Functional characterization of the PPAR targets ANGPTL4 and HILPDA in lipid metabolism

Frits Mattijssen

Thesis committee

Promotor
Prof. Dr A.H. Kersten
Personal chair at the Division of Human Nutrition
Wageningen University

Other members
Prof. Dr M.K. Hesselink, Maastricht University
Dr J.W. Jonker, University Medical Center Groningen
Prof. Dr P.C.N. Rensen, Leiden University Medical Center
Prof. Dr D. Weijers, Wageningen University

Functional characterization of the PPAR targets ANGPTL4 and HILPDA in lipid metabolism

Frits Mattijssen

Abstract

The peroxisomal proliferator activator receptors (PPARs) are ligand-activated transcription factors that play important roles in the regulation of lipid metabolism. Three PPAR isoforms have been identified: PPARα, PPARβ/δ, and PPARγ. Each isoform has specific functions determined by their relative abundance in a cell and regulation of specific target genes.

A highly sensitive PPAR target gene is represented by Angiopoietin-like 4 (ANGPTL4), which was discovered by three independent groups in 2000. ANGPTL4 is produced in a number of organs including liver and adipose tissue, where its expression is governed by PPARα and PPARγ, respectively. Upon secretion, ANGPTL4 is cleaved into N- and C-terminal fragments that have divergent functions. nANGPTL4 is known to function as an inhibitor of lipoprotein lipase, whereas cANGPTL4 is involved in a number of processes including tumorigenesis and wound healing, and is known to interact with integrins β1 and β5.

In this thesis we set out to expand our knowledge on the molecular function of ANGPTL4 in the regulation of lipid metabolism. We performed animal experiments, cell culture, biochemical assays, and other functional measurements to zoom in on previously unexplored aspects of ANGPTL4.

Feeding mice deficient in ANGPLT4 a diet rich in long-chain saturated fatty acids elicited a complex phenotype and *Angptl4*$^{-/-}$ mice ultimately died from fibrinopurulent peritonitis. In contrast, the lethal phenotype was not observed when the fat component of the high-fat diet was changed to medium-chain fatty acids, suggesting a role for increased chyle flow via the lymphatic system. Indeed, *Angptl4*$^{-/-}$ mice had dramatically enlarged mesenteric lymph nodes which contained numerous lipid laden macrophages. In vitro experiments showed that PPARβ/δ-mediated induction of ANGPTL4 results in inhibition of macrophage LPL. In the absence of ANGPTL4, lipid uptake in mesenteric lymph node resident macrophages is increased, leading to ER stress and subsequent pro-inflammatory response.

Additionally, *Angptl4*$^{-/-}$ mice initially gain more weight when fed a high-fat diet. The increased body weight and adiposity was unrelated to food intake, activity, or energy expenditure. Remarkably, we observed decreased fecal lipid excretion in *Angptl4*$^{-/-}$ mice, which coincided with increased lipase activity in the intestinal lumen. Using biochemical assays we reveal that ANGPTL4 inhibits pancreatic lipase.

In the second part of this thesis we identify a novel PPAR target gene named hypoxia inducible lipid droplet associated (HILPDA). We observed *Hilpda* expression to be increased in liver slices exposed to a synthetic PPARα ligand. Additionally, oral dosing of similar ligand induced a marked increase in HILPDA expression in livers of wild-type mice but

not *Ppara*$^{-/-}$ mice. Induction of HILPDA expression by PPAR was found to be mediated by a conserved and functional PPAR response element located 1200 base pair upstream of the transcription start site of *Hilpda*. Functional characterization of HILPDA in liver was performed via adeno-associated virus-mediated overexpression. Interestingly, increased hepatic expression of HILPDA was associated with the development of a fatty liver, which could be attributed to a decrease in hepatic very low-density lipoprotein (VLDL) production.

HILPDA was also found to be highly expressed in both human and mouse adipose tissue, where its expression is under the control of PPARγ and β-adrenergic receptor. Moreover, adipose tissue HILPDA expression was increased with fasting but decreased with high-fat feeding. HILPDA did not affect 3T3-L1 adipogenesis. Furthermore, adipose tissue specific *Hilpda* knock-out mice showed no major metabolic perturbations upon fasting. However, overexpression of HILPDA in adipocytes significantly reduced the release of NEFAs upon β-adrenergic receptor activation. Induction of HILPDA by β-adrenergic receptor stimulation may be part of feedback mechanism to regulate adipocyte lipolysis.

In conclusion, in thesis we have extended the current knowledge on the function of ANGPTL4. We show that ANGPTL4 serves as an important regulator in the process of lipid digestion and in the protection of macrophages that reside in mesenteric lymph nodes. HILPDA is a novel PPAR target that is involved in hepatic VLDL secretion and adipocyte lipolysis. Future research will focus on elucidating the mechanistic aspects of the regulation and function of HILPDA in liver and adipose tissue.

Contents

1

General introduction

Lipid digestion

Our diet contains three major macronutrients that can provide energy: carbohydrates, lipids, and proteins. Carbohydrates and proteins yield 4 kcal of energy per gram whereas lipids contribute 9 kcal of energy per gram. Around 34% of the energy in the current diet of the Dutch population is derived from lipids, which corresponds to 70-105 gram of fat per day, depending on age and gender (1). Dietary fat mainly consists of triglycerides (TGs) (95%), with minor fractions of phospholipids and cholesteryl esters. The human body is able to extract > 90% of these TGs with the aid of several lipases.

Digestion of TGs starts in the mouth by the enzyme lingual lipase followed by contractions of the stomach to mix lipids with water, gastric acid, and gastric lipase secreted by the chief cells of the stomach (2). However, the major fraction of dietary lipids is digested in the small intestine (3). In the duodenum, the predigested food is emulsified with bile acids to allow for efficient digestion. At the same time, the pancreas releases several digestive enzymes including lipases such as pancreatic lipase (PL), carboxyl ester hydrolase, and pancreatic lipase-related protein 2 (3). Among those PL is the major lipase involved in the digestion of dietary lipids and hydrolyzes the ester bonds at the sn-1 and sn-3 positions of TGs (3).

PL is a carboxyl esterase that is part of the family of extracellular lipases that includes lipoprotein lipase (LPL), hepatic lipase, and endothelial lipase (4). Inhibition of PL by pharmacological inhibitors such as Orlistat lowers the amount of lipid that is digested and subsequently absorbed by 30% and is used in the treatment of obesity (5). Similarly, many plant-derived components have been found to inhibit PL (6). Following PL mediated hydrolysis, 2-monoacylglycerol (2-MG) and fatty acids mix with bile acids to form micelles that subsequently migrate to the apical membrane of enterocytes (7). The precise mechanisms by which 2-MG and fatty acids enter enterocytes are not completely understood and several mechanism including passive diffusion and active transport via transporters such as CD36 and fatty acid binding proteins (FABPs) have been postulated (7, 8).

Chylomicron formation and secretion

Once taken up by enterocytes, 2-MG and fatty acids are re-esterified into TGs catalyzed by several monoacylglycerol acyltransferase (MGAT) and acyl-coenzyme A: diacylglycerol acyltransferase (DGAT) enzymes localized at the surface of the endoplasmic reticulum (ER) (9-11). Within the rough ER, apolipoprotein B48 (APOB48) is lipidated by the enzyme microsomal triglyceride transfer protein (MTTP) to form a primordial particle

(12, 13). These particles fuse with intraluminal ER-associated lipid droplets to form pre-chylomicrons that are subsequently transported to the Golgi via transport vesicles (14). After maturation in the Golgi, the chylomicrons are subsequently secreted into intercellular space by exocytosis after which the chylomicrons enter the intestinal lacteals (15, 16). Lacteals transporting chylomicrons merge into the mesenteric lymph duct, then into the thoracic duct. Chylomicrons ultimately enter the circulation in the subclavian vein. Following a high-fat meal the production and secretion of chyle and chylomicrons increases and TG concentrations in the mesenteric lymph duct can reach concentrations up to 55 mM (17). During the transport of chyle in the mesenteric lymphatics numerous mesenteric lymph nodes (MLNs) are encountered. MLNs contain a variety of immune cells including T cells and macrophages that sample chyle for the presence of antigens (18). As a consequence of their localization, mesenteric lymph node resident immune cells are exposed the high concentration of TGs as mentioned above. In contrast to long-chain fatty acids, short- and medium-chain fatty acids (SCFA/MCFA) are absorbed apically and secreted basolateral without being incorporated into chylomicrons. Instead, SCFA and MCFA are secreted in the portal vein and transported to the liver directly (19, 20).

Uptake of non-esterified fatty acids from lipoproteins via LPL

Chylomicrons that have entered the circulation deliver their TGs to peripheral tissues to serve as energy source of for storage. In the circulation chylomicrons acquire several additional apoliproteins such as APOC2 and APOE that aid in the clearance of TGs (21, 22). In order for peripheral tissues to efficiently hydrolyze fatty acids from chylomicrons, the presence of LPL is required (23). Expression of LPL is found in numerous tissues that are characterized by elevated uptake of lipids such as skeletal muscle, adipose tissue and heart (23). Production of LPL takes place in the parenchymal cells after which the enzyme is secreted and transported to the luminal surface of capillary endothelial cells. Here, LPL is anchored to heparin sulfate proteoglycans (HSPG) and glycosylphosphatidylinositol anchored high density lipoprotein binding protein 1 (GPIHBP1) (24, 25). Interestingly, GPIHBP1 is responsible for LPL translocation across the endothelial cells and prevents LPL from being inactivated by ANGPTL4 (see below) (26, 27). LPL functions as a homodimer and requires cofactors including APOC2 to catalyze the lipolysis of TGs from chylomicrons (21, 23, 28). The resulting products of LPL mediated hydrolysis, glycerol and non-esterified fatty acids (NEFAs) are then taken up by the parenchymal cells to be used in a variety of processes such as β-oxidation, synthesis of lipid derived components, or storage in lipid droplets after re-esterification to triglycerides.

NEFAs activate PPARS

Additionally, lipids that are taken up can activate transcription factors of the peroxisomal-proliferator activated receptor (PPAR) family (29). PPARs are part of a larger family of nuclear hormone receptors that includes additional members such as the glucocorticoid receptor, vitamin D receptor, and the liver X receptor (30, 31). To date, three PPAR isoforms have been identified: PPARα, PPARβ/δ and PPARγ, all of which function as a heterodimer with the retinoid X receptor (RXR) (32, 33). Similar to most nuclear receptors, PPARs contain several distinct domains: an N-terminal activation function 1 (AF1), a DNA binding domain (DBD), a ligand binding domain (LBD), and an activation function 2 (AF2) located within the LBD (34). Upon ligand activation PPARs dismiss several corepressors such as nuclear receptor co-repressor (NCoR) and silencing mediator of retinoic acid and thyroid hormone receptor (SMRT) and simultaneously recruit coactivators including CREB binding protein (CBP/p300) and peroxisome proliferator activated receptor gamma coactivator 1 alpha (PGC-1α) (35-37). Together, these actions initiate the binding of PPARs to specific loci in the DNA called PPAR response elements (PPREs) that are present in promoter regions but also in introns and intergenic regions (34, 38). Each PPAR displays a distinct expression profile: PPARα is mainly expressed in liver, brown adipose tissue, skeletal muscle, and heart, PPARβ/δ is expressed ubiquitously, while PPARγ expression is primarily localized to adipose tissue (34, 39-41). These differential expression profiles together with inherent biochemical properties and ligand specificity determine the genes that are regulated by each PPAR and consequently their specific function. PPARα regulates many genes that are involved in the oxidation of fatty acids, although it is increasingly recognized as an important regulator of other metabolic processes such as gluconeogenesis and bile metabolism (42). The function of PPARβ/δ is less well characterized though accumulating data suggest that it induces β-oxidation in skeletal muscle and heart (40). PPARγ was identified in adipose tissue where it plays a role in the development as well is in the maintenance of adipose tissue (43). Although all PPARs can be activated by fatty acids and fatty acid-derived components, the specific ligands are poorly defined. High affinity ligands such as fibrates and thiazolidinediones are used in the treatment of hyperlipidemia and type 2 diabetes and act via PPARα and PPARγ, respectively (44-46).

Induction of ANGPTL4 via PPARs

One of the genes that is under the control of the family of PPAR receptors is angiopoietin-like 4 (ANGPTL4). ANGPTL4 was identified as PPAR target when livers from wild-type

and *Ppara*⁻/⁻ mice were analyzed for differentially expressed genes (47). In later years, the PPAR dependent regulation was confirmed with the identification of a PPRE located within intron 3 (48). The *Angptl4* gene contains 6 introns and 7 exons that encode a protein of 406 amino acids. Expression of ANGPTL4 is ubiquitous with high expression levels in liver, adipose tissue, heart, and intestine (47, 49, 50). ANGPTL4 is subjected to several post-translational modifications that take place upon secretion, such as cleavage, glycosylation and sialylation (51-55). Proteolytic processing of ANGPTL4 yields an N-terminal fragment containing a coiled-coil domain and a C-terminal fragment that comprises a fibrinogen-like domain (56). cANGPTL4 circulates as a monomer, serves as a ligand for β1 and β5 integrins, and is involved in numerous processes including angiogenesis, wound healing, and tumorigenesis (56-58). In contrast, nANGPTL4 forms oligomers and plays an important role in the regulation of lipid uptake via regulation of LPL in a number of tissues and cells in an autocrine and endocrine manner (59). For instance, lipid accumulation in cardiomyocytes via LPL mediated hydrolysis of chylomicrons leads to the activation of PPARβ/δ, induction of *Angptl4* expression and ultimately inhibition of LPL activity by secreted ANGPTL4 (60). Hence, induction of ANGPTL4 by ligand-activated PPAR serves as a feedback mechanism to prevent aberrant lipid accumulation. The precise mechanism by which ANGPTL4 inhibits LPL is unclear. Several lines of evidence suggest that ANGPTL4 inhibits LPL by non-reversible degradation of LPL homodimers (61, 62). More recently an additional mechanism has been proposed in which ANGPTL4 reversibly inhibits LPL in the subendothelial space by forming a complex (63). In addition to the PPARs, several other transcription factors have been implicated in the regulation of ANGPTL4, including the glucocorticoid receptor and hypoxia-inducible factor (64-66).

Uptake of chylomicron remnants in liver and production of VLDL

After delivery of the vast majority of their TGs to peripheral tissues, chylomicron remnant particles are taken up by the liver via LDL receptor, LDL receptor related protein, and HSPG mediated pathways (67-70). The liver does not store major quantities of lipids although several conditions including obesity, cancer cachexia, and fasting are associated with an increase in hepatic lipid accumulation (71-73). Indeed, the majority of lipids in liver are secreted back in to the circulation incorporated in VLDL, a process that is generally believed to be largely driven by substrate availability (74). Assembly and secretion of VLDL in liver and chylomicrons in the intestine share many similarities and both processes rely on the lipidation process initiated by MTTP (75, 76). Nevertheless, there are some key differences. For instance, chylomicron synthesis starts with the lipidation of APOB48, whereas VLDL

synthesis starts with APOB100. Both apolipoproteins are derived from the same gene, yet in the intestine a stop codon is introduced via RNA editing by APOBEC1 and APOBEC1 complementation factor (ACF), resulting in the translation of a smaller protein (77, 78). It should be noted that rats and mice produce APOB48-containing particles in liver as well (79, 80). VLDL contains relatively more cholesterol and phospholipids compared to chylomicrons. Once secreted, VLDL redistributes TGs to LPL-expressing tissues including heart, muscle and adipose tissue.

Outline of this thesis

The main aim of this thesis is to increase our understanding regarding the function of ANGPTL4 in lipid metabolism. In **chapter 2** we present a contemporary overview of the knowledge on ANGPTL proteins and their role in triglyceride metabolism. **Chapter 3** uncovers the key role of ANGPTL4 in the regulation of lipid uptake by mesenteric lymph node resident macrophages. Using *Angptl4*$^{-/-}$ mice we show that a PPARβ/δ-ANGPTL4 feedback mechanism in these macrophages protects them from an inflammatory response provoked by uncontrolled influx of saturated fatty acids. In **chapter 4** we reveal a new role for ANGPTL4 in the regulation of lipid uptake in the intestine. Employing a combination of in vivo and in vitro experiments, we provide evidence for an ANGPTL4-mediated reduction in lipid harvest from dietary sources. As a result, *Angptl4*$^{-/-}$ animals are heavier and have increased fat mass. In **chapter 5** we identify hypoxia inducible lipid droplet associated (HILPDA) as a novel PPAR target gene involved in the regulation of VLDL production. **Chapter 6** describes the regulation and function of HILPDA in adipose tissue. We demonstrate that HILPDA plays a role as an inhibitor of β-adrenergic receptor induced lipolysis. Finally, in **chapter 7** we discuss our findings, integrate the different chapters and provide a general conclusion.

References

1.   van Rossum CTM, Fransen HP, Verkaik-Kloosterman J, Buurma-Rethans EJM, Ocké MC. Dutch National Food Consumption Survey 2007-2010. *National Institute for Public Health and the Environment (RIVM).* 2011.

2.   Armand M. Lipases and lipolysis in the human digestive tract: where do we stand? *Curr Opin Clin Nutr Metab Care.* 2007;10(2):156-164.

3.   Whitcomb DC, Lowe ME. Human pancreatic digestive enzymes. *Dig Dis Sci.* 2007;52(1):1-17.

4.   Wong H, Schotz MC. The lipase gene family. *J Lipid Res.* 2002;43(7):993-999.

5.   Drew BS, Dixon AF, Dixon JB. Obesity management: update on orlistat. *Vasc Health Risk Manag.* 2007;3(6):817-821.

6.   de la Garza AL, Milagro FI, Boque N, Campion J, Martinez JA. Natural inhibitors of pancreatic lipase as new players in obesity treatment. *Planta Med.* 2011;77(8):773-785.

7.   Wang TY, Liu M, Portincasa P, Wang DQ. New insights into the molecular mechanism of intestinal fatty acid absorption. *Eur J Clin Invest.* 2013;43(11):1203-1223.

8.   Schwenk RW, Holloway GP, Luiken JJ, Bonen A, Glatz JF. Fatty acid transport across the cell membrane: regulation by fatty acid transporters. *Prostaglandins Leukot Essent Fatty Acids.* 2010;82(4-6):149-154.

9.   Buhman KK, Smith SJ, Stone SJ, Repa JJ, Wong JS, Knapp FF, Jr., Burri BJ, Hamilton RL, Abumrad NA, Farese RV, Jr. DGAT1 is not essential for intestinal triacylglycerol absorption or chylomicron synthesis. *J Biol Chem.* 2002;277(28):25474-25479.

10.   Kindel T, Lee DM, Tso P. The mechanism of the formation and secretion of chylomicrons. *Atheroscler Suppl.* 2010;11(1):11-16.

11.   Hiramine Y, Tanabe T. Characterization of acyl-coenzyme A:diacylglycerol acyltransferase (DGAT) enzyme of human small intestine. *J Physiol Biochem.* 2011;67(2):259-264.

12.   Sharp D, Blinderman L, Combs KA, Kienzle B, Ricci B, Wager-Smith K, Gil CM, Turck CW, Bouma ME, Rader DJ, et al. Cloning and gene defects in microsomal triglyceride transfer protein associated with abetalipoproteinaemia. *Nature.* 1993;365(6441):65-69.

13.   Iqbal J, Hussain MM. Intestinal lipid absorption. *Am J Physiol Endocrinol Metab.* 2009;296(6):E1183-1194.

14.   Abumrad NA, Davidson NO. Role of the gut in lipid homeostasis. *Physiol Rev.* 2012;92(3):1061-1085.

15.   Mansbach CM, Siddiqi SA. The biogenesis of chylomicrons. *Annu Rev Physiol.* 2010;72:315-333.

16.   Dixon JB. Mechanisms of chylomicron uptake into lacteals. *Ann N Y Acad Sci.* 2010;1207 Suppl 1(E52-57.

17.   Lichtenstein L, Mattijssen F, de Wit NJ, Georgiadi A, Hooiveld GJ, van der Meer R, He Y, Qi L, Koster A, Tamsma JT, et al. Angptl4 protects against severe proinflammatory effects of saturated fat by inhibiting fatty acid uptake into mesenteric lymph node macrophages. *Cell Metab.* 2010;12(6):580-592.

18.   Ohtani O, Ohtani Y. Structure and function of rat lymph nodes. *Arch Histol Cytol.* 2008;71(2):69-76.

19.   Kiyasu JY, Bloom B, Chaikoff IL. The portal transport of absorbed fatty acids. *J Biol Chem.* 1952;199(1):415-419.

20.   Clement J. [Digestion and absorption of dietary triglycerides]. *J Physiol (Paris).* 1976;72(2):137-170.

21.   Kei AA, Filippatos TD, Tsimihodimos V, Elisaf MS. A review of the role of apolipoprotein C-II in lipoprotein metabolism and cardiovascular disease. *Metabolism.* 2012;61(7):906-921.

22.   Voshol PJ, Rensen PC, van Dijk KW, Romijn JA, Havekes LM. Effect of plasma triglyceride metabolism on lipid storage in adipose tissue: studies using genetically engineered mouse models. *Biochim Biophys Acta.* 2009;1791(6):479-485.

23.   Wang H, Eckel RH. Lipoprotein lipase: from gene to obesity. *Am J Physiol Endocrinol Metab.* 2009;297(2):E271-288.

24.   Eisenberg S, Sehayek E, Olivecrona T, Vlodavsky I. Lipoprotein lipase enhances binding of lipoproteins to heparan sulfate on cell surfaces and extracellular matrix. *J Clin Invest.* 1992;90(5):2013-2021.

25.   Beigneux AP, Davies BS, Gin P, Weinstein MM, Farber E, Qiao X, Peale F, Bunting S, Walzem RL, Wong JS, et al. Glycosylphosphatidylinositol-anchored high-density lipoprotein-binding protein 1 plays a critical role in the lipolytic processing of chylomicrons. *Cell Metab.* 2007;5(4):279-291.

26.   Davies BS, Beigneux AP, Barnes RH, 2nd, Tu Y, Gin P, Weinstein MM, Nobumori C, Nyren R, Goldberg I, Olivecrona G, et al. GPIHBP1 is responsible for the entry of lipoprotein lipase into capillaries. *Cell Metab.* 2010;12(1):42-52.

27.   Sonnenburg WK, Yu D, Lee EC, Xiong W, Gololobov G, Key B, Gay J, Wilganowski N, Hu Y, Zhao S, et al. GPIHBP1 stabilizes lipoprotein lipase and prevents its inhibition by angiopoietin-like 3 and angiopoietin-like 4. *J Lipid Res.* 2009;50(12):2421-2429.

28.   Kinnunen PK, Jackson RL, Smith LC, Gotto AM, Jr., Sparrow JT. Activation of lipoprotein lipase by native and synthetic fragments of human plasma apolipoprotein C-II. *Proc Natl Acad Sci U S A.* 1977;74(11):4848-4851.

29.   Kersten S, Wahli W. Peroxisome proliferator activated receptor agonists. *EXS.* 2000;89:141-151.

30.   Chawla A, Repa JJ, Evans RM, Mangelsdorf DJ. Nuclear receptors and lipid physiology: opening the X-files. *Science.* 2001;294(5548):1866-1870.

31.   Sonoda J, Pei L, Evans RM. Nuclear receptors: decoding metabolic disease. *FEBS Lett.* 2008;582(1):2-9.

32.   Dreyer C, Krey G, Keller H, Givel F, Helftenbein G, Wahli W. Control of the peroxisomal beta-oxidation pathway by a novel family of nuclear hormone receptors. *Cell.* 1992;68(5):879-887.

33.   Keller H, Dreyer C, Medin J, Mahfoudi A, Ozato K, Wahli W. Fatty acids and retinoids control lipid metabolism through activation of peroxisome proliferator-activated receptor-retinoid X receptor heterodimers. *Proc Natl Acad Sci U S A.* 1993;90(6):2160-2164.

34.   Poulsen L, Siersbaek M, Mandrup S. PPARs: fatty acid sensors controlling metabolism. *Semin Cell Dev Biol.* 2012;23(6):631-639.

35.   Dowell P, Ishmael JE, Avram D, Peterson VJ, Nevrivy DJ, Leid M. p300 functions as a coactivator for the peroxisome proliferator-activated receptor alpha. *J Biol Chem.* 1997;272(52):33435-33443.

36.   Yu S, Reddy JK. Transcription coactivators for peroxisome proliferator-activated receptors. *Biochim Biophys Acta.* 2007;1771(8):936-951.

37.   Perissi V, Jepsen K, Glass CK, Rosenfeld MG. Deconstructing repression: evolving models of co-repressor action. *Nat Rev Genet.* 2010;11(2):109-123.

38.   Tugwood JD, Issemann I, Anderson RG, Bundell KR, McPheat WL, Green S. The mouse peroxisome proliferator activated receptor recognizes a response element in the 5' flanking sequence of the rat acyl CoA oxidase gene. *EMBO J.* 1992;11(2):433-439.

39.   Mandard S, Muller M, Kersten S. Peroxisome proliferator-activated receptor alpha target genes. *Cell Mol Life Sci.* 2004;61(4):393-416.

40.   Bojic LA, Huff MW. Peroxisome proliferator-activated receptor delta: a multifaceted metabolic player. *Curr Opin Lipidol.* 2013;24(2):171-177.

41.   Tontonoz P, Hu E, Graves RA, Budavari AI, Spiegelman BM. mPPAR gamma 2: tissue-specific regulator of an adipocyte enhancer. *Genes Dev.* 1994;8(10):1224-1234.

42.   Rakhshandehroo M, Knoch B, Muller M, Kersten S. Peroxisome proliferator-activated receptor alpha target genes. *PPAR Res.* 2010;2010.pii:612089.

43.   Ahmadian M, Suh JM, Hah N, Liddle C, Atkins AR, Downes M, Evans RM. PPARgamma signaling and metabolism: the good, the bad and the future. *Nat Med.* 2013;19(5):557-566.

44.   Duval C, Muller M, Kersten S. PPARalpha and dyslipidemia. *Biochim Biophys Acta.* 2007;1771(8):961-971.

45.   Lalloyer F, Staels B. Fibrates, glitazones, and peroxisome proliferator-activated receptors. *Arterioscler Thromb Vasc Biol.* 2010;30(5):894-899.

46.   Tontonoz P, Spiegelman BM. Fat and beyond: the diverse biology of PPARgamma. *Annu Rev Biochem.* 2008;77:289-312.

1

47. Kersten S, Mandard S, Tan NS, Escher P, Metzger D, Chambon P, Gonzalez FJ, Desvergne B, Wahli W. Characterization of the fasting-induced adipose factor FIAF, a novel peroxisome proliferator-activated receptor target gene. *J Biol Chem.* 2000;275(37):28488-28493.

48. Mandard S, Zandbergen F, Tan NS, Escher P, Patsouris D, Koenig W, Kleemann R, Bakker A, Veenman F, Wahli W, et al. The direct peroxisome proliferator-activated receptor target fasting-induced adipose factor (FIAF/PGAR/ANGPTL4) is present in blood plasma as a truncated protein that is increased by fenofibrate treatment. *J Biol Chem.* 2004;279(33):34411-34420.

49. Romeo S, Yin W, Kozlitina J, Pennacchio LA, Boerwinkle E, Hobbs HH, Cohen JC. Rare loss-of-function mutations in ANGPTL family members contribute to plasma triglyceride levels in humans. *J Clin Invest.* 2009;119(1):70-79.

50. Kersten S, Lichtenstein L, Steenbergen E, Mudde K, Hendriks HF, Hesselink MK, Schrauwen P, Muller M. Caloric restriction and exercise increase plasma ANGPTL4 levels in humans via elevated free fatty acids. *Arterioscler Thromb Vasc Biol.* 2009;29(6):969-974.

51. Ge H, Yang G, Huang L, Motola DL, Pourbahrami T, Li C. Oligomerization and regulated proteolytic processing of angiopoietin-like protein 4. *J Biol Chem.* 2004;279(3):2038-2045.

52. Yang YH, Wang Y, Lam KS, Yau MH, Cheng KK, Zhang J, Zhu W, Wu D, Xu A. Suppression of the Raf/MEK/ERK signaling cascade and inhibition of angiogenesis by the carboxyl terminus of angiopoietin-like protein 4. *Arterioscler Thromb Vasc Biol.* 2008;28(5):835-840.

53. Yin W, Romeo S, Chang S, Grishin NV, Hobbs HH, Cohen JC. Genetic variation in ANGPTL4 provides insights into protein processing and function. *J Biol Chem.* 2009;284(19):13213-13222.

54. Lei X, Shi F, Basu D, Huq A, Routhier S, Day R, Jin W. Proteolytic processing of angiopoietin-like protein 4 by proprotein convertases modulates its inhibitory effects on lipoprotein lipase activity. *J Biol Chem.* 2011;286(18):15747-15756.

55. Clement LC, Avila-Casado C, Mace C, Soria E, Bakker WW, Kersten S, Chugh SS. Podocyte-secreted angiopoietin-like-4 mediates proteinuria in glucocorticoid-sensitive nephrotic syndrome. *Nat Med.* 2011;17(1):117-122.

56. Zhu P, Goh YY, Chin HF, Kersten S, Tan NS. Angiopoietin-like 4: a decade of research. *Biosci Rep.* 2012;32(3):211-219.

57. Goh YY, Pal M, Chong HC, Zhu P, Tan MJ, Punugu L, Lam CR, Yau YH, Tan CK, Huang RL, et al. Angiopoietin-like 4 interacts with integrins beta1 and beta5 to modulate keratinocyte migration. *Am J Pathol.* 2010;177(6):2791-2803.

58. Zhu P, Tan MJ, Huang RL, Tan CK, Chong HC, Pal M, Lam CR, Boukamp P, Pan JY, Tan SH, et al. Angiopoietin-like 4 protein elevates the prosurvival intracellular O2(-):H2O2 ratio and confers anoikis resistance to tumors. *Cancer Cell.* 2011;19(3):401-415.

59. Mattijssen F, Kersten S. Regulation of triglyceride metabolism by Angiopoietin-like proteins. *Biochim Biophys Acta.* 2012;1821(5):782-789.

60. Georgiadi A, Lichtenstein L, Degenhardt T, Boekschoten MV, van Bilsen M, Desvergne B, Muller M, Kersten S. Induction of cardiac Angptl4 by dietary fatty acids is mediated by peroxisome proliferator-activated receptor beta/delta and protects against fatty acid-induced oxidative stress. *Circ Res.* 2010;106(11):1712-1721.

61. Sukonina V, Lookene A, Olivecrona T, Olivecrona G. Angiopoietin-like protein 4 converts lipoprotein lipase to inactive monomers and modulates lipase activity in adipose tissue. *Proc Natl Acad Sci U S A.* 2006;103(46):17450-17455.

62. Lichtenstein L, Berbee JF, van Dijk SJ, van Dijk KW, Bensadoun A, Kema IP, Voshol PJ, Muller M, Rensen PC, Kersten S. Angptl4 upregulates cholesterol synthesis in liver via inhibition of LPL- and HL-dependent hepatic cholesterol uptake. *Arterioscler Thromb Vasc Biol.* 2007;27(11):2420-2427.

63. Lafferty MJ, Bradford KC, Erie DA, Neher SB. Angiopoietin-like protein 4 inhibition of lipoprotein lipase: evidence for reversible complex formation. *J Biol Chem.* 2013;288(40):28524-28534.

64. Koliwad SK, Kuo T, Shipp LE, Gray NE, Backhed F, So AY, Farese RV, Jr., Wang JC. Angiopoietin-like 4 (ANGPTL4, fasting-induced adipose factor) is a direct glucocorticoid receptor target and participates in glucocorticoid-regulated triglyceride metabolism. *J Biol Chem.* 2009;284(38):25593-25601.

65. Belanger AJ, Lu H, Date T, Liu LX, Vincent KA, Akita GY, Cheng SH, Gregory RJ, Jiang C. Hypoxia up-regulates expression of peroxisome proliferator-activated receptor gamma angiopoietin-related gene (PGAR) in cardiomyocytes: role of hypoxia inducible factor 1alpha. *J Mol Cell Cardiol.* 2002;34(7):765-774.

66. Drager LF, Yao Q, Hernandez KL, Shin MK, Bevans-Fonti S, Gay J, Sussan TE, Jun JC, Myers AC, Olivecrona G, et al. Chronic intermittent hypoxia induces atherosclerosis via activation of adipose angiopoietin-like 4. *Am J Respir Crit Care Med.* 2013;188(2):240-248.

67. Chappell DA, Medh JD. Receptor-mediated mechanisms of lipoprotein remnant catabolism. *Prog Lipid Res.* 1998;37(6):393-422.

68. Hassing HC, Surendran RP, Mooij HL, Stroes ES, Nieuwdorp M, Dallinga-Thie GM. Pathophysiology of hypertriglyceridemia. *Biochim Biophys Acta.* 2012;1821(5):826-832.

69. Foley EM, Gordts PL, Stanford KI, Gonzales JC, Lawrence R, Stoddard N, Esko JD. Hepatic remnant lipoprotein clearance by heparan sulfate proteoglycans and low-density lipoprotein receptors depend on dietary conditions in mice. *Arterioscler Thromb Vasc Biol.* 2013;33(9):2065-2074.

70. Gonzales JC, Gordts PL, Foley EM, Esko JD. Apolipoproteins E and AV mediate lipoprotein clearance by hepatic proteoglycans. *J Clin Invest.* 2013;123(6):2742-2751.

71. Cohen JC, Horton JD, Hobbs HH. Human fatty liver disease: old questions and new insights. *Science.* 2011;332(6037):1519-1523.

72. Berriel Diaz M, Krones-Herzig A, Metzger D, Ziegler A, Vegiopoulos A, Klingenspor M, Muller-Decker K, Herzig S. Nuclear receptor cofactor receptor interacting protein 140 controls hepatic triglyceride metabolism during wasting in mice. *Hepatology.* 2008;48(3):782-791.

73. Kersten S, Seydoux J, Peters JM, Gonzalez FJ, Desvergne B, Wahli W. Peroxisome proliferator-activated receptor alpha mediates the adaptive response to fasting. *J Clin Invest.* 1999;103(11):1489-1498.

74. Choi SH, Ginsberg HN. Increased very low density lipoprotein (VLDL) secretion, hepatic steatosis, and insulin resistance. *Trends Endocrinol Metab.* 2011;22(9):353-363.

75. Tiwari S, Siddiqi SA. Intracellular trafficking and secretion of VLDL. *Arterioscler Thromb Vasc Biol.* 2012;32(5):1079-1086.

76. Xiao C, Hsieh J, Adeli K, Lewis GF. Gut-liver interaction in triglyceride-rich lipoprotein metabolism. *Am J Physiol Endocrinol Metab.* 2011;301(3):E429-446.

77. Powell LM, Wallis SC, Pease RJ, Edwards YH, Knott TJ, Scott J. A novel form of tissue-specific RNA processing produces apolipoprotein-B48 in intestine. *Cell.* 1987;50(6):831-840.

78. Hirano K, Young SG, Farese RV, Jr., Ng J, Sande E, Warburton C, Powell-Braxton LM, Davidson NO. Targeted disruption of the mouse apobec-1 gene abolishes apolipoprotein B mRNA editing and eliminates apolipoprotein B48. *J Biol Chem.* 1996;271(17):9887-9890.

79. Chan L, Chang BH, Nakamuta M, Li WH, Smith LC. Apobec-1 and apolipoprotein B mRNA editing. *Biochim Biophys Acta.* 1997;1345(1):11-26.

80. Olofsson SO, Boren J. Apolipoprotein B: a clinically important apolipoprotein which assembles atherogenic lipoproteins and promotes the development of atherosclerosis. *J Intern Med.* 2005;258(5):395-410.

1

2

Regulation of triglyceride metabolism by Angiopoietin-like proteins

F Mattijssen, S Kersten

Abstract

Plasma triglyceride concentrations are determined by the balance between production of the triglyceride-rich lipoproteins VLDL and chylomicrons in liver and intestine, and their lipoprotein lipase-mediated clearance in peripheral tissues. In the last decade, the group of Angiopoietin-like proteins has emerged as important regulators of circulating triglyceride (TG) levels. Specifically, ANGPTL3 and ANGPTL4 impair TG clearance by inhibiting lipoprotein lipase (LPL). Whereas ANGPTL4 irreversibly inactivates LPL by promoting conversion of active LPL dimers into inactive monomers, ANGPTL3 reversibly inhibits LPL activity. Studies using transgenic or knockout mice have clearly demonstrated the stimulatory effect of ANGPTL3 and ANGPTL4 on plasma TG, which is further supported by human genetic data including genome wide association studies. Whereas ANGPTL3 is mainly active in the fed state, ANGPTL4 is elevated by fasting and mediates fasting-induced changes in plasma TG and free fatty acid metabolism. Both proteins undergo oligomerization and are subject to proteolytic cleavage to generate N- and C-terminal fragments with highly divergent biological activities. Expression of ANGPTL3 is exclusive to liver and governed by the liver X receptor (LXR). In contrast, ANGPTL4 is expressed ubiquitously and under sensitive control of the Peroxisome proliferator-activated receptor (PPAR) family. Induction of ANGPTL4 gene expression by fatty acids via PPARs is part of a feedback mechanism aimed at protecting cells against lipotoxicity. So far there is very little evidence that other ANGPTLs directly impact plasma lipoprotein metabolism.

Introduction

The extracellular lipase gene family represents one of the most robust gene families in living organisms. Members of the family, which include Hepatic Lipase (HL), Endothelial Lipase (EL), Lipoprotein Lipase (LPL), and Pancreatic Lipase (PL) share significant structural homology and are essential for maintaining lipid homeostasis. Pancreatic lipase is responsible for digesting dietary triglycerides, thereby permitting uptake of lipids from food. Hepatic lipase facilitates uptake of remnant lipoproteins, is involved in remodeling of HDL, and catalyzes conversion of IDL to LDL. Endothelial lipase targets circulating phospholipids and regulates plasma HDL levels. Finally, Lipoprotein lipase catalyzes breakdown of triglyceride-rich lipoproteins and as such is a major determinant of circulating TG levels. Given their importance in lipid homeostasis, the activity of extracellular lipases needs to be carefully controlled. In recent years it has become evident that the activity of some lipases is regulated by members of the family of Angiopoetin-like proteins. To date seven Angiopoietin-like proteins have been identified named ANGPTL1 through ANGPTL7. All ANGPTLs contain an N-terminal signal peptide that directs the proteins towards secretion, an N-terminal coiled-coil domain, a linker region, and a C-terminal fibrinogen-like domain. Here we review the current knowledge on ANGPTL2-6 and their role in regulation of metabolism of plasma lipids, moving from human genetic data to transgenic animal and in vitro data. No metabolic function has thus far been attributed to ANGPTL1 or ANGPTL7, which therefore are not discussed in this review.

ANGPTL2

No sequence variants in *ANGPTL2* have been identified that are associated with alterations in plasma lipoprotein levels. Deletion of *Angptl2* in mice leads to amelioration of adipose tissue inflammation and insulin resistance in obese mice, whereas *Angptl2* overexpression promotes adipose tissue inflammation and systemic insulin resistance [1]. However, unlike ANGPTL3 and ANGPTL4, there is no evidence that ANGPTL2 directly regulates plasma lipid levels. Administration of recombinant Angptl2 to diabetic *db/db* mice was recently shown to significantly reduce serum TG levels and free fatty acids. However, these changes are likely indirect via changes in insulin sensitivity in adipocytes [2]. Expression of *Angptl2* is found in several tissues including adipose tissue where it follows a circadian rhythmicity [1, 2]. Data on regulation of *Angptl2* mRNA are scarce and remain ambiguous with respect to the effect of obesity and endoplasmic reticulum stress [1, 2].

ANGPTL3

Human genetic studies

ANGPTL3 represents one of the many genes that have been linked to circulating lipids in recent genome wide association studies (3-5). Several SNPs at loci near *ANGPTL3* have been associated with plasma lipid concentrations. *ANGPTL3* rs12130333 is associated with the Fredrickson hyperlipoproteinemia type 5, representing a mixed hyperlipidaemia characterized by elevated VLDL and chylomicrons levels (6). More recently, rs2131925 was identified as the lead SNP in *ANGPTL3* and was shown to be associated with a mean reduction in plasma TG of 4.94 mg/dL (7). rs2131925 is located within the DOCK7 gene located upstream of the *ANGPTL3* gene and impacts ANGPTL3 expression, likely by being situated within regulatory elements (7). In another report, the *ANGPTL3* SNP rs12042319 was associated with lower LDL-C, TG, and IL-6 levels but counter-intuitively with increased risk for coronary heart disease (8). Re-sequencing of the seven exons of *ANGPTL3* in the Dallas Heart Study has provided further evidence for a link between the *ANGPTL3* gene and plasma TG levels in humans. A total of 35 non-synonymous sequence variants were identified and variants that yield a loss-of-function allele were all in the lowest quartile of TG levels. Fourteen out of 35 non-synonymous variants were in the lower quintile for TG, while 5 variations were found in the upper quintile. Variant M259T, which is mainly present in African Americans and rare among individuals of European descent, was associated with lower plasma TG levels in the Dallas Heart Study and among African Americans in the Atherosclerosis Risk in Communities study (9). Recently, exome sequencing of 15,994 genes of two individuals from a family with familial combined hypolipidemia led to the identification of two novel *ANGPTL3* gene variants that introduce a stop codon at positions 17 and 129. Subsequent sequencing of the first exon in all family members identified 13 normal heterozygotes and 4 compound heterozygotes, with the latter exhibiting significantly lower plasma LDL-C and TG levels. The normal heterozygotes in turn had significantly lower plasma LDL-C and TG levels compared to 21 non-mutant family members (10). Thus, human genetic studies clearly link the *ANGPTL3* gene to regulation of plasma lipid levels, with a primary effect on plasma TG.

Based on the above data, a positive association between plasma ANGPTL3 levels and plasma TG levels may be expected. However, in two Japanese studies, ANGPTL3 levels did not correlate with TG levels (11, 12). Also, no correlation between plasma ANGPTL3 and TG was found in a small group of 20 overweight and obese subjects (13). More recently, an inverse correlation between ANGPTL3 levels and TG concentration was found in a Finnish population. Interestingly, when HDL-C and ApoA-I were used as control variables, the

association between ANGPTL3 and TG was no longer apparent, indicating that the effect of ANGPTL3 on TG levels may be dependent on HDL concentration (14). It should be noted that the lack of a clear association between plasma ANGPTL3 and TG levels does not necessarily invalidate ANGPTL3 as a determinant of plasma TG in humans yet does raise questions about whether circulating ANGPTL3 represents the functional pool of protein. Proper interpretation of the data on circulating ANGPTL3 also requires additional information on what the ELISA actually detects, as ANGPTL3 undergoes cleavage to generate fragments that likely vary in their biological activity.

2

ANGPTL3 raises plasma triglycerides in mice via LPL inhibition

An abundance of data from animal studies supports an inhibitory effect of ANGPTL3 on plasma TG metabolism in mice. In an effort to explain the low plasma TG levels in the mutant KK/San mice, Koshi and colleagues discovered that the KK/San animals carry a 4 base pair insert in exon 6 of the *Angptl3* gene creating a stop codon at position 347. Adenoviral-mediated delivery of either mouse or human ANGPTL3 in both KK/San and C57BL/6J mice raised plasma TG levels, as did injection of recombinant ANGPTL3 in KK/San animals (15). Consistent with these findings, targeted deletion of *Angptl3* lowers plasma TG and cholesterol levels (16). The hypertriglyceridemic effect of ANGPTL3 is most prominent during the fed state, suggesting that ANGPTL3 mainly plays a role in regulation of peripheral lipid uptake after feeding (16).

Data abound indicating that the plasma TG raising effect of ANGPTL3 is mediated by inhibition of LPL activity (Figure 1). Low TG levels in the KK/San mice can be attributed to marked augmentation of the LPL-dependent clearance rate of VLDL-TG from the plasma, and not by changes in the hepatic VLDL triglyceride secretion rate (17). Consistent with these findings, absence of ANGPTL3 markedly increases post-heparin LPL activity, while HL activity is only mildly affected (17, 18). Despite its strong effects in vivo, recombinant ANGPTL3 only weakly inhibits LPL catalytic activity and does not cause permanent LPL inactivation in a biochemical assay (19). The discrepancy may be explained by the suggested stimulatory effect of ANGPTL3 on LPL cleavage mediated by endogenous FURIN and PCSK6, causing dissociation of LPL from the cell surface (20). Interestingly, while the inhibitory effect of ANGPTL3 on LPL activity in vitro and in vivo was found to be mitigated by heparin and the LPL anchor and transport protein GPIHBP1 (19, 21), ANGPTL3-induced LPL cleavage was unaffected by heparan-sulphate proteoglycans or GPIHBP1 in a cell based system (20). Inhibition of LPL activity by ANGPTL3 is dependent on a heparin-binding site and three polar residues located within the N-terminal coiled-coil region: Asn46, Gln50, and His53 (18, 22).
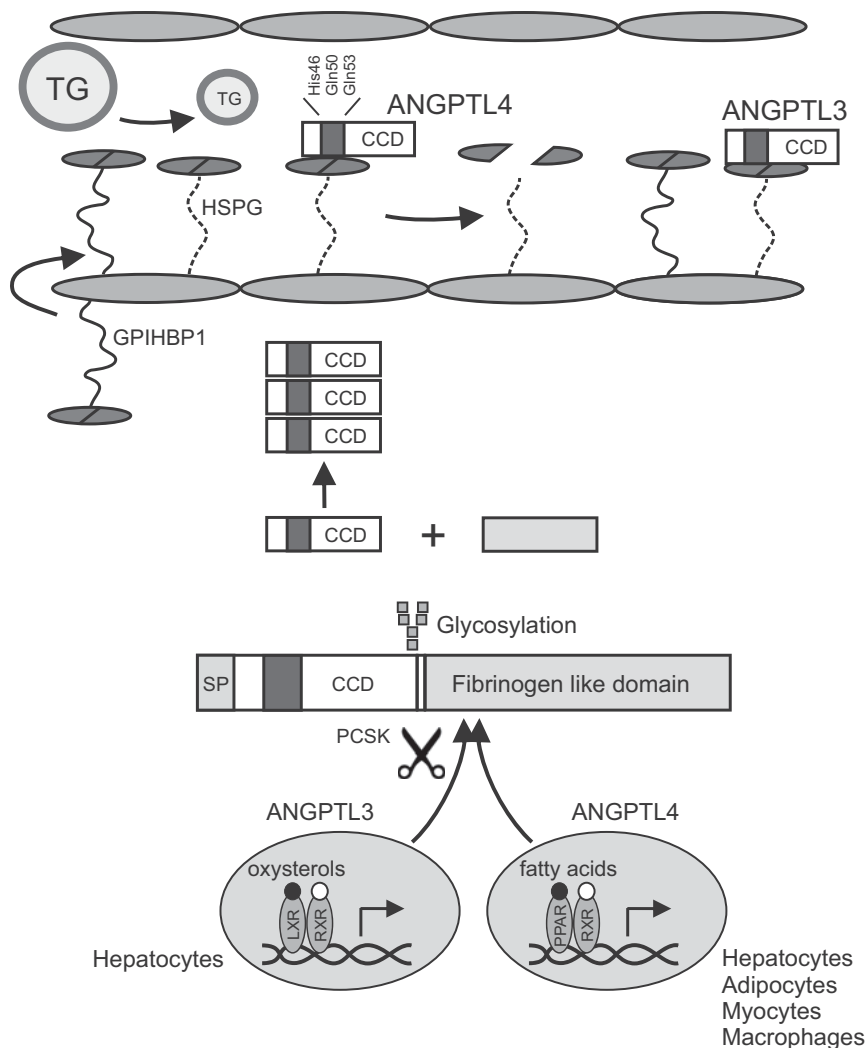
Figure 1. Current model on regulation of LPL-mediated lipolysis by ANGPTL3 and ANGPTL4
ANGPTL3 is predominantly expressed in hepatocytes and is under transcriptional control of the Liver X Receptor. ANGPTL4 is expressed in multiple cell types including adipocytes, hepatocytes, and macrophages, and expression is governed by PPARs. ANGPTL3 and ANGPTL4 undergo several post-translational modifications that include oligomerization, glycosylation and proprotein convertase (PCSK)-mediated cleavage. LPL inhibition by ANGPTL3 and ANGPTL4 is dependent on three polar residues on position 46, 50, and 53 within the N-terminal coiled-coil domain. ANGPTL4 permanently inactivates LPL at least partly by promoting the dissociation of LPL dimer into inactive LPL monomers. In contrast, ANGPTL3 reversibly inhibits LPL activity. The C-terminal fibrinogen-like domain (FLD) does not seem to have a direct function in regulation of TG metabolism.
GPIHBP1 = glycosylphosphatidylinositol anchored high density lipoprotein binding protein 1. HSPG = heparan-sulphate proteoglycan. SP = signal peptide.

Next to its role in regulation of TG homeostasis, ANGPTL3 is capable of inhibiting endothelial lipase (EL), leading to increased HDL cholesterol and phospholipids levels (12). It was suggested that hepatic proprotein convertases inhibit EL partly by promoting the activating cleavage of ANGPTL3, thus raising HDL levels (23).

Transcriptional and post-transcriptional regulation of ANGPTL3

Like many secreted proteins, ANGPTL3 is susceptible to numerous post-translational modifications including cleavage and glycosylation. The cleavage site has been located to amino acid sequence [221]RAPR[224], yielding an N-terminal fragment containing the coiled-coil region and a C-terminal fragment containing the fibrinogen-like domain (18) (Figure 1). Cleavage of ANGPTL3 is catalyzed by proprotein convertases and was found to be required to achieve a maximum increase in plasma TG upon injection of ANGPTL3 in mice (18, 23). Recently, it was shown that proprotein convertase-induced ANGPTL3 cleavage is blocked by GalNAc-T2 mediated O-glycosylation of Thr[225/226] residues (24). Interestingly, variants in the GALNT2 gene are associated with increased TG levels in GWAS studies. Future research will have to reveal whether this effect might be due to altered GalNac-T2 mediated O-glycosylation of ANGPTL3 (3, 4, 7). In addition to undergoing cleavage, ANGPTL3 forms higher order multi-subunit complexes, which does not seem to require formation of intermolecular disulfide bonds (25). It can be speculated that formation of oligomers may protect ANGPTL3 from degradation and/or glomerular filtration.

Expression of ANGPTL3 in mouse and human is predominant in liver, with minor expression in kidney, and is governed by a variety of signals. The nuclear receptor LXR induces ANGPTL3 mRNA via a LXR response element located within the promoter of ANGPTL3, possibly accounting for the stimulatory effect of LXR agonists on plasma TG levels (Figure 1) (26, 27). In contrast, the nuclear receptor PPARβ/δ inhibits *Angptl3* mRNA expression, likely by dissociating the binding between of LXR and RXRα and thereby hampering activation of *Angptl3* by LXR (28). More recently, hepatic *ANGPTL3* mRNA was shown to be decreased upon treatment with atorvastatin, suggesting that ANGPTL3 may play a role in VLDL-TG lowering by statins when used at high doses (29). In addition, insulin, leptin, thyroid hormone and LPS suppress hepatic *Angptl3* expression (30-33).

ANGPTL4

Human genetic studies

Human genetic studies unequivocally support a role of *ANGPTL4* in plasma TG homeostasis. Evidence was first provided by re-sequencing seven exons and intron-exon

boundaries of *ANGPTL4* in a large number of individuals. One particular variant, which is carried by approximately 2% of Caucasians and causes a substitution of glutamine to lysine at position 40 (E40K) was associated with decreased plasma TG and increased plasma HDL-C concentrations (34, 35). The lower TG levels in E40K carriers compared to non-carriers persisted over a nine-year period during which TG concentrations went up in both groups (36).

Another ANGPTL4 gene variant, T266M, was also found to be associated with lower plasma TG. However, the effect disappeared once E40K carriers were removed from analysis, suggesting linkage disequilibrium between T266M and E40K (35). Others have been unable to replicate the association between T266M and plasma TG, possibly due to the low number of E40K carriers in their sample (37, 38). Recently, Smart-Halajko found that even after removal of E40K carriers from the analysis, T266M was associated with lower plasma TG levels in type 2 diabetic patients (39). In contrast, the same authors failed to find an association between T266M and plasma TG in a meta-analysis of 5 studies involving patients with cardiovascular disease (35). Interestingly, T266M raised plasma ANGPTL4 levels, possibly by influencing ANGPTL4 secretion (40). In summary, while the effect of the E40K variant on circulating TGs and HDL has been firmly established, the effect of T266M remains unclear and may depend on the specific population studied.

Surprisingly, none of the GWAS studies performed so far have linked SNPs in or near the ANGPTL4 gene to plasma TG levels. However, a significant association was found between rs2967605, which is located 30 kb downstream from *ANGPTL4*, and HDL-C levels. Why an association was found with HDL-C but not with TG is unclear and could be related to the more pronounced role of environmental factors in determining plasma TG compared to HDL-C. Alternatively, the rs2967605 SNP may mediate the effect of another gene located in proximity to *ANGPTL4* (5).

Whereas ANGPTL4 genotype clearly influences plasma TG, the relation between plasma levels of ANGPTL4 and plasma TG is less clear-cut. An early report found a positive correlation between the two parameters (41). However, more recent studies have not been able to replicate those initial findings (14, 40, 42, 43). Similar to ANGPTL3, the absence of a correlation between plasma ANGPTL4 and plasma TG does not necessarily invalidate ANGPTL4 as a determinant of plasma TG in humans yet does raise questions about: a) whether circulating ANGPTL4 represents the functional pool of protein involved in LPL inhibition, and b) what functional form of ANGPTL4 is in fact detected by the ELISA assay.

ANGPTL4 raises plasma triglycerides in mice

Studies with mice lacking or overexpressing *Angptl4* have clearly demonstrated the impact of ANGPTL4 on plasma TG metabolism. Mice deficient in *Angptl4* exhibit low plasma TG levels coinciding with elevated post-heparin plasma LPL activity, while whole body *Angptl4* transgenic mice show high TG levels together with low plasma LPL activity (44). Similar to whole body *Angptl4* overexpression, liver-specific *Angptl4* overexpression raises plasma TG levels and decreases post-heparin plasma LPL activity, suggesting an endocrine effect of liver-derived ANGPTL4 (16). Interestingly, cardiac specific *Angptl4* transgenic animals are characterized by elevated plasma TG together with decreased cardiac LPL activity yet do not exhibit any change in post-heparin plasma LPL activity or LPL activity in other tissues (45). Hence, ANGPTL4 produced in heart may primarily act locally to protect the heart from lipid overload and consequent lipotoxicity (46). It is unclear what accounts for the primary autocrine/paracrine versus endocrine function of ANGPTL4 in tissues.

The hypertriglyceridemic effect of ANGPTL4 is unequivocally attributable to its N-terminus as injecting mice with an monoclonal antibody directed against the N-terminal portion of ANGPTL4 lowers plasma TG to levels comparable to *Angptl4*$^{-/-}$ animals (47). In support of this notion, mice homozygous for the E40K mutation, which alters a critical residue towards the N-terminus of ANGPTL4, have low plasma TG levels (48).

Besides raising circulating TG levels, ANGPTL4 potently increases plasma free fatty acids. Injection of recombinant ANGPTL4 acutely raises free fatty acids (49). In addition, whole body *Angptl4* overexpression augments the fasting-induced increase in free fatty acids, whereas this response is completely blunted in *Angptl4*$^{-/-}$ mice (50). Studies in cultured adipocytes support a direct effect of ANGPTL4 on TG hydrolysis in adipocytes (50). How ANGPTL4 stimulates intracellular lipolysis is unknown but involvement of the adipose triglyceride lipase ATGL/PNPLA2 has been proposed (44).

ANGPTL4 is an endogenous inhibitor of lipoprotein lipase

Like all Angiopoietin-like proteins, ANGPTL4 is composed of several distinct regions including an N-terminus signal peptide, a coiled-coil domain and fibrinogen-like domain (Figure 1). Numerous studies have provided firm evidence that the N-terminal portion of ANGPTL4 irreversibly inhibits LPL activity, which is at least partially accounted for by promoting the conversion of active LPL dimers into inactive monomers (22, 51, 52). Inhibition of LPL by ANGPTL4 is suppressed by GPIHBP1 but not by heparin (19, 21). Besides inducing LPL dimer dissociation, ANGPTL4 may inhibit LPL by potentiating proprotein convertase-mediated cleavage of LPL (53). Similar to ANGPTL3, the LPL inhibitory effect of ANGPTL4 is largely conferred by the polar residues His46, Gln50,

and Gln53 located within the N-terminal coiled-coil domain (Figure 1). Consistent with this notion, injection of mice with a synthetic 12 amino acid peptide encompassing this particular region increased plasma TG levels by 164% compared to saline injected animals, although it was less potent compared to recombinant ANGPTL4 encompassing the entire N-terminus including the coiled-coil domain (22). ANGPTL4 effectively inhibits LPL produced by a variety of cells including (cardio)myocytes, adipocytes, and also macrophages. Recently, we demonstrated that macrophage ANGPTL4 is induced by fatty acids and inhibits LPL to reduce postprandial lipid uptake from chyle into macrophages present in mesenteric lymph nodes, thereby preventing macrophage activation and foam cell formation (54).

Post-transcriptional modifications of ANGPTL4

In analogy with ANGPTL3, ANGPTL4 is cleaved into an N-terminal (nANGPTL4) and a C-terminal (cANGPTL4) part, which occurs at the conserved proprotein convertase recognition sequence [161]RRKR[164] (53, 55-57). Whereas rat ANGPTL4 seems to require serum for in vitro cleavage, human ANGPTL4 can be cleaved in cultured cells in the absence of serum (57, 58). Recent work has found that proprotein convertases PCSK5, FURIN, and PCSK7 are able to cleave ANGPTL4 (53). Several studies have investigated whether cleavage of ANGPTL4 influences its ability to inhibit LPL. Conditioned medium from cells overexpressing the cleavage-resistant [161]GSGS[164] variant of ANGPTL4 markedly inhibited LPL activity, yet was less effective compared to wild-type ANGPTL4 conditioned medium. Surprisingly, adenoviral-mediated overexpression of the GSGS mutant in mice caused more pronounced hypertriglyceridemia compared to injection of wild-type ANGPTL4, possibly because of higher protein stability (57). In contrast, adenoviral-mediated overexpression of the cleavage-resistant mutant R161A resulted in less pronounced hypertriglyceridemia compared to wild-type ANGPTL4 overexpression, concurrent with less inhibition of LPL (53). Thus, the importance of ANGPTL4 cleavage for regulating LPL inhibition remains ambiguous. It should be emphasized that cANGPTL4 does not seem to play a role in lipid metabolism but rather regulates a variety of biological processes including angiogenesis, wound healing and tumor cell behavior by binding integrin β1 and β5 (59, 60).

In addition to cleavage, ANGPTL4 is subject to a second post-translational modification via oligomerization (Figure 1), which takes place intracellularly and is dependent on disulfide bond-forming cysteine residues 76 and 80 (56-58, 61). Since these residues are located in the N-terminal portion, nANGPTL4 and full length ANGPTL4 but not cANGPTL4 form oligomers (57). ANGPTL4 mutated at both residues is much less effective at raising plasma TG levels upon adenoviral-mediated overexpression, concurrent with a

marked reduction in nANGPTL4 and full length ANGPTL4 oligomers but also monomers. The latter result suggests that oligomerization protects ANGPTL4 from degradation and thereby maintains its LPL inhibitory capacity (57, 61). Consistent with this notion, detailed kinetic analysis of LPL inhibition indicated that purified ANGPTL4 mutated at cysteine 76 and 80 was equally effective at inhibiting LPL compared to wild-type ANGPTL4 (19). In contrast, disruption of disulfide mediated oligomerization by reducing agent was shown to reduce the capacity of ANGPTL4 to inhibit LPL independent of the absolute amount of ANGPTL4 protein (22). Thus, while it is clear that oligomerization is important for ANGPTL4 stabilisation to ensure an active pool of functional ANGPTL4 protein, it is unclear whether oligomerization is an actual prerequisite for effective LPL inhibition, for instance by creating the proper interface for LPL inhibition.

Another potential modification altering protein function is glycosylation. ANGPTL4 contains several potential N- and O-glycosylation sites (62), and was found to be N-glycosylated in the fibrinogen-like domain at position 177, potentiating its anti-angiogenic capacity (Figure 1) (55, 58). It is unclear whether glycosylation impacts the ability of ANGPTL4 to inhibit LPL. N-glycosylation at position 177 does not seem to affect cleavage of ANGPTL4 by proprotein convertases (53).

Regulation of *ANGPTL4* expression

ANGPTL4 is ubiquitously expressed in both mouse and human. Highest expression levels in humans are found in liver, followed by small intestine, adipose tissue, and heart, whereas mouse *Angptl4* mRNA is most highly expression in adipose tissue, followed by liver, intestine, heart, lung and ovary (9, 63-65).

In these tissues, *Angptl4* gene expression is regulated by many signals. ANGPTL4 was originally identified as a PPARα and -γ target gene in liver and adipose tissue, respectively (Figure 1) (64, 66). Although many studies have employed *Angptl4* as marker gene for PPARβ/δ activation (67-70), it should be emphasized that the main PPAR isotype involved in *Angptl4* regulation depends on the cell or tissue studied and can be either PPARα (liver, intestine), PPARβ/δ (skeletal muscle, heart, macrophages), or PPARγ (adipocytes, colonocytes). Regulation by PPAR is mediated by a composite PPAR-response element within intron 3 of the gene that consists of a number of adjacent direct repeat-1 elements (71-73). Recently, TGFβ was shown to either positively or negatively modulate PPARβ/δ-induced *ANGPTL4* regulation via interactions between additional transcription factor and the PPREs (73, 74). Consistent with fatty acids being potent activators of PPARs, *Angptl4* gene expression is strongly induced by free fatty acids in a variety of tissues (42, 46, 54, 63). In fact, microarray analysis has shown that *Angptl4* is the most highly induced gene upon

fatty acid stimulation in several cell types (our unpublished observations). Accordingly, plasma ANGPTL4 levels in human are increased by conditions associated with elevated free fatty acid levels, including fasting, prolonged caloric restriction, and exercise (63, 75). As a consequence, a positive correlation exists between fasting free fatty acids and ANGPTL4 levels (14, 42).

Interestingly, ANGPTL4 expression seems to be negatively regulated by insulin in cultured adipocytes and hepatocytes (76, 77). In agreement with these data, plasma ANGPTL4 levels were significantly reduced during a hyperinsulinemic clamp (77). Suppression of ANGPTL4 by insulin and induction by fasting may contribute to the switch in fuel utilization from lipoprotein derived fatty acids in the post-prandial state to free fatty acids in the fasting state. In addition to regulation by insulin, ANGPTL4 was found to be upregulated in hepatocytes and adipocytes by the glucocorticoid receptor via a binding site located at the 3'-untranslated region of *Angptl4*. Hence, ANGPTL4 may be a critical intermediate in the changes in triglyceride metabolism elicited by glucocorticoid treatment, including the hypertriglyceridemia in patients chronically treated with glucocorticoids (78). Similarly, ANGPTL4 may mediate the inhibitory effect of chronic intermittent hypoxia on clearance of TG-rich lipoproteins and adipose lipoprotein lipase activity (79).

Expression of ANGPTL4 in the small intestine is under control of the intestinal microbiota. Evidence was provided that the reduction in ANGPTL4 expression upon conventionalization of germ-free mice mediates the associated expansion of adipose tissue mass by stimulating adipose LPL activity (80). In contrast, it was also reported that absence of gut microbiota does not provide a general protection from diet-induced obesity and that intestinal ANGPTL4 does not contribute to the effects of gut microbiota on fat storage (81). Currently, it is difficult to reconcile these obviously divergent reports. Interestingly, the probiotic Lactobacillus *paracasei ssp paracasei* F19 was found to increase the expression of ANGPTL4 in colonocytes and produce a trend towards elevated plasma TG in mice colonized with F19, indicating that regulation of ANGPTL4 by intestinal microbiota is strain dependent (82).

ANGPTL5

Re-sequencing *ANGPTL5* in the Dallas Heart Study indicated a significant excess of non-synonymous sequence variations in the lower quartile of TG levels. One non-synonymous variant (T268M) in *ANGPTL5* had a mean allele frequency exceeding 1% but no consistent association was found between this variant and plasma TG levels (9). Interestingly, 3 out of 7 missense mutations in *ANGPTL5* found within the lower quartile of TG levels give rise to a protein that cannot be secreted into cell medium (9). Although these data may

hint at a potential role of ANGPTL5 in the regulation of TG metabolism, there has been no experimental follow up to explore these speculations. Specifically, the absence of a mouse ortholog makes it very difficult to perform functional studies in animals. In contrast to ANGPTL3, ANGPTL4, and ANGPTL6, ANGPTL5 is hardly expressed in liver yet is expressed in adipose tissue, heart, vena cava, epididymis, and bronchus (9). Unfortunately, no data are available regarding regulation of ANGPTL5.

ANGPTL6

Although multiple sequence variants of *ANGPTL6* were found by re-sequencing of a large multiethnic population, none of them associated with plasma TG levels. A significant excess of variants was found in the upper quartile of plasma total cholesterol levels, though this was not the case when specifically examining LDL-C or HDL-C (9). In a French population, no association was apparent between any of the four SNPs that cover most of the genetic variability within *ANGPTL6*, and plasma TG levels (83). Hence, human genetic studies do not support a role for *ANGPTL6* in regulation of plasma TG metabolism.

Serum ANGPTL6 levels did not correlate with TG levels in a Korean population while a positive correlation was found between ANGPTL6 levels and visceral fat, leptin, insulin, BMI and waist circumference (84). Moreover, ANGPTL6 levels were increased in diabetic patients compared to non-diabetic individuals (85).

Illustrating the importance of ANGPTL6 for basal development, more than 80% of *Angptl6*$^{-/-}$ mice die at about embryonic day 13 due to cardiovascular defects. Surviving *Angptl6*$^{-/-}$ mice develop obesity and increased hepatic TG content compared to wild-type littermates (86). Moreover, *Angptl6*$^{-/-}$ mice show increased serum cholesterol and free fatty acid levels, whereas serum TG levels are comparable to control animals (86). Overexpression of *Angptl6* generates a reverse phenotype characterized by lean and insulin sensitive animals showing decreased hepatic TG levels while serum TG levels are again comparable to wild-type animals (86). These effects are thought to be partially conveyed by a p38 MAPK/PGC-1α mediated increase in energy expenditure (87). Thus, there is currently no evidence linking ANGPTL6 to regulation of plasma TG metabolism and in contrast to ANGPTL3 and ANGPTL4, ANGPTL6 does not inhibit LPL (9). Whether the elevated serum cholesterol levels in *Angptl6*$^{-/-}$ mice reflect a direct effect of ANGPTL6 on lipoprotein metabolism requires further investigation.

Perspectives

A major insight that has become apparent in recent years is that regulation of lipases is complex and involves many cooperating proteins. While the existence of an endogenous LPL inhibitor had been predicted by the Olivecrona group, many aspects of the structure, function, and regulation of ANGPTL3 and ANGPTL4 have been surprising, most notable the functional divergence between the N- and C-terminal fragments. It is tempting to speculate about proteins that may interact with ANGPTLs, including GPIHBP1, possibly directing them to specific targets or conferring site-specific roles. Identification of cooperating proteins will be challenging yet could provide important insights into the functioning of lipases and ANGPTLs.

Cleavage of ANGPTLs has been considered a mechanism to create the functional endogenous lipase inhibitor. However, since full length ANGPTL3 and ANGPTL4 are able to inhibit lipases as well, the purpose of proteolytic processing of ANGPTLs remains somewhat ambiguous. It can be hypothesized that cleavage primarily serves to release the soluble monomeric C-terminal fragment, which otherwise would remain sequestered in a large multimeric complex of full length ANGPTL. Cleavage also enables separation between lipase inhibition and ANGPTL functions conferred by the C-terminal domain. The greatest mystery regarding ANGPTL3 and especially ANGPTL4 is why the proteins are so exceptionally regulated at the transcriptional level, given that the two cleavage fragments of ANGPTL3 and ANGPTL4 differ completely in their biological activities. Conceivably, proteolytic processing of ANGPTLs is cell-specific and yields different fragments depending on the expression of specific proprotein convertases. So far, there is no evidence of any regulation of ANGPTLs at the level of protein clearance and/or inactivation.

In conclusion, data gathered in the last decade have clearly demonstrated a key function of several ANGPTLs in regulation of plasma TG metabolism. Effects of ANGPTL3 and ANGPTL4 on circulating lipoproteins can be almost entirely explained by inhibition of lipases, principally LPL. However, this observation does not exclude potential effects of ANGPTLs on lipid metabolism via other mechanisms. Currently, there is no evidence that any of the other ANGPTLs besides ANGPTL3 and ANGPTL4 function as inhibitors of lipases. While human genetic studies have provided preliminary data potentially linking ANGPTL5 to regulation of plasma lipid levels, biochemical follow-up analyses have been lacking.

References

1. Tabata M, Kadomatsu T, Fukuhara S, Miyata K, Ito Y, Endo M, Urano T, Zhu HJ, Tsukano H, Tazume H, et al. Angiopoietin-like protein 2 promotes chronic adipose tissue inflammation and obesity-related systemic insulin resistance. *Cell Metab.* 2009;10(3):178-188.

2. Kitazawa M, Nagano M, Masumoto KH, Shigeyoshi Y, Natsume T, Hashimoto S. Angiopoietin-like 2, a circadian gene, improves type 2 diabetes through potentiation of insulin sensitivity in mice adipocytes. *Endocrinology.* 2011;152(7):2558-2567.

3. Willer CJ, Sanna S, Jackson AU, Scuteri A, Bonnycastle LL, Clarke R, Heath SC, Timpson NJ, Najjar SS, Stringham HM, et al. Newly identified loci that influence lipid concentrations and risk of coronary artery disease. *Nat Genet.* 2008;40(2):161-169.

4. Kathiresan S, Melander O, Guiducci C, Surti A, Burtt NP, Rieder MJ, Cooper GM, Roos C, Voight BF, Havulinna AS, et al. Six new loci associated with blood low-density lipoprotein cholesterol, high-density lipoprotein cholesterol or triglycerides in humans. *Nat Genet.* 2008;40(2):189-197.

5. Kathiresan S, Willer CJ, Peloso GM, Demissie S, Musunuru K, Schadt EE, Kaplan L, Bennett D, Li Y, Tanaka T, et al. Common variants at 30 loci contribute to polygenic dyslipidemia. *Nat Genet.* 2009;41(1):56-65.

6. Hegele RA, Ban MR, Hsueh N, Kennedy BA, Cao H, Zou GY, Anand S, Yusuf S, Huff MW, Wang J. A polygenic basis for four classical Fredrickson hyperlipoproteinemia phenotypes that are characterized by hypertriglyceridemia. *Hum Mol Genet.* 2009;18(21):4189-4194.

7. Teslovich TM, Musunuru K, Smith AV, Edmondson AC, Stylianou IM, Koseki M, Pirruccello JP, Ripatti S, Chasman DI, Willer CJ, et al. Biological, clinical and population relevance of 95 loci for blood lipids. *Nature.* 2010;466(7307):707-713.

8. Angelakopoulou A, Shah T, Sofat R, Shah S, Berry DJ, Cooper J, Palmen J, Tzoulaki I, Wong A, Jefferis BJ, et al. Comparative analysis of genome-wide association studies signals for lipids, diabetes, and coronary heart disease: Cardiovascular Biomarker Genetics Collaboration. *Eur Heart J.* 2012;33(3):393-407.

9. Romeo S, Yin W, Kozlitina J, Pennacchio LA, Boerwinkle E, Hobbs HH, Cohen JC. Rare loss-of-function mutations in ANGPTL family members contribute to plasma triglyceride levels in humans. *J Clin Invest.* 2009;119(1):70-79.

10. Musunuru K, Pirruccello JP, Do R, Peloso GM, Guiducci C, Sougnez C, Garimella KV, Fisher S, Abreu J, Barry AJ, et al. Exome sequencing, ANGPTL3 mutations, and familial combined hypolipidemia. *N Engl J Med.* 2010;363(23):2220-2227.

11. Hatsuda S, Shoji T, Shinohara K, Kimoto E, Mori K, Fukumoto S, Koyama H, Emoto M, Nishizawa Y. Association between plasma angiopoietin-like protein 3 and arterial wall thickness in healthy subjects. *J Vasc Res.* 2007;44(1):61-66.

12. Shimamura M, Matsuda M, Yasumo H, Okazaki M, Fujimoto K, Kono K, Shimizugawa T, Ando Y, Koishi R, Kohama T, et al. Angiopoietin-like protein3 regulates plasma HDL cholesterol through suppression of endothelial lipase. *Arterioscler Thromb Vasc Biol.* 2007;27(2):366-372.

13. Nakajima K, Kobayashi J, Mabuchi H, Nakano T, Tokita Y, Nagamine T, Imamura S, Ai M, Otokozawa S, Schaefer EF. Association of angiopoietin-like protein 3 with hepatic triglyceride lipase and lipoprotein lipase activities in human plasma. *Ann Clin Biochem.* 2010;47(Pt 5):423-431.

14. Robciuc MR, Tahvanainen E, Jauhiainen M, Ehnholm C. Quantitation of serum angiopoietin-like proteins 3 and 4 in a Finnish population sample. *J Lipid Res.* 2010;51(4):824-831.

15. Koishi R, Ando Y, Ono M, Shimamura M, Yasumo H, Fujiwara T, Horikoshi H, Furukawa H. Angptl3 regulates lipid metabolism in mice. *Nat Genet.* 2002;30(2):151-157.

2

16. Koster A, Chao YB, Mosior M, Ford A, Gonzalez-DeWhitt PA, Hale JE, Li D, Qiu Y, Fraser CC, Yang DD, et al. Transgenic angiopoietin-like (angptl)4 overexpression and targeted disruption of angptl4 and angptl3: regulation of triglyceride metabolism. *Endocrinology.* 2005;146(11):4943-4950.

17. Shimizugawa T, Ono M, Shimamura M, Yoshida K, Ando Y, Koishi R, Ueda K, Inaba T, Minekura H, Kohama T, et al. ANGPTL3 decreases very low density lipoprotein triglyceride clearance by inhibition of lipoprotein lipase. *J Biol Chem.* 2002;277(37):33742-33748.

18. Ono M, Shimizugawa T, Shimamura M, Yoshida K, Noji-Sakikawa C, Ando Y, Koishi R, Furukawa H. Protein region important for regulation of lipid metabolism in angiopoietin-like 3 (ANGPTL3): ANGPTL3 is cleaved and activated in vivo. *J Biol Chem.* 2003;278(43):41804-41809.

19. Shan L, Yu XC, Liu Z, Hu Y, Sturgis LT, Miranda ML, Liu Q. The angiopoietin-like proteins ANGPTL3 and ANGPTL4 inhibit lipoprotein lipase activity through distinct mechanisms. *J Biol Chem.* 2009;284(3):1419-1424.

20. Liu J, Afroza H, Rader DJ, Jin W. Angiopoietin-like protein 3 inhibits lipoprotein lipase activity through enhancing its cleavage by proprotein convertases. *J Biol Chem.* 2010;285(36):27561-27570.

21. Sonnenburg WK, Yu D, Lee EC, Xiong W, Gololobov G, Key B, Gay J, Wilganowski N, Hu Y, Zhao S, et al. GPIHBP1 stabilizes lipoprotein lipase and prevents its inhibition by angiopoietin-like 3 and angiopoietin-like 4. *J Lipid Res.* 2009;50(12):2421-2429.

22. Yau MH, Wang Y, Lam KS, Zhang J, Wu D, Xu A. A highly conserved motif within the NH2-terminal coiled-coil domain of angiopoietin-like protein 4 confers its inhibitory effects on lipoprotein lipase by disrupting the enzyme dimerization. *J Biol Chem.* 2009;284(18):11942-11952.

23. Jin W, Wang X, Millar JS, Quertermous T, Rothblat GH, Glick JM, Rader DJ. Hepatic proprotein convertases modulate HDL metabolism. *Cell Metab.* 2007;6(2):129-136.

24. Schjoldager KT, Vester-Christensen MB, Bennett EP, Levery SB, Schwientek T, Yin W, Blixt O, Clausen H. O-glycosylation modulates proprotein convertase activation of angiopoietin-like protein 3: possible role of polypeptide GalNAc-transferase-2 in regulation of concentrations of plasma lipids. *J Biol Chem.* 2010;285(47):36293-36303.

25. Ge H, Cha JY, Gopal H, Harp C, Yu X, Repa JJ, Li C. Differential regulation and properties of angiopoietin-like proteins 3 and 4. *J Lipid Res.* 2005;46(7):1484-1490.

26. Kaplan R, Zhang T, Hernandez M, Gan FX, Wright SD, Waters MG, Cai TQ. Regulation of the angiopoietin-like protein 3 gene by LXR. *J Lipid Res.* 2003;44(1):136-143.

27. Inaba T, Matsuda M, Shimamura M, Takei N, Terasaka N, Ando Y, Yasumo H, Koishi R, Makishima M, Shimomura I. Angiopoietin-like protein 3 mediates hypertriglyceridemia induced by the liver X receptor. *J Biol Chem.* 2003;278(24):21344-21351.

28. Matsusue K, Miyoshi A, Yamano S, Gonzalez FJ. Ligand-activated PPARbeta efficiently represses the induction of LXR-dependent promoter activity through competition with RXR. *Mol Cell Endocrinol.* 2006;256(1-2):23-33.

29. Pramfalk C, Parini P, Gustafsson U, Sahlin S, Eriksson M. Effects of high-dose statin on the human hepatic expression of genes involved in carbohydrate and triglyceride metabolism. *J Intern Med.* 2011;269(3):333-339.

30. Inukai K, Nakashima Y, Watanabe M, Kurihara S, Awata T, Katagiri H, Oka Y, Katayama S. ANGPTL3 is increased in both insulin-deficient and -resistant diabetic states. *Biochem Biophys Res Commun.* 2004;317(4):1075-1079.

31. Shimamura M, Matsuda M, Ando Y, Koishi R, Yasumo H, Furukawa H, Shimomura I. Leptin and insulin down-regulate angiopoietin-like protein 3, a plasma triglyceride-increasing factor. *Biochem Biophys Res Commun.* 2004;322(3):1080-1085.

32. Fugier C, Tousaint JJ, Prieur X, Plateroti M, Samarut J, Delerive P. The lipoprotein lipase inhibitor ANGPTL3 is negatively regulated by thyroid hormone. *J Biol Chem.* 2006;281(17):11553-11559.

33. Lu B, Moser A, Shigenaga JK, Grunfeld C, Feingold KR. The acute phase response stimulates the expression of angiopoietin like protein 4. *Biochem Biophys Res Commun.* 2010;391(4):1737-1741.

34. Romeo S, Pennacchio LA, Fu Y, Boerwinkle E, Tybjaerg-Hansen A, Hobbs HH, Cohen JC. Population-based resequencing of ANGPTL4 uncovers variations that reduce triglycerides and increase HDL. *Nat Genet.* 2007;39(4):513-516.

35. Talmud PJ, Smart M, Presswood E, Cooper JA, Nicaud V, Drenos F, Palmen J, Marmot MG, Boekholdt SM, Wareham NJ, et al. ANGPTL4 E40K and T266M: effects on plasma triglyceride and HDL levels, postprandial responses, and CHD risk. *Arterioscler Thromb Vasc Biol.* 2008;28(12):2319-2325.

36. Nettleton JA, Volcik KA, Demerath EW, Boerwinkle E, Folsom AR. Longitudinal changes in triglycerides according to ANGPTL4[E40K] genotype and longitudinal body weight change in the atherosclerosis risk in communities study. *Ann Epidemiol.* 2008;18(11):842-846.

37. Staiger H, Machicao F, Werner R, Guirguis A, Weisser M, Stefan N, Fritsche A, Haring HU. Genetic variation within the ANGPTL4 gene is not associated with metabolic traits in white subjects at an increased risk for type 2 diabetes mellitus. *Metabolism.* 2008;57(5):637-643.

38. Legry V, Bokor S, Cottel D, Beghin L, Catasta G, Nagy E, Gonzalez-Gross M, Spinneker A, Stehle P, Molnar D, et al. Associations between common genetic polymorphisms in angiopoietin-like proteins 3 and 4 and lipid metabolism and adiposity in European adolescents and adults. *J Clin Endocrinol Metab.* 2009;94(12):5070-5077.

39. Smart-Halajko MC, Kelley-Hedgepeth A, Montefusco MC, Cooper JA, Kopin A, McCaffrey JM, Balasubramanyam A, Pownall HJ, Nathan DM, Peter I, et al. ANGPTL4 variants E40K and T266M are associated with lower fasting triglyceride levels in Non-Hispanic White Americans from the Look AHEAD Clinical Trial. *BMC Med Genet.* 2011;12(1):89.

40. Smart-Halajko MC, Robciuc MR, Cooper JA, Jauhiainen M, Kumari M, Kivimaki M, Khaw KT, Boekholdt SM, Wareham NJ, Gaunt TR, et al. The relationship between plasma angiopoietin-like protein 4 levels, angiopoietin-like protein 4 genotype, and coronary heart disease risk. *Arterioscler Thromb Vasc Biol.* 2010;30(11):2277-2282.

41. Stejskal D, Karpisek M, Reutova H, Humenanska V, Petzel M, Kusnierova P, Vareka I, Varekova R, Stejskal P. Angiopoietin-like protein 4: development, analytical characterization, and clinical testing of a new ELISA. *Gen Physiol Biophys.* 2008;27(1):59-63.

42. Staiger H, Haas C, Machann J, Werner R, Weisser M, Schick F, Machicao F, Stefan N, Fritsche A, Haring HU. Muscle-derived angiopoietin-like protein 4 is induced by fatty acids via peroxisome proliferator-activated receptor (PPAR)-delta and is of metabolic relevance in humans. *Diabetes.* 2009;58(3):579-589.

43. Robciuc MR, Naukkarinen J, Ortega-Alonso A, Tyynismaa H, Raivio T, Rissanen A, Kaprio J, Ehnholm C, Jauhiainen M, Pietilainen KH. Serum angiopoietin-like 4 protein levels and expression in adipose tissue are inversely correlated with obesity in monozygotic twins. *J Lipid Res.* 2011;52(8):1575-1582.

44. Mandard S, Zandbergen F, van Straten E, Wahli W, Kuipers F, Muller M, Kersten S. The fasting-induced adipose factor/angiopoietin-like protein 4 is physically associated with lipoproteins and governs plasma lipid levels and adiposity. *J Biol Chem.* 2006;281(2):934-944.

45. Yu X, Burgess SC, Ge H, Wong KK, Nassem RH, Garry DJ, Sherry AD, Malloy CR, Berger JP, Li C. Inhibition of cardiac lipoprotein utilization by transgenic overexpression of Angptl4 in the heart. *Proc Natl Acad Sci U S A.* 2005;102(5):1767-1772.

2

46.   Georgiadi A, Lichtenstein L, Degenhardt T, Boekschoten MV, van Bilsen M, Desvergne B, Muller M, Kersten S. Induction of cardiac Angptl4 by dietary fatty acids is mediated by peroxisome proliferator-activated receptor beta/delta and protects against fatty acid-induced oxidative stress. *Circ Res.* 2010;106(11):1712-1721.

47.   Desai U, Lee EC, Chung K, Gao C, Gay J, Key B, Hansen G, Machajewski D, Platt KA, Sands AT, et al. Lipid-lowering effects of anti-angiopoietin-like 4 antibody recapitulate the lipid phenotype found in angiopoietin-like 4 knockout mice. *Proc Natl Acad Sci U S A.* 2007;104(28):11766-11771.

48.   Lee EC, Desai U, Gololobov G, Hong S, Feng X, Yu XC, Gay J, Wilganowski N, Gao C, Du LL, et al. Identification of a new functional domain in angiopoietin-like 3 (ANGPTL3) and angiopoietin-like 4 (ANGPTL4) involved in binding and inhibition of lipoprotein lipase (LPL). *J Biol Chem.* 2009;284(20):13735-13745.

49.   Yoshida K, Shimizugawa T, Ono M, Furukawa H. Angiopoietin-like protein 4 is a potent hyperlipidemia-inducing factor in mice and inhibitor of lipoprotein lipase. *J Lipid Res.* 2002;43(11):1770-1772.

50.   Sanderson LM, Degenhardt T, Koppen A, Kalkhoven E, Desvergne B, Muller M, Kersten S. Peroxisome proliferator-activated receptor beta/delta (PPARbeta/delta) but not PPARalpha serves as a plasma free fatty acid sensor in liver. *Mol Cell Biol.* 2009;29(23):6257-6267.

51.   Lichtenstein L, Berbee JF, van Dijk SJ, van Dijk KW, Bensadoun A, Kema IP, Voshol PJ, Muller M, Rensen PC, Kersten S. Angptl4 upregulates cholesterol synthesis in liver via inhibition of LPL- and HL-dependent hepatic cholesterol uptake. *Arterioscler Thromb Vasc Biol.* 2007;27(11):2420-2427.

52.   Sukonina V, Lookene A, Olivecrona T, Olivecrona G. Angiopoietin-like protein 4 converts lipoprotein lipase to inactive monomers and modulates lipase activity in adipose tissue. *Proc Natl Acad Sci U S A.* 2006;103(46):17450-17455.

53.   Lei X, Shi F, Basu D, Huq A, Routhier S, Day R, Jin W. Proteolytic processing of angiopoietin-like protein 4 by proprotein convertases modulates its inhibitory effects on lipoprotein lipase activity. *J Biol Chem.* 2011;286(18):15747-15756.

54.   Lichtenstein L, Mattijssen F, de Wit NJ, Georgiadi A, Hooiveld GJ, van der Meer R, He Y, Qi L, Koster A, Tamsma JT, et al. Angptl4 protects against severe proinflammatory effects of saturated fat by inhibiting fatty acid uptake into mesenteric lymph node macrophages. *Cell Metab.* 2010;12(6):580-592.

55.   Yang YH, Wang Y, Lam KS, Yau MH, Cheng KK, Zhang J, Zhu W, Wu D, Xu A. Suppression of the Raf/MEK/ERK signaling cascade and inhibition of angiogenesis by the carboxyl terminus of angiopoietin-like protein 4. *Arterioscler Thromb Vasc Biol.* 2008;28(5):835-840.

56.   Chomel C, Cazes A, Faye C, Bignon M, Gomez E, Ardidie-Robouant C, Barret A, Ricard-Blum S, Muller L, Germain S, et al. Interaction of the coiled-coil domain with glycosaminoglycans protects angiopoietin-like 4 from proteolysis and regulates its antiangiogenic activity. *Faseb J.* 2009;23(3):940-949.

57.   Yin W, Romeo S, Chang S, Grishin NV, Hobbs HH, Cohen JC. Genetic variation in ANGPTL4 provides insights into protein processing and function. *J Biol Chem.* 2009;284(19):13213-13222.

58.   Ge H, Yang G, Huang L, Motola DL, Pourbahrami T, Li C. Oligomerization and regulated proteolytic processing of angiopoietin-like protein 4. *J Biol Chem.* 2004;279(3):2038-2045.

59.   Goh YY, Pal M, Chong HC, Zhu P, Tan MJ, Punugu L, Lam CR, Yau YH, Tan CK, Huang RL, et al. Angiopoietin-like 4 interacts with integrins beta1 and beta5 to modulate keratinocyte migration. *Am J Pathol.* 2010;177(6):2791-2803.

60.   Goh YY, Pal M, Chong HC, Zhu P, Tan MJ, Punugu L, Tan CK, Huang RL, Sze SK, Tang MB, et al. Angiopoietin-like 4 interacts with matrix proteins to modulate wound healing. *J Biol Chem.* 2010;285(43):32999-33009.

61. Ge H, Yang G, Yu X, Pourbahrami T, Li C. Oligomerization state-dependent hyperlipidemic effect of angiopoietin-like protein 4. *J Lipid Res.* 2004;45(11):2071-2079.

62. Clement LC, Avila-Casado C, Mace C, Soria E, Bakker WW, Kersten S, Chugh SS. Podocyte-secreted angiopoietin-like-4 mediates proteinuria in glucocorticoid-sensitive nephrotic syndrome. *Nat Med.* 2011;17(1):117-122.

63. Kersten S, Lichtenstein L, Steenbergen E, Mudde K, Hendriks HF, Hesselink MK, Schrauwen P, Muller M. Caloric restriction and exercise increase plasma ANGPTL4 levels in humans via elevated free fatty acids. *Arterioscler Thromb Vasc Biol.* 2009;29(6):969-974.

64. Kersten S, Mandard S, Tan NS, Escher P, Metzger D, Chambon P, Gonzalez FJ, Desvergne B, Wahli W. Characterization of the fasting-induced adipose factor FIAF, a novel peroxisome proliferator-activated receptor target gene. *J Biol Chem.* 2000;275(37):28488-28493.

65. Zandbergen F, van Dijk S, Muller M, Kersten S. Fasting-induced adipose factor/angiopoietin-like protein 4: a potential target for dyslipidemia? *Future Lipidol.* 2006;1(2):227-236.

66. Yoon JC, Chickering TW, Rosen ED, Dussault B, Qin Y, Soukas A, Friedman JM, Holmes WE, Spiegelman BM. Peroxisome proliferator-activated receptor gamma target gene encoding a novel angiopoietin-related protein associated with adipose differentiation. *Mol Cell Biol.* 2000;20(14):5343-5349.

67. Schug TT, Berry DC, Shaw NS, Travis SN, Noy N. Opposing effects of retinoic acid on cell growth result from alternate activation of two different nuclear receptors. *Cell.* 2007;129(4):723-733.

68. Rieck M, Meissner W, Ries S, Muller-Brusselbach S, Muller R. Ligand-mediated regulation of peroxisome proliferator-activated receptor (PPAR) beta/delta: a comparative analysis of PPAR-selective agonists and all-trans retinoic acid. *Mol Pharmacol.* 2008;74(5):1269-1277.

69. Naruhn S, Meissner W, Adhikary T, Kaddatz K, Klein T, Watzer B, Muller-Brusselbach S, Muller R. 15-hydroxyeicosatetraenoic acid is a preferential peroxisome proliferator-activated receptor beta/delta agonist. *Mol Pharmacol.* 2010;77(2):171-184.

70. Palkar PS, Borland MG, Naruhn S, Ferry CH, Lee C, Sk UH, Sharma AK, Amin S, Murray IA, Anderson CR, et al. Cellular and pharmacological selectivity of the peroxisome proliferator-activated receptor-beta/delta antagonist GSK3787. *Mol Pharmacol.* 2010;78(3):419-430.

71. Mandard S, Zandbergen F, Tan NS, Escher P, Patsouris D, Koenig W, Kleemann R, Bakker A, Veenman F, Wahli W, et al. The direct peroxisome proliferator-activated receptor target fasting-induced adipose factor (FIAF/PGAR/ANGPTL4) is present in blood plasma as a truncated protein that is increased by fenofibrate treatment. *J Biol Chem.* 2004;279(33):34411-34420.

72. Heinaniemi M, Uski JO, Degenhardt T, Carlberg C. Meta-analysis of primary target genes of peroxisome proliferator-activated receptors. *Genome Biol.* 2007;8(7):R147.

73. Kaddatz K, Adhikary T, Finkernagel F, Meissner W, Muller-Brusselbach S, Muller R. Transcriptional profiling identifies functional interactions of TGF beta and PPAR beta/delta signaling: synergistic induction of ANGPTL4 transcription. *J Biol Chem.* 2010;285(38):29469-29479.

74. Stockert J, Adhikary T, Kaddatz K, Finkernagel F, Meissner W, Muller-Brusselbach S, Muller R. Reverse crosstalk of TGFbeta and PPARbeta/delta signaling identified by transcriptional profiling. *Nucleic Acids Res.* 2011;39(1):119-131.

75. Jonker JT, Smit JW, Hammer S, Snel M, van der Meer RW, Lamb HJ, Mattijssen F, Mudde K, Jazet IM, Dekkers OM, et al. Dietary modulation of plasma angiopoietin-like protein 4 concentrations in healthy volunteers and in patients with type 2 diabetes. *Am J Clin Nutr.* 2013;97(2):255-260.

76. Yamada T, Ozaki N, Kato Y, Miura Y, Oiso Y. Insulin downregulates angiopoietin-like protein 4 mRNA in 3T3-L1 adipocytes. *Biochem Biophys Res Commun.* 2006;347(4):1138-1144.

2

77. van Raalte DH, Brands M, Serlie MJ, Mudde K, Stienstra R, Sauerwein HP, Kersten S, Diamant M. Angiopoietin-like protein 4 is differentially regulated by glucocorticoids and insulin in vitro and in vivo in healthy humans. *Exp Clin Endocrinol Diabetes.* 2012;120(10):598-603.

78. Koliwad SK, Kuo T, Shipp LE, Gray NE, Backhed F, So AY, Farese RV, Jr., Wang JC. Angiopoietin-like 4 (ANGPTL4, fasting-induced adipose factor) is a direct glucocorticoid receptor target and participates in glucocorticoid-regulated triglyceride metabolism. *J Biol Chem.* 2009;284(38):25593-25601.

79. Drager LF, Li J, Shin MK, Reinke C, Aggarwal NR, Jun JC, Bevans-Fonti S, Sztalryd C, O'Byrne SM, Kroupa O, et al. Intermittent hypoxia inhibits clearance of triglyceride-rich lipoproteins and inactivates adipose lipoprotein lipase in a mouse model of sleep apnoea. *Eur Heart J.* 2011;33(6):783-90.

80. Backhed F, Manchester JK, Semenkovich CF, Gordon JI. Mechanisms underlying the resistance to diet-induced obesity in germ-free mice. *Proc Natl Acad Sci U S A.* 2007;104(3):979-984.

81. Fleissner CK, Huebel N, Abd El-Bary MM, Loh G, Klaus S, Blaut M. Absence of intestinal microbiota does not protect mice from diet-induced obesity. *Br J Nutr.* 2010;104(6):919-929.

82. Aronsson L, Huang Y, Parini P, Korach-Andre M, Hakansson J, Gustafsson JA, Pettersson S, Arulampalam V, Rafter J. Decreased fat storage by Lactobacillus paracasei is associated with increased levels of angiopoietin-like 4 protein (ANGPTL4). *PLoS One.* 2010;5(9).

83. Legry V, Goumidi L, Huyvaert M, Cottel D, Ferrieres J, Arveiler D, Bingham A, Wagner A, Ruidavets JB, Ducimetiere P, et al. Association between angiopoietin-like 6 (ANGPTL6) gene polymorphisms and metabolic syndrome-related phenotypes in the French MONICA Study. *Diabetes Metab.* 2009;35(4):287-292.

84. Namkung J, Koh SB, Kong ID, Choi JW, Yeh BI. Serum levels of angiopoietin-related growth factor are increased in metabolic syndrome. *Metabolism.* 2011;60(4):564-568.

85. Ebert T, Bachmann A, Lossner U, Kratzsch J, Bluher M, Stumvoll M, Fasshauer M. Serum levels of angiopoietin-related growth factor in diabetes mellitus and chronic hemodialysis. *Metabolism.* 2009;58(4):547-551.

86. Oike Y, Akao M, Yasunaga K, Yamauchi T, Morisada T, Ito Y, Urano T, Kimura Y, Kubota Y, Maekawa H, et al. Angiopoietin-related growth factor antagonizes obesity and insulin resistance. *Nat Med.* 2005;11(4):400-408.

87. Oike Y, Akao M, Kubota Y, Suda T. Angiopoietin-like proteins: potential new targets for metabolic syndrome therapy. *Trends Mol Med.* 2005;11(10):473-479.

2

3

ANGPTL4 protects against severe proinflammatory effects of saturated fat by inhibiting fatty acid uptake into mesenteric lymph node macrophages

L Lichtenstein*, F Mattijssen*, NJ de Wit*,
A Georgiadi, GJ Hooiveld, R van der Meer, Y He, L Qi,
A Köster, JT Tamsma, NS Tan, M Müller, S Kersten

*Equal contribution

Abstract

Dietary saturated fat is linked to numerous chronic diseases, including cardiovascular disease. Here we study the role of the lipoprotein lipase inhibitor ANGPTL4 in the response to dietary saturated fat. Strikingly, in mice lacking *Angptl4*, saturated fat induces a severe and lethal phenotype characterized by fibrinopurulent peritonitis, ascites, intestinal fibrosis, and cachexia. These abnormalities are preceded by a massive acute phase response induced by saturated but not unsaturated fat or medium-chain fat, originating in mesenteric lymph nodes (MLNs). MLNs undergo dramatic expansion and contain numerous lipid-laden macrophages. In peritoneal macrophages incubated with chyle, ANGPTL4 dramatically reduced foam cell formation, inflammatory gene expression, and chyle-induced activation of ER stress. Induction of macrophage ANGPTL4 by fatty acids is part of a mechanism that serves to reduce postprandial lipid uptake from chyle into MLN-resident macrophages by inhibiting triglyceride hydrolysis, thereby preventing macrophage activation and foam cell formation and protecting against progressive, uncontrolled saturated fat-induced inflammation.

Introduction

Studies indicate that elevated saturated fat consumption is associated with increased risk for chronic diseases, including cardiovascular disease and type 2 diabetes. However, the underlying mechanisms and why specifically saturated fat is harmful largely remain unknown. Consequently, there is a need to better understand the molecular mechanisms that govern the response to dietary (saturated) fat ingestion.

After digestion of dietary fat, absorbed long-chain fatty acids are incorporated into chylomicrons as triglycerides (TGs) and released into the circulation after passage through the intestinal lymphatics. Hydrolysis of chylomicron-TG is catalyzed by the enzyme lipoprotein lipase (LPL), which is anchored to the capillary endothelium via heparin–sulphate proteoglycans and is a key determinant of cellular fatty acid uptake (1). LPL is expressed at high levels in tissues that depend on fatty acids as fuel (heart, skeletal muscle), or synthesize fats for storage or secretion (adipose tissue, mammary tissue), but high expression is also found in macrophages (2, 3).

Activity of LPL is governed via numerous mechanisms that act primarily at the posttranscriptional and posttranslational level. One important modulator of LPL activity is Angiopoietin-like protein 4 (ANGPTL4) (4). ANGPTL4 was discovered as transcriptional target of the peroxisome proliferator activated receptor alpha and gamma and is expressed in numerous cell types including adipocytes, hepatocytes, (cardio)myocytes and endothelial cells (5, 6). Studies using different transgenic mouse models of ANGPTL4 overexpression or deletion show that ANGPTL4 potently raises plasma TG levels by suppressing LPL-mediated clearance of plasma TG-rich lipoproteins (7-9).

Recently, it was shown that deletion of other members of the Angiopoietin-like protein family influences the development of obesity-related complications in the C57Bl/6 mouse high fat-induced obesity model. Specifically, surviving *Angptl6$^{-/-}$* mice developed marked obesity, ectopic fat storage and insulin resistance. In contrast, mice over-expressing *Angptl6* were leaner and had improved insulin sensitivity (10). Deletion of *Angptl2* ameliorated adipose tissue inflammation and insulin resistance in obese mice, whereas *Angptl2* over-expression promoted adipose tissue inflammation and systemic insulin resistance (11). Given the role of ANGPTL4 in plasma clearance of dietary TGs, we set out to study the effect of ANGPTL4 deletion in the context of chronically elevated dietary fat intake.

3

Results

Angptl4⁻/⁻ mice fed HFD develop fibrinopurulent peritonitis and ascites

To examine the effect of ANGPTL4 on diet-induced obesity and its metabolic consequences, wild-type and *Angptl4⁻/⁻* mice were fed a high fat diet (HFD) containing saturated fat-rich palm oil and compared with mice fed low fat diet (LFD) (Table S1). As expected based on its ability to inhibit LPL, *Angptl4⁻/⁻* mice had decreased plasma TGs (Figure 1A) and showed faster initial weight gain (Figure 1B) (12). Remarkably, bodyweights of *Angptl4⁻/⁻* mice fed HFD reached a plateau after around 12 weeks and declined thereafter (Figure 1B). The decrease in bodyweight was related to anorexia noticeable after about 10 weeks of HFD (Figure 1C). All *Angptl4⁻/⁻* mice fed HFD ultimately die anywhere between 15 and 25 weeks. The cause of death was identified by an animal pathologist as severe fibrinopurulent peritonitis connected with ascites.

Large amounts of fibrin exudate covered the abdominal organs in *Angptl4⁻/⁻* mice fed HFD (Figure 1D). Other macroscopic abnormalities included intestinal fibrosis (Figure 1E), a compressed liver (Supplemental Figure 1A), and a hyperplasic spleen (data not shown). No such abnormalities were observed in *Angptl4⁻/⁻* mice fed LFD, even at high age (>1.5 years). Routine clinical tests were performed on the ascites fluid, which varied in color from purulent white to purulent red (Figure 1D, inset). Ascites white blood cell count was extremely high in all animals (25.5-34.1*109/l, diagnostic threshold: ≤0.5*109/l), as was the endotoxin concentration (50-120 EU/ml, zero threshold), strongly suggesting bacterial peritonitis. Ascites fluid of some animals tested positive for E. Coli. The high protein concentration (3.43-4.28 g/dl, diagnostic threshold: >2.5 g/dl) and low serum-ascites albumin gradient (SAAG, 0.11-0.34 g/dl, diagnostic threshold: <1.1 g/dl) indicated exudative ascites, thereby excluding portal hypertension. The ascites TG concentration was highly variable but clearly elevated (4.8-75.5 mM, diagnostic threshold: ~1.25 mM). Analysis of chylous ascites fluid by lipoprotein profiling indicated an abundance of TG-rich


Figure 1. *Angptl4⁻/⁻* mice chronically fed HFD develop fibrinopurulent peritonitis and ascites
(A) Four-hour fasting plasma TG levels during the course of chronic LFD or HFD intervention (Study 1). Differences between LFD and HFD within each genotype were not statistically significant (n = 10 per group).
(B) Bodyweight changes in wild-type and *Angptl4⁻/⁻* mice fed LFD or HFD for 19 weeks.
(C) Mean daily food intake in wild-type and *Angptl4⁻/⁻* mice fed LFD or HFD for 19 weeks.
(D) Whole animal photographs taken immediately following sacrifice of representative wild-type and *Angptl4⁻/⁻* mice fed either LFD or HFD for 19 weeks. Pictures at far right were taken after removal of peritoneum. Ascites fluid collected from two *Angptl4⁻/⁻* mice fed HFD is shown at the bottom.
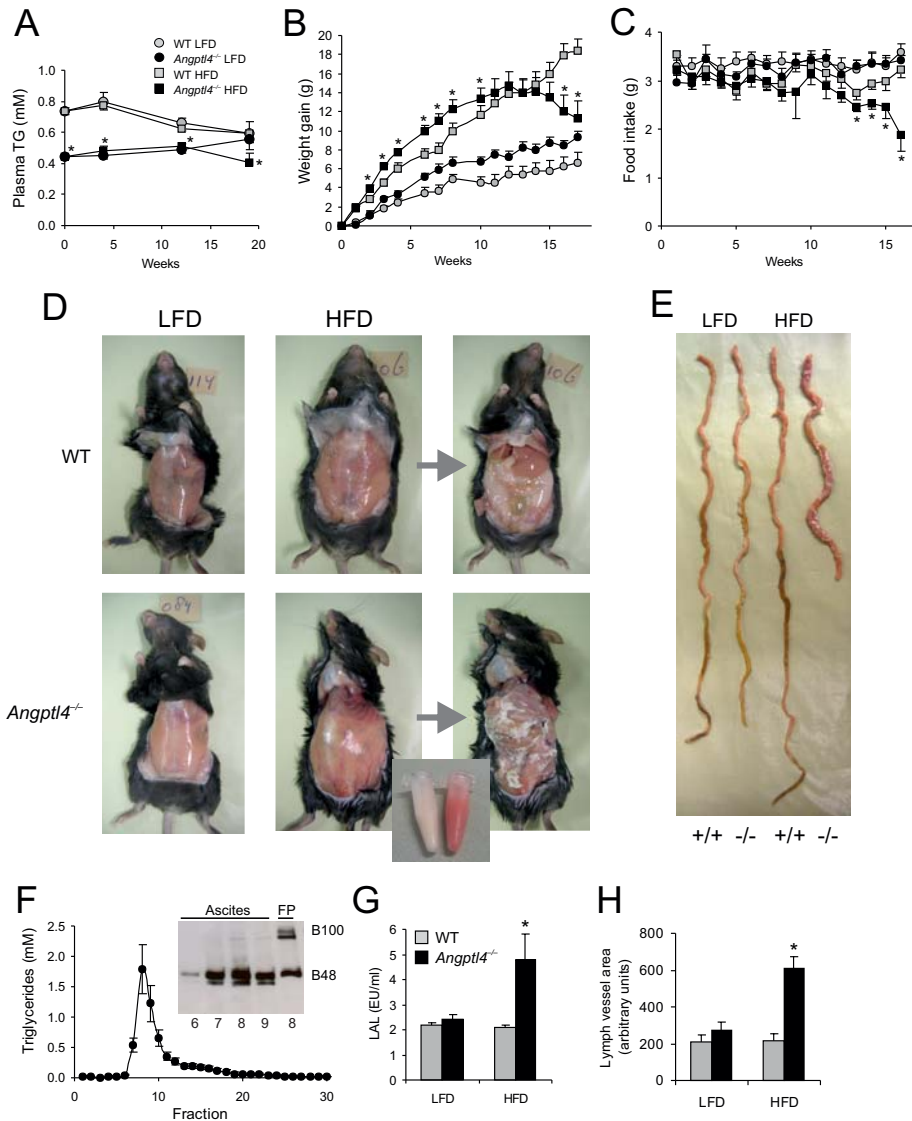
(E) Photograph of small intestine of wild-type and *Angptl4**⁻/⁻* mouse fed LFD or HFD for 19 weeks.

(F) FLPC lipoprotein profiling of ascites fluid of *Angptl4⁻/⁻* mice fed HFD for 19 weeks (n = 5). Inset: APOB immunoblot of FPLC fractions from ascites fluid of *Angptl4⁻/⁻* mice or mouse fasting plasma (FP).

(G) Plasma endotoxin levels in wild-type and *Angptl4⁻/⁻* mice fed LFD or HFD for 19 weeks.

(H) Lymph vessel area in jejunum of wild-type and *Angptl4⁻/⁻* mice fed LFD or HFD for 19 weeks determined after Lyve-1 staining.

Error bars represent SEM. * indicates significantly different from corresponding wild-type mice according to Student's *t*-test (*P* < 0.05).

lipoproteins representing chylomicrons, as shown by immunostaining for APOB (Figure 1F), suggesting leakage of chyle from lymphatic vessels. Additionally, significant vascular leakage occurred, as shown by the much lower protein concentration in chyle (1.38-1.83 g/dl) compared to ascites fluid (3.43-4.28 g/dl).

Plasma endotoxin levels were significantly elevated in *Angptl4*$^{-/-}$ mice fed HFD for 19 weeks (Figure 1G). Microscopic examination indicated that the fibrin exudate contained an abundance of foam cells, polynuclear giant cells, and other leukocytes (data not shown). The same cells as well as focal lymphocyte infiltrates were observed in the small intestine (Figure 2A, inset) and mesenteric fat (Figure 2B), in the former encapsulated by collagen (Figure 2C). Intestinal lymph vessels were dilated, suggesting mesenteric lymphatic obstruction (Figure 1H). Epididymal adipose tissue had a red appearance (Supplemental Figure 1C), and exhibited coagulation necrosis and steatitis as shown by presence of lymphocytes, granulocytes and other leukocytes (Supplemental Figure 1D, inset).

Livers of *Angptl4*$^{-/-}$ mice fed HFD for 19 weeks were not fibrotic but resembled an ischemic liver. Portal triads, cords and sinusoids were poorly visible, and clumping of nuclei was seen, indicating collapse of liver (Supplemental Figures 1A and 1B). Focal infiltrates of neutrophils, eosinophils and macrophages were observed (Supplemental Figure 1B, inset), as were rod-shaped bacteria. Liver fat was almost absent, whereas it was elevated in *Angptl4*$^{-/-}$ mice on LFD (Supplemental Figure 1E). Weights of liver and epididymal fat pads were significantly lower in *Angptl4*$^{-/-}$ mice after 19 weeks of HFD (Supplemental Figures 1F and 1G), while epididymal fat pads were heavier in *Angptl4*$^{-/-}$ mice on the LFD. Taken together, *Angptl4*$^{-/-}$ mice chronically fed HFD develop a severe phenotype characterized by anorexia, cachexia, intestinal inflammation and fibrosis, chylous ascites, and fibrinopurulent peritonitis, leading to the death of the animal.

Ascites and other clinical abnormalities are not related to a primary lymph vessel defect

Angptl4$^{-/-}$ mice on a mixed genetic background were reported to die shortly after birth due to defective separation of intestinal lymphatic and blood microvasculature (13). Although we did not find these abnormalities in *Angptl4*$^{-/-}$ mice on pure C57Bl/6 background and adult mice in proper Mendelian ratios were obtained, there might be an underlying primary weakness in intestinal lymphatics that becomes manifest when chyle flow is increased as with HFD, causing leakage of chyle into intestinal lumen and peritoneal cavity. However, none of the clinical abnormalities including chylous ascites were observed in *Angptl4*$^{-/-}$ mice fed a safflower oil-based HFD rich in polyunsaturated fat (Table S2) (data not shown). Furthermore, if lymphatic vessels are intrinsically more permeable,

ascites and diarrhea, the latter due to loss of protein and fat from lymph into the intestinal lumen, should develop upon starting the HFD, which was not observed. Surprisingly, fecal fat excretion was markedly decreased in *Angptl4*⁻/⁻ mice, indicating more efficient fat absorption (Supplemental Figure 2A). An acute intestinal lipid absorption test using
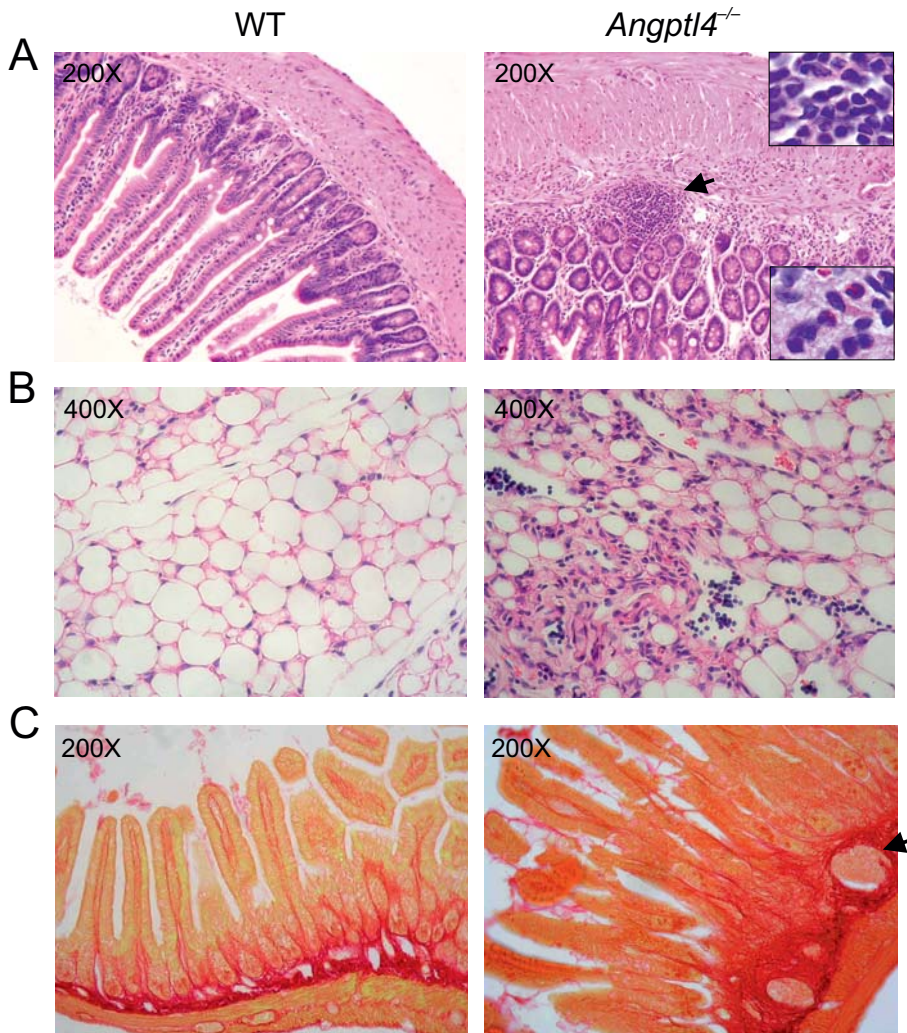

Figure 2. Severe intestinal inflammation in *Angptl4*⁻/⁻ mice chronically fed HFD

(A and B) Representative H&E staining of small intestine (A) or mesenteric fat (B) of wild-type and *Angptl4*⁻/⁻ mice fed HFD for 19 weeks (Study 1). Inset: high magnification image of lymphocyte infiltrate (top) or presence of granulocytes (bottom).

(C) Sirius red staining of small intestine of wild-type and *Angptl4*⁻/⁻ mice fed HFD for 19 weeks. Arrow indicates inflammatory infiltrate.

[3]H-triolein and ^{14}C-palmitic acid failed to show any differences in rate of appearance of either label in blood between wild-type and *Angptl4^{−/−}* mice (Supplemental Figures 2B and 2C), suggesting chylomicron formation and release is similar between wild-type and *Angptl4^{−/−}* mice. In contrast, in all intestinal parts, accumulation of both labels 5 hours after lipid load was markedly higher in *Angptl4^{−/−}* mice (Supplemental Figures 2D and 2E). The similarity in results between ^{3}H-triolein and ^{14}C-palmitic acid argue against an effect of ANGPTL4 inactivation on TG digestion but suggest enhanced fatty acid uptake into enterocytes. This is supported by elevated expression of target genes of PPARα in small intestine of *Angptl4^{−/−}* mice, suggesting enhanced gene regulation by fatty acids (Supplemental Figures 2F and 2G). Overall, the data argue against a primary lymph vessel defect forming the basis for the severe pathology.

A massive acute phase response precedes ascites in Angptl4^{−/−} mice fed HFD

To investigate the cause of the severe pathology, wild-type and *Angptl4^{−/−}* mice were studied before onset of anorexia and cachexia at 8 weeks of HFD (Figures 1A and 1B), and before ascites or other macroscopic abnormalities were observed. Strikingly, after 8 weeks of HFD, plasma levels of serum amyloid A (SAA) and other inflammatory markers were dramatically increased in *Angptl4^{−/−}* mice (Figures 3A and 3B). Whereas IL-6 was undetectable in plasma of wild-type mice, levels averaged 63±26 pg/ml in *Angptl4^{−/−}* mice (normal values <15 pg/ml). These changes were paralleled by massive induction of hepatic mRNA for SAA2 and other acute phase proteins haptoglobin and lipocalin 2 (Figure 3C). Furthermore, increased expression of macrophage/Kupffer cell marker *Cd68* (Figure 3D) and enhanced CD68 immunostaining was observed (Figure 3E). Consistent with these data, serum levels of negative acute phase protein albumin were decreased (Figure 3F). Thus, *Angptl4^{−/−}* mice fed HFD exhibit systemic inflammation and a massive acute phase response several weeks prior to development of ascites and other clinical symptoms.

Chronic HFD is known to induce adipose tissue inflammation, characterized by adipose infiltration of macrophages. However, no signs of enhanced macrophage or other leukocyte infiltration were observed in epididymal fat of *Angptl4^{−/−}* mice after 8 weeks of HFD (Supplemental Figures 3A and 3B), suggesting that enhanced systemic inflammation does not originate in the adipose tissue.

Inflammation in Angptl4^{−/−} mice fed HFD originates in mesenteric lymph nodes

Interestingly, a trend towards increased plasma SAA levels in *Angptl4^{−/−}* mice was already visible after one week of HFD (Figure 4A). HFD has been proposed to lead to inflammatory
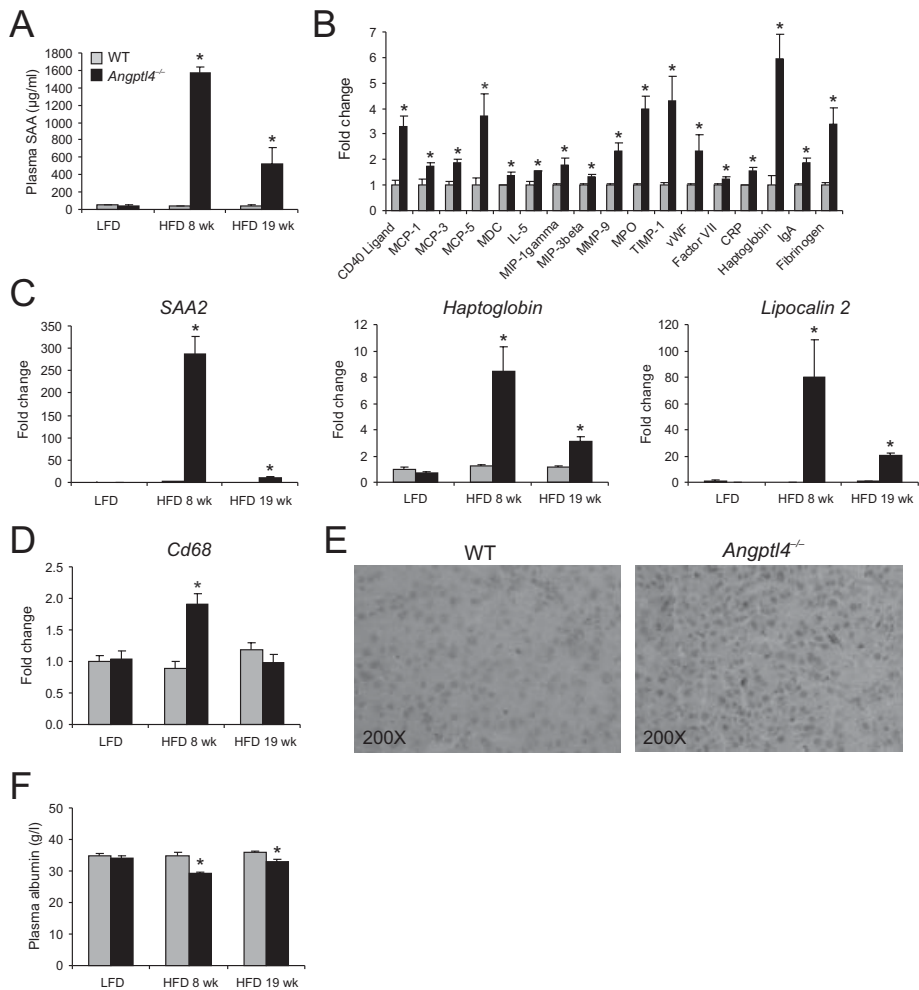
3

Figure 3. High fat feeding provokes massive acute phase response in *Angptl4*$^{-/-}$ mice

(A) Plasma serum amyloid (SAA) levels in wild-type and *Angptl4*$^{-/-}$ mice fed LFD or HFD (Study 1).

(B) Plasma levels of numerous cytokines in wild-type and *Angptl4*$^{-/-}$ fed HFD for 8 weeks. Values are expressed relative to wild-type.

(C) Hepatic mRNA levels of *SAA2, haptoglobin* and *lipocalin 2* determined by qPCR. Expression was normalized against *36b4*.

(D) Hepatic mRNA levels of macrophage marker *Cd68*.

(E) CD68 immunostaining of liver sections of wild-type and *Angptl4*$^{-/-}$ mice fed HFD for 8 weeks.

(F) Plasma serum albumin levels.

Error bars represent SEM. * indicates significantly different from corresponding wild-type mice according to Student's *t*-test ($P < 0.05$) (n = 4-11 mice per group).
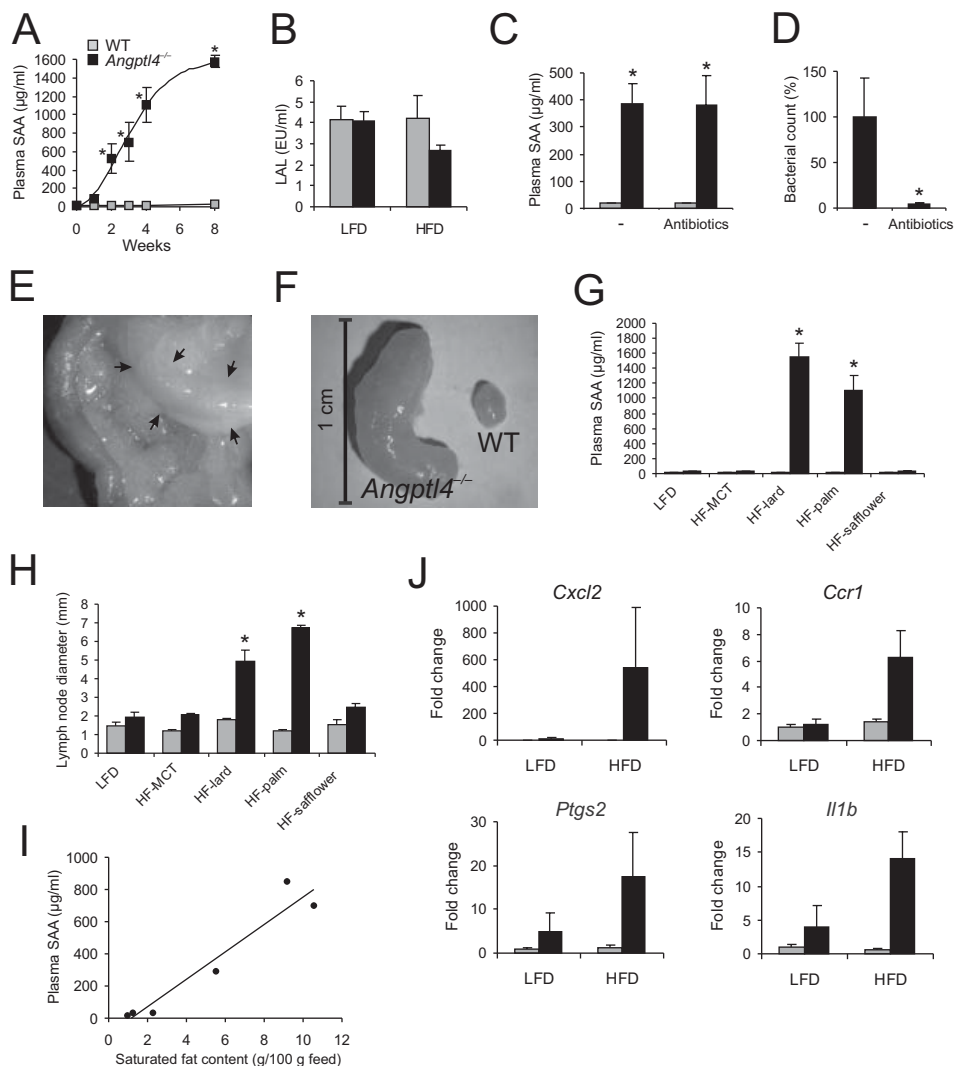
Figure 4. Chyle containing saturated fat elicits massive mesenteric lymphadenitis in *Angptl4⁻/⁻* mice

(A) Kinetics of change in plasma SAA in wild-type and *Angptl4⁻/⁻* mice fed HFD (n = 6-7 per group). (B) Post-prandial endotoxin levels in portal plasma from wild-type and *Angptl4⁻/⁻* mice fed LFD or HFD for 5 weeks (Study 2) (n = 6-7 per group).

(C) Plasma SAA levels in wild-type and *Angptl4⁻/⁻* mice fed HFD for 5 weeks being given oral antibiotics or vehicle (Study 3) (n = 6-10 per group).

(D) Relative abundance of total bacteria expressed per weight of colonic content in *Angptl4⁻/⁻* mice fed HFD and given oral antibiotics or vehicle. * indicates significantly different from corresponding wild-type mice according to Student's *t*-test (*P* < 0.05).

(E) Photograph of mesenteric fat of *Angptl4⁻/⁻* mouse fed HFD for 5 weeks (Study 2). Position of dramatically enlarged lymph node is indicated.

stress via changes in intestinal microflora and/or increased release of LPS (14). However, portal LPS levels were lowest in *Angptl4$^{-/-}$* mice fed HFD (Figure 4B). Importantly, the increase in plasma SAA levels in *Angptl4$^{-/-}$* mice by HFD was unaffected by chronic oral antibiotic treatment (Figure 4C), which effectively reduced intestinal bacterial counts (Figure 4D and Supplemental Figure 4A) and resulted in a severely enlarged caecum (data not shown). These data suggest that induction of systemic inflammation in *Angptl4$^{-/-}$* mice by HFD is independent of the intestinal microbiota.

Remarkably, we noticed that the mesenteric lymph nodes (MLNs) were dramatically enlarged in *Angptl4$^{-/-}$* mice already after 5 weeks of HFD, indicating massive mesenteric lymphadenitis (Figures 4E and 4F). Inflammation extended to mesenteric fat which exhibited mesenteric panniculitis (Supplemental Figure 4B). High fat feeding is known to promote intestinal lymph flow and formation of chylomicrons, which pass through the MLNs as chyle before reaching the circulation. Hence, MLNs are exposed to extremely high TG concentrations, which reach 55 mM in rats fed HFD (mean 35±11 mM). To investigate the role of increased chyle flow, mice were fed for 5 weeks a diet rich in medium chain TGs (MCT) (Table S2), which are not processed via the lymph but enter the portal vein as free fatty acids. Remarkably, induction of plasma SAA and mesenteric lymphadenitis were absent in *Angptl4$^{-/-}$* mice fed MCT (Figures 4G and 4H), suggesting the response is mediated by chylomicrons. A safflower oil-based HFD, which as mentioned previously did not provoke a clinical phenotype, also did not promote inflammation in *Angptl4$^{-/-}$* mice, whereas a lard-based high saturated fat diet gave similar results as the palm-oil based HFD (Figures 4G and 4H). Use of a palm oil-based diet with intermediate fat content supported a clear correlation between dietary saturated fat content and plasma SAA in *Angptl4$^{-/-}$* mice (Figure 4I). Consistent with a direct proinflammatory effect of saturated fat via chylomicrons, there

(F) MLN of a wild-type and *Angptl4$^{-/-}$* mouse fed HFD for 5 weeks after dissection and removal of adipose tissue.

(G) Plasma SAA levels in wild-type and *Angptl4$^{-/-}$* mice fed LFD or different types of HFD for 5 weeks (Study 2). HF-MCT = high fat medium-chain triglycerides, HF-lard = high fat lard-based, HF-palm = high fat palm oil-based, HF-safflower = high fat safflower oil-based.

(H) Size of MLNs in wild-type and *Angptl4$^{-/-}$* mice fed LFD or different types of HFD for 5 weeks (n = 6-7 mice per group). Means of HF-palm and HF-lard groups were significantly different from the other groups as determined by one-way ANOVA followed by Tukey's post-hoc test.

(I) Close correlation between saturated fat content of the diet and the mean plasma level of SAA in *Angptl4$^{-/-}$* mice after 3 weeks of feeding.

(J) Expression of inflammatory marker genes in MLNs of wild-type and *Angptl4$^{-/-}$* mice fed HFD for 24 hours (Study 4). Error bars represent SEM (n = 3 per group).

was a clear trend towards increased expression of several inflammatory mediators in MLNs of *Angptl4*^{−/−} mice already after one day of HFD (Figure 4J and Supplemental Figure 4C). These data indicate that in *Angptl4*^{−/−} mice, a diet rich in saturated fat rapidly causes severe mesenteric lymphadenitis and panniculitis via chylomicrons, leading to a massive hepatic acute phase response via the connecting portal circulation.

Absence of ANGPTL4 stimulates foam cell formation and inflammation in MLN macrophages

MLNs are packed with numerous immune cells including macrophages. Microscopic examination of MLNs from *Angptl4*^{−/−} mice but not wild-type mice fed HFD for 5 weeks showed an abundance of multinucleated Touton giant cells (Figures 5A and 5B), originating from fusion of aberrant lipid-laden tissue macrophages as verified by F4/80 immunostaining (Figure 5C). Formation of Touton cells is known to occur as reaction to lipid material in lymph nodes and is characteristic of lipid lymphadenopathy (15). Accumulation of neutral lipids in Touton cells was confirmed by Oil red O (Figure 5D) and Sudan Black staining (Figure 5E). Importantly, Touton cells were spotted in *Angptl4*^{−/−} mice already after 1 day of HFD (Supplemental Figure 4D). The data suggest a major role of MLN macrophages in initiating inflammation in *Angptl4*^{−/−} fed HFD.

Previously, TG-rich VLDL particles were shown to stimulate foam cell formation and provoke release of cytokines by mouse peritoneal macrophages by serving as source of proinflammatory saturated fatty acids (16, 17). This effect required LPL, which is highly expressed in macrophages (2, 18, 19) and lymph nodes (http://biogps.gnf.org/) (20). Microarray analysis indicated that LPL was among the top 25 of genes with the highest microarray expression signal in peritoneal mouse macrophages (Table S3). Since ANGPTL4 is also expressed in macrophages, is dramatically induced by chyle (Supplemental Figure 5A), and can inhibit macrophage LPL (Supplemental Figure 5B), we hypothesized that ANGPTL4 minimizes lipolysis of chylomicrons by MLN macrophages and accordingly suppress uptake of proinflammatory saturated fatty acids. To test this hypothesis, peritoneal macrophages from *Angptl4*^{−/−} mice were incubated with chyle obtained from the mesenteric lymph duct of rats fed palm oil-based HFD. Chyle dramatically increased lipid storage in macrophages leading to foam cell formation, which was strongly reduced by the LPL inhibitor orlistat (Supplemental Figure 5C). Increased lipid uptake was verified by elevated expression of PPAR-LXR target *Abca1* and decreased expression of SREBP targets, as shown by whole genome expression profiling (Figure 6A) and qPCR (Supplemental Figure 5D). Importantly, increased lipid uptake was associated with pronounced induction of numerous inflammation and immune-related genes, as shown by significant over-representation of
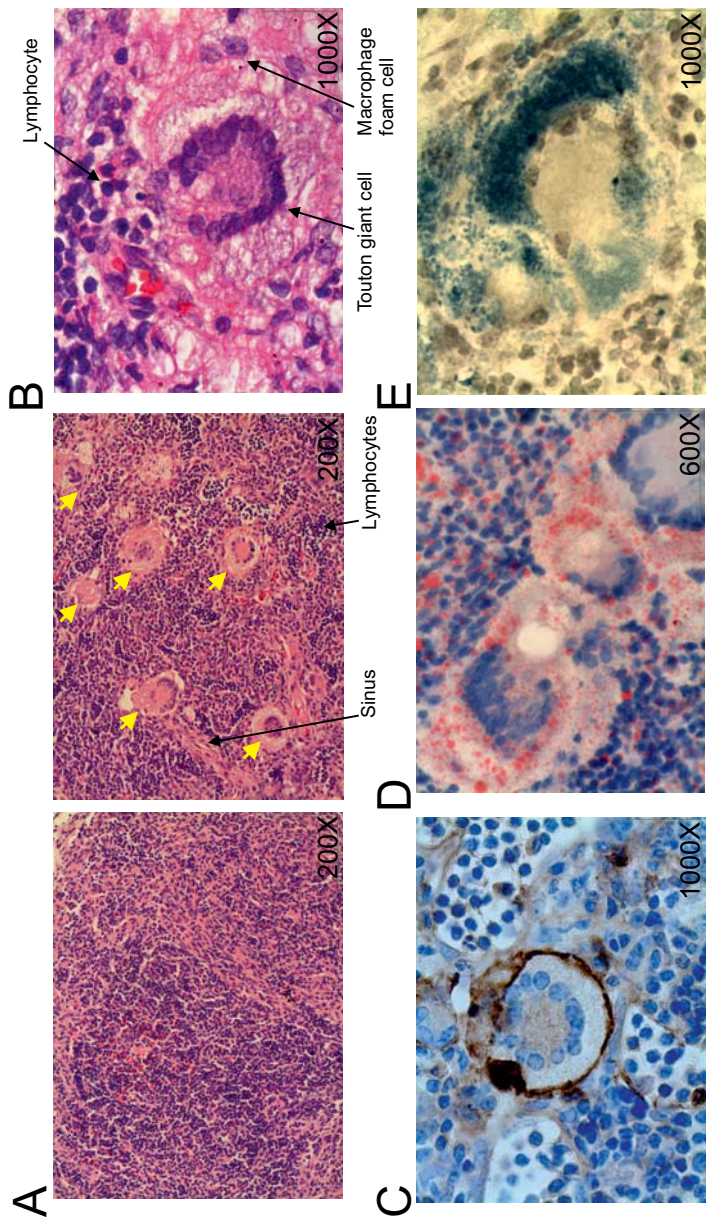
Figure 5. Touton giant cells are abundant in MLNs of *Angptl4−/−* mice fed HFD

(A) Low magnification image of H&E staining of MLNs from wild-type and *Angptl4−/−* mice fed HFD for 5 weeks (Study 2). Touton giant cells are indicated by yellow arrows.

(B) High magnification image of MLN with Touton giant cells from an *Angptl4−/−* animal fed HFD for 5 weeks.

(C) F4/80 immunostaining of a MLN with Touton giant cell.

(D) Oil red O staining counterstained with Hematoxylin.
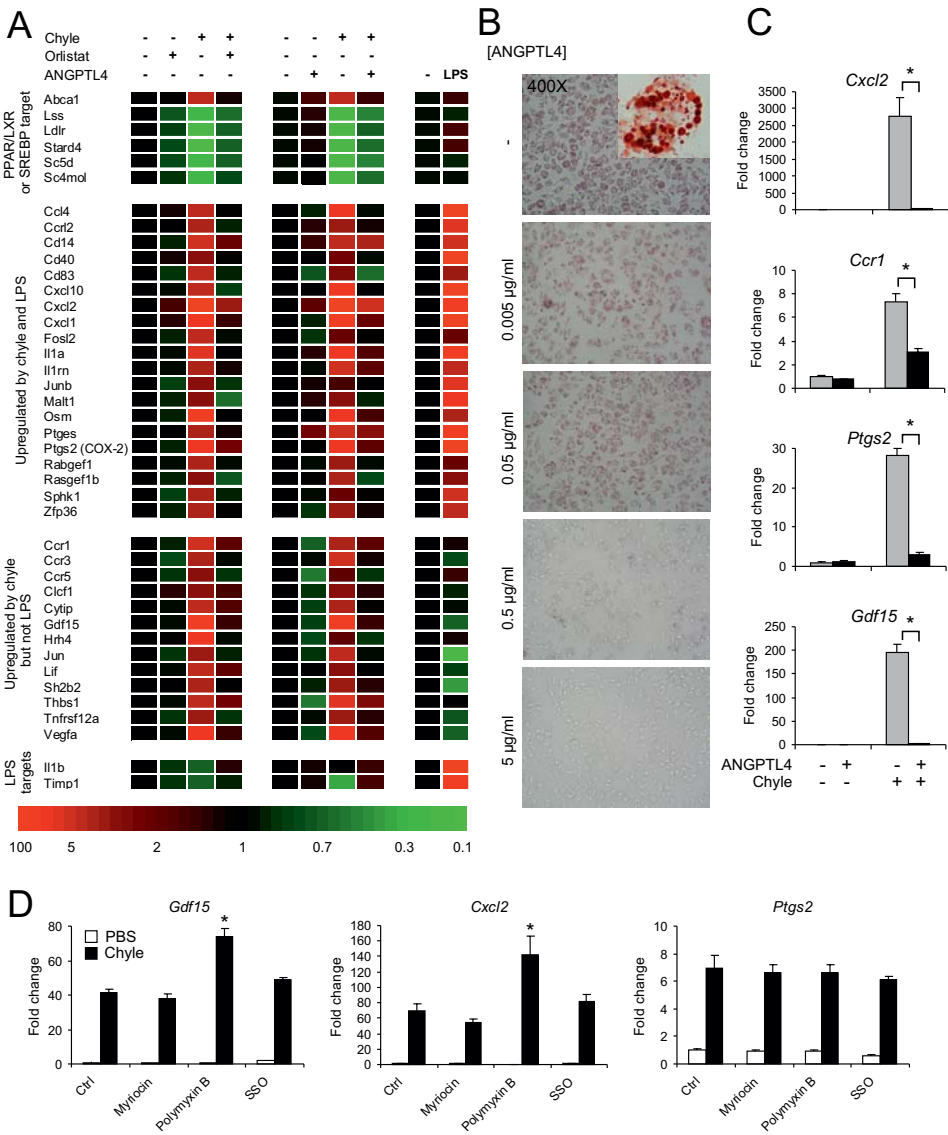
(E) Sudan black staining.

3

Figure 6. ANGPTL4 inhibits macrophage foam cell formation and inflammatory gene expression

(A) Heat map showing changes in expression of selected genes in *Angptl4*$^{-/-}$ mouse peritoneal macrophages incubated for 6 hours with chyle (final TG concentration 2 mM) and/or Orlistat (20 μM), or with chyle and/or recombinant ANGPTL4 (2.5 μg/ml). Expression in untreated macrophages was set at 1. In parallel, expression changes are shown of same genes in peritoneal macrophages treated for 4 hours with LPS (100ng/ml). All genes induced by chyle by at least 2.5-fold and which are labeled with "cytokine or chemokine activity" or "immune or inflammatory response" by Gene Ontology (Biological Process) or are involved in immunity/inflammation based on literature study were included. Also, SREBP target genes that were >75% suppressed by chyle were included.

GO-classes corresponding to those pathways and by Ingenuity Canonical Pathway analysis (Supplemental Figures 6A and 6B). Induction of inflammation, exemplified by *Cxcl2*, *Gdf15*, *oncostatin M*, *Ptgs2* (COX-2) and other genes, was almost entirely blunted by orlistat, indicating lipolysis and LPL-dependency (Figure 6A). Some overlap in macrophage gene regulation was observed between chyle and LPS, but overall effects were mostly divergent (Supplemental Figure 6C). Specifically, typical targets of LPS such as *Il1b* were not induced by chyle, while numerous inflammatory genes upregulated by chyle were not induced by LPS, including *Gdf15* and *Vegfa*.

To examine whether ANGPTL4 can mimic the effect of orlistat on macrophage inflammation, macrophages were loaded with chyle in the presence of recombinant ANGPTL4. ANGPTL4 did not influence cell viability, which was equally high in ANGPTL4- and PBS-treated cells (>85%). At a concentration that causes maximal inhibition of LPL (21), ANGPTL4 prevented lipid uptake from chyle (Figure 6B) and markedly reduced inflammation (Figures 6A and 6C), as shown by strongly blunted induction of inflammatory markers *Ptgs2*, *Cxcl2*, *Ccr1* and *Gdf15*. Inhibitory effects of ANGPTL4 and orlistat on chyle-elicited changes in inflammatory gene expression were highly similar and support a common mechanism of action (Figure 6A). No clear differences in foam cell formation upon chyle loading were observed between wild-type and *Angptl4*^{−/−} macrophages (Supplemental Figure 5C), likely because induction of ANGPTL4 protein by chyle in wild-type macrophages and subsequent feedback inhibition of lipid uptake via LPL lag behind the extremely rapid rate of lipid uptake.

ANGPTL4 abolishes chyle-induced ER stress in macrophages

To explore the mechanism mediating the proinflammatory effect of chyle, peritoneal macrophages were incubated with different chemical modulators including an inhibitor of LPS-induced TLR4 signaling (Polymyxin B), sphingolipid biosynthesis (Myriocin), and fatty acid translocase/Cd36 (Sulfosuccinimidyl oleate) (Figure 6D). None of the compounds

(B) Oil red O staining of *Angptl4*^{−/−} mouse peritoneal macrophages incubated for 6 hours with chyle (TG concentration 2 mM) and increasing concentrations of mouse recombinant ANGPTL4. Chyle was collected from rats fed palm oil-based HFD. Inset: high magnification image of macrophage foam cell. (C) qPCR expression of inflammatory genes in *Angptl4*^{−/−} macrophages treated with chyle and/or ANGPTL4 (2.5 µg/ml). * significantly different according to Student's *t*-test ($P < 0.05$). (D) qPCR expression of inflammatory genes in *Angptl4*^{−/−} macrophages treated with chyle and various pharmacologic inhibitors. SSO = Sulfosuccinimidyl oleate. Differences were evaluated for statistical significance by one-way ANOVA followed by Tukey's post-hoc test. * significantly different from control-treated cells ($P < 0.05$). Error bars represent SEM.

showed any repressive effect on chyle-induced inflammation, although the LPS inhibitor polymyxin B augmented expression of *Gdf15* and *Cxcl2*.

Since ER stress was one of the Canonical Pathways significantly altered by chyle (Table S6B), and is linked to activation of inflammation (22), we further focused our investigation on the ER stress pathway. The mammalian ER stress pathway consists of three major branches: IRE1α, PERK and ATF6. Upon ER stress activation, IRE1α and PERK undergo autophosphorylation and initiate downstream targets. IRE1α mediates the splicing of *XBP1* mRNA while PERK phosphorylates eIF2α, leading to attenuation of global translation and induction of expression of *Atf4* and *Ddit3* (*CHOP*). Remarkably, similar to the effect of ER stress inducers thapsigargin and tunicamycin, chyle significantly increased total IRE1α protein and IRE1α phosphorylation (Figure 7A), and dramatically stimulated *XBP1* splicing (Figure 7B). Moreover, chyle stimulated phosphorylation of PERK and its target eIF2α, markedly increased CHOP protein, and upregulated expression of many ER stress target genes including *XBP1s*, *CHOP*, and *Atf4* (Figure 7C). Importantly and consistent with its anti-lipolytic role, effects of chyle on ER stress marker genes were entirely abolished by ANGPTL4 (Figure 7D). Taken together, chyle induces ER stress in macrophages, which may account for the pronounced activation of inflammation.

Saturated and unsaturated fatty acids differentially modulate *Angptl4* mRNA and ER stress

As mentioned above, chyle dramatically increased *Angptl4* mRNA in wild-type peritoneal macrophages (Figure 7E). Similarly, individual fatty acids markedly increased *Angptl4* mRNA in mouse peritoneal and human U937 macrophages (Figure 7F). Compared to unsaturated oleic and linoleic acid, the saturated palmitic acid was significantly less potent in inducing *Angptl4*. In contrast, expression of *IRE1α*, *XBP1s*, *CHOP*, *Atf4*, and *Gdf15* and to a lesser extent *Cxcl2* was specifically stimulated by palmitic acid (Figure 7G). Palmitic, oleic and linoleic acid represent 95% of fatty acids present in the various diets used, excluding the MCT diet.

Figure 7. ANGPTL4 prevents chyle-induced ER stress

(A) Immunoblots of IRE1α, PERK, eIF2α and CHOP using regular gels or Phos-tag gels (IRE1α only) of *Angptl4*^{−/−} macrophages treated with chyle (TG concentration 2 mM), thapsigargin (100 nM) or tunicamycin (2.5 µg/ml) for 6 hours. "P" represents phosphorylated form.

(B) Regular RT-PCR of XBP1 processing revealing spliced and unspliced XBP1 mRNA.

(C) qPCR expression of ER stress genes. Differences were evaluated for statistical significance by one-way ANOVA followed by Tukey's post-hoc test. * significantly different from control-treated cells ($P < 0.05$).
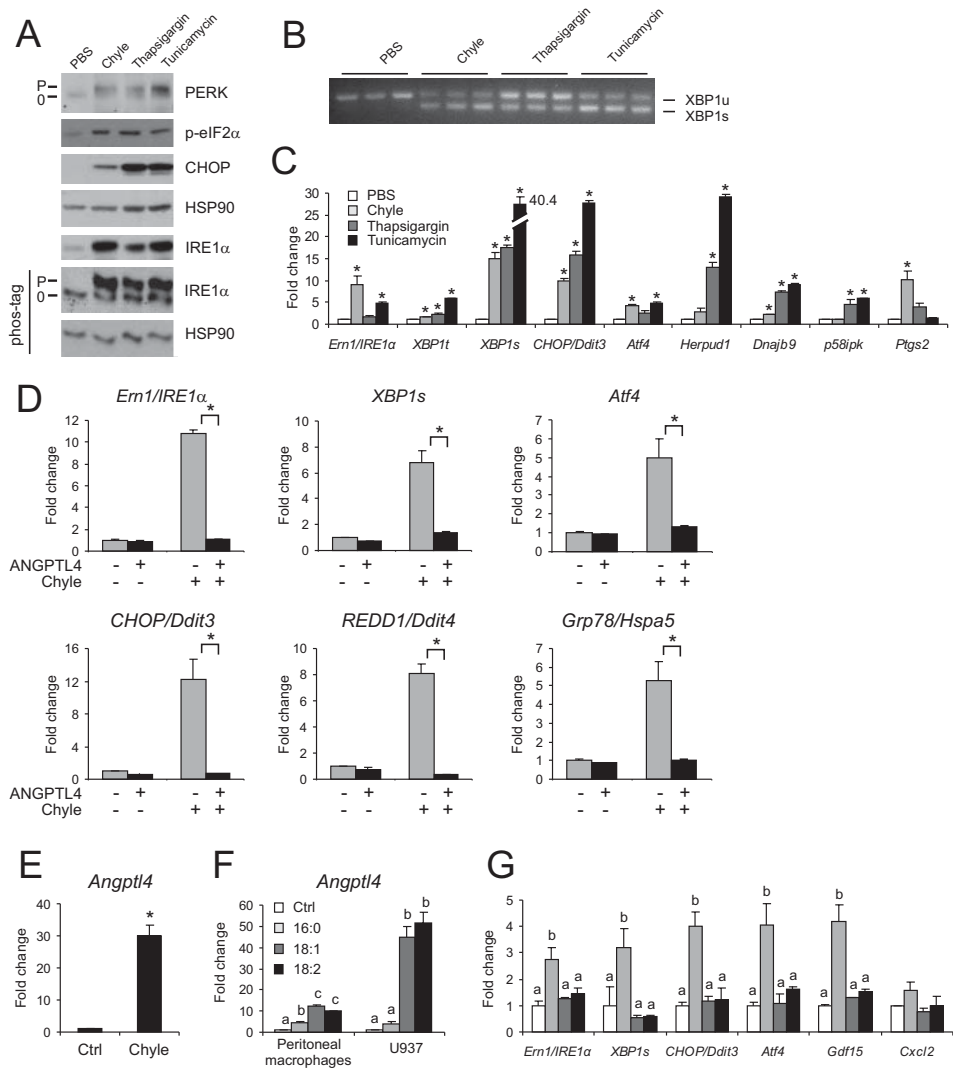
(D) qPCR expression of selected genes involved in ER stress in *Angptl4*^{-/-} mouse peritoneal macrophages incubated for 6 hours with chyle and/or recombinant ANGPTL4 (2.5 μg/ml). * significantly different according to Student's *t*-test ($P < 0.05$).

(E) *Angptl4* mRNA expression in wild-type mouse peritoneal macrophages treated for 6 hours with chyle (TG concentration 1.3 mM).

(F) *Angptl4* mRNA expression in wild-type mouse peritoneal macrophages or human U937 macrophages treated for 6 hours with albumin-bound free fatty acids (500 μM).

(G) qPCR expression of selected genes in wild-type mouse peritoneal macrophages treated with albumin-bound free fatty acids (500 μM). Control-treated cells were treated with albumin only. Differences were evaluated for statistical significance by one-way ANOVA followed by Tukey's post-hoc test. Bars with different letters are significantly different ($P < 0.05$). Error bars represent SEM.

Finally, to study which specific PPAR isotype is involved in *Angptl4* regulation by fatty acids, three types of macrophages were treated with synthetic agonists for PPARα, PPARδ, and PPARγ. No induction of *Angptl4* expression was observed with PPARα agonist Wy14643 (Supplemental Figure 7A). The PPARδ agonist GW501516 consistently induced *Angptl4* mRNA in all three cell types, whereas the PPARγ agonist rosiglitazone increased *Angptl4* mRNA in peritoneal macrophages and to a minor extent in U937 cells. These data suggest that PPARδ most likely mediates the effect of chylomicron-derived fatty acids on *Angptl4* expression.

Taken together, these results demonstrate that ANGPTL4 protects MLN macrophages from uncontrolled lipid accumulation after high fat feeding, thereby preventing lipid-induced ER stress and consequent inflammation.

Discussion

After a saturated fat-rich meal, MLNs are exposed to extremely high concentrations of chylomicrons via the chyle, which might lead to generation of large amounts of proinflammatory saturated fatty acids upon TG lipolysis. Our data indicate that MLNs and specifically resident macrophages are protected from the proinflammatory effect of saturated fatty acids via expression of ANGPTL4, which is strongly induced by chyle and fatty acids and which via inhibition of LPL prevents lipolysis of chylomicron-TG. In the absence of this protective autocrine mechanism, feeding a diet rich in saturated fat rapidly leads to enhanced lipid uptake into MLN-resident macrophages, triggering foam (Touton) cell formation and a massive inflammatory response characterized by severe mesenteric lymphadenitis. Concomitant induction of numerous cytokines leads to a massive hepatic acute phase response via the connecting portal circulation, further evolving into a progressive, uncontrolled inflammation that culminates in chylous ascites and fibrinopurulent peritonitis. The data thus show that ANGPTL4 is a key player in the protection against the severe proinflammatory effects of dietary saturated fat. Based on our data in mice, it can be hypothesized that human subjects homozygous for the E40K mutation in *ANGPTL4*, which has reduced ability to inhibit LPL and is associated with lower plasma TGs (23-25), may be particularly sensitive to the proinflammatory effects of dietary saturated fat.

According to microarray analysis, LPL was among the most highly expressed genes in mouse peritoneal macrophages. The ability of macrophage LPL to facilitate lipid uptake into macrophages is well recognized (2, 18). The locally released fatty acids may serve as energy source for active macrophages (26), but may also constitute a potential proinflammatory

stimulus. Consistent with this notion, fatty acids offered to macrophages as VLDL-TG are taken up and engage MAPK-mediated inflammatory pathways along with increased expression of several proinflammatory cytokines (17). Our data indicate that exposure of macrophages to elevated yet physiologically relevant concentrations of chylomicrons containing saturated fatty acids unleashes a vast inflammatory response characterized by marked induction of numerous chemokines and other inflammation-related genes, which is entirely dependent on TG-lipolysis. We propose that expression of ANGPTL4 in macrophages and its potent induction by chylomicron-derived fatty acids are part of a feedback mechanism aimed at protecting MLN-resident macrophages against post-prandial lipid overload and associated inflammation.

Ablation of ANGPTL4 is associated with decreased plasma TG levels caused by increased peripheral LPL activity (7). Recent data indicate that endothelium-bound LPL is stabilized by the protein GPIHBP1, which partially prevents LPL inhibition by ANGPTL4 (27). Perhaps the almost complete blockage of lipid uptake by ANGPTL4 in macrophages as opposed to its more modest effect in muscle and adipose tissue may be explained by the minimal expression of *Gpihbp1* in macrophages (Supplemental Figure 7B) (27). Future studies will have to address this issue in more detail.

Feeding *Angptl4*$^{-/-}$ mice a diet rich in polyunsaturated fatty acids did not elicit an inflammatory response, consistent with data in peritoneal macrophages showing lack of induction of *Gdf15* and *Cxcl2* by oleic and linoleic acid. In contrast, oleic and linoleic acid were much more potent inducers of *Angptl4* expression compared to palmitic acid, suggesting that the ANGPTL4-mediated feedback inhibition of lipid uptake and inflammation is disturbed in presence of saturated fatty acids.

An important question is how chyle induces inflammation in macrophages. Use of chemical inhibitors indicated that the response is not mediated by LPS, is not dependent on Cd36-mediated fatty acid transport, and does not require sphingolipid synthesis. Strikingly, chyle caused pronounced activation of different branches of the ER stress pathway. It has been shown that ER stress can promote inflammation by various mechanisms, including via IRE1α-mediated activation of stress kinases such as the c-Jun N-terminal kinase (28), and via PERK-mediated activation of NF-κB (29). We found that chyle stimulated IRE1α phosphorylation to promote *XBP1* splicing, and activated PERK, eIF2α and their downstream targets. Activation of ER stress in peritoneal macrophages could be reproduced by free palmitic acid but not oleic or linoleic acid, suggesting the response is mediated by saturated fatty acids.

The mechanism by which saturated fatty acids induce ER stress has been the subject of recent investigations. Palmitate but not palmitoleate induced ER stress in pancreatic

beta cells (30). In liver cells saturated fatty acids induced ER stress independently of ceramide synthesis (31). Stimulation of ER stress by palmitate may occur via increasing the saturated lipid content of ER membrane phospholipids and TGs, leading to compromised ER morphology and integrity and impaired function of protein-folding chaperones (32). Data also point to an important role for aP2 (FABP4) in linking saturated fatty acids to ER stress in macrophages via alterations in lipid composition (33).

Several studies have attributed the proinflammatory effect of saturated fatty acids to activation of TLR4 (34-36). Recently, interplay between TLR4 (and TLR2) and the ER stress pathway was demonstrated (37). IRE1α was shown to be a positive regulator of the inflammatory response to TLR activation in macrophages, while the PERK pathway was not induced by TLR signaling (38). These data hint at a possible role for TLR signaling in the response to chyle in macrophages. However, unlike TLR signaling, chyle dramatically induced ER stress as evidenced by the activation of ER stress sensors IRE1α and PERK as well as their downstream targets. Additionally, whole genome analysis of gene regulation by chyle versus LPS revealed some overlap, but chyle clearly did not mimic LPS, as illustrated by the differential response of classic LPS/TLR4-target *Il1b*. Although these data do not rule out a role for TLR signaling in mediating the inflammatory effects of chyle, induction of ER stress seems a much more plausible mechanism.

A previous report briefly alluded to development of chylous ascites in *Angptl4*$^{-/-}$ mice after 20 weeks of HFD (39). In that study it was found that repeated injections of wild-type mice fed HFD with a monoclonal antibody recapitulated the phenotype of *Angptl4*$^{-/-}$ mice. Since the antibody is directed against the N-terminal portion of ANGPTL4 and abolishes its ability to inhibit LPL, the data support the notion that the clinical abnormalities in *Angptl4*$^{-/-}$ mice fed HFD are related to altered LPL activity, and are independent of C-terminal ANGPTL4.

Chylous ascites has been observed in mice heterozygous for the transcription factor prospero homeobox 1 (*Prox1*) as well as in mice lacking angiopoietin2 (*Angpt2*). Both proteins are essential for development of the lymphatic vasculature (40, 41). Accordingly, it is tempting to hypothesize a similar role for ANGPTL4. However, *Prox1*$^{+/-}$ and *Angpt2*$^{-/-}$ mice develop chylous ascites shortly after birth, reflecting a severe developmental defect. In contrast, *Angptl4*$^{-/-}$ mice do not exhibit ascites unless challenged with HFD for at least 12 weeks. Rather, the data indicate that ascites was secondary to progressive inflammation originating in MLN macrophages, leading to massive lymphadenitis and consequent obstruction in mesenteric lymph flow, which in turn caused dilation of intestinal lymphatic vessels. Furthermore, inflammation of MLNs and mesenteric fat led to increased local lymphatic and vascular permeability, as shown by chylous ascites and

low SAAG, respectively, which is indicative of exudative ascites. The more than two-fold higher protein concentration in ascites fluid compared to chyle supports an important contribution of vascular leakage next to leakage from chyle. Increased circulatory leakage caused fibrinogen extravasation, which after clotting accumulated as fibrin and covered abdominal organs. Chronic inflammation likely gave rise to impaired intestinal barriers function and translocation of enteric bacteria, causing peritonitis and death of the animals.

In conclusion, ANGPTL4 protects against the severe proinflammatory effects of dietary saturated fat in MLNs by inhibiting macrophage LPL, thereby reducing lipolytic release of fatty acids, macrophage foam cell formation, ER stress, and initiation of a marked inflammatory response. The data illustrate how the unique anatomy of the intestinal lymphatic system in which immune cells residing in MLNs are exposed to excessive postprandial TG concentrations, requires activation of an effective cellular mechanism that protects against elevated lipid uptake and its complications. It can be speculated that the inability to effectively recruit this mechanism may contribute to proinflammatory changes related to elevated saturated fat consumption.

Methods

Animals

Animal studies were done using pure-bred wild-type and *Angptl4*$^{-/-}$ mice on C57Bl/6 background (7). In study 1, male 11-week old mice were fed LFD or HFD for 8 or 19 weeks, providing 10 or 45% energy percent as TGs (D12450B or D12451, Research Diets, Inc., Table S1) (Research Diets Services, Wijk bij Duurstede, Netherlands), after 3 weeks run-in (adaptation period) with LFD. In study 2, male 10- to 18-week old mice were fed LFD or HFD for 5 weeks, after 2 weeks run-in with LFD. Fat source of the HFD was either palm oil (standard HFD used in study 1, 3 and 4, Table S1), lard, MCT oil, or safflower oil (Table S2). Blood was collected from tail vein at weekly intervals. In study 3, male 12-week old mice were fed standard HFD for 5 weeks, after 2 weeks run-in with standardized low fat diet AIN93G (see http://testdiet.purina-mills.com/PDF/57W5.pdf and Table S2). The following antibiotics were provided in drinking water: ampicillin (1g/l), neomycin (1g/l), metronidazole (0.5g/l). Blood was collected from tail vein at weekly intervals. In study 4, mice were fed low fat AIN93G or standard HFD for 24 hours, after 1 week run-in with AIN93G. In the latter studies low fat AIN93G was chosen instead of D12450B to achieve minimal dietary saturated fat intake. Diet composition is provided in Table S1 and S2. At the end of each study, mice were anaesthetized with mixture of isoflurane (1.5%), nitrous oxide (70%) and oxygen (30%). Blood was collected by orbital puncture into EDTA tubes. Mice were killed by cervical dislocation, after which tissues were excised and directly frozen in liquid nitrogen or prepared for histology.

Wistar rats were fed palm-oil based HFD (D12451) overnight. The next morning, animals were anesthetized using isoflurane and mesenteric lymph ducts were cannulated. Chyle was collected for 1-2 hours and stored at -20°C. Chyle TG concentrations averaged at 35±11 mM as determined by enzymatic assay (Instruchemie, Delfzijl, Netherlands). Animal studies were approved by the local animal ethics committee at Wageningen University.

Two terminally ill animals were transferred to the Small Animal Pathology laboratory of the Faculty of Veterinary Medicine at Utrecht University for formal autopsy by a licensed animal pathologist.

Lipid excretion and absorption

During week 3-5 of high fat feeding, the amount of lipid excreted was measured in the faecal samples as previously described (42). Measurement of intestinal lipid absorption using ^{3}H-labeled triolein and ^{14}C-labeled palmitic acid was carried out exactly as previously described (43).

Plasma and ascites analyses

All analyses were performed on non-fasting plasma unless specifically indicated. ELISA was used to determine plasma levels of serum amyloid A (Biosource International, Breda, Netherlands) and endotoxins (Limulus Amoebocyte Lysate, SanBio, Uden, Netherlands) following instructions from the manufacturer. Plasma concentrations of multiple inflammation markers were measured by multiplex immunoassay (RodentMAP) (Rules Based Medicine, Austin, TX). Plasma, ascites, and liver triglycerides were determined enzymatically as previously described (8). Plasma and ascites albumin concentration were determined by a photometric colorometric test according to the bromocresol green method (44) (Instruchemie, Delfzijl, Netherlands). Ascites protein concentration was determined using Bradford assay (45) (Biorad, Veenendaal, Netherlands). Ascites WBC was determined using a Sysmex XE-2100 haematology automated analyzer following instructions from the manufacturer. Lipoprotein profiling of the ascites fluid and mouse plasma was carried out by FPLC as previously described (21). Chylous ascites and plasma FPLC fractions were resolved by 6% SDS-PAGE and blotted onto PVDF membrane overnight (Millipore, Amsterdam, Netherlands). Membranes were blocked using 5% (w/v) milk powder in PBS with 0.1% Tween 20 and subsequently probed with rabbit anti-mouse APOB48/APOB100 (Meridian Life Sciences Inc, Saco, ME) followed by HRP-conjugated goat anti-rabbit (Sigma, Zwijndrecht, Netherlands). Membranes were incubated with ECL (Amersham ECL Plus, GE Healthcare, Diegem, Belgium) and exposed to film.

Bacterial counts in feces

Colonic content was freeze-dried overnight and subsequently weighed. Feces were homogenized in 500 µl lysis buffer using FastPrep at 4°C and 5.5 ms for 3 minutes. 130 µl of 10 M ammonium acetate was added, followed by centrifugation. After transfer of the supernatant to a new tube, one volume of isopropanol was added. Samples were incubated on ice for 30 minutes, centrifuged, washed with 70% ethanol, and air-dried. The pellet was dissolved in 200 µl TE buffer. Genomic DNA was purified using QIAmp DNA Mini Kit to a final volume of 200 µl. Samples were diluted 100X before PCR analysis. DNA from all

bacteria was amplified by real-time PCR using primers: forward, ACTCCTACGGGAGGCAGCAG; reverse, ATTACCGCGGCTGCTGG. DNA from bacteroidetes was amplified using primers: forward, GGARCATGTGGTTTAATTCGATGAT; reverse, AGCTGACGACAACCATGCAG. Bacterial PCR-based counts were normalized to the weight of fecal sample.

Cell culture

U937 human monocytes were differentiated into macrophages by 24 hours treatment with phorbol myristate acetate (10 ng/µl). U937 macrophages were subsequently incubated for 6 hours with fatty acids (C16:0, C18:1, C18:2) coupled to fatty acid free BSA to a final concentration of 500 µM as previously described (46).

To obtain peritoneal macrophages, wild-type and $Angptl4^{-/-}$ mice were injected intraperitoneally with 1 ml 4% thioglycollate. Three days later, animals were anesthesized with isoflurane, bled via orbital puncture, and peritoneal cavities washed using 10 ml ice-cold RPMI medium supplemented with 100 U/ml penicillin and 100 µg/ml streptomycin (Lonza, Verviers, Belgium). Cell pellets were incubated with RBC lysis buffer on ice for 5 minutes and subsequently washed with RPMI medium supplemented with 10% fetal bovine serum (FBS) (Lonza) and antibiotics, re-pelletized and seeded at density of 3×10^5 cells/cm^2. Two hours later, cells were washed twice with PBS to remove non-adherent cells and provided with medium. Two days later, cells were exposed to chyle at TG concentration of 2 mM for 6 hours preceded by preincubation with 20 µM Orlistat (Sigma Zwijndrecht, Netherlands) or 2.5 µg/ml mouse recombinant ANGPTL4 (R&D Systems, Abingdon, UK) for 1.5 hours. To explore mechanism of chyle, $Angptl4^{-/-}$ macrophages were preincubated with 10 µM myriocin, 10 µg/ml Polymyxin B or 0.5 mM Sulfosuccinimidyl oleate (SSO) for 30 minutes followed by exposure of cells to either PBS or chyle at TG concentration of 2 mM for 6 hours. In ER stress experiments, $Angptl4^{-/-}$ macrophages were exposed to 100 nM thapsigargin, 2.5 µg/ml tunicamycin or chyle (TG 2 mM) for 6 hours. Analysis of ER stress in peritoneal macrophages was carried out as described (47).

Histology/Immunohistochemistry

Haematoxylin and Eosin staining of sections was performed using standard protocols. For detection of macrophages, immunohistochemistry was performed using antibody against CD68 (liver, adipose tissue) or F4/80 (lymph nodes) (Serotec, Oxford, UK). Paraffin-embedded sections were preincubated with 20% normal goat serum followed by overnight incubation at 4°C with primary antibody diluted 1:50 in PBS/1% BSA. After incubation with primary antibody, goat anti rat IgG conjugated to horseradish peroxidase (Serotec) was used as secondary antibody. Visualization was performed using AEC Substrate Chromogen (Cd68) or 3,3'-Diaminobenzidine (F4/80). Negative controls were prepared by omitting primary antibody.

For Sirius Red staining paraffin-embedded sections of small intestine were mounted on Superfrost microscope slides. Sections were dewaxed in xylene and rehydrated in series of graded alcohols. Slides were stained in picrosirius red 0.1% picric acid for 90 minutes and rinced in acidified H$_2$O 0.5% acetic acid.

Oil red O stock solution was prepared by dissolving 0.5g Oil red O (Sigma, #O0625) in 500 ml isopropanol. Oil red O working solution was prepared by mixing 30 ml Oil red O stock with 20 ml dH$_2$O, followed by filtration. 5μm sections were cut from frozen MLNs embedded in OCT. Sections were air dried for 30 minutes, rehydrated in dH$_2$O, and fixated for 10 minutes in formal calcium (4% formaldehyde, 1% CaCl$_2$). Sections were immersed in Oil red O working solution for 10 minutes, followed by two rinses with dH$_2$O. Haematoxylin Nuclei staining was subsequently carried out for 5 minutes followed by several rinses with dH$_2$O. Sections were mounted in aqueous mountant (Imsol, Preston, UK).

For Sudan Black staining, 0.5 g Sudan black (Sigma, #86015) was dissolved in 100 ml warm 70% ethanol and subsequently filtered. Sections were fixed and rehydrated as above. After two 3 minutes rinses with 50% ethanol and two quick rinses with dH$_2$O, sections were immersed in Sudan black solution for 10 minutes, followed by two rinses with dH$_2$O. Sections were mounted in aqueous mountant (Imsol, Preston, UK).

LPL activity assay

Angptl4$^{-/-}$ macrophages were isolated and cultured as described in the main text. After extensive washing with PBS, cells were incubated in serum-free medium containing either PBS or recombinant mouse ANGPTL4 (5 μg/ml) (R&D Systems, Abingdon, United Kingdom) for 45 minutes. LPL was subsequently solubilized by adding 100 IU/ml heparin for 10 minutes. LPL activity was determined in 15 μl of medium using the Roar LPL Activity Assay Kit (Roar Biomedical, Inc, New York, USA).

Gene expression analysis

Isolation of RNA and subsequent analysis of gene expression by qPCR was carried out as previously described (48). *Cyclophilin*, *18S*, or *36b4* were used as housekeeping genes. PCR primer sequences were taken from the PrimerBank and ordered from Eurogentec (Seraing, Belgium). Sequences of the primers used are available upon request.

RNA was isolated from mouse peritoneal macrophages using RNeasy mini columns (Qiagen, Venlo, The Netherlands). RNA quality was verified on an Agilent 2100 Bioanalyzer (Agilent Technologies, Amsterdam, The Netherlands) using 6000 Nano Chips according to manufacturer's instructions. RNA was considered suitable for array hybridization only if RNA integrity number exceeded 8.0. RNA from 3 samples per group was pooled for microarray analysis. One hundred nanogram of RNA was used for Whole Transcript cDNA synthesis (Affymetrix, Santa Clara, CA). Hybridization, washing, and scanning of Affymetrix GeneChip Mouse Gene 1.0 ST Arrays were carried out according to standard Affymetrix protocols. Scans of the Affymetrix arrays were processed using packages from the Bioconductor project. Arrays were normalized using the Robust Multi-array Average method (49, 50). Probe sets were defined by assigning probes to unique gene identifiers, e.g. Entrez ID (51), which total 20985 on the Gene 1.0 ST arrays. Changes in gene expression were calculated as signal log ratios between treatment and control. These ratios were used to create heatmaps within Excel.

Affymetrix GeneChip analysis was carried out on wild-type mouse peritoneal macrophages incubated with lipopolysaccharide (LPS, 100 ng/ml) for 4 hours (52). CEL files were downloaded from the internet via Gene Expression Omnibus (GSE14891) and processed as described above.

Acknowledgements

3

References

1. Merkel M, Eckel RH, Goldberg IJ. Lipoprotein lipase: genetics, lipid uptake, and regulation. *J Lipid Res.* 2002;43(12):1997-2006.
2. Ostlund-Lindqvist AM, Gustafson S, Lindqvist P, Witztum JL, Little JA. Uptake and degradation of human chylomicrons by macrophages in culture. Role of lipoprotein lipase. *Arteriosclerosis.* 1983;3(5):433-440.
3. Wang H, Eckel RH. Lipoprotein lipase: from gene to obesity. *Am J Physiol Endocrinol Metab.* 2009;297(2):E271-288.
4. Yoshida K, Shimizugawa T, Ono M, Furukawa H. Angiopoietin-like protein 4 is a potent hyperlipidemia-inducing factor in mice and inhibitor of lipoprotein lipase. *J Lipid Res.* 2002;43(11):1770-1772.
5. Kersten S, Mandard S, Tan NS, Escher P, Metzger D, Chambon P, Gonzalez FJ, Desvergne B, Wahli W. Characterization of the fasting-induced adipose factor FIAF, a novel peroxisome proliferator-activated receptor target gene. *J Biol Chem.* 2000;275(37):28488-28493.
6. Yoon JC, Chickering TW, Rosen ED, Dussault B, Qin Y, Soukas A, Friedman JM, Holmes WE, Spiegelman BM. Peroxisome proliferator-activated receptor gamma target gene encoding a novel angiopoietin-related protein associated with adipose differentiation. *Mol Cell Biol.* 2000;20(14):5343-5349.
7. Koster A, Chao YB, Mosior M, Ford A, Gonzalez-DeWhitt PA, Hale JE, Li D, Qiu Y, Fraser CC, Yang DD, et al. Transgenic angiopoietin-like (angptl)4 overexpression and targeted disruption of angptl4 and angptl3: regulation of triglyceride metabolism. *Endocrinology.* 2005;146(11):4943-4950.
8. Mandard S, Zandbergen F, van Straten E, Wahli W, Kuipers F, Muller M, Kersten S. The Fasting-induced Adipose Factor/Angiopoietin-like Protein 4 Is Physically Associated with Lipoproteins and Governs Plasma Lipid Levels and Adiposity. *J Biol Chem.* 2006;281(2):934-944.
9. Xu A, Lam MC, Chan KW, Wang Y, Zhang J, Hoo RL, Xu JY, Chen B, Chow WS, Tso AW, et al. Angiopoietin-like protein 4 decreases blood glucose and improves glucose tolerance but induces hyperlipidemia and hepatic steatosis in mice. *Proc Natl Acad Sci U S A.* 2005;102(17):6086-6091.

10. Oike Y, Akao M, Yasunaga K, Yamauchi T, Morisada T, Ito Y, Urano T, Kimura Y, Kubota Y, Maekawa H, et al. Angiopoietin-related growth factor antagonizes obesity and insulin resistance. *Nat Med.* 2005;11(4):400-408.

11. Tabata M, Kadomatsu T, Fukuhara S, Miyata K, Ito Y, Endo M, Urano T, Zhu HJ, Tsukano H, Tazume H, et al. Angiopoietin-like protein 2 promotes chronic adipose tissue inflammation and obesity-related systemic insulin resistance. *Cell Metab.* 2009;10(3):178-188.

12. Voshol PJ, Rensen PC, van Dijk KW, Romijn JA, Havekes LM. Effect of plasma triglyceride metabolism on lipid storage in adipose tissue: studies using genetically engineered mouse models. *Biochim Biophys Acta.* 2009;1791(6):479-485.

13. Backhed F, Crawford PA, O'Donnell D, Gordon JI. Postnatal lymphatic partitioning from the blood vasculature in the small intestine requires fasting-induced adipose factor. *Proc Natl Acad Sci U S A.* 2007;104(2):606-611.

14. Cani PD, Amar J, Iglesias MA, Poggi M, Knauf C, Bastelica D, Neyrinck AM, Fava F, Tuohy KM, Chabo C, et al. Metabolic endotoxemia initiates obesity and insulin resistance. *Diabetes.* 2007;56(7):1761-1772.

15. Aterman K, Remmele W, Smith M. Karl Touton and his "xanthelasmatic giant cell." A selective review of multinucleated giant cells. *Am J Dermatopathol.* 1988;10(3):257-269.

16. Gianturco SH, Bradley WA, Gotto AM, Jr., Morrisett JD, Peavy DL. Hypertriglyceridemic very low density lipoproteins induce triglyceride synthesis and accumulation in mouse peritoneal macrophages. *J Clin Invest.* 1982;70(1):168-178.

17. Saraswathi V, Hasty AH. The role of lipolysis in mediating the proinflammatory effects of very low density lipoproteins in mouse peritoneal macrophages. *J Lipid Res.* 2006;47(7):1406-1415.

18. Babaev VR, Fazio S, Gleaves LA, Carter KJ, Semenkovich CF, Linton MF. Macrophage lipoprotein lipase promotes foam cell formation and atherosclerosis in vivo. *J Clin Invest.* 1999;103(12):1697-1705.

19. Skarlatos SI, Dichek HL, Fojo SS, Brewer HB, Kruth HS. Absence of triglyceride accumulation in lipoprotein lipase-deficient human monocyte-macrophages incubated with human very low density lipoprotein. *J Clin Endocrinol Metab.* 1993;76(3):793-796.

20. Lattin JE, Schroder K, Su AI, Walker JR, Zhang J, Wiltshire T, Saijo K, Glass CK, Hume DA, Kellie S, et al. Expression analysis of G Protein-Coupled Receptors in mouse macrophages. *Immunome Res.* 2008;4(1):5.

21. Lichtenstein L, Berbee JF, van Dijk SJ, van Dijk KW, Bensadoun A, Kema IP, Voshol PJ, Muller M, Rensen PC, Kersten S. Angptl4 upregulates cholesterol synthesis in liver via inhibition of LPL- and HL-dependent hepatic cholesterol uptake. *Arterioscler Thromb Vasc Biol.* 2007;27(11):2420-2427.

22. Hotamisligil GS. Endoplasmic reticulum stress and the inflammatory basis of metabolic disease. *Cell.* 2010;140(6):900-917.

23. Romeo S, Pennacchio LA, Fu Y, Boerwinkle E, Tybjaerg-Hansen A, Hobbs HH, Cohen JC. Population-based resequencing of ANGPTL4 uncovers variations that reduce triglycerides and increase HDL. *Nat Genet.* 2007;39(4):513-516.

24. Shan L, Yu XC, Liu Z, Hu Y, Sturgis LT, Miranda ML, Liu Q. The angiopoietin-like proteins ANGPTL3 and ANGPTL4 inhibit lipoprotein lipase activity through distinct mechanisms. *J Biol Chem.* 2008.

25. Yin W, Romeo S, Chang S, Grishin NV, Hobbs HH, Cohen JC. Genetic variation in ANGPTL4 provides insights into protein processing and function. *J Biol Chem.* 2009;284(19):13213-13222.

26. Yin B, Loike JD, Kako Y, Weinstock PH, Breslow JL, Silverstein SC, Goldberg IJ. Lipoprotein lipase regulates Fc receptor-mediated phagocytosis by macrophages maintained in glucose-deficient medium. *J Clin Invest.* 1997;100(3):649-657.

27.   Sonnenburg WK, Yu D, Lee EC, Xiong W, Gololobov G, Key B, Gay J, Wilganowski N, Hu Y, Zhao S, et al. GPIHBP1 stabilizes lipoprotein lipase and prevents its inhibition by angiopoietin-like 3 and angiopoietin-like 4. *J Lipid Res.* 2009;50(12):2421-2429.

28.   Urano F, Wang X, Bertolotti A, Zhang Y, Chung P, Harding HP, Ron D. Coupling of stress in the ER to activation of JNK protein kinases by transmembrane protein kinase IRE1. *Science.* 2000;287(5453):664-666.

29.   Jiang HY, Wek SA, McGrath BC, Scheuner D, Kaufman RJ, Cavener DR, Wek RC. Phosphorylation of the alpha subunit of eukaryotic initiation factor 2 is required for activation of NF-kappaB in response to diverse cellular stresses. *Mol Cell Biol.* 2003;23(16):5651-5663.

30.   Diakogiannaki E, Welters HJ, Morgan NG. Differential regulation of the endoplasmic reticulum stress response in pancreatic beta-cells exposed to long-chain saturated and monounsaturated fatty acids. *J Endocrinol.* 2008;197(3):553-563.

31.   Wei Y, Wang D, Topczewski F, Pagliassotti MJ. Saturated fatty acids induce endoplasmic reticulum stress and apoptosis independently of ceramide in liver cells. *Am J Physiol Endocrinol Metab.* 2006;291(2):E275-281.

32.   Borradaile NM, Han X, Harp JD, Gale SE, Ory DS, Schaffer JE. Disruption of endoplasmic reticulum structure and integrity in lipotoxic cell death. *J Lipid Res.* 2006;47(12):2726-2737.

33.   Erbay E, Babaev VR, Mayers JR, Makowski L, Charles KN, Snitow ME, Fazio S, Wiest MM, Watkins SM, Linton MF, et al. Reducing endoplasmic reticulum stress through a macrophage lipid chaperone alleviates atherosclerosis. *Nat Med.* 2009;15(12):1383-1391.

34.   Lee JY, Sohn KH, Rhee SH, Hwang D. Saturated fatty acids, but not unsaturated fatty acids, induce the expression of cyclooxygenase-2 mediated through Toll-like receptor 4. *J Biol Chem.* 2001;276(20):16683-16689.

35.   Shi H, Kokoeva MV, Inouye K, Tzameli I, Yin H, Flier JS. TLR4 links innate immunity and fatty acid-induced insulin resistance. *J Clin Invest.* 2006;116(11):3015-3025.

36.   Suganami T, Tanimoto-Koyama K, Nishida J, Itoh M, Yuan X, Mizuarai S, Kotani H, Yamaoka S, Miyake K, Aoe S, et al. Role of the Toll-like receptor 4/NF-kappaB pathway in saturated fatty acid-induced inflammatory changes in the interaction between adipocytes and macrophages. *Arterioscler Thromb Vasc Biol.* 2007;27(1):84-91.

37.   Woo CW, Cui D, Arellano J, Dorweiler B, Harding H, Fitzgerald KA, Ron D, Tabas I. Adaptive suppression of the ATF4-CHOP branch of the unfolded protein response by toll-like receptor signalling. *Nat Cell Biol.* 2009;11(12):1473-1480.

38.   Martinon F, Chen X, Lee AH, Glimcher LH. TLR activation of the transcription factor XBP1 regulates innate immune responses in macrophages. *Nat Immunol.* 2010;11(5):411-418.

39.   Desai U, Lee EC, Chung K, Gao C, Gay J, Key B, Hansen G, Machajewski D, Platt KA, Sands AT, et al. Lipid-lowering effects of anti-angiopoietin-like 4 antibody recapitulate the lipid phenotype found in angiopoietin-like 4 knockout mice. *Proc Natl Acad Sci U S A.* 2007;104(28):11766-11771.

40.   Gale NW, Thurston G, Hackett SF, Renard R, Wang Q, McClain J, Martin C, Witte C, Witte MH, Jackson D, et al. Angiopoietin-2 is required for postnatal angiogenesis and lymphatic patterning, and only the latter role is rescued by Angiopoietin-1. *Dev Cell.* 2002;3(3):411-423.

41.   Harvey NL, Srinivasan RS, Dillard ME, Johnson NC, Witte MH, Boyd K, Sleeman MW, Oliver G. Lymphatic vascular defects promoted by Prox1 haploinsufficiency cause adult-onset obesity. *Nat Genet.* 2005;37(10):1072-1081.

42.   Govers MJ, Termont DS, Van der Meer R. Mechanism of the antiproliferative effect of milk mineral and other calcium supplements on colonic epithelium. *Cancer Res.* 1994;54(1):95-100.

3

43. Goudriaan JR, Dahlmans VE, Febbraio M, Teusink B, Romijn JA, Havekes LM, Voshol PJ. Intestinal lipid absorption is not affected in CD36 deficient mice. *Mol Cell Biochem.* 2002;239(1-2):199-202.

44. Doumas BT, Watson WA, Biggs HG. Albumin standards and the measurement of serum albumin with bromcresol green. *Clin Chim Acta.* 1971;31(1):87-96.

45. Bradford MM. A rapid and sensitive method for the quantitation of microgram quantities of protein utilizing the principle of protein-dye binding. *Anal Biochem.* 1976;72(248-254.

46. de Vogel-van den Bosch HM, de Wit NJ, Hooiveld GJ, Vermeulen H, van der Veen JN, Houten SM, Kuipers F, Muller M, van der Meer R. A cholesterol-free, high-fat diet suppresses gene expression of cholesterol transporters in murine small intestine. *Am J Physiol Gastrointest Liver Physiol.* 2008;294(5):G1171-1180.

47. Yang L, Xue Z, He Y, Sun S, Chen H, Qi L. A Phos-tag-based approach reveals the extent of physiological endoplasmic reticulum stress. *PLoS ONE.* 2010;5(7):e11621.

48. Sanderson LM, de Groot PJ, Hooiveld GJ, Koppen A, Kalkhoven E, Muller M, Kersten S. Effect of synthetic dietary triglycerides: a novel research paradigm for nutrigenomics. *PLoS ONE.* 2008;3(2):e1681.

49. Bolstad BM, Irizarry RA, Astrand M, Speed TP. A comparison of normalization methods for high density oligonucleotide array data based on variance and bias. *Bioinformatics.* 2003;19(2):185-193.

50. Irizarry RA, Bolstad BM, Collin F, Cope LM, Hobbs B, Speed TP. Summaries of Affymetrix GeneChip probe level data. *Nucleic Acids Res.* 2003;31(4):e15.

51. Dai M, Wang P, Boyd AD, Kostov G, Athey B, Jones EG, Bunney WE, Myers RM, Speed TP, Akil H, et al. Evolving gene/transcript definitions significantly alter the interpretation of GeneChip data. *Nucleic Acids Res.* 2005;33(20):e175.

52. Matsushita K, Takeuchi O, Standley DM, Kumagai Y, Kawagoe T, Miyake T, Satoh T, Kato H, Tsujimura T, Nakamura H, et al. Zc3h12a is an RNase essential for controlling immune responses by regulating mRNA decay. *Nature.* 2009;458(7242):1185-1190.
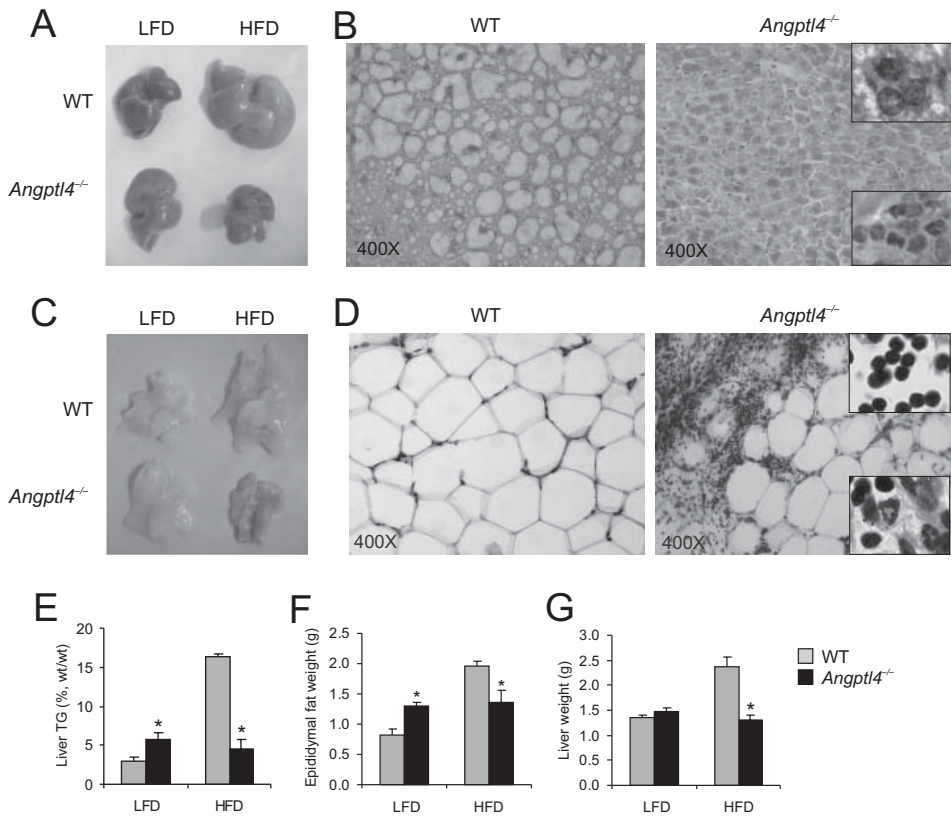
Supplemental Figure 1. Micro- and macroscopic alteration in liver and adipose tissue

(A) Photograph of livers of wild-type and *Angptl4*$^{-/-}$ mouse fed LFD or HFD for 19 weeks. Livers of wild-type mice fed HFD were enlarged and pale, indicating steatosis. Livers of *Angptl4*$^{-/-}$ mice fed HFD were rigid and compressed.

(B) H&E staining of livers of wild-type and *Angptl4*$^{-/-}$ mouse fed HFD for 19 weeks. Staining reveals missing cords and sinusoids, poorly visible portal triads and lack of hepatic fat in *Angptl4*$^{-/-}$ mice fed HFD. Clumping of nuclei and focal infiltrates of neutrophils, eosinophils and macrophages were observed (insets).

(C) Photograph of epididymal fat of wild-type and *Angptl4*$^{-/-}$ mouse fed LFD or HFD for 19 weeks. Adipose tissue of *Angptl4*$^{-/-}$ mice fed HFD had red appearance and was small in size compared to wild-type mice fed HFD.

(D) H&E staining of epididymal fat of wild-type and *Angptl4*$^{-/-}$ fed HFD for 19 weeks. *Angptl4*$^{-/-}$ mice reveal steatitis as shown by massive infiltration of granulocytes and lymphocytes around the periphery (insets).

(E) Liver triglycerides after 19 weeks of LFD or HFD.

(F and G) Weights of epididymal fat (F) and liver (G) after 19 weeks of LFD or HFD.

Error bars represent SEM. * indicates significantly different according to Student's *t*-test (*P* < 0.05).
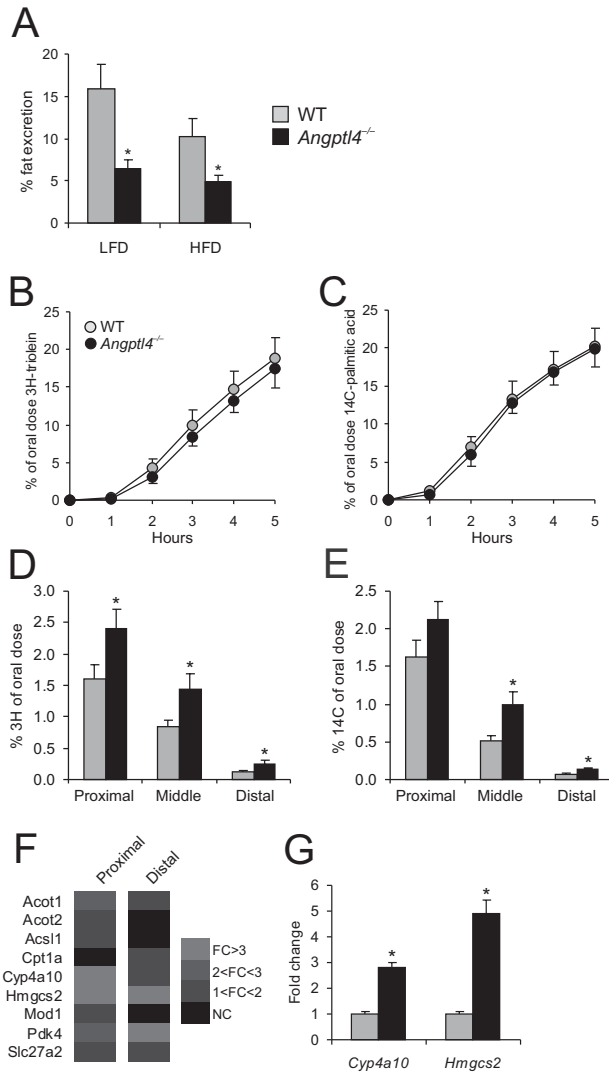
Supplemental Figure 2. Absence of fat malabsorption in *Angptl4*^{–/–} mice

(A) Fat excretion expressed as a percentage of dietary fat intake during week 2-5 of LFD or HFD.

(B and C) Mice fasted for 5 hours were given 400 µl of olive oil containing 7µCi glycerol-tri[^{3}H] oleate (triolein) and 2 µCi [^{14}C]palmitate. Blood was collected every hour. ^{3}H- (B) and ^{14}C-radioactivity (C) are expressed as a percentage of total oral dose.

(D and E) Five hours thereafter, small intestine was collected and cut into 3 parts. ^{3}H- (D) and ^{14}C-radioactivity (E) are expressed as a percentage of total oral dose.

(F) Heat map showing fold changes in expression of PPARα-target genes in small intestine of *Angptl4*^{–/–} vs. wild-type mice.

(G) mRNA expression of selected PPARα targets in small intestine of wild-type and *Angptl4*^{–/–} mice.

Error bars represent SEM. * indicates significantly different between wild-type and *Angptl4*^{–/–} mice according to Student's *t*-test ($P < 0.05$).

A

WT   Angptl4⁻ᐟ⁻

B
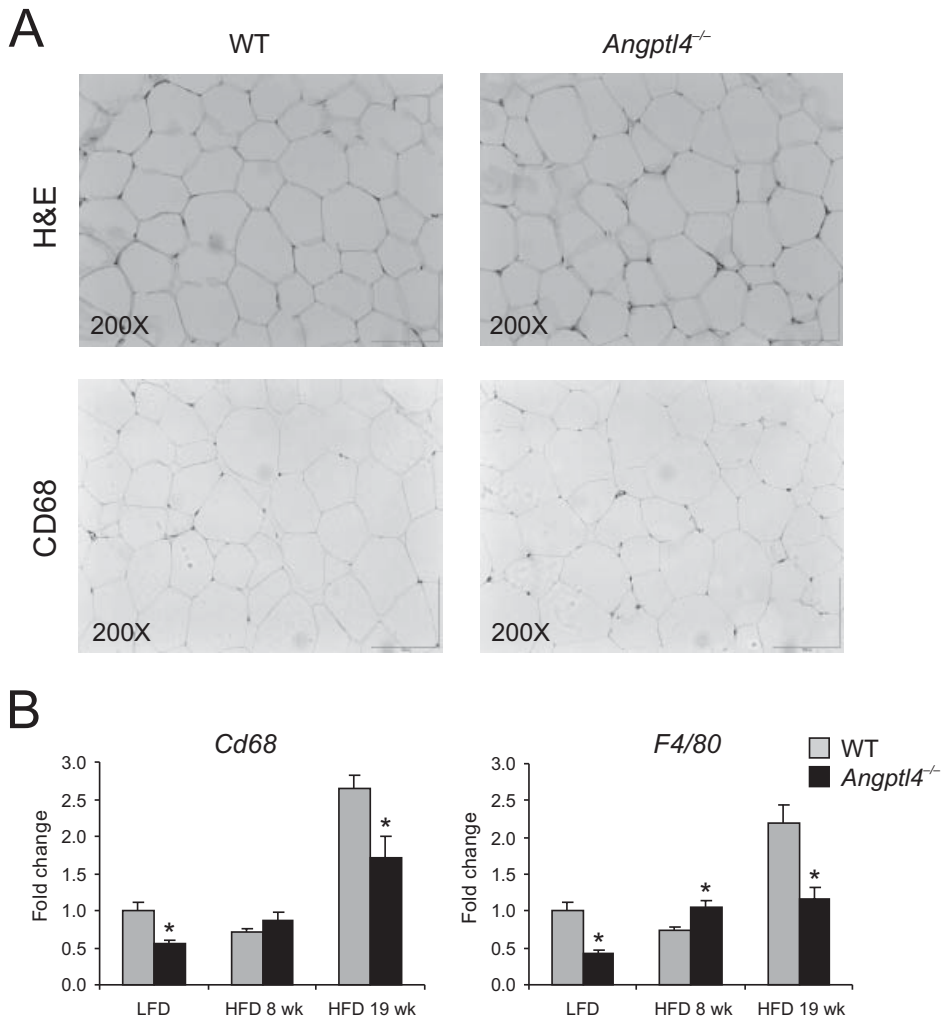
Supplemental Figure 3. Epididymal adipose tissue does not show signs of enhanced inflammation in *Angptl4⁻ᐟ⁻* mice fed HFD

(A) H&E staining and CD68 immunostaining of epididymal adipose tissue of wild-type and *Angptl4⁻ᐟ⁻* fed HFD for 8 weeks. No signs of enhanced macrophage or other leukocyte infiltration were observed. (B) mRNA levels of macrophage marker *Cd68* and *F4/80* in epididymal adipose tissue of wild-type and *Angptl4⁻ᐟ⁻* mice fed LFD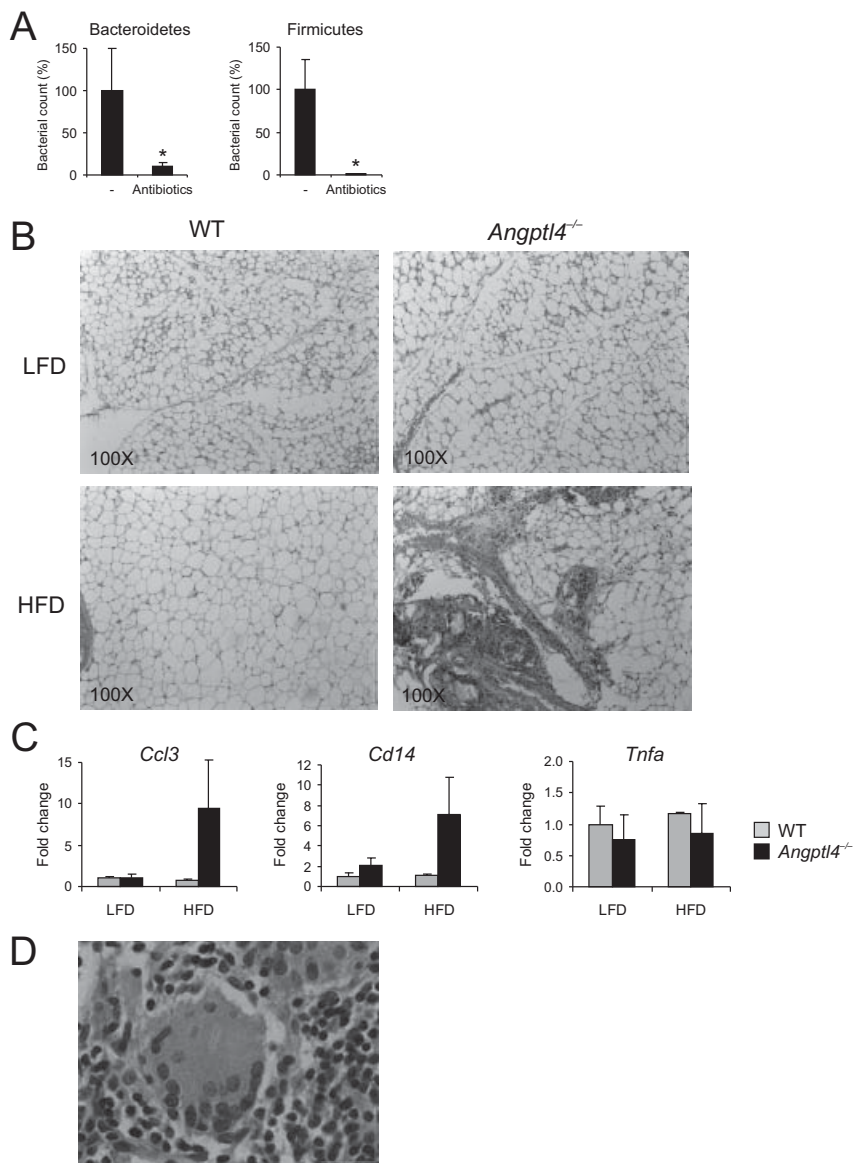 or HFD. * indicates significantly different between wild-type and *Angptl4⁻ᐟ⁻* mice according to Student's *t*-test ($P < 0.05$).

Supplemental Figure 4. Inflammatory changes in *Angptl4*−/− mice fed HFD

(A) Relative abundance of bacterial phyla bacteroidetes and firmicutes per weight of colonic content in *Angptl4*−/− mice fed HFD and given oral antibiotics or vehicle. Error bars represent SEM. * = significantly different between mice given antibiotics or vehicle according to Student's *t*-test (*P* < 0.05).

(B) Mesenteric panniculitis in *Angptl4*−/− mice fed HFD for 5 weeks.

(C) Expression of inflammatory genes in MLNs of wild-type and *Angptl4*−/− mice fed HFD for 24 hours. n = 3 per group. Error bars represent SEM.

(D) High magnification (1000X) image of lipid-laden Touton giant cell in a MLN of an *Angptl4*−/− animal fed HFD for 24 hours.
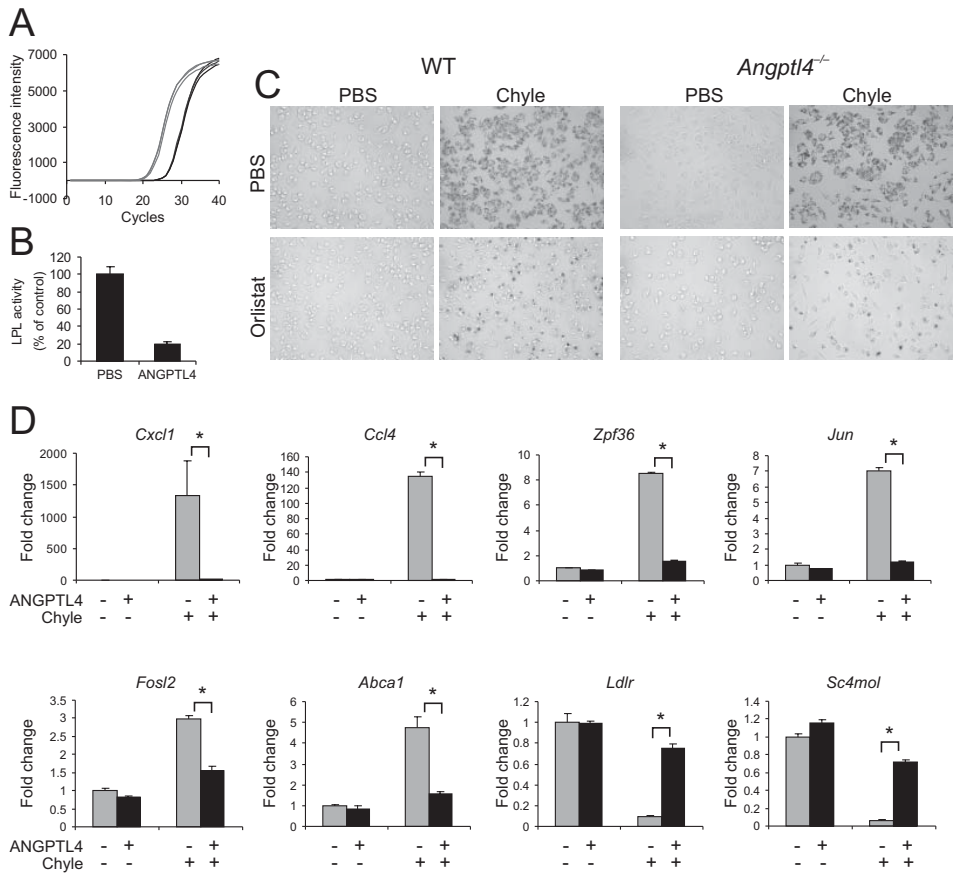
Supplemental Figure 5. The LPL inhibitor Orlistat prevents formation of lipid loaden macrophages

(A) Real-time PCR amplification plot of *Angptl4* in wild-type peritoneal macrophages cultured in the absence of chyle (black lines, triplicates) and the presence of chyle (red lines, triplicates) (6 hours, final triglyceride concentration 2mM).

(B) Heparin-releasable LPL activity in *Angptl4⁻ᐟ⁻* peritoneal macrophages treated with recombinant ANGPTL4 (5 µg/ml)

(C) Oil red O staining of wild-type and *Angptl4⁻ᐟ⁻* peritoneal macrophages incubated for 6 hours with chyle (final triglyceride concentration 2 mM) and/or 20 µM Orlistat. Chyle was collected from rats provided with palm oil-based HFD overnight. Magnification 200X.

(D) qPCR expression of selected genes in *Angptl4⁻ᐟ⁻* macrophages treated with chyle and/or Angptl4 (2.5 µg/ml). * significantly different according to Student's *t*-test ($P < 0.05$).

A   ErmineJ - Gene Ontology (Biological Processes)

Bar chart with categories (top to bottom): sterol biosynthetic process, sterol metabolic process, steroid biosynthetic process, cholesterol biosynthetic process, cholesterol metabolic process, innate immune response, I-kappaB kinase/NF-kappaB cascade, regulation of cytokine production, regulation of T cell proliferation, regulation of interleukin-6 production, regulation of leukocyte proliferation, mismatch repair, regulation of interleukin-6 biosynthetic process, regulation of lymphocyte activation, regulation of leukocyte activation, regulation of B cell differentiation, determination of adult lifespan, purine ribonucleoside metabolic process, positive regulation of protein secretion, immune-regulating cell surface receptor sign. pathway, regulation of protein amino acid phosphorylation, nucleoside bisphosphate metabolic process, negative regulation of DNA recombination. X-axis: -log(P-value), 0 to 10.

B   Ingenuity - Canonical pathways

Bar chart with categories (top to bottom): Pattern Recognition Receptors in Recognition of Bacteria and Viruses, Toll-like Receptor Signaling, p38 MAPK Signaling, IL-10 Signaling, TREM1 Signaling, LXR/RXR Activation, Communication between Innate and Adaptive Immune Cells, HMGB1 Signaling, PDGF Signaling, Cell Cycle: G2/M DNA Damage Checkpoint Regulation, ILK Signaling, NF-κB Signaling, TR/RXR Activation, IL-6 Signaling, NRF2-mediated Oxidative Stress Response, Endoplasmic Reticulum Stress Pathway, Biosynthesis of Steroids, Prolactin Signaling. X-axis: -log(P-value), 0 to 7.

C Chyle LPS

141	68	557

Top 10 genes

|		
Gdf15	Cxcl2	Il1b
Osm	Inhba	Ccl5
Dusp10	Hspa1a	Ifit2
2310016C0	Cxcl1	Cxcl3
Dusp1	Gem	Ifit1
Ankrd33b	Csmp1	Gpr84
Vegfa	Ier3	Tnf
Car6	Ptgs2	Cmpk2
Ptp4a1	Tnfaip6	Rsad2
Trib3	Il1a	Lcn2

3

Supplemental Figure 6. Chyle triggers inflammation in *Angptl4*$^{-/-}$ peritoneal macrophages
(A) Gene Ontology classes (Biological Processes) significantly overrepresented in *Angptl4*$^{-/-}$ mouse peritoneal macrophages treated with chyle (6 hours, triglyceride concentration 2 mM) compared to PBS-treated macrophages. Only GO classes with corrected $P > 0.01$ were included.
(B) Ingenuity Canonical Pathways significantly altered in *Angptl4*$^{-/-}$ mouse peritoneal macrophages treated with chyle (6 hours, triglyceride concentration 2 mM) compared to PBS-treated macrophages. Only Canonical Pathways with $P < 0.001$ were included.
(C) Venn diagram showing overlap in gene regulation by chyle (6 hours, 2 mM triglycerides) and LPS (4 hours, 100 ng/ml) in primary mouse macrophages. Only genes present on both arrays and exceeding the minimal expression threshold (signal intensity >20 on at least one array) were included in the analysis (7517 genes in total). Overlap in gene induction (threshold 2.5-fold) by chyle and LPS was determined. The top 10 of most highly induced genes are shown.
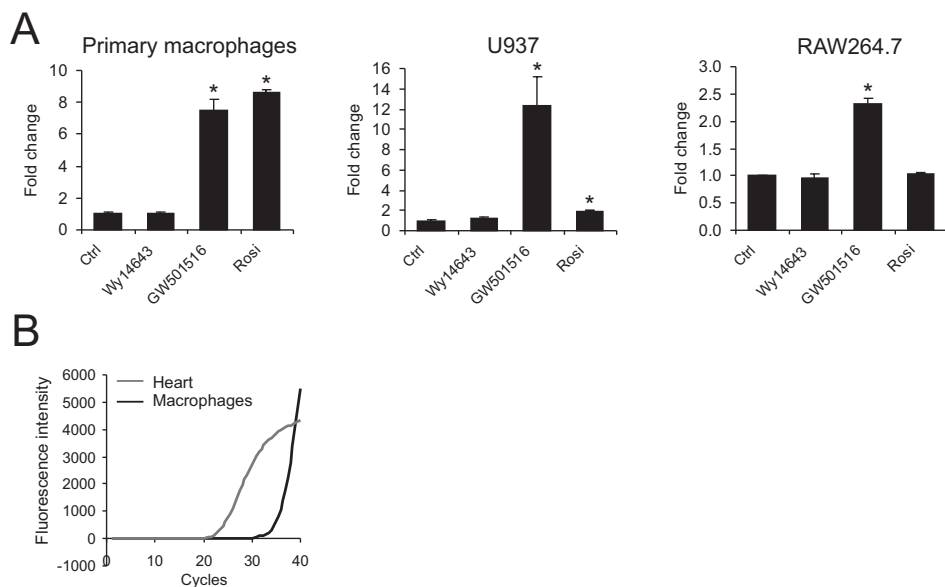
Supplemental Figure 7. Regulation of *Angptl4* and *Gpihbp1* expression in macrophages
(A) Primary wild-type mouse peritoneal macrophages, human U937 and mouse RAW 264.7 macrophages were treated for 6 hours with synthetic agonists of PPARα (Wy14643, 1 μM), PPARβ/δ (GW501516, 0.5 μM) and PPARγ (rosiglitazone, 0.5 μM). *Angptl4* gene expression was determined by qPCR.
(B) cDNA was prepared from whole mouse heart and mouse peritoneal macrophages. Real-time PCR amplification curves of *Gpihbp1* were created using forward primer: ATGGGGCTAACTTGCCTAAGA and reverse primers: CTGAGCAGGGAGGGCTATATTAC.

Supplemental Table 1. Macronutrient and ingredient composition of the various diets

	LFD- palm oil		MFD-palm oil		HFD-palm oil	
Based on formula #	D12450B		D12451		D12451	
	g%	*kcal%*	**g%**	*kcal%*	**g%**	*kcal%*
Protein	19	*20*	21	*20*	24	*20*
Carbohydrate	67	*70*	54	*51.3*	41	*35*
Fat	4	*10*	13	*27.7*	24	*45*
Total		*100*		*100*		*100*
kcal/g	3.8		4.7		4.7	
Ingredient	**g**	*kcal*	**g**	*kcal*	**g**	*kcal*
Casein, lactic	200	*800*	200	*800*	200	*800*
L-Cystine	3	*12*	3	*12*	3	*12*
Corn Starch	427.2	*1709*	247.25	*989*	72.8	*291*
Maltodextrin	100	*400*	100	*400*	100	*400*
Sucrose	172.8	*691*	172.8	*691*	172.8	*691*
Cellulose, BW200	50	*0*	50	*0*	50	*0*
Soybean Oil	25	*225*	25	*225*	25	*225*
Palm oil	20	*180*	100	*900*	177.5	*1598*
Mineral Mix S10026	10	*0*	10	*0*	10	*0*
DiCalcium Phosphate	13	*0*	13	*0*	13	*0*
Calcium Carbonate	5.5	*0*	5.5	*0*	5.5	*0*
Potassium Citrate	16.5	*0*	16.5	*0*	16.5	*0*
Vitamin Mix V10001	10	*40*	10	*40*	10	*40*
Choline Bitartrate	2	*0*	2	*0*	2	*0*
Total (grams)	**1055**	*4057*	**955.1**	*4057*	**858.15**	*4057*

3

Supplemental Table 2A. Fatty acid composition of the various diets expressed as percentage of total fatty acids

% of total FAs	Diet						
	LFD-palm	MFD-palm	HFD-palm	HFD-lard	HFD-safflower	HFD-MCT	AIN93G
8:0	0.0	0.0	0.0	0.0	0.0	52.6	0.0
10:0	0.0	0.0	0.0	0.0	0.0	35.1	0.0
12:0	0.0	0.0	0.0	0.0	0.0	0.0	0.0
14:0	0.5	0.8	0.9	1.3	0.0	0.0	0.1
16:0	25.5	38.0	40.7	23.2	6.5	1.2	10.0
16:1	0.0	0.0	0.0	2.2	0.0	0.0	0.0
18:0	4.0	4.0	4.0	14.5	3.1	0.5	4.0
18:1	30.3	36.5	37.8	40.5	13.3	2.8	22.5
18:2	35.0	19.0	15.5	14.2	75.2	6.8	55.0
18:3	4.2	1.5	0.9	2.7	0.9	0.9	7.5
Other	0.5	0.2	0.1	1.4	1.0	0.1	0.9
Total	**100.0**	**100.0**	**100.0**	**100.0**	**100.0**	**100.0**	**100.0**

Supplemental Table 2B. Fatty acid composition of the various diets expressed as percent by weight

g/100 g feed	Diet						
	LFD-palm	MFD-palm	HFD-palm	HFD-lard	HFD-safflower	HFD-MCT	AIN93G
8:0	0.0	0.0	0.0	0.0	0.0	12.4	0.0
10:0	0.0	0.0	0.0	0.0	0.0	8.3	0.0
12:0	0.0	0.0	0.0	0.0	0.0	0.0	0.0
14:0	0.0	0.1	0.2	0.3	0.0	0.0	0.0
16:0	1.1	5.0	9.6	5.5	1.5	0.3	0.7
16:1	0.0	0.0	0.0	0.5	0.0	0.0	0.0
18:0	0.2	0.5	0.9	3.4	0.7	0.1	0.3
18:1	1.3	4.8	8.9	9.6	3.1	0.7	1.6
18:2	1.5	2.5	3.7	3.4	17.7	1.6	3.9
18:3	0.2	0.2	0.2	0.6	0.2	0.2	0.5
Other	0.0	0.0	0.0	0.3	0.2	0.0	0.1
Total	**4.3**	**13.1**	**23.6**	**23.6**	**23.6**	**23.6**	**7.0**

Supplemental Table 3. Lipoprotein lipase (LPL) is among the most highly expressed genes in mouse peritoneal macrophages

Affymetrix microarray analysis was performed on mouse peritoneal macrophages using mouse Gene 1.0 ST arrays. Arrays were normalized using the Robust Multi-array Average method. Genes were ranked according to expression signal.

Rank	Expression signal	Gene symbol	Gene name
1	9618	Apoe	apolipoprotein E
2	9178	Ctsd	cathepsin D
3	8976	Psap	prosaposin
4	8411	Gpnmb	glycoprotein (transmembrane) nmb
5	8096	Fth1	ferritin heavy chain 1
6	8055	Ctss	cathepsin S
7	7977	Lyz2	lysozyme 2
8	7898	Eef1a1	eukaryotic translation elongation factor 1 alpha 1
9	7601	Actb	actin, beta
10	7423	Ctsb	cathepsin B
11	7396	Spp1	secreted phosphoprotein 1
12	7354	Mmp12	matrix metallopeptidase 12
13	6916	Ctsz	cathepsin Z
14	6786	Cd68	CD68 antigen
15	6387	Ctsl	cathepsin L
16	6371	Cd36	CD36 antigen
17	6340	Gm13882	glyceraldehyde-3-phosphate dehydrogenase pseudogene
18	6235	Cst3	cystatin C
19	5908	Txn1	thioredoxin 1
20	5813	Lpl	lipoprotein lipase
21	5810	Lgals3	lectin, galactose binding, soluble 3
22	5795	Akr1a4	aldo-keto reductase family 1, member A4 (aldehyde reductase)
23	5759	Cybb	cytochrome b-245, beta polypeptide
24	5467	Vim	vimentin
25	5464	Lipa	lysosomal acid lipase A

3

4

ANGPTL4 serves as an endogenous inhibitor of intestinal lipid digestion

F Mattijssen, S Alex, HJ Swarts, AK Groen,
EM van Schothorst, S Kersten

Abstract

Dietary triglycerides are hydrolyzed in the small intestine principally by pancreatic lipase. Following uptake by enterocytes and secretion as chylomicrons, dietary lipids are cleared from the bloodstream via lipoprotein lipase. Whereas lipoprotein lipase is inhibited by several proteins including Angiopoietin-like 4 (ANGPTL4), no endogenous regulator of pancreatic lipase has yet been identified. Here we present evidence that ANGPTL4 is an endogenous inhibitor of dietary lipid digestion. $Angptl4^{-/-}$ mice were heavier compared to their wild-type counterparts without any difference in food intake, energy expenditure or locomotor activity. However, $Angptl4^{-/-}$ mice showed decreased lipid content in the stools and increased accumulation of dietary triglycerides in the small intestine, which coincided with elevated luminal lipase activity in $Angptl4^{-/-}$ mice. Furthermore, recombinant ANGPTL4 reduced the activity of pancreatic lipase as well as the lipase activity in human ileostomy output. In conclusion, our data suggest that ANGPTL4 is an endogenous inhibitor of intestinal lipase activity.

Introduction

Dietary triglycerides (TGs) contribute a major portion of our daily energy requirement. TGs are digested in the gastrointestinal tract through the action of several lipases including lingual lipase and gastric lipase (1, 2). However, the far majority of dietary TGs are digested in the small intestine by pancreatic lipase (PL) assisted by pancreatic colipase, pancreatic lipase-related protein 2, and carboxyl ester lipase (3, 4). To increase the accessibility of PL to dietary TGs at the oil-water interphase, dietary lipids are emulsified by the action of bile acids, which are produced in the liver, stored in the gallbladder, and subsequently released upon ingestion of a high-fat meal (2, 5). The resulting mono-acylglycerol and free fatty acids are taken up by enterocytes and resynthesized into TGs, followed by the lipidation of apolipoproteins to yield chylomicrons that are subsequently secreted into the lacteals (6-8). After traveling through the splanchnic lymphatic system and the thoracic duct, chylomicrons are released into the blood stream and ultimately reach the heart, skeletal muscle and adipose tissue as their primary target organs.

Clearance of circulating chylomicrons is mediated by lipoprotein lipase (LPL), which is anchored to the capillary endothelium via the protein GPIHBP1 (9-11). LPL catalyzes the hydrolysis of TGs to free fatty acids, which are taken up by the parenchymal cells to serve as energy source, building blocks for membranes, or to be used for storage. LPL is thought to function as an active homodimer and its activity in tissues is profoundly influenced by various physiological stimuli, including nutritional status, exercise and cold (9). In the last decade it has become evident that the activity of LPL is carefully controlled by three proteins belonging to the Angiopoietin-like protein family: ANGPTL3, ANGPTL4, and ANGPTL8 (12, 13). All three proteins have been shown to inhibit LPL activity in vitro and in vivo and accordingly raise circulating TG levels (12, 14, 15). ANGPTL3 is produced primarily by the liver and its expression is regulated by the Liver X Receptor (16, 17). ANGPTL8, a paralog of ANGPTL3, was recently identified as the latest member of the ANGPTL family (13). Deletion of ANGPTL8 results in decreased plasma TG levels due to decreased hepatic VLDL production and elevated LPL activity (14). ANGPTL4 has previously been shown to potently inhibit LPL in several tissues and cells under a variety of circumstances. Indeed, we and others have identified ANGPTL4 as an important regulator of LPL in adipose tissue, heart, and macrophages (18-22). ANGPTL4 forms higher order oligomers and is subject to proteolytic cleavage to yield C- as well as N-terminal ANGPTL4. The precise mechanism by which ANGPTL4 inhibits LPL as well as the localization of the inhibitory effect are not fully understood. It was reported that ANGPTL4 inhibits LPL by promoting the irreversible conversion of active homodimeric

units into inactive monomers (23), whereas recent data suggest that ANGPTL4 functions as a reversible noncompetitive inhibitor of LPL (24). The expression of *Angptl4* is governed by a multitude of dietary and hormonal cues including fatty acids and glucocorticoids via peroxisome proliferator-activated receptors (PPARs) and glucocorticoid receptor (GR), respectively (25-27).

LPL is part of the same family of extracellular lipases as PL, which also include endothelial lipase and hepatic lipase (28). However, little is known about regulation of the activity of PL. Here we report that ANGPTL4 reduces intestinal lipase activity by inhibition of PL. As a result, *Angptl4*$^{-/-}$ animals harvest more lipids from ingested food resulting in increased fat mass and body weight.

Results

ANGPTL4 deletion leads to increased bodyweight independent of food intake, energy intake, or locomotor activity

We observed that chow-fed *Angptl4*$^{-/-}$ mice have a significantly higher bodyweight than age-matched wild-type mice (Figure 1A). Body composition analysis by DEXA indicated that the difference in body weight can be attributed to a higher amount of body fat (Figure 1B). In contrast, no difference in lean mass was observed between the two sets of mice, which was supported by the weight of major organs including liver, heart, and various muscles (Supplemental Figures 1A-1F). Also, no differences in food intake could be recorded (Figure 1C). Supporting a role of ANGPTL4 in dietary fat-induced weight gain, *Angptl4*$^{-/-}$ mice gained weight much faster compared to wild-type mice when switched to a high fat diet (Figure 1D), which again was independent of food intake (Figure 1E).

A difference in body weight can be explained by several mechanisms including differences in locomotor activity and/or energy expenditure. To explore these options we determined the total energy balance of wild-type and *Angptl4*$^{-/-}$ mice using indirect calorimetry. For 1 week prior to and during the measurements the mice were given access to HFD. The metabolic phenotyping revealed no differences in food intake (Figures 2A and 2B) and energy expenditure (Figures 2C and 2D), which was confirmed with ANCOVA analysis. Respiratory exchange ratios for wild-type and *Angptl4*$^{-/-}$ animals were equal at 0.85, indicative of the combustion of a mixture of fat and carbohydrates (Figure 2E). Moreover, locomotor activity did not differ between wild-type and *Angptl4*$^{-/-}$ animals (Figure 2F). These data indicate that the enhanced fat mass in *Angptl4*$^{-/-}$ mice is not due to increased food intake or decreased energy expenditure.
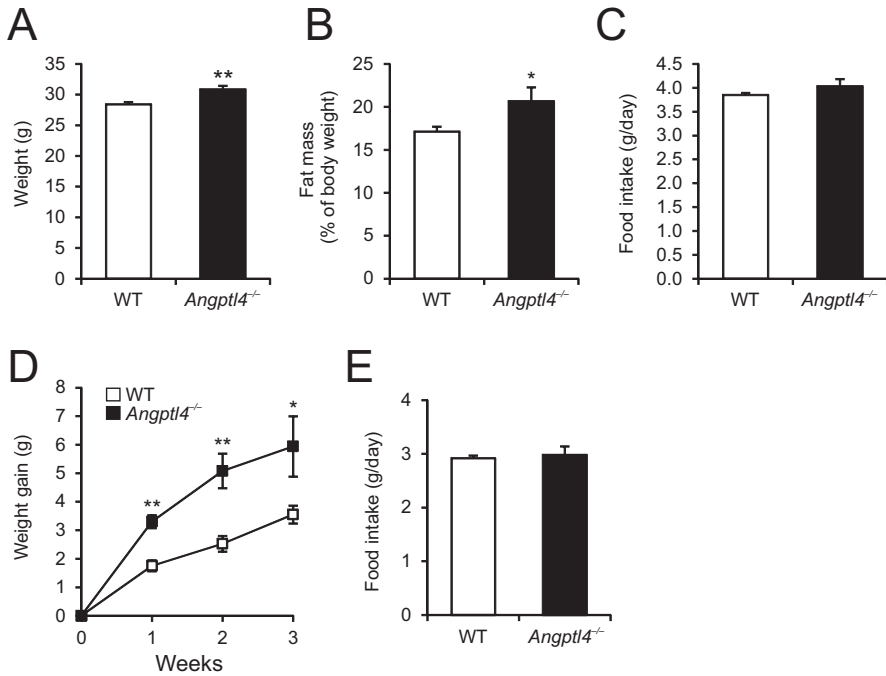
Figure 1. *Angptl4*⁻/⁻ **mice are heavier despite equal food intake**
(A-D) Body weight (A), fat mass as determined with DEXA scan (B), average food intake per day over a 2-week period (C) of wild-type and *Angptl4*⁻/⁻ mice on a standard chow diet (n = 10-11 per group). (D and E) Body weight development (D) and food intake (E) of wild-type and *Angptl4*⁻/⁻ mice after a switch to HFD (n = 4-5 per group).
Data are mean ± SEM. Asterisks indicate significant differences according to Student's *t*-test; *$P < 0.05$, **$P < 0.01$.

4

To examine if lipid absorption is elevated in *Angptl4*⁻/⁻ mice, we determined the amount of fat in the feces in mice fed low fat diet or high fat diet. Strikingly, the amount of fat in the feces was significantly lower in *Angptl4*⁻/⁻ mice as compared to wild-type mice (Figure 2G), indicating enhanced lipid absorption. Thus, the data suggest that *Angptl4*⁻/⁻ mice harvest more lipids from the ingested food, pointing to the intestine as a key site of ANGPTL4 action.

Although ANGPTL4 is known to be produced by a number of intestinal cell lines (29, 30), little is known about intestinal ANGPTL4 expression in vivo. In mouse small intestine, *Angptl4* mRNA levels were highest at the top of the villi and lowest in the crypts (Figure 3A). Expression of *Angptl4* did not vary much along the longitudinal axis of the murine
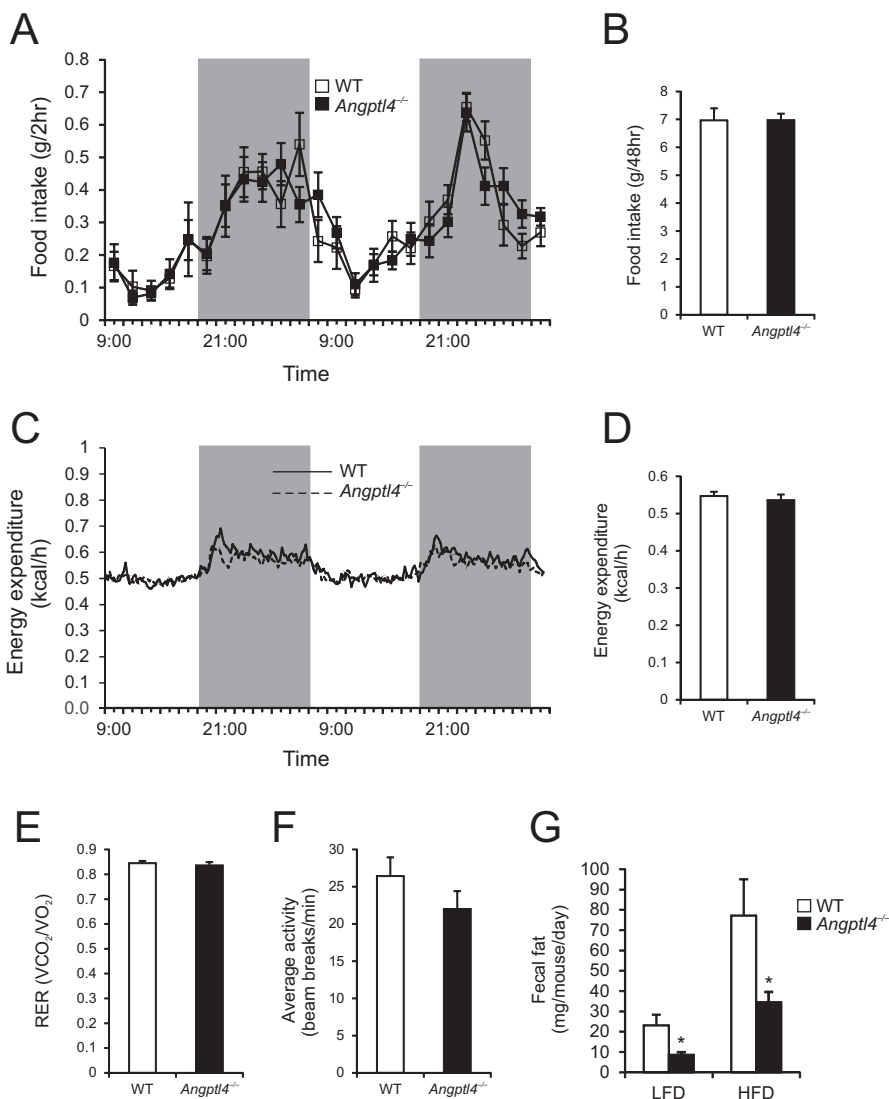
Figure 2. Metabolic phenotyping reveals no differences in energy expenditure, food intake or locomotor activity between wild-type and *Angptl4*−/− mice

(A and B) Food intake per 2 hours (A) or accumulated over 2 days (B) of wild-type and *Angptl4*−/− mice on a 45en% HFD diet (n = 11-12 per group).

(C) Energy expenditure as determined every 13 minutes over the course of 2 days (n = 11-12 per group)

(D) Average energy expenditure over 2 days of wild-type and *Angptl4*−/− animals (n = 11-12 per group)

(E) RER of wild-type and *Angptl4*−/− animals (n = 11-12 per group).

(F) Locomotor activity of wild-type and *Angptl4*−/− animals (n = 7-8 group).

(G) Fecal fat content in wild-type and *Angptl4*−/− mice after a 3-week HFD intervention (n = 4-5 group). Data are mean ± SEM. Asterisk indicates significant differences according to two-way ANOVA with Bonferroni post-hoc test; *$P < 0.05$.
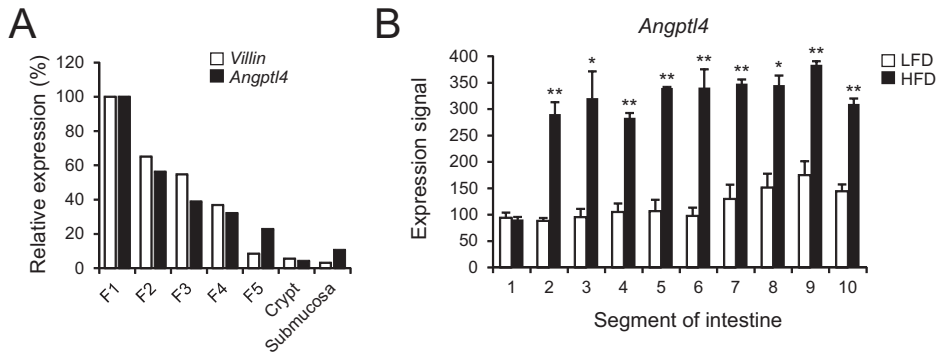
Figure 3. Increased intestinal *Angptl4* mRNA expression after a HFD intervention
(A) *Villin* and *Angptl4* expression in isolated epithelial fractions enriched for villi (n = 2).
(B) *Angptl4* expression in 10 parts of the small intestine after 2 weeks HFD intervention, determined with Affymetrix Microarray (n = 3).
Data are mean ± SEM. Asterisks indicate significant differences according to Student's *t*-test; *$P < 0.05$, **$P < 0.01$.

small intestine (Figure 3B). Interestingly, except in the most proximal portion of the small intestine, *Angptl4* mRNA levels were 2-3 fold elevated by high fat feeding (Figure 3B).

To explore the possible cause for the increased harvesting of dietary fat we carried out a lipid absorption test via oral dosing of ³H-triolein. No difference was observed in the rate of appearance of ³H-tracer in the circulation between wild-type and *Angptl4*⁻/⁻ mice (Figure 4A), indicating that chylomicron synthesis and secretion, which are rate-limiting for dietary TG entry into the blood, are not different between the two sets of mice. However, a significant increase in tracer abundance was observed in small intestinal tissue of *Angptl4*⁻/⁻ mice (Figure 4B), suggesting a higher rate of fatty acid uptake and possibly digestion. This finding was confirmed by higher TG levels in small intestine of *Angptl4*⁻/⁻ mice after a 1-day HFD intervention (Figure 4C). In accordance with activation of the lipid-sensitive transcription factor PPARα by dietary fat, HFD or lipid gavage caused marked induction of numerous PPARα target genes in the small intestine. Consistent with enhanced lipid uptake in *Angptl4*⁻/⁻ mice, induction of PPARα targets by HFD or lipid gavage was markedly augmented in *Angptl4*⁻/⁻ mice in comparison with wild-type mice (Figures 5A and 5B). These data suggest that ANGPTL4 regulates the amount of luminal TG entering the enterocytes while having no effect on the amount of TG released from the intestine into the circulation.
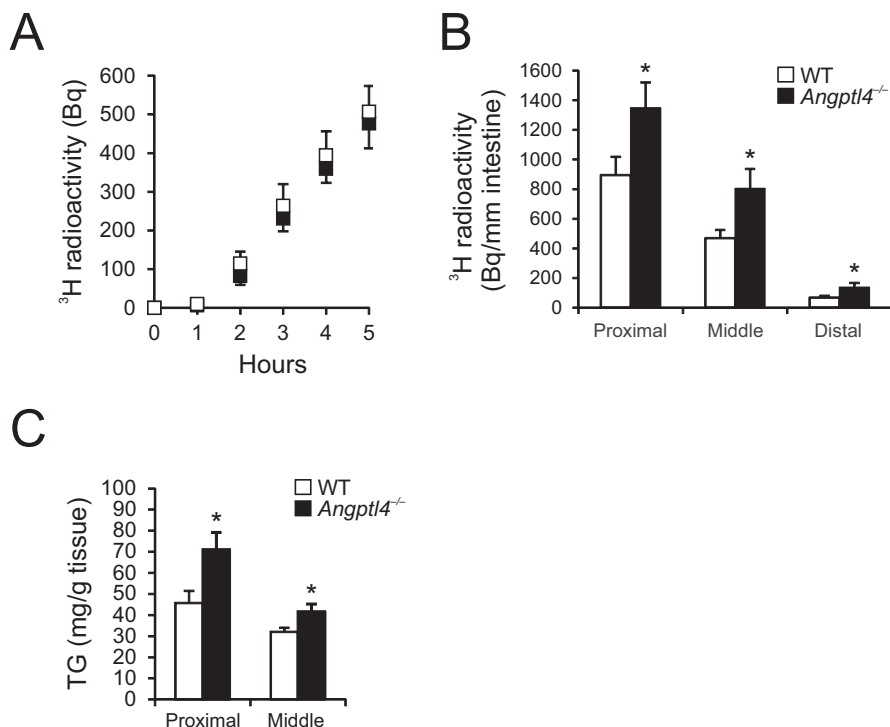
Figure 4. *Angptl4*^{−/−} mice accumulate fat in their intestine
(A and B) ³H-triolein appearance in plasma (A) and intestine (B) after gavage with ³H-triolein in fasted wild-type and *Angptl4*⁻/⁻ mice (n = 8-10 per group).
(C) Triglyceride content of wild-type and *Angptl4*⁻/⁻ intestine after one day HFD intervention (n = 6-7 per group).
Data are mean ± SEM. Asterisk indicates significant differences according to Student's *t*-test; *P < 0.05.

Increased lipid digestion in Angptl4⁻/⁻ mice is independent of intestinal length, gastrointestinal transit time, and bile acid secretion or composition

An increase in intestinal lipid uptake might be explained by several factors, including a decrease in gastrointestinal (GI) transit time, allowing more time for lipases to digest dietary TGs and causing a higher overall rate of lipid digestion. To explore this possibility we fed overnight fasted mice a semi-synthetic diet colored with Fast Green FCF and recorded the time until arrival of the first dropping. No difference was observed in GI transit time between wild-type and *Angptl4*⁻/⁻ mice (Figure 6A). In addition, total length of the small intestinal was unchanged between wild-type and *Angptl4*⁻/⁻ mice (Figure 6B).
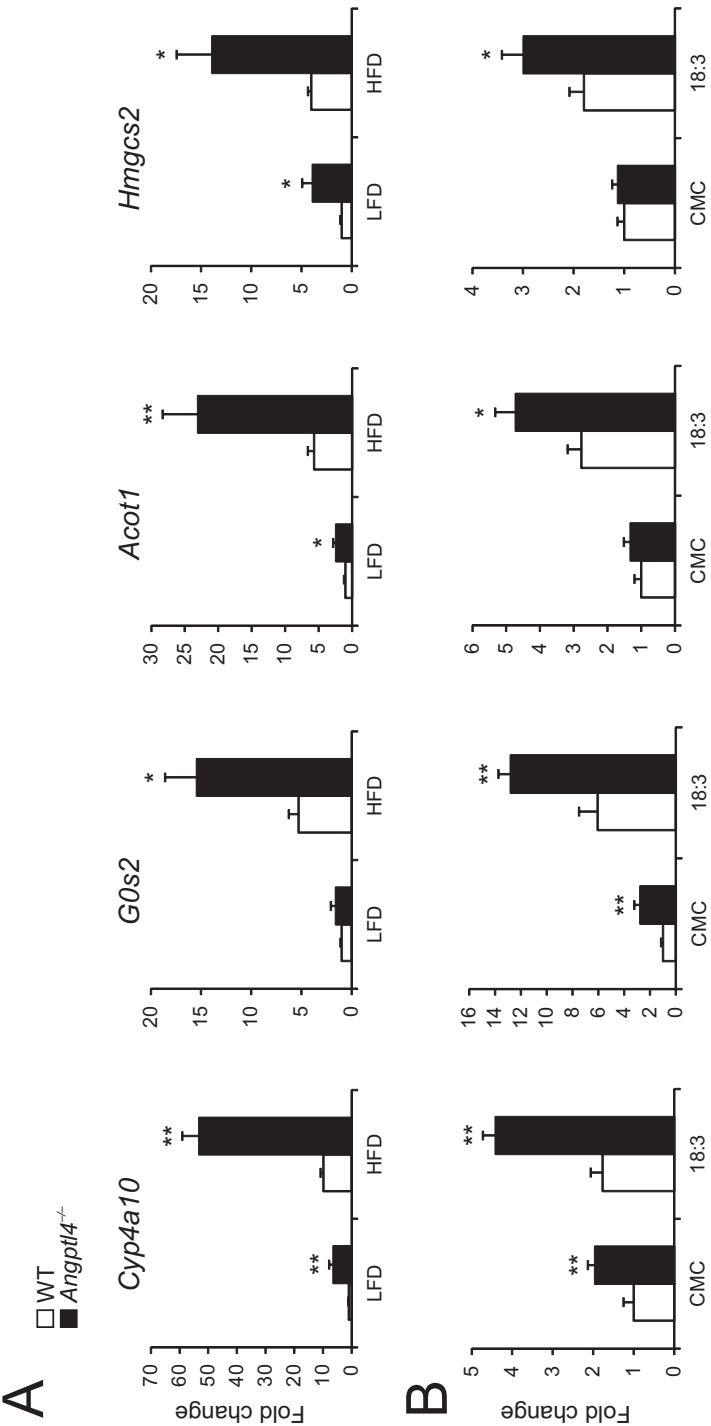
Figure 5. Expression of PPARα target genes is increased in *Angptl4−/−* mice intestine

(A and B) Expression of selected PPARα targets in the proximal part of the small intestine after a 6-week HFD intervention (A, n = 6-7 per group) or oral gavage with 0.5% carboxymethyl cellulose (CMC) or C18:3 TGs (B, n = 5-6 per group) in wild-type and *Angptl4−/−* mice.

Data are mean ± SEM. Asterisks indicate significant differences according to two-way ANOVA with Bonferroni post-hoc test; *P < 0.05, **P < 0.01.

4

Bile acids play an important role in lipid digestion by emulsifying lipids and thereby allowing for increased efficiency of lipid harvesting. Hence, a difference in the composition or in the total amount of bile acids may contribute to increased lipid uptake. We found no difference in the fecal amount of cholic- or deoxycholic acid (Figure 6C), nor in the amount of primary-, secondary-, or total bile acids between wild-type and *Angptl4*$^{-/-}$ mice (Figure 6D and E). Together, these observations indicate that enhanced lipid uptake in intestine of *Angptl4*$^{-/-}$ mice is unrelated to changes in intestinal transit time, intestinal length or bile acid composition/secretion.

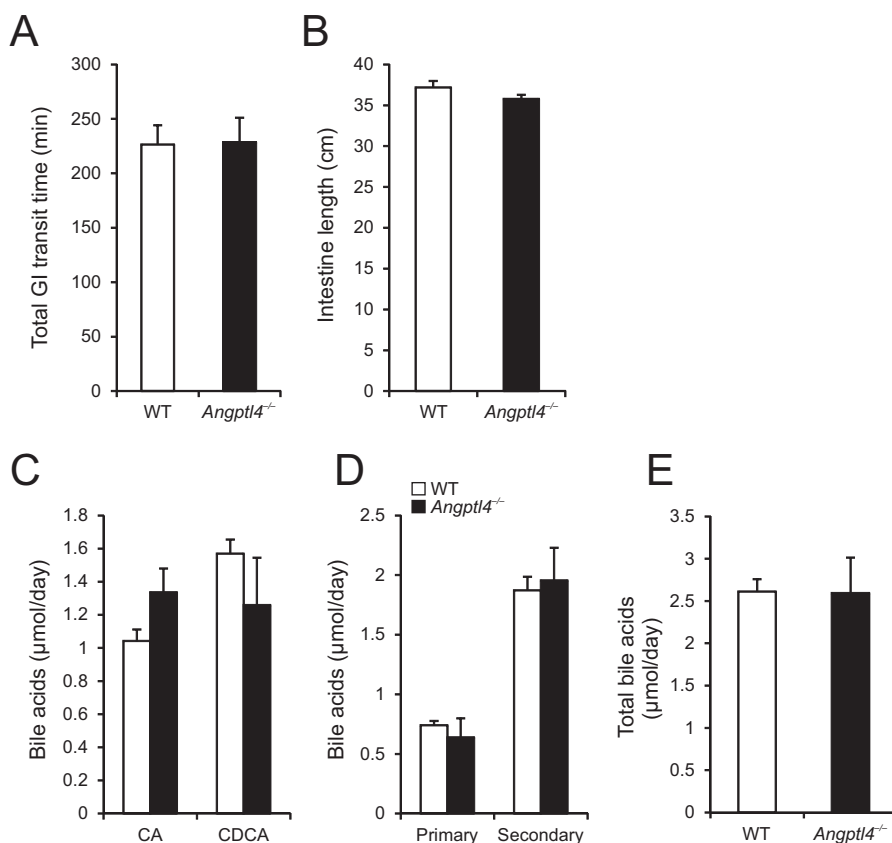**Figure 6. Increased lipid uptake in *Angptl4*$^{-/-}$ mice is independent of transit time or bile acid secretion**

(A and B) GI transit time (A) and intestinal length (B) of wild-type and *Angptl4*$^{-/-}$ mice (n = 8-9 per group). (C-E) Fecal bile acids in wild-type and *Angptl4*$^{-/-}$ mice expressed as CA vs. CDCA (C), primary vs. secondary (D), or total (E) bile acids (n = 8-9 per group).

Data are mean ± SEM.

ANGPTL4 inhibits pancreatic lipase

ANGPTL4 serves as an endogenous inhibitor of LPL and there is evidence that it inhibits hepatic lipase as well (31). Since PL, which serves as the principal intestinal lipase, belongs to the same family of extra-cellular lipases, we asked whether increased lipid uptake in *Angptl4*$^{-/-}$ mice may be explained by enhanced lipid digestion due to a lack of ANGPTL4-mediated inhibition of intestinal lipase activity. To test this hypothesis we collected the luminal content from (refed) wild-type and *Angptl4*$^{-/-}$ mice and assayed fecal water for lipase activity. Consistent with our hypothesis, *Angptl4*$^{-/-}$ mice had a significantly higher luminal lipase activity in comparison to wild-type mice (Figure 7A).

Inasmuch as PL is responsible for the major portion of intestinal lipase activity, we determined the direct effect of ANGPTL4 on PL by assaying the activity of recombinant PL in the presence of increasing amounts of recombinant ANGPTL4. As shown in Figure 7B, ANGPTL4 inhibited PL activity in a dose-dependent manner. To extend these findings we collected ileostomy output from three otherwise healthy humans. Similar to mouse intestinal content, human material contained high lipase activity, which was repressed by the PL inhibitor Orlistat (Figure 7C). Importantly, adding recombinant human ANGPTL4 significantly decreased the luminal lipase activity (Figure 7C). Together, these data indicate that ANGPTL4 inhibits intestinal lipase activity.
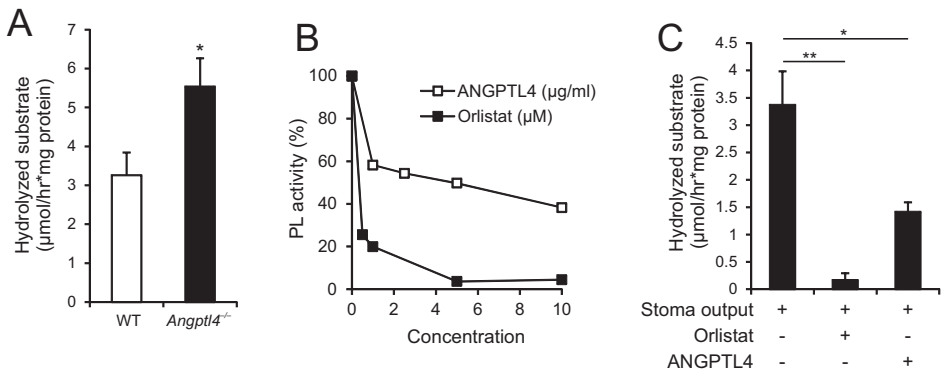

Figure 7. ANGPTL4 inhibits pancreatic lipase

(A) Luminal lipase activity in fecal water derived from wild-type and *Angptl4*$^{-/-}$ mice (n = 9 per group).

(B) Recombinant PL activity in the presence of increasing concentrations of Orlistat or recombinant ANGPTL4.

(C) Lipase activity in stoma output of human volunteers in the absence or presence of Orlistat 25 µM) or recombinant human ANGPTL4 (10 µg/ml) (n = 3).

Data are mean ± SEM. Asterisks indicate significant differences according to Student's *t*-test (A) or one-way ANOVA with Tukey's post-hoc test (C); *$P < 0.05$, **$P < 0.01$.

Discussion

Our results indicate that ANGPTL4 serves as an endogenous inhibitor of dietary lipid digestion via inhibition of PL, reducing the amount of energy that is harvested from dietary fat. As a result, mice lacking *Angptl4* have less fat in their feces and gain more weight over time. Loss of ANGPTL4 does not appear to have any effect on energy expenditure or food intake. A key question elicited by our study is: what is the physiological relevance of an endogenous intestinal lipase inhibitor, production of which is increased by dietary fat? It is generally accepted that chylomicron secretion is rate limiting for lipid absorption, as evidenced by the constant rate of TG entry into the blood during an oral lipid loading test. Following consumption of a copious fat-rich meal, absence of any regulation on TG digestion may be expected to lead to excess fatty acid uptake into enterocytes, exceeding the capacity for re-esterification and chylomicron secretion and thus leading to lipid overload. To avoid such a scenario, production of ANGPTL4 is quickly stimulated upon entry of dietary fatty acids into enterocytes, putting a brake on dietary TG digestion. We propose that ANGPTL4 is an essential component of a feedback mechanism aimed at matching lipid uptake into enterocytes to the capacity for TG secretion. Previously, a similar role for ANGPTL4 in protection against lipid overload was demonstrated in cardiomyocytes and macrophages (19, 20).

The mechanism by which ANGPTL4 inhibits PL at the biochemical level requires further investigation. While we present a compelling case for direct inhibition of PL by ANGPTL4 as the underlying mechanism accounting for enhanced fat uptake in *Angptl4*$^{-/-}$ mice, we cannot completely exclude a potential effect of *Angptl4* deletion on total PL secretion. Indeed, an increase in PL secretion in *Angptl4*$^{-/-}$ mice would lead to increased lipid uptake and decreased fat secretion in the stools. However, recombinant ANGPTL4 was able to inhibit pancreatic lipase, pointing to a direct effect on PL. Since PL does not function as a homodimer, ANGPTL4 cannot inhibit PL by promoting the irreversible dimer to monomer conversion, as has been proposed for LPL (23). Interestingly, recent data suggest that ANGPTL4 may reversibly inhibit LPL independent of dimer dissociation by forming an inhibitory complex with LPL that regains lipase activity upon dissociation (24). It can be hypothesized that a similar mechanism may underlie inhibition of PL by ANGPTL4. It should be noted that ANGPTL4 was able to inhibit PL in the absence of colipase, and we therefore believe it is unlikely that the inhibitory effect is attributable to interference of the interaction between PL and colipase. Although the ANGPTL4 concentrations required for in vitro PL inhibition were relatively high, in vitro inhibition of LPL by ANGPTL4 under similar conditions also requires relatively high concentrations of ANGPTL4, yet there

is unequivocal evidence that ANGPTL4 serves as physiological inhibitor of LPL in vivo (18, 23, 32). It can be hypothesized that the high concentrations of ANGPTL4 required for in vitro LPL and PL inhibition may be related to absence of specific factors that shift the dose response curve.

Whereas numerous exogenous intestinal lipase inhibitors have been characterized, mainly representing plant derived components such as saponins, polyphenols, and terpenes (33, 34), to our knowledge we have identified the first endogenous inhibitor of PL. Interestingly, several endogenous inhibitors of the major protein digestive enzymes including trypsin and chemotrypsin have been described (35, 36). Although the majority is thought to function in the pancreas to prevent premature activation of zymogens (35), expression of some of these inhibitors is found in the intestine (37, 38), suggesting a role in controlling luminal protease activity.

In recent years, the gut microbiota has received much attention as alleged critical contributor to weight gain and obesity (39, 40). In this context, a role of ANGPTL4 in linking gut microbiota to fat storage has been proposed. Specifically, introducing microbiota into germ-free mice or zebrafish was found to markedly reduce intestinal *Angptl4* expression (41, 42). Furthermore, whereas wild-type and *Angptl4*$^{-/-}$ mice have similar amounts of body fat on a germ-free background, introducing microbiota leads to a much smaller increase in body fat in *Angptl4*$^{-/-}$ mice compared to wild-type mice, suggesting that microbial suppression of ANGPTL4 contributes to increased fat deposition. Suppression of ANGPTL4 was suggested to promote fat storage by loss of inhibition of LPL activity in adipose tissue and reduction in expression of Pgc1α and fatty acid oxidation enzymes in liver and skeletal muscle (43). Based on our data, it can be envisaged that microbial suppression of ANGPTL4 may also promote weight gain via loss of local action of ANGPTL4 in the gut, leading to elevated intestinal lipase activity and increased harvesting of dietary TGs. In apparent conflict with the decrease in *Angptl4* expression upon colonization of germ-free animals, recent data suggest that short-chain fatty acids derived from microbial fermentation of dietary fibers induce *Angptl4* expression in intestinal cells via PPARγ (29). Although most of the short-chain fatty acids are produced in the colon, relatively high concentrations are also found in the small intestine (29). It can be speculated that induction of ANGPTL4 may play a role in mediating the repressive effect of dietary fibers on lipid absorption (44, 45). ANGPTL4 undergoes cleavage to form N-terminal and C-terminal ANGPTL4 fragments. Recently, we found that C-terminal ANGPTL4, which is unable to inhibit lipase activity, is produced by entero-endocrine cells in human intestine, suggesting secretion towards the bloodstream (46). We hypothesize that N-terminal ANGPTL4, which is able to inhibit lipase activity, is released selectively by

4

enterocytes towards the lumen to inhibit PL. Future experiments will have to clarify both the exact site of N-terminal ANGPTL4 production as well as its presence in the lumen.

We have previously shown that *Angptl4*$^{-/-}$ mice develop a progressive and ultimately lethal inflammatory condition when chronically fed a HFD containing mainly saturated fatty acids (19). However, it is highly unlikely that the enhanced intestinal lipid uptake in *Angptl4*$^{-/-}$ mice is related to underlying inflammatory processes, as enhanced weight gain is already apparent on a LFD and becomes more pronounced very quickly upon shifting to a HFD. Furthermore, the effect of ANGPTL4 on luminal lipase activity is apparent in mice fed a LFD or with tests that last only a few hours.

Recently, Kim and colleagues postulated that *Angptl4* deletion leads to increased body weight due to an inhibitory effect of ANGPTL4 on hypothalamic AMPK and a subsequent increase in energy expenditure (47). In our study we were unable to find a difference in energy expenditure when comparing wild-type and *Angptl4*$^{-/-}$ mice after 1 week acclimatization to HFD, when the difference in weight gain between the two sets of mice is the most pronounced. Additionally, Kim and colleagues found that *Angptl4*$^{-/-}$ mice have increased food intake during fasting-refeeding, but not under ad libitum conditions (47). Similarly, we have never observed any differences in food intake between ad libitum-fed wild-type and *Angptl4*$^{-/-}$ mice, either on chow diet, semi-synthetic LFD or a HFD. Interestingly, the *Angptl4*$^{-/-}$ mice employed in the studies by Kim et al. were resistant to diet induced obesity, while we have found several times that mice lacking *Angptl4* gain more weight on a HFD, at least during the first 2 months. A potential explanation for the difference is that the development of the previously reported dietary saturated fat-induced inflammation in *Angptl4*$^{-/-}$ mice was greatly accelerated in the study by Kim and colleagues due to extremely high saturated fat content of the diet, leading to reduced food intake as described previously (19).

Collectively, we describe a novel function of ANGPTL4 in the regulation of lipid metabolism. By acting as a gatekeeper in the regulation of intestinal lipid uptake, ANGPTL4 decreases the amount of lipid being harvested from the ingested food and protects against enterocyte lipid overload.

Methods

Animal studies

Animals used for all experiments were pure-bred male wild-type and *Angptl4*$^{-/-}$ animals on a C57BL/6 background (48). Body composition was determined by DEXA (Lunar, PIXImus) on chow-fed 24 weeks old wild-type and *Angptl4*$^{-/-}$ mice. Food intake was recorded over a 2-week period. Animals were sacrificed by cervical dislocation after being anesthetized using isoflurane and several organs were excised.

Eleven-week-old wild-type and *Angptl4*⁻ᐟ⁻ animals were given access to HFD providing 45en% fat (D12451, Research Diets Services, Wijk bij Duurstede, The Netherlands). Food intake and body weight were recorded weekly for a period of 3 weeks.

Wild-type and *Angptl4*⁻ᐟ⁻ animals (28 weeks old) were analyzed in an open-circuit LabMaster Metabolism Research Platform (TSE systems GmbH, Bad Homburg, Germany) as described previously (49), with minor adaptations. Animals were acclimatized for 24 hours followed by 48-hour measurements. Eight of the 12 cages were also equipped for locomotor activity measurements. Body composition analysis (Echo-MRI, Houston, USA) was performed immediately before and after the indirect calorimetric analyses, which showed similar lean mass between wild-type and *Angptl4*⁻ᐟ⁻ mice. One week before the actual metabolic phenotyping, the animals were switched to HFD. During the analysis, mice were kept on the same HFD. Fecal fat was extracted from feces of 11-week-old wild-type and *Angptl4*⁻ᐟ⁻ animals after a 3-week HFD intervention using published methods (50). Fatty acids were subsequently measured using an enzymatic assay (NEFA-HR(2), Wako Chemicals, Neuss, Germany).

Intestinal lipid absorption tests were performed using ³H-labeled triolein according to published methods (51). For determination of intestinal TG content, wild-type and *Angptl4*⁻ᐟ⁻ animals were fed a HFD for 24 hours after a 1-week run in with LFD. Mice were killed by cervical dislocation and the small intestine was collected, washed with ice-cold PBS and snap frozen. Samples were homogenized in sucrose buffer (10 mM Tris, 2 mM EDTA, 0.25 M sucrose, pH 7.5) with a Qiagen TissueLyser II (Qiagen, Hilden, Germany) and subsequently analyzed for TGs using a Triglycerides liquicolor^mono kit (HUMAN, Wiesbaden, Germany).

qPCR analysis of PPARα target genes was performed in proximal small intestine of 10- to 15-week-old wild-type and *Angptl4*⁻ᐟ⁻ mice fed LFD or a safflower oil-based HFD for 6 weeks. qPCR analysis of PPARα target genes was also performed on small intestine of 4-months-old wild-type and *Angptl4*⁻ᐟ⁻ animals fasted for 4 hours and subsequently intragastrically gavaged with 400 μl carboxymethyl cellulose (CMC) or synthetic trilinolenin. Proximal small intestines were excised, washed with ice-cold PBS, and subsequently snap frozen in liquid nitrogen.

To assess intestinal transit time, wild-type and *Angptl4*⁻ᐟ⁻ mice (16 weeks old) were fed AIN-93W low fat semi-purified diet (Research Diets Services, Wijk bij Duurstede, Netherlands) for 3 days prior to the experiment. Next, the mice were fasted for 16 hours and subsequently given access to AIN-93W diet which was colored with 60 mg/kg Fast Green FCF (Sigma-Aldrich, Schnelldorf, Germany). The time until the first green dropping appeared was recorded. Feces from 12- to 15-week-old wild-type and *Angptl4*⁻ᐟ⁻ mice on standard chow were collected and analyzed for several bile acids as described previously (52).

Animal studies were performed according to protocols approved by the local animal ethics committee of Wageningen University.

Gene expression analysis

Proximal intestine samples from wild-type and *Angptl4*⁻ᐟ⁻ animals after HFD or lipid gavage were homogenized in TRIzol® (Life Technologies Europe BV, Bleiswijk, The Netherlands) using a Qiagen

4

TissueLyser II (Qiagen, Hilden, Germany) for RNA isolation. cDNA was synthesized with the First Strand cDNA synthesis kit (Thermo Scientific, Landsmeer, The Netherlands). qPCR was performed using SensiMix (Bioline, GC biotech, Alphen aan den Rijn, The Netherlands) and primers from the Harvard PrimerBank on a CFX384 platform (BioRad, Veenendaal, The Netherlands). For normalization 36b4 was used as a housekeeping gene.

Affymetrix GeneChip analysis was performed on 10 longitudinal small intestine fragments collected along the total length of the small intestine of C57BL/6 mice fed LFD or HFD for 2 weeks. RNA was extracted as described above and subsequently purified using the RNeasy Minikit (Qiagen, Venlo, The Netherlands). RNA quality was assessed on RNA 6000 Nano chips with the Agilent 2100 Bioanalyzer (Agilent Technologies, Amsterdam, the Netherlands). Labeled RNA was hybridized to Affymetrix Mouse Gene 1.1 ST array plate on the Affymetrix GeneTitan platform, and scans were processed using Bioconductor followed by RMA normalization (53, 54). Probe sets were generated based on published methods (55) using chip definition file (CDF) version 15 derived from the Entrez gene database. Analysis of *Villin* and *Angptl4* mRNA levels along the crypt-villus axis was performed according to published methods (56) using qPCR as described above.

Mouse luminal lipase activity

Luminal content collected from the small intestine was mixed with 19 volumes ice-cold PBS, vortexed vigorously and centrifuged at 15,000 g for 10 minutes at 4°C. Supernatants were collected and diluted 1:100 in PBS for subsequent analysis. Lipase activity was measured using the Roar LPL activity assay kit (Roar Biomedical, Inc., New York, USA) according to the manufacturer's protocol. The LPL activity kit employs a substrate that becomes fluorescent upon hydrolysis of an ester and can be used to assess the activity of other lipases too. Lipase activity was calculated as µmole per hour using a pre-hydrolyzed substrate and subsequently normalized for protein concentration of the fecal water as determined with BCA protein assay (Thermo Fisher Scientific, Landsmeer, The Netherlands).

Human luminal lipase activity

Three otherwise healthy volunteers with a distal ileostomy volunteered to provide stoma output. Volunteers were aged 50-67 years and included one male and two females. Collected material was transported on ice and centrifuged at 5,000 *g* for 10 minutes at 4°C. Supernatants were collected and stored at -80°C until lipase activity assays. Samples were diluted 1:100 before determining lipase activity with the Roar LPL Activity Assay Kit. Recombinant mouse ANGPTL4 (R&D Systems, Abingdon United Kingdom) or Orlistat (Sigma-Aldrich, Schnelldorf, Germany) were allowed to preincubate with stoma output at 37°C for 45 minutes after which the fluorescent substrate was added. Fluorescence was measured after an additional incubation period of 45 minutes at 37°C. Fluorescent units were converted to µmol of hydrolyzed substrate per hour using the pre-hydrolyzed substrate, and normalized for protein content determined with a BCA protein assay.

Pancreatic lipase activity

Recombinant PL (Sigma-Aldrich, Schnelldorf, Germany) at an amount of 250 units was added to the fluorescent substrate of the Roar LPL Activity Assay Kit. Recombinant mouse ANGPTL4 or Orlistat were included to address the inhibitory capacity of these compounds on PL mediated hydrolysis. Fluorescence was measured after incubation at 37°C for 45 minutes.

Statistical analysis

Unpaired two-tailed Student's *t*-tests and analysis of variances with corresponding post-hoc tests were performed using GraphPad Prism (GraphPad Software, La Jolla, CA, USA). The cutoff for significance level was set at $P < 0.05$.

Acknowledgements

4

References

1. Armand M. Lipases and lipolysis in the human digestive tract: where do we stand? *Curr Opin Clin Nutr Metab Care.* 2007;10(2):156-164.
2. Wilde PJ, Chu BS. Interfacial & colloidal aspects of lipid digestion. *Adv Colloid Interface Sci.* 2011;165(1):14-22.
3. Carriere F, Barrowman JA, Verger R, Laugier R. Secretion and contribution to lipolysis of gastric and pancreatic lipases during a test meal in humans. *Gastroenterology.* 1993;105(3):876-888.
4. Whitcomb DC, Lowe ME. Human pancreatic digestive enzymes. *Dig Dis Sci.* 2007;52(1):1-17.
5. Brownlee IA, Forster DJ, Wilcox MD, Dettmar PW, Seal CJ, Pearson JP. Physiological parameters governing the action of pancreatic lipase. *Nutr Res Rev.* 2010;23(1):146-154.
6. Wang TY, Liu M, Portincasa P, Wang DQ. New insights into the molecular mechanism of intestinal fatty acid absorption. *Eur J Clin Invest.* 2013;43(11):1203-1223.
7. Demignot S, Beilstein F, Morel E. Triglyceride-rich lipoproteins and cytosolic lipid droplets in enterocytes: Key players in intestinal physiology and metabolic disorders. *Biochimie.* 2013.
8. Iqbal J, Hussain MM. Intestinal lipid absorption. *Am J Physiol Endocrinol Metab.* 2009;296(6):E1183-1194.
9. Wang H, Eckel RH. Lipoprotein lipase: from gene to obesity. *Am J Physiol Endocrinol Metab.* 2009;297(2):E271-288.
10. Beigneux AP, Davies BS, Gin P, Weinstein MM, Farber E, Qiao X, Peale F, Bunting S, Walzem RL, Wong JS, et al. Glycosylphosphatidylinositol-anchored high-density lipoprotein-binding protein 1 plays a critical role in the lipolytic processing of chylomicrons. *Cell Metab.* 2007;5(4):279-291.

11. Davies BS, Beigneux AP, Barnes RH, 2nd, Tu Y, Gin P, Weinstein MM, Nobumori C, Nyren R, Goldberg I, Olivecrona G, et al. GPIHBP1 is responsible for the entry of lipoprotein lipase into capillaries. *Cell Metab.* 2010;12(1):42-52.

12. Mattijssen F, Kersten S. Regulation of triglyceride metabolism by Angiopoietin-like proteins. *Biochim Biophys Acta.* 2012;1821(5):782-789.

13. Quagliarini F, Wang Y, Kozlitina J, Grishin NV, Hyde R, Boerwinkle E, Valenzuela DM, Murphy AJ, Cohen JC, Hobbs HH. Atypical angiopoietin-like protein that regulates ANGPTL3. *Proc Natl Acad Sci U S A.* 2012;109(48):19751-19756.

14. Wang Y, Quagliarini F, Gusarova V, Gromada J, Valenzuela DM, Cohen JC, Hobbs HH. Mice lacking ANGPTL8 (Betatrophin) manifest disrupted triglyceride metabolism without impaired glucose homeostasis. *Proc Natl Acad Sci U S A.* 2013;110(40):16109-16114.

15. Zhang R. Lipasin, a novel nutritionally-regulated liver-enriched factor that regulates serum triglyceride levels. *Biochem Biophys Res Commun.* 2012;424(4):786-792.

16. Kaplan R, Zhang T, Hernandez M, Gan FX, Wright SD, Waters MG, Cai TQ. Regulation of the angiopoietin-like protein 3 gene by LXR. *J Lipid Res.* 2003;44(1):136-143.

17. Inaba T, Matsuda M, Shimamura M, Takei N, Terasaka N, Ando Y, Yasumo H, Koishi R, Makishima M, Shimomura I. Angiopoietin-like protein 3 mediates hypertriglyceridemia induced by the liver X receptor. *J Biol Chem.* 2003;278(24):21344-21351.

18. Mandard S, Zandbergen F, van Straten E, Wahli W, Kuipers F, Muller M, Kersten S. The fasting-induced adipose factor/angiopoietin-like protein 4 is physically associated with lipoproteins and governs plasma lipid levels and adiposity. *J Biol Chem.* 2006;281(2):934-944.

19. Lichtenstein L, Mattijssen F, de Wit NJ, Georgiadi A, Hooiveld GJ, van der Meer R, He Y, Qi L, Koster A, Tamsma JT, et al. Angptl4 protects against severe proinflammatory effects of saturated fat by inhibiting fatty acid uptake into mesenteric lymph node macrophages. *Cell Metab.* 2010;12(6):580-592.

20. Georgiadi A, Lichtenstein L, Degenhardt T, Boekschoten MV, van Bilsen M, Desvergne B, Muller M, Kersten S. Induction of cardiac Angptl4 by dietary fatty acids is mediated by peroxisome proliferator-activated receptor beta/delta and protects against fatty acid-induced oxidative stress. *Circ Res.* 2010;106(11):1712-1721.

21. Yu X, Burgess SC, Ge H, Wong KK, Nassem RH, Garry DJ, Sherry AD, Malloy CR, Berger JP, Li C. Inhibition of cardiac lipoprotein utilization by transgenic overexpression of Angptl4 in the heart. *Proc Natl Acad Sci U S A.* 2005;102(5):1767-1772.

22. Kroupa O, Vorrsjo E, Stienstra R, Mattijssen F, Nilsson SK, Sukonina V, Kersten S, Olivecrona G, Olivecrona T. Linking nutritional regulation of Angptl4, Gpihbp1, and Lmf1 to lipoprotein lipase activity in rodent adipose tissue. *BMC Physiol.* 2012;12:13.

23. Sukonina V, Lookene A, Olivecrona T, Olivecrona G. Angiopoietin-like protein 4 converts lipoprotein lipase to inactive monomers and modulates lipase activity in adipose tissue. *Proc Natl Acad Sci U S A.* 2006;103(46):17450-17455.

24. Lafferty MJ, Bradford KC, Erie DA, Neher SB. Angiopoietin-like Protein 4 inhibition of lipoprotein lipase: evidence for reversible complex formation. *J Biol Chem.* 2013;288(40):28524-28534.

25. Kersten S, Lichtenstein L, Steenbergen E, Mudde K, Hendriks HF, Hesselink MK, Schrauwen P, Muller M. Caloric restriction and exercise increase plasma ANGPTL4 levels in humans via elevated free fatty acids. *Arterioscler Thromb Vasc Biol.* 2009;29(6):969-974.

26. Koliwad SK, Kuo T, Shipp LE, Gray NE, Backhed F, So AY, Farese RV, Jr., Wang JC. Angiopoietin-like 4 (ANGPTL4, fasting-induced adipose factor) is a direct glucocorticoid receptor target and participates in glucocorticoid-regulated triglyceride metabolism. *J Biol Chem.* 2009;284(38):25593-25601.

27. Staiger H, Haas C, Machann J, Werner R, Weisser M, Schick F, Machicao F, Stefan N, Fritsche A, Haring HU. Muscle-derived angiopoietin-like protein 4 is induced by fatty acids via peroxisome proliferator-activated receptor (PPAR)-delta and is of metabolic relevance in humans. *Diabetes.* 2009;58(3):579-589.

28. Wong H, Schotz MC. The lipase gene family. *J Lipid Res.* 2002;43(7):993-999.

29. Alex S, Lange K, Amolo T, Grinstead JS, Haakonsson AK, Szalowska E, Koppen A, Mudde K, Haenen D, Al-Lahham S, et al. Short-chain fatty acids stimulate angiopoietin-like 4 synthesis in human colon adenocarcinoma cells by activating peroxisome proliferator-activated receptor gamma. *Mol Cell Biol.* 2013;33(7):1303-1316.

30. Korecka A, de Wouters T, Cultrone A, Lapaque N, Pettersson S, Dore J, Blottiere HM, Arulampalam V. ANGPTL4 expression induced by butyrate and rosiglitazone in human intestinal epithelial cells utilizes independent pathways. *Am J Physiol Gastrointest Liver Physiol.* 2013;304(11):G1025-1037.

31. Lichtenstein L, Berbee JF, van Dijk SJ, van Dijk KW, Bensadoun A, Kema IP, Voshol PJ, Muller M, Rensen PC, Kersten S. Angptl4 upregulates cholesterol synthesis in liver via inhibition of LPL- and HL-dependent hepatic cholesterol uptake. *Arterioscler Thromb Vasc Biol.* 2007;27(11):2420-2427.

32. Yoshida K, Shimizugawa T, Ono M, Furukawa H. Angiopoietin-like protein 4 is a potent hyperlipidemia-inducing factor in mice and inhibitor of lipoprotein lipase. *J Lipid Res.* 2002;43(11):1770-1772.

33. de la Garza AL, Milagro FI, Boque N, Campion J, Martinez JA. Natural inhibitors of pancreatic lipase as new players in obesity treatment. *Planta Med.* 2011;77(8):773-785.

34. Birari RB, Bhutani KK. Pancreatic lipase inhibitors from natural sources: unexplored potential. *Drug Discov Today.* 2007;12(19-20):879-889.

35. Marchbank T, Freeman TC, Playford RJ. Human pancreatic secretory trypsin inhibitor. Distribution, actions and possible role in mucosal integrity and repair. *Digestion.* 1998;59(3):167-174.

36. Laskowski M, Jr., Kato I. Protein inhibitors of proteinases. *Annu Rev Biochem.* 1980;49:593-626.

37. Bohe H, Bohe M, Lundberg E, Polling A, Ohlsson K. Production and secretion of pancreatic secretory trypsin inhibitor in normal human small intestine. *J Gastroenterol.* 1997;32(5):623-627.

38. Wang J, Ohmuraya M, Hirota M, Baba H, Zhao G, Takeya M, Araki K, Yamamura K. Expression pattern of serine protease inhibitor kazal type 3 (Spink3) during mouse embryonic development. *Histochem Cell Biol.* 2008;130(2):387-397.

39. Tremaroli V, Backhed F. Functional interactions between the gut microbiota and host metabolism. *Nature.* 2012;489(7415):242-249.

40. Turnbaugh PJ, Ley RE, Mahowald MA, Magrini V, Mardis ER, Gordon JI. An obesity-associated gut microbiome with increased capacity for energy harvest. *Nature.* 2006;444(7122):1027-1031.

41. Backhed F, Ding H, Wang T, Hooper LV, Koh GY, Nagy A, Semenkovich CF, Gordon JI. The gut microbiota as an environmental factor that regulates fat storage. *Proc Natl Acad Sci U S A.* 2004;101(44):15718-15723.

42. Camp JG, Jazwa AL, Trent CM, Rawls JF. Intronic cis-regulatory modules mediate tissue-specific and microbial control of angptl4/fiaf transcription. *PLoS Genet.* 2012;8(3):e1002585.

43. Backhed F, Manchester JK, Semenkovich CF, Gordon JI. Mechanisms underlying the resistance to diet-induced obesity in germ-free mice. *Proc Natl Acad Sci U S A.* 2007;104(3):979-984.

44. Santas J, Espadaler J, Cune J, Rafecas M. Partially hydrolyzed guar gums reduce dietary fatty acid and sterol absorption in guinea pigs independent of viscosity. *Lipids.* 2012;47(7):697-705.

45. Vahouny GV, Satchithanandam S, Chen I, Tepper SA, Kritchevsky D, Lightfoot FG, Cassidy MM. Dietary fiber and intestinal adaptation: effects on lipid absorption and lymphatic transport in the rat. *Am J Clin Nutr.* 1988;47(2):201-206.

4

46.   Alex S, Lichtenstein L, Dijk W, Mensink RP, Tan NS, Kersten S. ANGPTL4 is produced by entero-endocrine cells in the human intestinal tract. *Histochem Cell Biol.* 2013.

47.   Kim HK, Youn BS, Shin MS, Namkoong C, Park KH, Baik JH, Kim JB, Park JY, Lee KU, Kim YB, et al. Hypothalamic Angptl4/Fiaf is a novel regulator of food intake and body weight. *Diabetes.* 2010;59(11):2772-2780.

48.   Koster A, Chao YB, Mosior M, Ford A, Gonzalez-DeWhitt PA, Hale JE, Li D, Qiu Y, Fraser CC, Yang DD, et al. Transgenic angiopoietin-like (angptl)4 overexpression and targeted disruption of angptl4 and angptl3: regulation of triglyceride metabolism. *Endocrinology.* 2005;146(11):4943-4950.

49.   Hoevenaars FP, Keijer J, Swarts HJ, Snaas-Alders S, Bekkenkamp-Grovenstein M, van Schothorst EM. Effects of dietary history on energy metabolism and physiological parameters in C57BL/6J mice. *Exp Physiol.* 2013;98(5):1053-1062.

50.   Govers MJ, Van der Meet R. Effects of dietary calcium and phosphate on the intestinal interactions between calcium, phosphate, fatty acids, and bile acids. *Gut.* 1993;34(3):365-370.

51.   Goudriaan JR, Dahlmans VE, Febbraio M, Teusink B, Romijn JA, Havekes LM, Voshol PJ. Intestinal lipid absorption is not affected in CD36 deficient mice. *Mol Cell Biochem.* 2002;239(1-2):199-202.

52.   Plosch T, Kok T, Bloks VW, Smit MJ, Havinga R, Chimini G, Groen AK, Kuipers F. Increased hepatobiliary and fecal cholesterol excretion upon activation of the liver X receptor is independent of ABCA1. *J Biol Chem.* 2002;277(37):33870-33877.

53.   Gentleman RC, Carey VJ, Bates DM, Bolstad B, Dettling M, Dudoit S, Ellis B, Gautier L, Ge Y, Gentry J, et al. Bioconductor: open software development for computational biology and bioinformatics. *Genome Biol.* 2004;5(10):R80.

54.   Irizarry RA, Hobbs B, Collin F, Beazer-Barclay YD, Antonellis KJ, Scherf U, Speed TP. Exploration, normalization, and summaries of high density oligonucleotide array probe level data. *Biostatistics.* 2003;4(2):249-264.

55.   Dai M, Wang P, Boyd AD, Kostov G, Athey B, Jones EG, Bunney WE, Myers RM, Speed TP, Akil H, et al. Evolving gene/transcript definitions significantly alter the interpretation of GeneChip data. *Nucleic Acids Res.* 2005;33(20):e175.

56.   Bunger M, van den Bosch HM, van der Meijde J, Kersten S, Hooiveld GJ, Muller M. Genome-wide analysis of PPARalpha activation in murine small intestine. *Physiol Genomics.* 2007;30(2):192-204.
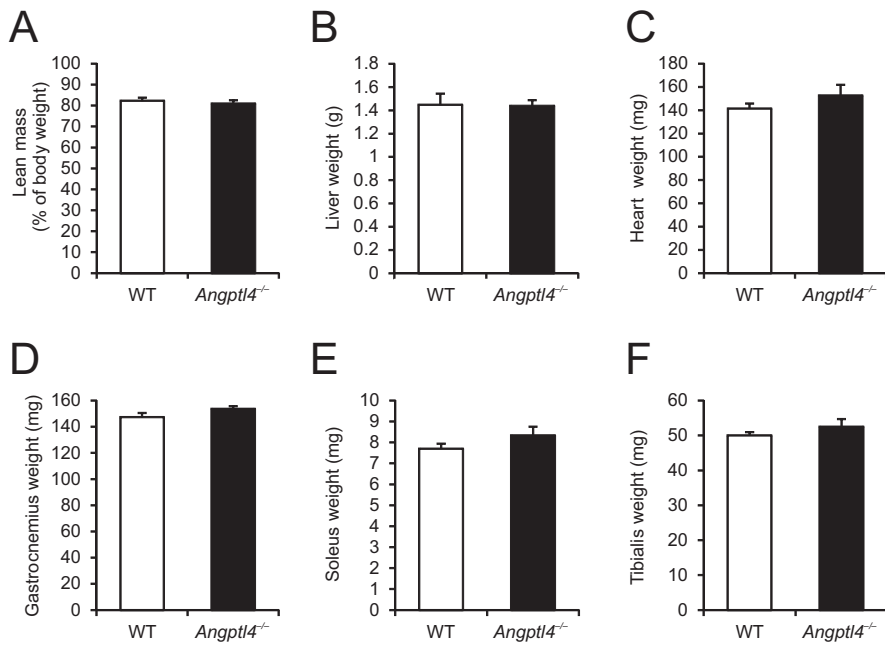
Supplemental Figure 1. Tissue weights of wild-type and *Angptl4*$^{-/-}$ animals

(A-E) Liver (A), heart (B), gastrocnemius (C), soleus (D), and tibialis weight of wild-type and *Angptl4*$^{-/-}$ mice fed a standard chow diet (n = 10-11 per group).

Data are mean ± SEM.

4

5

Hypoxia inducible lipid droplet associated (HILPDA) is a novel PPAR target involved in hepatic triglyceride secretion

F Mattijssen, E Szalowska, A Zota, C Heier, D Ratman,
K De Bosscher, R Zechner, S Herzig, S Kersten

Abstract

Peroxisome proliferator-activated receptors (PPARs) play major roles in the regulation of hepatic lipid metabolism through the control of numerous genes involved in processes such as lipid uptake and fatty acid oxidation. Here we identify hypoxia inducible lipid droplet associated (*Hilpda*) as a novel PPAR target gene involved in hepatic lipid metabolism. Microarray and qPCR analysis showed that *Hilpda* expression is markedly induced by the PPARα agonist Wy14643 in mouse liver slices. Induction of *Hilpda* mRNA by Wy14643 was confirmed in mouse and human hepatocytes. Oral dosing with Wy14643 similarly induced *Hilpda* mRNA levels in livers of wild-type mice but not *Ppara*$^{-/-}$ mice. Transactivation studies and chromatin immunoprecipitation showed that *Hilpda* is a direct PPARα target gene via a conserved PPAR response element (PPRE) located 1200 base pair upstream of the transcription start site. Hepatic overexpression of HILPDA in mice via adeno-associated virus led to a 4-fold increase in liver triglyceride storage, without any changes in key genes involved in de-novo lipogenesis, β-oxidation, or lipolysis. Moreover, HILPDA did not affect intracellular lipase activity. Strikingly, HILPDA overexpression significantly impaired hepatic triglyceride secretion. Taken together, our data uncover HILPDA as a novel PPAR target that raises hepatic triglyceride storage via regulation of triglyceride secretion.

Introduction

The liver is a key organ in the control of carbohydrate and lipid metabolism. During the postprandial phase the liver is exposed to high concentrations of glucose and chylomicron remnants, which are taken up, processed, and subsequently stored as glycogen and triglycerides, respectively. In the fasted state, the liver assures the maintenance of stable plasma glucose and lipid levels to provide peripheral organs with the necessary nutrients. Indeed, gluconeogenesis, VLDL production, and ketogenesis are important metabolic processes in the liver aimed at maintaining energy homeostasis in times of food deprivation (1-4). Many genes involved in these processes are regulated by nuclear receptors (5-7).

Nuclear receptors comprise a family of transcription factors that bind to specific response elements across the genome and regulate the expression of a large network of genes (8). As a group they are activated by a variety of steroid hormones and other lipid-derived compounds, including fat-soluble vitamins, cholesterol, and fatty acids (9). Binding of ligand to nuclear receptors promotes the recruitment and release of coactivators and corepressors, respectively, to form multiprotein complexes that induce transcription of target genes (10-14). A group of nuclear receptors that has been extensively studied and that plays a central role in the regulation of nutrient homeostasis in liver and other organs are the peroxisome proliferator activated receptors (PPARs) (15-17). PPARs are ligand-activated transcription factors that bind a variety of (dietary) fatty acids and fatty-acid derived compounds, including various eicosanoids (18, 19). Furthermore, PPARs are the molecular target of the thiazolidinedione and fibrate classes of drugs used in the treatment of diabetes and dyslipidemia, respectively (20-23).

PPARs share a common structure with other nuclear receptors consisting of several distinct domains: a DNA-binding domain (DBD) containing two zinc-fingers, a ligand binding domain (LBD), and two transcriptional activation functions located in the N-terminal domain (AF1) or the LBD (AF2) (24). All domains can contribute to PPAR activation via ligand dependent and independent mechanisms.

Induction of gene transcription by PPARs requires the cooperative binding to retinoid X receptors (RXR), a nuclear receptor that is ligand-activated by 9-cis retinoic acid, to form an active heterodimer (25). The PPAR-RXR heterodimer binds to so called PPAR response elements (PPRE) composed of the consensus sequence AGGTCAnAGGTCA located in proximal promoters, introns, and more distant regions of target genes (26, 27).

Three different PPARs can be distinguished: PPARα (Nr1c1), PPARβ/δ (Nr1c2), and PPARγ (Nr1c3) (24, 28, 29). PPARγ is highly expressed in adipose tissue where it regulates genes involved in fat cell development, lipid deposition, insulin signaling, and inflammation

5

(30). PPARβ/δ is found at high levels in many tissues and compelling evidence indicates that it stimulates fatty acid oxidation, at least in skeletal muscle and adipose tissue (31). Expression of PPARα is highest in tissues that oxidize fatty acids at a rapid rate, including liver, brown adipose tissue, heart and kidney (32).

Activation of PPARα leads to induction of a large set of target genes involved in various pathways of lipid metabolism, including fatty acid transport, activation, storage, and oxidation (33, 34). Indeed, PPARα can be considered as the master regulator of hepatic lipid metabolism. As a consequence, mice lacking PPARα suffer from hepatic steatosis, hypoglycemia, hypoketonemia, and elevated plasma free fatty acids, all of which are aggravated during fasting (35). Inasmuch as most of our knowledge about the biological function of PPARα is directly coupled to the function of its target genes, the identification of genes regulated by PPARα may help in further deciphering the role of PPARα in vivo.

In this study we set out to identify novel PPARα targets using mouse liver slices. We identify *Hilpda* as a PPAR target in mouse and human hepatocytes and show it plays an important role in hepatic triglyceride storage and secretion.

Results

Hildpa is regulated by PPARα in liver slices and hepatocytes

To identify potential novel target genes of PPARα, mouse liver slices were treated with the PPARα ligand Wy14643. Whole genome microarray analysis using Affymetrix GeneChips revealed increased expression of numerous classical PPARα target with roles in β-oxidation (e.g. *Ehhadh*, *Slc22a5*, *Pdk4*, *Abcd2*, Cpt1b) and other lipid metabolic pathways (e.g. *Acot2*, *Creb3l3*, *Fabp4*, *Mgll*, *Cidec*) (Figure 1A). However, several genes in the top 40 of most highly induced genes by Wy14643 have not or have only been very poorly characterized. Among those genes 2310016C08Rik, later annotated as *Hilpda*, was of particular interest as it has recently been identified as a putative lipid droplet associated protein that is regulated via a hypoxia-dependent mechanism involving HIF1 (36). Induction of *Hildpa* expression by Wy14643 was confirmed by qPCR analysis, which revealed a ~3 fold increase of *Hilpda* mRNA (Figure 1B). The *Hilpda* gene contains one intron and two exons and encodes a highly conserved protein of 63 and 64 amino acids in human and mouse, respectively (Figure 1C). In mice, an isoform of 95 amino acids has been suggested to be translated from an alternative start codon in the first exon. In silico analysis revealed neither a signal peptide nor other putative conserved sequences. In addition, no homologous proteins were identified.
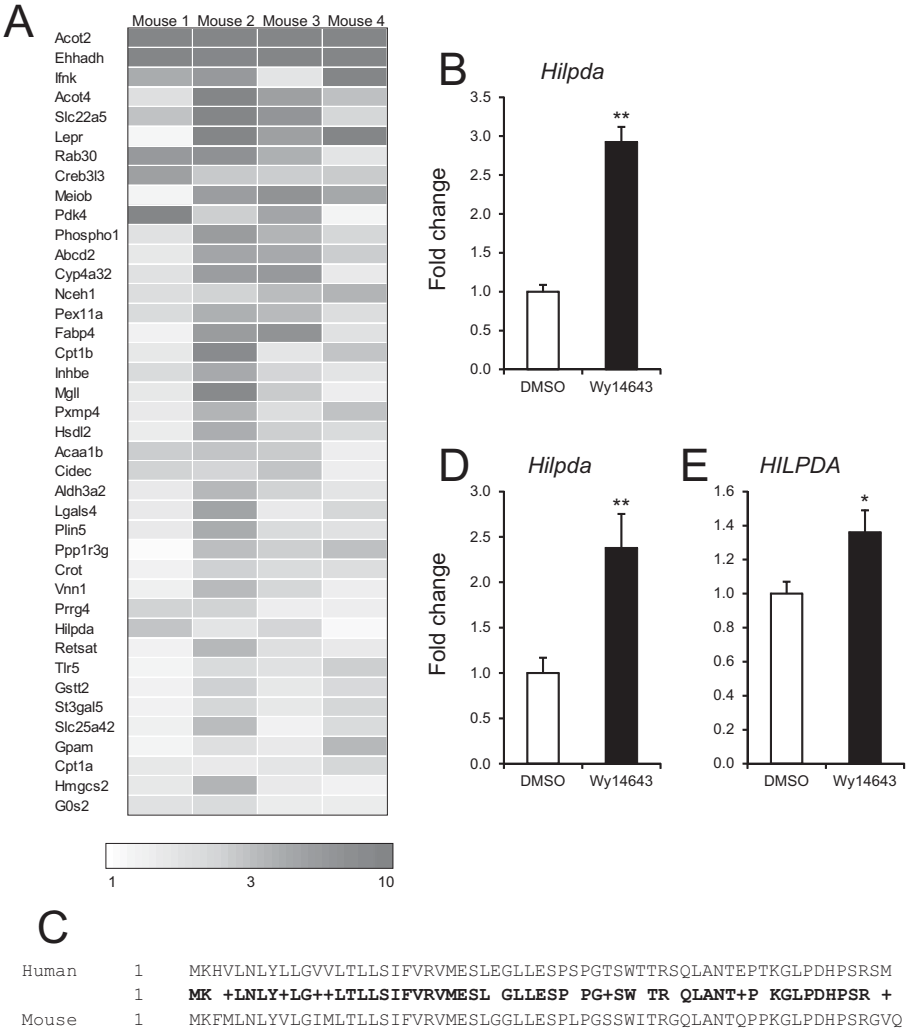
Figure 1. Wy14643 increases *Hilpda* expression in liver slices and hepatocytes

(A) Top 40 of most highly induced genes in mouse liver slices exposed to 20 μM Wy14643 for 24 hours. Values are expressed as fold changes over DMSO treated slices from the same animal (n = 4).

(B) *Hilpda* mRNA determined by qPCR in mouse liver slices exposed to 20 μM Wy14643 for 6 hours. Samples include the 4 described in A plus two additional animals (n = 6).

(C) Amino acid sequence of mouse and human HILPDA.

(D and E) *Hilpda* mRNA levels in mouse (D, n = 6 animals from different strains) and human (E, n = 6) hepatocytes after exposure to Wy14643 for 6 hours.

Data are mean ± SEM. Asterisks indicate significant differences according to Student's *t*-test; *$P < 0.05$, **$P < 0.01$.

To substantiate our findings in mouse liver slices we analyzed *Hilpda* expression in isolated mouse and human hepatocytes exposed to DMSO or Wy14643 for 6 hours. In congruence with the data from liver slices, we found a significant increase in *Hilpda* mRNA levels following Wy14643 treatment in mouse and human hepatocytes (Figures 1D and 1E). Together these data indicate that expression of *Hilpda* is positively regulated by PPARα in mouse and human hepatocytes, suggesting that *Hilpda* may represent a novel putative PPARα target.

Hepatic Hilpda expression is regulated by PPARs in vivo

We next sought to explore the PPARα dependent regulation of *Hilpda* in vivo by employing wild-type and *Ppara*$^{-/-}$ animals which were fed either a control diet or the same diet supplemented with aforementioned Wy14643. Five days after switching the mice to the diet containing Wy14643 their livers were excised and analyzed for *Hilpda* expression. Interestingly, *Hilpda* mRNA levels were significantly increased in wild-type mice fed Wy14643, whereas the response was absent in *Ppara*$^{-/-}$ animals, suggesting a PPARα mediated regulation of *Hilpda* (Figure 2A). Moreover, increased *Hilpda* mRNA levels were associated with a marked induction of HILPDA protein levels (Figure 2B).

PPARα is an important regulator in the metabolic response to fasting and the expression of many PPARα regulated genes increases upon fasting (35). However, we found a much less pronounced increase in *Hilpda* mRNA and protein in livers of fasted wild-type mice compared to *Ppara*$^{-/-}$ mice. Indeed, *Hilpda* mRNA was increased 1.4-fold and 9.2-fold by fasting in wild-type and *Ppara*$^{-/-}$ mice, respectively (Figure 2C), which was confirmed by Western blot (Figure 2D). It has been observed that PPARγ is able to partially compensate for PPARα deletion during high-fat diet feeding or fasting (37, 38). Indeed, *Pparg* expression was increased in livers of *Ppara*$^{-/-}$ animals (Figure 2E). Moreover, we found markedly increased *Hilpda* mRNA expression upon adenoviral-mediated hepatic *Pparg1* overexpression (Figure 2E). Together, these data suggest that *Hilpda* expression in liver is regulated by both PPARα and PPARγ.

Hilpda is a direct PPAR target

In silico screening revealed the presence of a potential PPRE around 1200 base pair (bp) upstream of the transcription start site (TSS) of *Hilpda* that is highly conserved between mouse and human. To determine whether this PPRE is indeed contributing to PPAR dependent regulation of *Hilpda*, we generated luciferase reporter vectors containing a ~200 bp genomic fragment flanking the mouse or human PPRE (Figure 3A). Notably, all
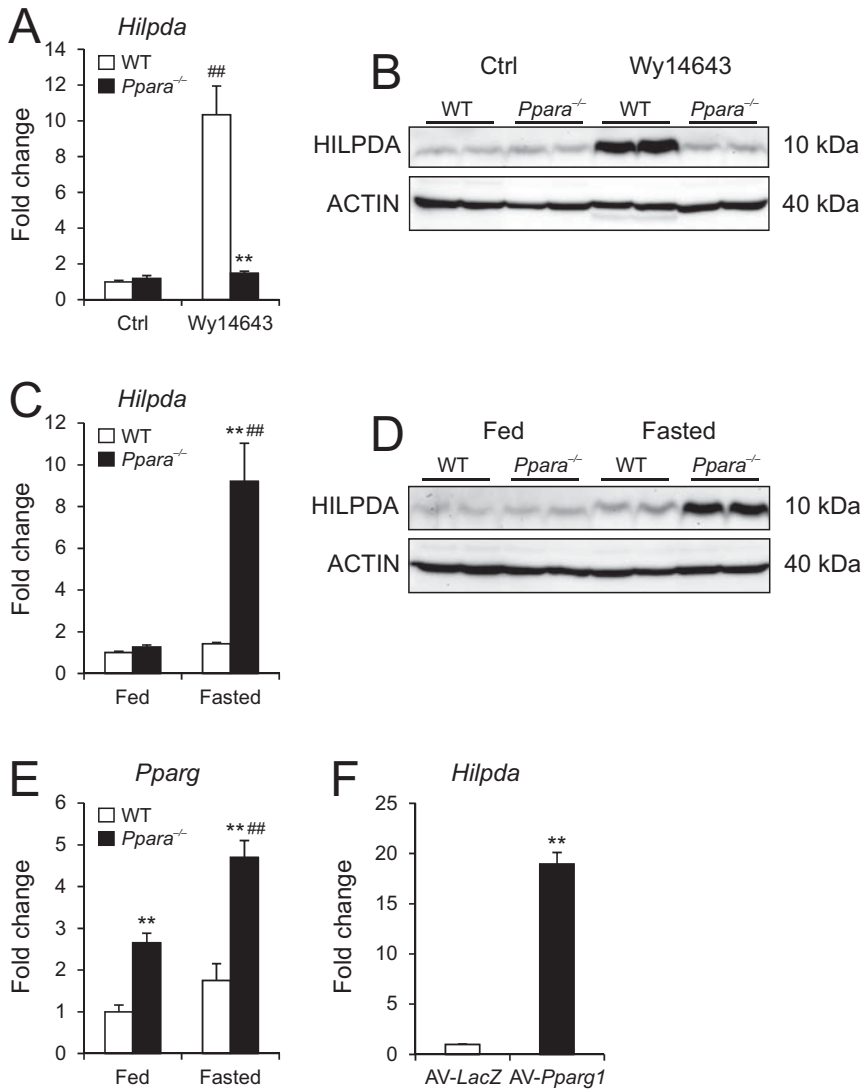
Figure 2. PPAR dependent regulation of *Hilpda* expression in vivo

(A and B) *Hilpda* gene expression (A, n = 4-5 per group) and Western blot (B) analysis of livers from wild-type and *Ppara*−/− mice fed a control diet or similar diet supplemented with Wy14643 for 5 days.

(C and D) *Hilpda* gene expression (C, n = 4-5 per group) and Western blot (D) analysis of livers from wild-type and *Ppara*−/− mice after 24 hours fasting.

(E) Analysis of *Pparg* mRNA levels in same samples as in C (n = 4-5 per group).

(F) *Hilpda* mRNA levels in livers from *Ppara*−/− mice intravenously injected with adenovirus encoding *LacZ* or *Pparg1* (n = 4 per group).

Data are mean ± SEM. Two-way ANOVA with Bonferroni post-hoc test (A, C, and E) or Student's *t*-test (F) were performed; *$P < 0.05$, **$P < 0.01$, ##$P < 0.01$. *, difference between WT and *Ppara*−/− (A, C, and E); #, difference between Ctrl/Wy14643 (A) or Fed/Fasted (C and E).

5

A

Mouse	AAAGT<u>AGGGG</u>**AAA**GGTCACAG	wild-type
Human	AAAGG<u>AGGGG</u>**AAA**GGTCGCAG	

Mouse	AAAGT<u>AGGGG</u>**CCC**GGTCACAG	mutant
Human	AAAGG<u>AGGGG</u>**CCC**GGTCGCAG	

B Mouse
Relative Luc activity
Wy14643   - + - +
PPARα-RXRα - - + +

C Mouse
Relative Luc activity
GW501516   - + - +
PPARβ/δ-RXRα - - + +

D Mouse
Relative Luc activity
Rosiglitazone - + - +
PPARγ-RXRα   - - + +
□ WT ■ Mut

E Human
Relative Luc activity
Wy14643   - + - +
PPARα-RXRα - - + +

F Human
Relative Luc activity
GW501516   - + - +
PPARβ/δ-RXRα - - + +

G Human
Relative Luc activity
Rosiglitazone - + - +
PPARγ-RXRα   - - + +
□ WT ■ Mut

H
Fold enrichment over IgG
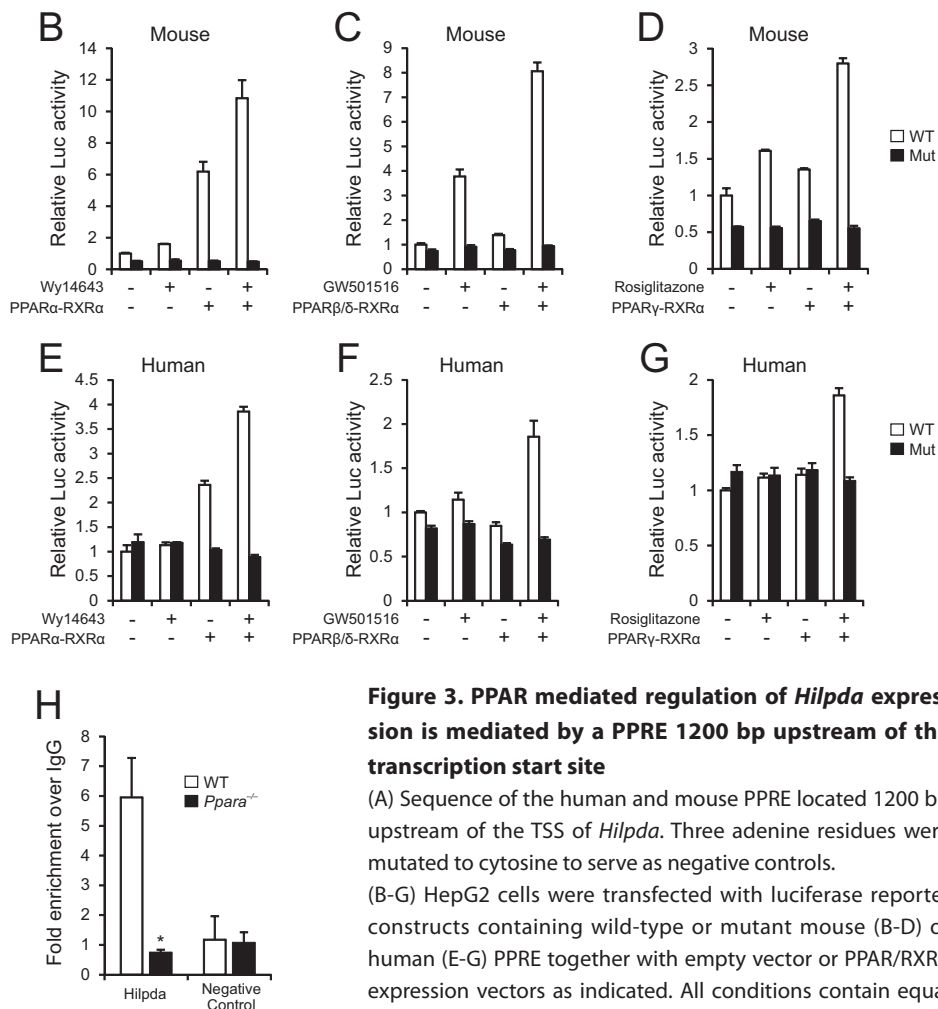□ WT ■ Ppara$^{-/-}$
Hilpda   Negative Control

Figure 3. PPAR mediated regulation of *Hilpda* expression is mediated by a PPRE 1200 bp upstream of the transcription start site

(A) Sequence of the human and mouse PPRE located 1200 bp upstream of the TSS of *Hilpda*. Three adenine residues were mutated to cytosine to serve as negative controls.

(B-G) HepG2 cells were transfected with luciferase reporter constructs containing wild-type or mutant mouse (B-D) or human (E-G) PPRE together with empty vector or PPAR/RXRα expression vectors as indicated. All conditions contain equal amounts of DNA and β-galactosidase was co-transfected for normalization. Transfected cells were subsequently exposed to DMSO, 50 μM Wy14643, 5 μM GW501516, or 5 μM rosiglitazone for 24 hours. Luciferase readings in cell lysates were normalized against β-galactosidase activity (n = 3).

(H) Chromatin was extracted from wild-type and *Ppara*$^{-/-}$ primary hepatocytes and ChIP assay was performed using antibodies specific for PPARα or IgG. PCR was performed using primers flanking the conserved PPRE 1200 bp upstream of the *Hilpda* TSS or negative control primers to amplify an intergenic region 100 kb upstream of *Pdk4* (n = 3).

Data are mean ± SEM. Asterisk indicates significant difference according to Student's *t*-test; *$P < 0.01$.

PPARs were able to stimulate luciferase activity driven by the mouse and human wild-type PPRE (Figures 3B-G). By contrast, mutating the indicated adenine residues (Figure 3A) completely abolished the PPAR dependent increase in luciferase activity (Figures 3B-G).

To explore if the characterized PPRE is occupied by PPARα in liver, we performed chromatin immunoprecipitation experiments using primary hepatocytes from wild-type and $Ppara^{-/-}$ mice. Consistent with direct PPAR binding, we efficiently recovered a 125-bp region surrounding the conserved PPRE from PPARα immunoprecipitates in wild-type hepatocytes compared with $Ppara^{-/-}$ hepatocytes (Figure 3H). Taken together, these data demonstrate the presence of a functional PPRE 1200 bp upstream of the TSS of *Hilpda*, suggesting that *Hilpda* is a novel PPAR target gene.

Hepatic overexpression of HILPDA results in a fatty liver

To address the functional role of HILPDA in liver we employed adeno-associated viruses expressing GFP (AAV-GFP) or HILPDA (AAV-HILPDA) under the control of a modified albumin promoter. Intravenous injection of a dose as low as $1x10^{11}$ genomic copies (GC) caused a marked increase in HILPDA expression 4 weeks after injection (Supplemental Figure 1A). Consistent with the absence of a signal peptide as observed by in silico analysis, we were unable to detect Hilpda in the circulation, even after injecting higher doses (Supplemental Figure 1B). We subsequently injected $2.5x10^{11}$ GC for further characterization of hepatic HILPDA. Fluorescent microscopy of AAV-GFP injected animals indicated that almost all cells were infected at the dosage used (Figure 4A). Injecting equal amounts of AAV-HILPDA markedly increased HILPDA protein levels (Figure 4B). Importantly, HILPDA protein expressed by the AAV had the same molecular weight as the endogenous protein (Figure 4C). No differences were found in body weight between AAV-GFP and AAV-HILPDA mice 4 weeks post-injection (Figure 4D). Similarly, we did not observe any change in the weight of livers, epididymal fat pads (eWAT) or brown adipose tissue (BAT) (Figures 4E-G) between the two sets of mice. Furthermore, EchoMRI analysis did not show any difference in lean mass or fat mass (Supplemental Figure 1C).

However, during dissections we noticed that livers from AAV-HILPDA animals showed a different, slightly more yellowish color compared to AAV-GFP animals (Figure 5A), which is often indicative of increased liver fat deposition. Hematoxylin and eosin staining of livers from AAV-GFP and AAV-HILPDA animals indicated no major histological perturbations associated with HILPDA overexpression (Figure 5B). However, qualitative and quantitative analysis revealed a significant increase in hepatic triglyceride (TG) deposition upon Hilpda overexpression (Figures 5C and 5D), whereas there was no effect

5

on hepatic glycogen content (Figure 5E). Analysis of multiple plasma parameters including TG, NEFAs, glycerol, ketone bodies, and cholesterol revealed no significant differences between AAV-GFP and AAV-HILPDA mice (Figures 5F-K). Thus, HILPDA is involved in the regulation of hepatic TG metabolism, but has no effect on plasma lipid levels.
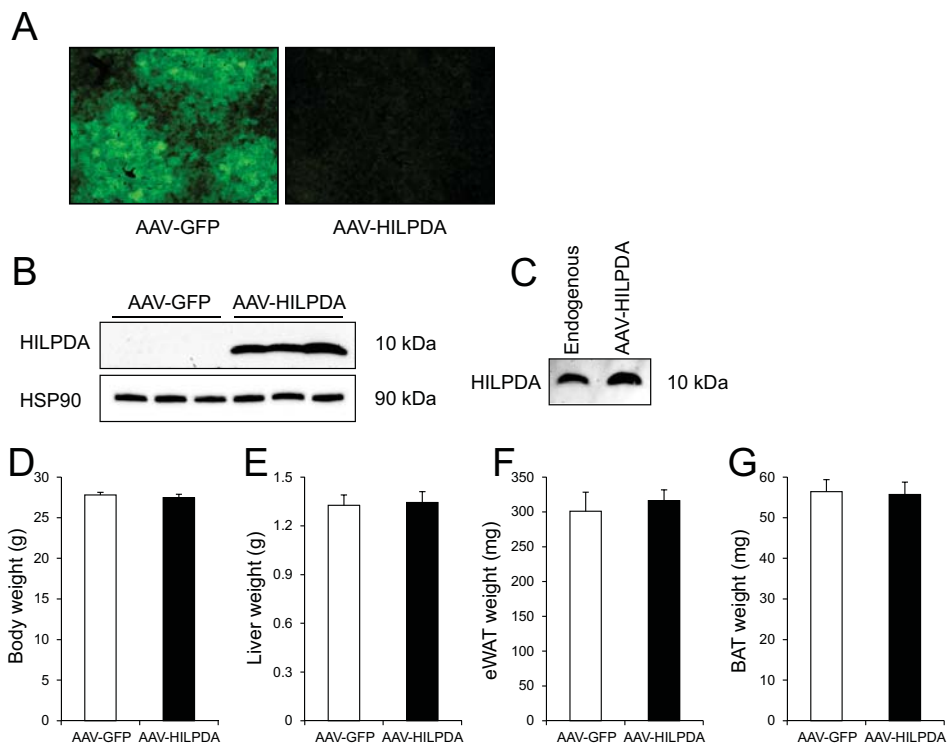

Figure 4. Hepatic overexpression of HILPDA does not impact body weight

(A) Fluorescent microscopy of liver sections from AAV-GFP and AAV-HILPDA mice 4 weeks post-injection of according AAVs.

(B) HILPDA protein expression in livers from AAV-GFP and AAV-HILPDA animals. HSP90 serves as loading control.

(C) Western blot analysis of endogenous and overexpressed HILPDA. For endogenous protein an aliquot of a sample used in Figure 2B (wild-type animal fed diet supplemented with Wy14643) was loaded.

(D) Body weight of AAV-GFP and AAV-HILPDA animals 4 weeks after injection of corresponding AAVs (n = 10-13 animals per group).

(E-G) Liver (E), eWAT (F), and BAT (G) weight of AAV-GFP and AAV-HILPDA animals (n = 8 animals per group). Data are mean ± SEM.
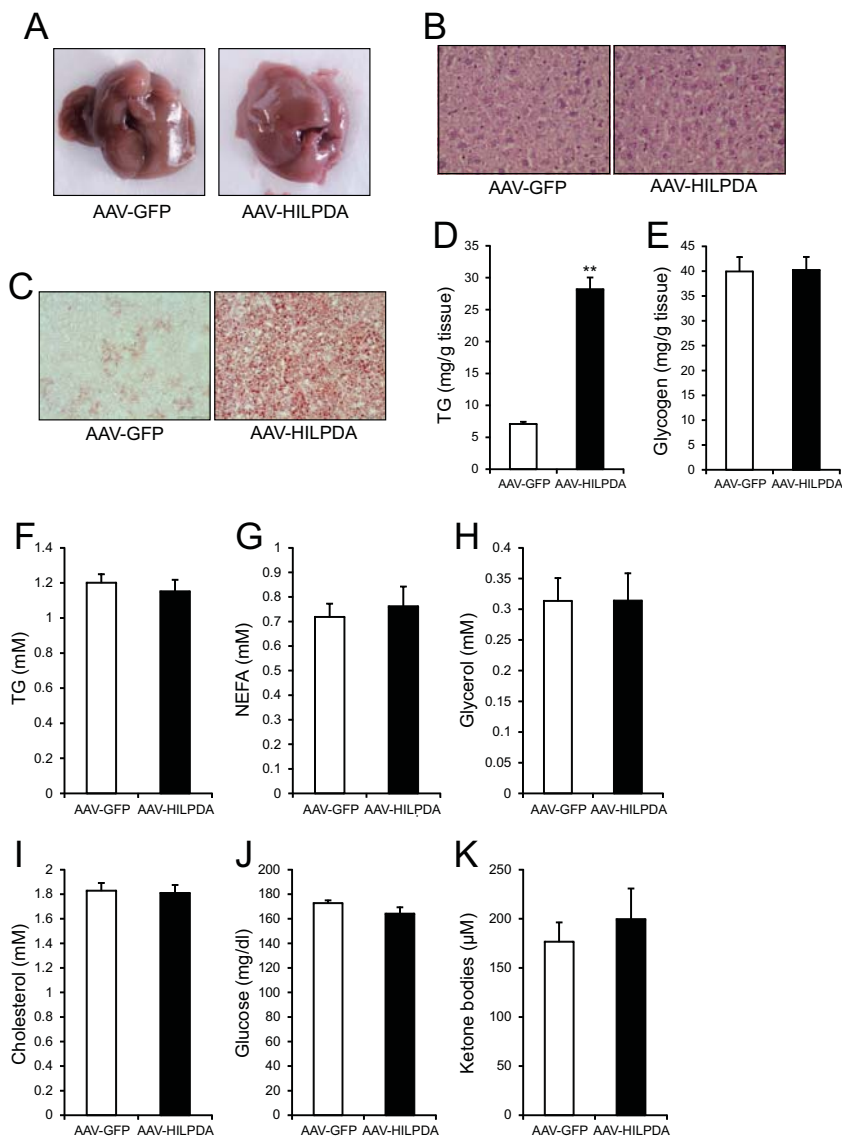
Figure 5. AAV mediated HILPDA overexpression induces hepatic steatosis

(A) Gross morphology of livers from AAV-GFP and AAV-HILPDA animals 4 weeks after injection of viruses. Animals were sacrificed under fed conditions.

(B) Representative H&E staining of livers from AAV-GFP and AAV-HILPDA animals.

(C) Oil Red O staining of liver sections from AAV-GFP and AAV-HILPDA animals.

(D) Hepatic TG content determined 4 weeks post-injection of AAVs (n = 8 animals per group).

(E) Hepatic glycogen levels in AAV-GFP and AAV-HILPDA animals (n = 8 animals per group).

(F-K) Plasma TG (F), NEFAs (G), glycerol (H), cholesterol (I), glucose (J), ketone bodies (K) levels in AAV-GFP and AAV-HILPDA animals 4 weeks post-injection of respective viruses (n = 7-8 animals per group).

Data are mean ± SEM. Asterisks indicate significant difference according to Student's t-test; ** $P < 0.01$.

HILPDA does not affect neutral lipase activity

Hepatic TG storage is the net result of several processes, including fatty acid β-oxidation, de-novo lipogenesis, fatty acid uptake, TG hydrolysis, and TG secretion as VLDL. To identify the mechanism underlying the increased lipid deposition in livers of AAV-HILPDA mice, we analyzed the expression of a selection of genes involved in abovementioned metabolic pathways. However, no differences were found in the expression of relevant genes (Figure 6).

Gene expression profiling by microarray identified only 139 genes to be significantly altered upon HILPDA overexpression (*P* value < 0.01), with more than 75% of these genes altered less than 1.5-fold. *Gadd45g*, a PPARγ target, was the most highly induced gene showing a 2.5-fold increase in expression. Together, these data suggest that increased HILPDA expression does not induce major changes in the expression of genes involved in hepatic lipid metabolism.

Previously we identified *G0s2* as a novel PPAR target in liver (39). Similar to HILPDA, G0S2 is a small protein (103 amino acids) with no conserved sequences or homology to other proteins. Recently, G0S2 was characterized as a critical regulation of adipose tissue triglyceride lipase (ATGL/PNPLA2) (40). In liver, similar to our data for HILPDA, overexpression of G0S2 increases TG storage, whereas G0S2 knock-down decreases TG levels associated with decreased or increased TG hydrolase activity, respectively (41, 42). To explore a possible effect of HILPDA overexpression on intracellular lipase activity we performed a TG hydrolase activity assay. No difference in total TG hydrolase activity was observed between AAV-GFP and AAV-HILPDA livers (Figure 7A). HILPDA also did not affect the activity of ATGL and HSL in vitro (Figure 7B). Thus, the development of a fatty liver upon HILPDA overexpression seems independent of neutral lipase activity.
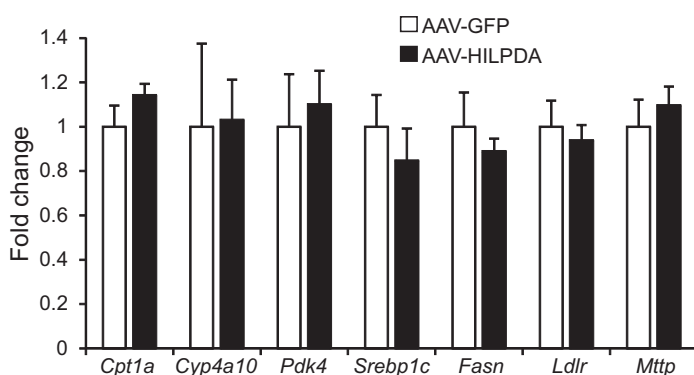

Figure 6. Hepatic overexpression of HILPDA does not affect the expression of key genes involved in β-oxidation or de-novo lipogenesis

qPCR analysis of important genes related to β-oxidation, lipogenesis, hepatic lipid uptake, and VLDL production in livers of AAV-GFP and AAV-HILPDA animals (n = 7-8 animals per group).
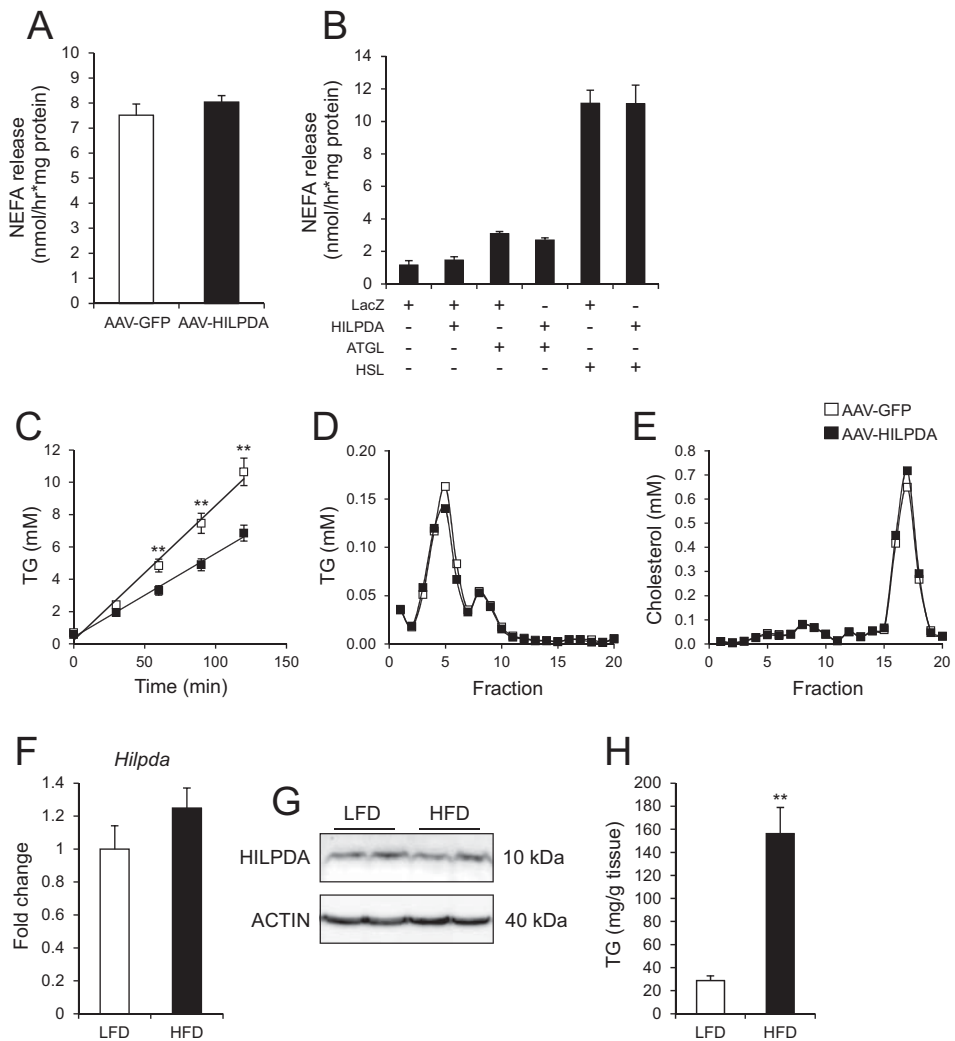Data are mean ± SEM.

Figure 7. AAV-HILPDA animals secrete less triglyceride

(A) Total TG hydrolyase activity in liver samples from AAV-GFP and AAV-HILPDA animals (n= 8 animals per group).

(B) Mouse ATGL or HSL was overexpressed in COS-7 cells and lysates were assayed for hydrolase activity in the presence of COS-7 lysates from cells transfected with expression vectors for LacZ or HILPDA (n = 2).

(C) Plasma TG levels after intravenous administration of tyloxapol to determine hepatic TG secretion in 16-hour fasted AAV-GFP and AAV-HILPDA animals (n = 7 animals per group).

(D and E) Lipoprotein-associated TG (D) and cholesterol (E) levels in HPLC fractions of pooled plasma samples from AAV-GFP and AAV-HILPDA animals.

(F-H) *Hilpda* mRNA (F) and protein levels (G) in wild-type animals after a 16-week HFD intervention resulting in the development of hepatic steatosis (H) (n = 8-10 animals per group).

Data are mean ± SEM. Asterisks indicate significant differences according to Student's t-test; **$P < 0.01$.

5

Hepatic TG secretion is decreased with HILPDA overexpression

To determine if HILPDA might impact TG secretion, we performed a VLDL production test in AAV-GFP and AAV-HILPDA mice using the lipase inhibitor tyloxapol. Remarkably, we noticed a robust reduction in hepatic TG secretion with HILPDA overexpression that was already apparent 1 hour after administration of tyloxapol (Figure 7C). Despite the inhibitory effect of HILPDA on hepatic TG secretion, we were unable to find significant changes in plasma total TG levels after 16 hours fasting (Figure 7C, time point 0) or in the fed state (Figure 5F). To investigate if HILPDA overexpression is associated with a difference in VLDL particle size or VLDL-TG content we performed lipoprotein profiling using gel-filtration high-performance liquid chromatography (HPLC). However, chylomicron and VLDL particle size and TG content, as well as LDL and HDL size and cholesterol content were unchanged between the two sets of mice (Table 1, Figures 7D and 7E). Finally, we explored the potential role of HILPDA in high fat diet-induced fatty liver. Interestingly, feeding wild-type mice a high-fat diet for 16 weeks did not elicit a change in liver HILPDA expression (Figures 7F and 7G), despite the development of severe hepatic steatosis (Figure 7H).

Table 1. VLDL, LDL, and HDL particle size in AAV-GFP and AAV-HILPDA animals

	AAV-GFP	AAV-HILPDA
Chylomicron (nm)	>100	>100
VLDL (nm)	46.46	46.99
LDL (nm)	24.67	24.78
HDL (nm)	11.08	11.15

Discussion

PPARα plays important roles in hepatic lipid metabolism by regulating the transcription of numerous genes involved in lipid metabolic pathways (33, 43). Here we provide evidence that *Hilpda* is a novel PPARα target gene that promotes hepatic TG deposition by reducing TG secretion.

One of our main findings is the inhibition of VLDL-TG secretion by hepatic HILPDA overexpression (Figure 7C). VLDL assembly and secretion have been studied extensively over the last decades (44). Central to the synthesis of VLDL is the lipidation of

apolipoprotein B100 (APOB100) in the endoplasmic reticulum (ER) by the microsomal triglyceride transfer protein (MTTP) to generate pre-VLDL (45-48). Next, large amount of lipids are transferred to pre-VLDL to yield mature VLDL, though it is not exactly clear whether this lipidation takes place solely in the ER or whether the Golgi-apparatus is involved as well (49-52). Indeed, many details regarding VLDL synthesis, ER to Golgi transport, and VLDL exocytosis remain unknown. Recently, additional players have been implicated in the lipidation and secretion of VLDL, including other apolipoproteins (APOC3), lipid droplet associated proteins (CIDEB), and sorting receptors (SORT1) (53-58). In vitro studies have previously identified HILPDA as a lipid droplet associated protein (36) and it is therefore of particular interest that the lipid droplet associated protein PLIN2 has been shown to inhibit VLDL synthesis due to increased shunting of triglycerides to cytosolic lipid droplets (55, 59). Future studies will have to determine the precise molecular mechanism underlying regulation of hepatic TG levels and secretion by HILPDA, as well as the molecular details of its association with lipids droplets.

Reduced hepatic VLDL-TG secretion might be expected to lead to a decrease in plasma TG levels. However, we did not observe a change in plasma TG levels when comparing AAV-GFP and AAV-HILPDA animals under either random fed conditions or after an overnight fast. A possible explanation is that VLDL produced in livers of mice overexpressing HILPDA is cleared from the circulation less efficiently, potentially due to an altered apolipoprotein make up decorating the VLDL.

The limited data available on HILPDA suggest that it may represent a lipid droplet associated protein that is induced by hypoxia (36, 60). Hypoxia is known to elicit numerous metabolic changes driven by the HIF transcription factors, including upregulation of many glycolytic genes (61-63). The specific regulatory effect of hypoxia/HIF1 on lipid metabolism is less well characterized, yet it is well known that hypoxia raises intracellular lipids (64-66). The rationale for hypoxia-induced lipid accumulation is not well characterized but it may be part of a general mechanism aimed at directing non-oxidized fatty acids towards storage, and thus shifting them away from potential lipotoxic effects. Taking into account the ability of HILPDA to promote intracellular lipid storage, it can be hypothesized that HILPDA may play a role in hypoxia-induced lipid accumulation.

The far majority of PPARα target genes identified so far are induced by fasting and by synthetic PPARα agonists in wild-type mice but not *Ppara*$^{-/-}$ mice, including *Fgf21*, *Cpt1a*, *Ehhadh*, *Hmcgcs2* and many others (67). In contrast, HILPDA expression was induced by fasting specifically in *Ppara*$^{-/-}$ mice but much less in wild-type mice, resembling the expression pattern of a small set of PPARα targets that include *Lpin2*. A number of genes with similar expression pattern were found to be regulated by PPARβ/δ, which may also

5

be true for Hilpda (67). Alternatively, upregulation of HILPDA in fasted *Ppara*$^{-/-}$ mice may be mediated by PPARγ, expression of which is elevated in livers of *Ppara*$^{-/-}$ mice and which potently induces *Hilpda* expression in liver, as shown by adenoviral overexpression of PPARγ. Transactivation experiments indicated that all three PPARs were able to activate a reporter construct driven by a portion of the *Hilpda* promoter, suggesting that *Hilpda* likely represents a pan-PPAR target gene. Accordingly, it can be hypothesized that depending on the specific stimulus, *Hilpda* can be regulated by either PPARα, PPARβ/δ, or PPARγ.

Synthetic PPARα agonists in the form of fibrates are used clinically for their ability to raise plasma HDL and reduce plasma TG levels (68). The plasma TG-lowering action of fibrates is primarily achieved via augmentation of plasma TG clearance, although there is in vivo and in vitro evidence that PPARα agonists also lower VLDL-TG production, potentially due to induction of PLIN2 and FABP1 and subsequent storage of TGs in cytosolic lipid droplets (69-72). Conversely, deletion of PPARα leads to elevated VLDL-TG production (73, 74). Conceivably, HILPDA may be involved in mediating the suppressive effect of synthetic PPARα agonists on TG secretion by the liver. Overall, it is evident that the role of PPARs in regulation of hepatic lipid homeostasis goes beyond the induction of genes involved in β-oxidation and ketogenesis. The direct effect of HILPDA on β-oxidation, lipid uptake, and lipogenesis has not been tested; nevertheless, we did not observe any difference in mRNA levels of key genes involved in these processes between AAV-GFP and AAV-HILPDA animals.

In conclusion, we identify *Hilpda* as a novel PPAR regulated gene involved in the regulation of hepatic TG metabolism. Increased HILPDA expression decreases the production of VLDL-TG resulting in the development of a fatty liver. Future experiments aim to elucidate the mechanism underlying the decrease in VLDL production.

Methods

Recombinant adeno-associated viruses (AAVs)
AAVs were made by Vector Biolabs (Philadelphia, PA, USA). In short, mouse *Hilpda* cDNA was inserted in pAAV-ALBp-3'iALB, a vector containing a modified albumin promoter flanked by two AAV2 derived Inverted Terminal Repeats (ITRs). To produce viruses, the above construct was packaged into AAV8 capsid in HEK293 cells by transfecting pAAV-ALBp-3'iALB, AAV2/AAV8 rep/cap vector, and Ad helper vector. Viral particles were purified by two sequential CsCl2 gradients and titrated by qPCR to determine viral genomes. The same amount of AAV2/AAV8 hybrid virus expressing GFP was injected to serve as control.

Animal studies

Wild-type and *Ppara*$^{-/-}$ mice on a Sv129 background were obtained from The Jackson Laboratory (Bar Harbor, ME, USA). Five-months-old wild-type and *Ppara*$^{-/-}$ mice were fed a diet containing Wy14643 at a concentration of 0.1% for 5 days after which the livers were excised and snap-frozen. Five-months-old wild-type and *Ppara*$^{-/-}$ mice were fasted for 24 hours and their livers were collected for analysis of HILPDA mRNA and protein levels.

Male 8-week-old C57BL/6J mice were purchased from Charles River Laboratories (Sulzfeld, Germany) and maintained on a 12-hour light-dark cycle with ad libitum access to chow and water. Adeno-associated viruses were administrated in a volume of 100 µl via the tail vein. Ten animals were injected with different amounts of AAV ranging from $1x10^{11}$ – $5x10^{11}$ genomic copies to determine the dose required for a significant increase in hepatic HILPDA expression. Subsequent experiments were performed after injection of $2.5x10^{11}$ GC. Body composition analysis of AAV-GFP and AAV-HILPDA animals 4 weeks post-injection was performed using EchoMRI (Echo Medical Systems, Houston, TX, USA).

Wild-type C57BL/6 animals (9-12 weeks old) were fed a low-fat or high-fat diet containing 10 or 45en% fat, respectively (D12450B/D12451, Research Diets Services, Wijk bij Duurstede, The Netherlands). After 16 weeks the livers where analyzed for triglyceride content and HILPDA expression.

All animal experiments were approved by the local animal welfare committees of Wageningen University or the German Cancer Research Center (DKFZ, Heidelberg, Germany), respectively.

VLDL production test

AAV-GFP and AAV-HILPDA animals were fasted for 16 hours and subsequently anesthetized via intra-peritoneal injection of a mixture of Dormicum (midazolam, Roche, Woerden, The Netherlands) and Hypnorm (fentanyl/fluanisone, VetaPharma, Leeds, United Kingdom) prepared in saline at 7 and 14/0.5 mg/kg, respectively. Then, a blood sample was drawn and the animals were injected intravenously with 500 mg/kg bodyweight tyloxapol (Sigma-Aldrich, Schnelldorf, Germany) diluted in saline to a 10% w/v solution. Every 30 minutes thereafter blood was collected via the tail vein over the course of 2 hours. Serum samples were assayed for triglycerides using a Triglycerides liquicolor^{mono} kit (HUMAN, Wiesbaden, Germany).

Hepatic Ppary1 overexpression

Ppara$^{-/-}$ mice were injected with adenovirus encoding *LacZ* or *Ppary1* via the tail vein and sacrificed 6 days later (75).

Liver slices

Livers from C57BL/6 mice were briefly perfused with saline, excised and submerged in ice-cold Krebs-Henseleit Buffer (KHB) supplemented with 11 mM glucose, 25 mM sodium bicarbonate, 10 mM HEPES, and penicillin/streptomycin. Next, 5 mm cylindrical liver cores were prepared with a surgical biopsy punch and sectioned to 200 µm slices using a Krumedieck tissue slicer (Alabama Research and

5

Development, Munford, AL, USA) filled with carbonated KHB. Liver slices were incubated in William's E Medium (Lonza, Verviers, Belgium) in 6-well plates at 37°C/5% CO_2 under continuous agitation. After 1 hour the media were replaced with fresh William's E Medium containing 0.1% DMSO or 20 µM Wy14643 and the slices were incubated for 6 or 24 hours.

Transactivation assays

A fragment of 645 bp and 519 bp containing the PPRE localized 1200 bp upstream of the TSS was amplified from human and mouse genomic DNA, respectively, using the primers: human Fwd1 5'-GCCTTCACCTGGCAAAGTAG-3', human Rev1 5'-AAGAGCCAGGAGGTCACAGA-3', mouse Fwd1 5'-GGATGACTCCCAGAAGTGGA-3', mouse Rev1 5'-GACCTGCCTTACCAGTCACC-3'. The resulting fragments were gel-purified using a QIAquick Gel Extraction Kit (Qiagen, Venlo, The Netherlands) and employed in a second PCR to introduce *KpnI* and *BglII* restriction sites to the resulting 278 bp and 219 bp fragments containing the human and mouse PPRE, respectively. Primers used for this PCR were: human Fwd2 5'-aaggtaccAGTTGGCTCCAAATGTCTGC-3', human Rev2 5'-cgaaagatctTGGTGGCTTTAGAACTGGCG-3', mouse Fwd2 5'-aaggtaccATTTCCACCTCCTGTGCTTG-3', mouse Rev2 5'-cgacagatctTGCGTTCTCATGACTTCCAG-3'. To introduce mutations in both the human and mouse PPRE an overlap PCR strategy was carried out. First, to generate partially overlapping fragments, the human Fwd2 primer was used together with reverse primer 5'-TCCCCACTGCGACCGGGCCCCTCCTTTCCT-3', and human Rev2 primer with forward primer 5'-AGGAAAGGAGGGGCCCGGTCGCAGTGGGGA-3' using wild-type insert as template. The resulting fragments were gel-purified and used in a second PCR with human Fwd2 and Rev2 primers. For mouse: Fwd2 primer was combined with reverse primer 5'-CTTCCGCTGTGACCGGGCCCCTACTTTTCA-3', and Rev2 primer with forward primer 5'-TGAAAAGTAGGGGCCCGGTCACAGCGGAAG-3'. For the final PCR, purified fragments were combined in a PCR to generate mutant insert using mouse Fwd2 and Rev2 primers. Resulting fragments were cloned in the *KpnI* and *BglII* sites of the pGL3-Promoter vector (Promega, Leiden, The Netherlands). The presence of the correct insert was confirmed with sequencing (EZ-Seq, Macrogen, Amsterdam, The Netherlands) using RV3primer: 5'-CTAGCAAAATAGGCTGTCCC-3' (Promega). Reporter vectors were transfected into the human hepatocellular cell line HepG2 (ATCC, Manassas, VA, USA) in the presence or absence of pSG5 vector expressing either PPARα, PPARβ/δ, PPARγ, or pSG5 empty vector. pSG5 expression vector encoding RXR was co-transfected with PPAR expression vectors. A β-galactosidase expression vector was co-transfected in all cases for determination of transfection efficiency. All transfections were performed using polyethylenimine (PEI). Sixteen hours post-transfection the cells were incubated with Wy14643 (50 µM), GW510516 (5 µM), Rosiglitazone (5 µM), or DMSO, respectively. Reporter activity was measured 24 hours after adding the corresponding ligands using the Promega luciferase assay kit (Promega) on a Fluoroskan Ascent apparatus (Thermo Scientific). β-Galactosidase activity in cell lysates was determined using 2-Nitrophenyl β-D-galactopyranoside (ONPG) as a substrate, and absorbance values were used to normalize the luciferase measurements. Data presented are based on 3 individual experiments.

ChIP

Primary hepatocytes were isolated from 10- to 12-week-old wild-type or *Ppara*$^{-/-}$ animals on a C57BL/6 background according to published methods (76). Hepatocytes were plated on 15 cm dished coated with rat-tail collagen at a density of 1×10^5 cells per cm^2. To cross-link proteins to DNA, the cells were incubated with 1% formaldehyde for 10 minutes after which glycine was added to a final concentration of 0.125 M to stop the cross-linking reaction. Cells were collected in ice-cold PBS, washed twice and snap-frozen in liquid nitrogen. Cell pellets were lysed in 500 µl lysis buffer containing 0.1% SDS, 1% Triton X-100, 0.15 M NaCl, 1 mM EDTA, 20 mM Tris pH 8, and protease inhibitor cocktail (Pierce). Following 30 cycles of sonication (30 seconds on, 30 seconds off, high intensity) at 4°C, the samples were centrifuged at 20,000 *g* for 30 minutes. Next, 100 µl of the supernatant was diluted 4 times with incubation buffer (0.15% SDS, 1% Triton X-100, 0.15 M NaCl, 1 mM EDTA, 20 mM HEPES) and subsequently mixed with antibodies (anti-PPARα (Santa-Cruz, H-98) or IgG (Santa Cruz, sc2027)) for 2 hours at 4°C on a rotating wheel. To reduce non-specific binding, Protein A Sepharose beads (GE Healthcare Life Sciences) were washed twice and pre-incubated with incubation buffer supplemented with 1 µg/µl BSA for 2 hours at 4°C on a rotating wheel. Then, blocked Protein A Sepharose mixture was combined with chromatin/antibody mixtures and incubated overnight at 4°C on a rotating wheel. The beads were subsequently washed in a series of buffers: twice in buffer 1 (0.1% SDS, 0.1% NaDOC, 1% Triton X-100, 0.15 M NaCl, 1 mM EDTA, 20 mM HEPES), once in buffer 2 (0.1% SDS, 0.1% NaDOC, 1% Triton X-100, 0.5 M NaCl, 1 mM EDTA, 20 mM HEPES), once in buffer 3 (0.25 M LiCl, 0.5% NaDOC, 0.5% NP-40, 1 mM EDTA, 20 mM HEPES) and twice in buffer 4 (1 mM EDTA, 20 mM HEPES). Protein-DNA complexes were eluted in 200 µl elution buffer (1% SDS + 0.1 M NaHCO3). To disrupt the cross-links between protein-DNA, eluted samples were supplemented with 8 µl of 5 M NaCl, 8 µl of RNAse A (0.5 mg/ml), and 10 µl of Proteinase K (20 mg/ml, Qiagen) and incubated overnight at 65°C. DNA was purified using a QiAQuick PCR purification kit (Qiagen) according to the manufacturer's protocol and analyzed by real-time PCR using primers directed against a 125 bp fragment encompassing the PPRE located 1200 base pair upstream of the TSS of *Hilpda*. Sequences of the primers that were used: Hilpda Fwd 5'-GCACGTCTCTCTTCTTCTAGGT-3', Hilpda Rev 5' TCGCCTCTAAACTAAACGGAA-3'. Primers against an intergenic region 100 kb upstream of *Pdk4* served as control: Fwd 5'-TTGGCTTGCCAAGCTTCTTC-3', Rev 5'-AGGGAACGCATTTCCATCAC-3'.

Plasma analysis

Non-esterified fatty acids were measured using a NEFA-HR(2) kit and ketone bodies using a Autokit Total Ketone Bodies assay (Wako Chemicals GmbH, Neuss, Germany). Triglycerides were determined with a Triglycerides liquicolor^{mono} kit (HUMAN). Glucose, glycerol, and cholesterol were measured using kits from DiaSys (DiaSys Diagnostic Systems, Holzheim, Germany).

5

Plasma lipoprotein analysis

Pooled plasma samples from AAV-GFP and AAV-HILPDA animals were fractionated using gel-filtration high-performance liquid chromatography (HPLC) offered by LipoSEARCH (Skylight Biotech, Inc., Akita, Japan). Effluent was subsequently analyzed for triglycerides and cholesterol content.

Histology

For GFP fluorescence microscopy, samples were fixed in 4% formaldehyde (Sigma-Aldrich) overnight, soaked in PBS containing 15% w/v sucrose for 12 hours then incubated in PBS containing 30% w/v sucrose overnight. Tissues were subsequently frozen in Tissue-Tek® O.C.T.™ (Sakura Finetek Holland B.V., Alphen aan de Rijn, The Netherlands) and sectioned to 5 μm and mounted on Superfrost microscopy slides. GFP fluorescence was determined using an Olympus CKX31 fluorescent microscope (Olympus Nederland B.V, Zoeterwoude, The Netherlands).

For hematoxylin and eosin staining liver pieces were fixed in 4% formaldehyde for 24 hours and subsequently embedded in paraffin. Samples were sectioned to 5 μM and stained in hematoxylin for 8 minutes and eosin for 30 seconds. Following dehydration in 95% ethanol and 2 xylene changes, the sections were mounted using a xylene based mounting medium.

To visualize neutral lipids, liver samples were frozen in Tissue-Tek® O.C.T.™, sectioned to 5 μm using a cryostat and mounted on Superfrost microscopy slides. After drying at room temperature for 30 minutes, the tissue sections were fixed in 4% formaldehyde (Sigma-Aldrich) for 10 minutes. Following 3 washes with ddH$_2$O the slides were incubated in Oil Red O (Sigma-Aldrich) solution (30 mg/ml in 60% isopropanol) for 10 minutes. Finally, the slides were rinsed with ddH2O twice and mounted using an aqueous mounting medium.

Hepatic triglycerides

Liver pieces of ~50 mg were homogenized to a 5% lysate (m/v) using 10 mM Tris, 2 mM EDTA, 0.25 M sucrose, pH 7.5. Lysates were assayed for TGs using a Triglycerides liquicolor^{mono} kit (HUMAN). TG levels were normalized against liver weight.

Hepatic glycogen

Tissues (~50 mg) were homogenized in 0.5 ml 30% KOH, incubated at 95°C for 30 minutes. And centrifuged at 15,000 g to pellet undigested material. Glycogen was precipitated from the supernatants by adding 0.75 ml 95% ethanol and subsequent centrifugation at 3,000 g for 20 minutes. Glycogen pellets were washed with fresh 95% ethanol, centrifuged, and air-dried. Pellets were dissolved in 0.25 ml ddH2O and incubated at 37°C for 30 minutes. To digest the glycogen, 5 mg of amyloglucosidase (#A7420, Sigma-Aldrich) was dissolved in 15 ml 0.2 M sodium acetate pH 4.8, and 450 μl of the resulting enzyme solution was mixed with 50 μl glycogen solution. After incubation at 40°C for 2 hours the samples were neutralized using 10 μl 30% KOH. Glucose concentrations were determined with a kit from DiaSys, protein concentrations were measured with a Pierce BCA kit (Thermo Scientific, Landsmeer, The Netherlands).

Western blot

Liver samples were homogenized in 50 mM Tris, pH 8.0, 150 mM NaCl, 1% v/v NP-40, 0.5% v/v sodium deoxycholate, 0.1% SDS, supplemented with Complete EDTA-free protease inhibitor cocktail with a Qiagen TissueLyser II. Samples were incubated on a rotating wheel for 30 minutes at 4ºC and subsequently centrifuged at 15,000 *g* for 15 minutes at 4°C. Protein concentration was determined using a Pierce BCA kit (Thermo Scientific) and equal amounts of protein were diluted with 2x Laemmli sample buffer. After boiling, the samples were separated on 4-20% or 8-16% gradient Criterion gels. For plasma analysis, 1 µl plasma from AAV-GFP or AAV-HILPDA animals was loaded on an 8-16% Criterion gel. Proteins were transferred to PVDF membrane using the Transblot turbo system (Bio-Rad, Veenendaal, The Netherlands). Antibodies against HILPDA (1:1000, Santa Cruz Biotechnology, Inc, #sc-137518), ACTIN (1:2000, Sigma-Aldrich #A2066), HSP90 (1:4000, Cell Signaling Technology, Inc, #4874), and goat anti-rabbit (1:5000, Jackson ImmunoResearch, #111-035-003) were diluted in 5% w/v skimmed milk powder in PBS-T. Primary antibodies were applied overnight at 4ºC, secondary antibody for 1 hour at room temperature. Bands were visualized using Pierce ECL Plus (Thermo Scientific) and a ChemiDoc MP (Bio-Rad). The presence of plasma proteins on the PVDF membrane was confirmed using Ponceau S solution (Sigma-Aldrich).

Gene expression analysis including microarrays

Mouse liver slices and tissues were homogenized in TRIzol® (Life Technologies Europe BV, Bleiswijk, The Netherlands) using the Qiagen TissueLyser II and stainless steel beads. One microgram of RNA was subsequently employed for cDNA synthesis using the First Strand cDNA synthesis kit (Thermo Scientific). RNA from a selection of slices and tissues was purified with RNeasy Minikit columns (Qiagen) and analyzed for quality with RNA 6000 Nano chips on the Agilent 2100 Bioanalyzer (Agilent Technologies, Amsterdam, the Netherlands). Purified RNA (100 ng) was labeled with the Ambion WT expression kit (Life Technologies, Bleiswijk, The Netherlands kit and hybridized to Affymetrix Mouse Gene 1.1 ST array plate (Affymetrix, Santa Clara, CA). Hybridization, washing, and scanning was carried out on an Affymetrix GeneTitan platform, and readouts were processed and analyzed according to published methods (77). qPCRs were performed using SensiMix (Bioline, GC biotech, Alphen aan den Rijn, The Netherlands) and a CFX384 Real-Time PCR Detection System (Bio-Rad). Primer sequences were derived from the Harvard PrimerBank and synthesized by Eurogentec (Eurogentec S.A., Seraing, Belgium). Primer sequences are listed in Table 2. Normalization was performed using the expression of 36b4. qPCR analysis of mouse and human hepatocytes exposed to DMSO or Wy14643 for 6 hours was performed as described above using RNA from hepatocytes of 6 different mouse strains and 6 human hepatocyte sample sets as described (78).

ATGL and HSL activity assay

COS-7 cells were grown in DMEM (Invitrogen, Carlsbad, CA) supplemented with 10% fetal calf serum (Sigma-Aldrich) and 100 IU/ml penicillin / 100 µg/ml streptomycin (Invitrogen). cDNAs encoding ATGL/PNPLA2, HSL, HILPDA, and LacZ were cloned in the pcDNA4/His Max vector (Invitrogen)

5

125

Table 2. Primers sequences of forward and reverse primers used in qPCR analysis

Gene	Forward (5'-3')	Reverse (5'-3')
36b4	ATGGGTACAAGCGCGTCCTG	GCCTTGACCTTTTCAGTAAG
Hilpda	TGCTGGGCATCATGTTGACC	TGACCCCTCGTGATCCAGG
Pparg	CACAATGCCATCAGGTTTGG	GCTGGT CGATATCACTGGAGATC
Cpt1a	CTCAGTGGGAGCGACTCTTCA	GGCCTCTGTGGTACACGACAA
Cyp4a10	ACCACAATGTGCATCAAGGAGGCC	AGGAATGAGTGGCTGTGTCGGGGAGAG
Pdk4	TCTACAAACTCTGACAGGGCTTT	CCGCTTAGTGAACACTCCTTC
Srebp1c	GGAGCCATGGATTGCACATT	CCTGTCTCACCCCCAGCATA
Fasn	TCCTGGGAGGAATGTAAACAGC	CACAAATTCATTCACTGCAGCC
Ldlr	GCATCAGCTTGGACAAGGTGT	GGGAACAGCCACCATTGTTG
Mttp	ATACAAGCTCACGTACTCCACT	TCCACAGTAACACAACGTCCA

and transfected into COS-7 cells using Metafectene (Biontex GmbH, München, Germany). 50 μg of either ATGL or HSL recombinant lysate was combined with 50 μg LacZ or HILPDA lysate. Radioactive emulsion was prepared by sonication of 0.3 mM triolein, phosphatidylcholine/phosphatidylinositol, and 9,10-[³H] triolein (PerkinElmer Life Sciences) in 100 mM potassium phosphate buffer (pH 7) supplemented with 2% BSA (essentially fatty acid free, Sigma). Protein lysates and radioactive emulsion were incubated for 60 minutes at 37°C. Next, the reactions were stopped by adding 3.25 ml of methanol/chloroform/heptane (10:9:7) and 1 ml of 0.1 M potassium carbonate/boric acid buffer (pH 10.5). Samples were centrifuged at 800 g for 20 minutes and radioactivity was determined in 1 ml of the supernatant using a scintillation counter (Beckman Coulter, Fullerton, CA)

Total TG hydrolase activity assay
Liver TG hydrolase activity was measured using published methods (79, 80). In short, samples from AAV-GFP and AAV-HILPDA animals were homogenized in lysis buffer (0.25 M sucrose, 1 mM EDTA, protease inhibitor cocktail, pH 7.0) and centrifuged at 20,000 g for 30 minutes at 4°C to collect the soluble infranatant fraction. Triolein and 9,10-[³H]triolein (PerkinElmer Life Sciences) were sonicated with phosphatidylcholine and phosphatidylinositol in 100mM potassium phosphate buffer (pH 7.0) to a final concentration of 1.67 mM triolein. 200 μg of infranatant from each liver sample was incubated with 0.1 ml radioactive substrate at 37°C for 60 minutes. The reaction was terminated by adding 3.25 ml of methanol/chloroform/heptane (10:9:7) and 1 ml of 0.1 M potassium carbonate/boric acid buffer (pH 10.5). Following centrifugation at 800 g for 20 minutes, radioactivity was determined in 1 ml of the upper phase using a LS 6500 Multi-Purpose Scintillation Counter (Beckman Coulter).

Statistical analysis
Student's t-tests or two-way ANOVA with Bonferroni post-hoc tests where appropriate were calculated using GraphPad Prism (GraphPad Software, Inc., La Jolla, CA). Results were considered significant at $P < 0.05$.
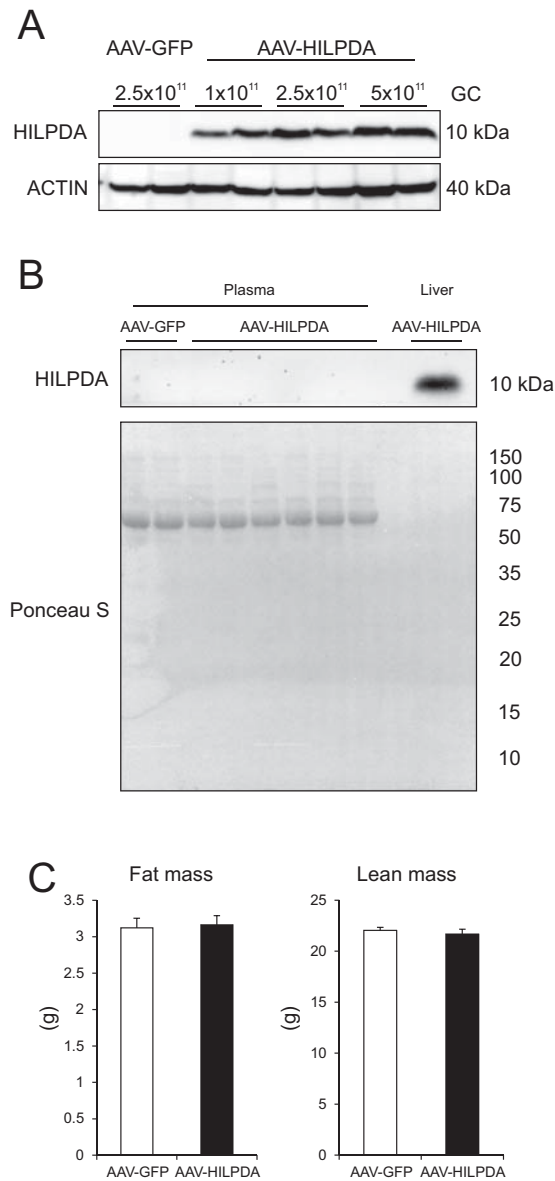
Acknowledgements

References

1. Mashek DG. Hepatic Fatty Acid Trafficking: Multiple Forks in the Road. *Adv Nutr.* 2013;4(6):697-710.
2. McPherson PA, McEneny J. The biochemistry of ketogenesis and its role in weight management, neurological disease and oxidative stress. *J Physiol Biochem.* 2012;68(1):141-151.
3. Sun Z, Lazar MA. Dissociating fatty liver and diabetes. *Trends Endocrinol Metab.* 2013;24(1):4-12.
4. Oh KJ, Han HS, Kim MJ, Koo SH. Transcriptional regulators of hepatic gluconeogenesis. *Arch Pharm Res.* 2013;36(2):189-200.
5. Kersten S. Effects of fatty acids on gene expression: role of peroxisome proliferator-activated receptor alpha, liver X receptor alpha and sterol regulatory element-binding protein-1c. *Proc Nutr Soc.* 2002;61(3):371-374.
6. Nakamura MT, Cheon Y, Li Y, Nara TY. Mechanisms of regulation of gene expression by fatty acids. *Lipids.* 2004;39(11):1077-1083.
7. Renga B, Mencarelli A, D'Amore C, Cipriani S, Baldelli F, Zampella A, Distrutti E, Fiorucci S. Glucocorticoid receptor mediates the gluconeogenic activity of the farnesoid X receptor in the fasting condition. *FASEB J.* 2012;26(7):3021-3031.
8. Chawla A, Repa JJ, Evans RM, Mangelsdorf DJ. Nuclear receptors and lipid physiology: opening the X-files. *Science.* 2001;294(5548):1866-1870.
9. Sonoda J, Pei L, Evans RM. Nuclear receptors: decoding metabolic disease. *FEBS Lett.* 2008;582(1):2-9.
10. Bulynko YA, O'Malley BW. Nuclear receptor coactivators: structural and functional biochemistry. *Biochemistry.* 2011;50(3):313-328.
11. Han SJ, Lonard DM, O'Malley BW. Multi-modulation of nuclear receptor coactivators through posttranslational modifications. *Trends Endocrinol Metab.* 2009;20(1):8-15.
12. Rodgers JT, Lerin C, Gerhart-Hines Z, Puigserver P. Metabolic adaptations through the PGC-1 alpha and SIRT1 pathways. *FEBS Lett.* 2008;582(1):46-53.
13. Perissi V, Jepsen K, Glass CK, Rosenfeld MG. Deconstructing repression: evolving models of co-repressor action. *Nat Rev Genet.* 2010;11(2):109-123.
14. Mottis A, Mouchiroud L, Auwerx J. Emerging roles of the corepressors NCoR1 and SMRT in homeostasis. *Genes Dev.* 2013;27(8):819-835.
15. Issemann I, Green S. Activation of a member of the steroid hormone receptor superfamily by peroxisome proliferators. *Nature.* 1990;347(6294):645-650.
16. Kersten S, Desvergne B, Wahli W. Roles of PPARs in health and disease. *Nature.* 2000;405(6785):421-424.
17. Montagner A, Rando G, Degueurce G, Leuenberger N, Michalik L, Wahli W. New insights into the role of PPARs. *Prostaglandins Leukot Essent Fatty Acids.* 2011;85(5):235-243.
18. Forman BM, Chen J, Evans RM. The peroxisome proliferator-activated receptors: ligands and activators. *Ann N Y Acad Sci.* 1996;804:266-275.
19. Schupp M, Lazar MA. Endogenous ligands for nuclear receptors: digging deeper. *J Biol Chem.* 2010;285(52):40409-40415.

5

20. Ahmadian M, Suh JM, Hah N, Liddle C, Atkins AR, Downes M, Evans RM. PPARgamma signaling and metabolism: the good, the bad and the future. *Nat Med.* 2013;19(5):557-566.

21. Vu-Dac N, Schoonjans K, Kosykh V, Dallongeville J, Fruchart JC, Staels B, Auwerx J. Fibrates increase human apolipoprotein A-II expression through activation of the peroxisome proliferator-activated receptor. *J Clin Invest.* 1995;96(2):741-750.

22. Lalloyer F, Staels B. Fibrates, glitazones, and peroxisome proliferator-activated receptors. *Arterioscler Thromb Vasc Biol.* 2010;30(5):894-899.

23. Rosenson RS, Wright RS, Farkouh M, Plutzky J. Modulating peroxisome proliferator-activated receptors for therapeutic benefit? Biology, clinical experience, and future prospects. *Am Heart J.* 2012;164(5):672-680.

24. Poulsen L, Siersbaek M, Mandrup S. PPARs: fatty acid sensors controlling metabolism. *Semin Cell Dev Biol.* 2012;23(6):631-639.

25. Keller H, Dreyer C, Medin J, Mahfoudi A, Ozato K, Wahli W. Fatty acids and retinoids control lipid metabolism through activation of peroxisome proliferator-activated receptor-retinoid X receptor heterodimers. *Proc Natl Acad Sci U S A.* 1993;90(6):2160-2164.

26. Tugwood JD, Issemann I, Anderson RG, Bundell KR, McPheat WL, Green S. The mouse peroxisome proliferator activated receptor recognizes a response element in the 5' flanking sequence of the rat acyl CoA oxidase gene. *EMBO J.* 1992;11(2):433-439.

27. Lemay DG, Hwang DH. Genome-wide identification of peroxisome proliferator response elements using integrated computational genomics. *J Lipid Res.* 2006;47(7):1583-1587.

28. Dreyer C, Krey G, Keller H, Givel F, Helftenbein G, Wahli W. Control of the peroxisomal beta-oxidation pathway by a novel family of nuclear hormone receptors. *Cell.* 1992;68(5):879-887.

29. Evans RM, Barish GD, Wang YX. PPARs and the complex journey to obesity. *Nat Med.* 2004;10(4):355-361.

30. Tontonoz P, Spiegelman BM. Fat and beyond: the diverse biology of PPARgamma. *Annu Rev Biochem.* 2008;77:289-312.

31. Bojic LA, Huff MW. Peroxisome proliferator-activated receptor delta: a multifaceted metabolic player. *Curr Opin Lipidol.* 2013;24(2):171-177.

32. Mandard S, Muller M, Kersten S. Peroxisome proliferator-activated receptor alpha target genes. *Cell Mol Life Sci.* 2004;61(4):393-416.

33. Rakhshandehroo M, Sanderson LM, Matilainen M, Stienstra R, Carlberg C, de Groot PJ, Muller M, Kersten S. Comprehensive analysis of PPARalpha-dependent regulation of hepatic lipid metabolism by expression profiling. *PPAR Res.* 2007;2007:26839.

34. Rakhshandehroo M, Knoch B, Muller M, Kersten S. Peroxisome proliferator-activated receptor alpha target genes. *PPAR Res.* 2010;2010.pii:612089.

35. Kersten S, Seydoux J, Peters JM, Gonzalez FJ, Desvergne B, Wahli W. Peroxisome proliferator-activated receptor alpha mediates the adaptive response to fasting. *J Clin Invest.* 1999;103(11):1489-1498.

36. Gimm T, Wiese M, Teschemacher B, Deggerich A, Schodel J, Knaup KX, Hackenbeck T, Hellerbrand C, Amann K, Wiesener MS, et al. Hypoxia-inducible protein 2 is a novel lipid droplet protein and a specific target gene of hypoxia-inducible factor-1. *FASEB J.* 2010;24(11):4443-4458.

37. Patsouris D, Reddy JK, Muller M, Kersten S. Peroxisome proliferator-activated receptor alpha mediates the effects of high-fat diet on hepatic gene expression. *Endocrinology.* 2006;147(3):1508-1516.

38. Hashimoto T, Cook WS, Qi C, Yeldandi AV, Reddy JK, Rao MS. Defect in peroxisome proliferator-activated receptor alpha-inducible fatty acid oxidation determines the severity of hepatic steatosis in response to fasting. *J Biol Chem.* 2000;275(37):28918-28928.

39.   Zandbergen F, Mandard S, Escher P, Tan NS, Patsouris D, Jatkoe T, Rojas-Caro S, Madore S, Wahli W, Tafuri S, et al. The G0/G1 switch gene 2 is a novel PPAR target gene. *Biochem J.* 2005;392(Pt 2):313-324.

40.   Yang X, Lu X, Lombes M, Rha GB, Chi YI, Guerin TM, Smart EJ, Liu J. The G(0)/G(1) switch gene 2 regulates adipose lipolysis through association with adipose triglyceride lipase. *Cell Metab.* 2010;11(3):194-205.

41.   Wang Y, Zhang Y, Qian H, Lu J, Zhang Z, Min X, Lang M, Yang H, Wang N, Zhang P. The g0/g1 switch gene 2 is an important regulator of hepatic triglyceride metabolism. *PLoS One.* 2013;8(8):e72315.

42.   Zhang X, Xie X, Heckmann BL, Saarinen AM, Czyzyk TA, Liu J. Target Disruption of G0/G1 Switch Gene 2 Enhances Adipose Lipolysis, Alters Hepatic Energy Balance, and Alleviates High Fat Diet-Induced Liver Steatosis. *Diabetes.* 2014;63(3):934-46.

43.   Pyper SR, Viswakarma N, Yu S, Reddy JK. PPARalpha: energy combustion, hypolipidemia, inflammation and cancer. *Nucl Recept Signal.* 2010;8:e002.

44.   Tiwari S, Siddiqi SA. Intracellular trafficking and secretion of VLDL. *Arterioscler Thromb Vasc Biol.* 2012;32(5):1079-1086.

45.   Gordon DA, Jamil H, Sharp D, Mullaney D, Yao Z, Gregg RE, Wetterau J. Secretion of apolipoprotein B-containing lipoproteins from HeLa cells is dependent on expression of the microsomal triglyceride transfer protein and is regulated by lipid availability. *Proc Natl Acad Sci U S A.* 1994;91(16):7628-7632.

46.   Gordon DA, Jamil H, Gregg RE, Olofsson SO, Boren J. Inhibition of the microsomal triglyceride transfer protein blocks the first step of apolipoprotein B lipoprotein assembly but not the addition of bulk core lipids in the second step. *J Biol Chem.* 1996;271(51):33047-33053.

47.   Jamil H, Gordon DA, Eustice DC, Brooks CM, Dickson JK, Jr., Chen Y, Ricci B, Chu CH, Harrity TW, Ciosek CP, Jr., et al. An inhibitor of the microsomal triglyceride transfer protein inhibits apoB secretion from HepG2 cells. *Proc Natl Acad Sci U S A.* 1996;93(21):11991-11995.

48.   Mitchell DM, Zhou M, Pariyarath R, Wang H, Aitchison JD, Ginsberg HN, Fisher EA. Apoprotein B100 has a prolonged interaction with the translocon during which its lipidation and translocation change from dependence on the microsomal triglyceride transfer protein to independence. *Proc Natl Acad Sci U S A.* 1998;95(25):14733-14738.

49.   Gusarova V, Brodsky JL, Fisher EA. Apolipoprotein B100 exit from the endoplasmic reticulum (ER) is COPII-dependent, and its lipidation to very low density lipoprotein occurs post-ER. *J Biol Chem.* 2003;278(48):48051-48058.

50.   Higgins JA. Evidence that during very low density lipoprotein assembly in rat hepatocytes most of the triacylglycerol and phospholipid are packaged with apolipoprotein B in the Golgi complex. *FEBS Lett.* 1988;232(2):405-408.

51.   Yamaguchi J, Gamble MV, Conlon D, Liang JS, Ginsberg HN. The conversion of apoB100 low density lipoprotein/high density lipoprotein particles to apoB100 very low density lipoproteins in response to oleic acid occurs in the endoplasmic reticulum and not in the Golgi in McA RH7777 cells. *J Biol Chem.* 2003;278(43):42643-42651.

52.   Borchardt RA, Davis RA. Intrahepatic assembly of very low density lipoproteins. Rate of transport out of the endoplasmic reticulum determines rate of secretion. *J Biol Chem.* 1987;262(34):16394-16402.

53.   Qin W, Sundaram M, Wang Y, Zhou H, Zhong S, Chang CC, Manhas S, Yao EF, Parks RJ, McFie PJ, et al. Missense mutation in APOC3 within the C-terminal lipid binding domain of human ApoC-III results in impaired assembly and secretion of triacylglycerol-rich very low density lipoproteins: evidence that ApoC-III plays a major role in the formation of lipid precursors within the microsomal lumen. *J Biol Chem.* 2011;286(31):27769-27780.

5

54. Ye J, Li JZ, Liu Y, Li X, Yang T, Ma X, Li Q, Yao Z, Li P. Cideb, an ER- and lipid droplet-associated protein, mediates VLDL lipidation and maturation by interacting with apolipoprotein B. *Cell Metab.* 2009;9(2):177-190.

55. Li X, Ye J, Zhou L, Gu W, Fisher EA, Li P. Opposing roles of cell death-inducing DFF45-like effector B and perilipin 2 in controlling hepatic VLDL lipidation. *J Lipid Res.* 2012;53(9):1877-1889.

56. Tiwari S, Siddiqi S, Siddiqi SA. CideB protein is required for the biogenesis of very low density lipoprotein (VLDL) transport vesicle. *J Biol Chem.* 2013;288(7):5157-5165.

57. Musunuru K, Strong A, Frank-Kamenetsky M, Lee NE, Ahfeldt T, Sachs KV, Li X, Li H, Kuperwasser N, Ruda VM, et al. From noncoding variant to phenotype via SORT1 at the 1p13 cholesterol locus. *Nature.* 2010;466(7307):714-719.

58. Strong A, Ding Q, Edmondson AC, Millar JS, Sachs KV, Li X, Kumaravel A, Wang MY, Ai D, Guo L, et al. Hepatic sortilin regulates both apolipoprotein B secretion and LDL catabolism. *J Clin Invest.* 2012;122(8):2807-2816.

59. Magnusson B, Asp L, Bostrom P, Ruiz M, Stillemark-Billton P, Linden D, Boren J, Olofsson SO. Adipocyte differentiation-related protein promotes fatty acid storage in cytosolic triglycerides and inhibits secretion of very low-density lipoproteins. *Arterioscler Thromb Vasc Biol.* 2006;26(7):1566-1571.

60. Denko N, Schindler C, Koong A, Laderoute K, Green C, Giaccia A. Epigenetic regulation of gene expression in cervical cancer cells by the tumor microenvironment. *Clin Cancer Res.* 2000;6(2):480-487.

61. Webster KA. Evolution of the coordinate regulation of glycolytic enzyme genes by hypoxia. *J Exp Biol.* 2003;206(Pt 17):2911-2922.

62. Shaw RJ. Glucose metabolism and cancer. *Curr Opin Cell Biol.* 2006;18(6):598-608.

63. Semenza GL. Regulation of metabolism by hypoxia-inducible factor 1. *Cold Spring Harb Symp Quant Biol.* 2011;76:347-353.

64. Gordon GB, Barcza MA, Bush ME. Lipid accumulation of hypoxic tissue culture cells. *Am J Pathol.* 1977;88(3):663-678.

65. Nath B, Levin I, Csak T, Petrasek J, Mueller C, Kodys K, Catalano D, Mandrekar P, Szabo G. Hepatocyte-specific hypoxia-inducible factor-1alpha is a determinant of lipid accumulation and liver injury in alcohol-induced steatosis in mice. *Hepatology.* 2011;53(5):1526-1537.

66. Qu A, Taylor M, Xue X, Matsubara T, Metzger D, Chambon P, Gonzalez FJ, Shah YM. Hypoxia-inducible transcription factor 2alpha promotes steatohepatitis through augmenting lipid accumulation, inflammation, and fibrosis. *Hepatology.* 2011;54(2):472-483.

67. Sanderson LM, Degenhardt T, Koppen A, Kalkhoven E, Desvergne B, Muller M, Kersten S. Peroxisome proliferator-activated receptor beta/delta (PPARbeta/delta) but not PPARalpha serves as a plasma free fatty acid sensor in liver. *Mol Cell Biol.* 2009;29(23):6257-6267.

68. Duval C, Muller M, Kersten S. PPARalpha and dyslipidemia. *Biochim Biophys Acta.* 2007;1771(8):961-971.

69. Shah A, Rader DJ, Millar JS. The effect of PPAR-alpha agonism on apolipoprotein metabolism in humans. *Atherosclerosis.* 2010;210(1):35-40.

70. Kersten S. Peroxisome proliferator activated receptors and lipoprotein metabolism. *PPAR Res.* 2008;2008:132960.

71. Edvardsson U, Ljungberg A, Linden D, William-Olsson L, Peilot-Sjogren H, Ahnmark A, Oscarsson J. PPARalpha activation increases triglyceride mass and adipose differentiation-related protein in hepatocytes. *J Lipid Res.* 2006;47(2):329-340.

72. Linden D, Lindberg K, Oscarsson J, Claesson C, Asp L, Li L, Gustafsson M, Boren J, Olofsson SO. Influence of peroxisome proliferator-activated receptor alpha agonists on the intracellular turnover and secretion of apolipoprotein (Apo) B-100 and ApoB-48. *J Biol Chem.* 2002;277(25):23044-23053.

73. Linden D, Alsterholm M, Wennbo H, Oscarsson J. PPARalpha deficiency increases secretion and serum levels of apolipoprotein B-containing lipoproteins. *J Lipid Res.* 2001;42(11):1831-1840.

74. Tordjman K, Bernal-Mizrachi C, Zemany L, Weng S, Feng C, Zhang F, Leone TC, Coleman T, Kelly DP, Semenkovich CF. PPARalpha deficiency reduces insulin resistance and atherosclerosis in apoE-null mice. *J Clin Invest.* 2001;107(8):1025-1034.

75. Yu S, Matsusue K, Kashireddy P, Cao WQ, Yeldandi V, Yeldandi AV, Rao MS, Gonzalez FJ, Reddy JK. Adipocyte-specific gene expression and adipogenic steatosis in the mouse liver due to peroxisome proliferator-activated receptor gamma1 (PPARgamma1) overexpression. *J Biol Chem.* 2003;278(1):498-505.

76. Berry MN, Friend DS. High-yield preparation of isolated rat liver parenchymal cells: a biochemical and fine structural study. *J Cell Biol.* 1969;43(3):506-520.

77. Lichtenstein L, Mattijssen F, de Wit NJ, Georgiadi A, Hooiveld GJ, van der Meer R, He Y, Qi L, Koster A, Tamsma JT, et al. Angptl4 protects against severe proinflammatory effects of saturated fat by inhibiting fatty acid uptake into mesenteric lymph node macrophages. *Cell Metab.* 2010;12(6):580-592.

78. Rakhshandehroo M, Hooiveld G, Muller M, Kersten S. Comparative analysis of gene regulation by the transcription factor PPARalpha between mouse and human. *PLoS One.* 2009;4(8):e6796.

79. Haemmerle G, Lass A, Zimmermann R, Gorkiewicz G, Meyer C, Rozman J, Heldmaier G, Maier R, Theussl C, Eder S, et al. Defective lipolysis and altered energy metabolism in mice lacking adipose triglyceride lipase. *Science.* 2006;312(5774):734-737.

80. Lass A, Zimmermann R, Haemmerle G, Riederer M, Schoiswohl G, Schweiger M, Kienesberger P, Strauss JG, Gorkiewicz G, Zechner R. Adipose triglyceride lipase-mediated lipolysis of cellular fat stores is activated by CGI-58 and defective in Chanarin-Dorfman Syndrome. *Cell Metab.* 2006;3(5):309-319.

5

A

AAV-GFP   AAV-HILPDA

2.5x10^{11} 1x10^{11} 2.5x10^{11} 5x10^{11} GC

HILPDA   10 kDa

ACTIN   40 kDa

B

Plasma   Liver

AAV-GFP   AAV-HILPDA   AAV-HILPDA

HILPDA   10 kDa

Ponceau S
150
100
75
50
35
25
20
15
10

C

Fat mass   Lean mass

(g)   (g)

AAV-GFP   AAV-HILPDA   AAV-GFP   AAV-HILPDA

Supplemental Figure 1.

(A) Western blot analysis of hepatic HILPDA expression after administration of 1, 2.5, and 5x10^{11} genomic copies of AAV-HILPDA. Livers were dissected 4 weeks after injection of respective viruses.

(B) HILPDA Western blot on plasma samples of the same animals as in A. An aliquot of diluted liver lysate from an animal injected with 2.5x10^{11} GC AAV-HILPDA virus was used as positive control. Ponceau S staining is shown to illustrate the presence of plasma proteins.

(C) Fat mass and lean mass in AAV-GFP and AAV-HILPDA animals determined using EchoMRI (n = 10-13 animals per group).

Data are mean ± SEM.

5

6

Hypoxia inducible lipid droplet associated (HILPDA) is a PPARγ and β-adrenergic receptor target gene involved in adipose tissue lipolysis

F Mattijssen, Z Xue, W Dijk, I Tasdelen, A Vegiopoulos,
W Kalkhoven, R Stienstra, S Mandrup, L Qi, S Kersten

Abstract

Peroxisomal-proliferator activator receptor gamma (PPARγ) is a ligand-activated transcription factor of eminent importance in the development and maintenance of adipose tissue. Hypoxia inducible lipid droplet associated protein (HILPDA) is a newly recognized PPAR target gene involved in the regulation of hepatic VLDL secretion. Here we study the regulation of and function of HILPDA in adipose tissue. HILPDA expression increased upon fasting whereas high-fat feeding induced the opposite effect. In congruence with PPARγ binding as determined by ChIP-seq, we revealed *Hilpda* to be regulated by PPARγ in a number of mouse and human adipocyte models. Moreover, HILPDA was potently induced upon β-adrenergic receptor stimulation. Manipulation of HILPDA expression in vitro did not affect the adipogenic capacity of 3T3-L1 cells. Adipose tissue-specific *Hilpda* knockout mice showed no major metabolic perturbations when fasted. However, overexpression of HILPDA in adipocytes was found to reduce the amount of NEFAs released upon β-adrenergic receptor activation. Thus, HILPDA is regulated by PPARγ and β-adrenergic receptor and is potentially part of a feedback mechanism to regulate adipocyte lipolysis.

Introduction

The peroxisomal-proliferator activator receptor gamma (PPARγ, NR1C3) is a ligand activated transcription factor that is part of the PPAR family of nuclear receptors (1). Whereas the other two family members, PPARα and PPARβ/δ, are expressed ubiquitously, PPARγ expression is predominant in adipose tissue (2-4). PPARs have a classical structure observed in many nuclear receptors that includes an N-terminal activation function (AF1), a DNA-binding domain, and a ligand binding domain that contains a ligand-dependent activation function (AF2) (5). All three PPARs function in conjunction with their obligatory binding partner, the retinoid x receptor (RXR). Ligand activation of PPARs initiates the recruitment of coactivators including CBP, SRC-1, and TBL1/TBLR1 (6-10) and at the same time the dismissal of corepressors such as NCoR/SMRT (11, 12), although many mechanistic aspects regarding cofactor recruitment and dismissal remain elusive (13). PPARs bind to specific loci in the DNA, called PPAR response elements (PPRE) that are localized across the genome in promoter regions but also in intronic or intergenic regions.

Shortly after the initial cloning of PPARs (14, 15), PPARγ was found to drive adipocyte differentiation (1). Subsequent studies using in vivo gene targeting have shown that PPARγ is indispensable for normal development of adipose tissue (16, 17). There are two variants of PPARγ, PPARγ1 and PPARγ2, due to alternative promoter usage and alternative splicing (4). PPARγ2 contains 30 additional amino acids at its N-terminus and is exclusively expressed in adipose tissue, whereas PPARγ1 is expressed in several tissues including colon and liver (18). Both isoforms are capable of inducing adipogenesis, with PPARγ2 being the most potent (4). Target genes of PPARγ include genes related to adipogenesis (*Cebpa*), lipid uptake and transport (*Lpl*, *Cd36*, *Fabp4*), uncoupling (*Ucp1*), lipid droplets associated proteins (*Plin1*, *Plin2*, *Cidea*, *Cidec*) and glucose metabolism (*Adipoq*, *Pck1*, *Slc2a4*) (4, 19-26).

The complete set of endogenous ligands for PPARγ has not been well characterized, though the general consensus is that fatty acids and mainly their derivatives such as prostaglandins can serve as PPARγ activators (27, 28). The most well-known PPARγ ligands are the insulin-sensitizing thiazolidinedione (TZD) class of drugs utilized in the treatment of type 2 diabetes (18). The PPARγ mediated insulin-sensitizing effects are not completely understood but include the redirection of fatty acids away from ectopic storage to adipose tissue depots, production and section of adiponectin, and inhibition of inflammatory signaling in macrophages (4).

Recently, we identified hypoxia inducible lipid droplet associated (HILPDA) as a novel PPAR regulated gene involved in hepatic VLDL-TG secretion (Chapter 5). HILPDA is a

6

relatively small protein of 63 and 64 amino acids in human and mouse, respectively, with no homologous proteins. HILPDA expression is highly induced upon hypoxia and several studies have identified HILPDA to be expressed in a variety of carcinomas where it might contribute to tumor growth via inhibition of apoptosis (29-33). Recently, HILPDA was found to localize to lipid droplets and to be involved in lipid storage (34).

In chapter 5 we showed that HILPDA can be transactivated by PPARα, PPARδ, and PPARγ. Furthermore, PPARγ overexpression in liver markedly induced *Hilpda* expression. Given the regulation of HILPDA by PPARs and its potential localization to lipid droplets we set out to study the role of HILPDA in other organs. In this study we identify *Hilpda* as a PPARγ- and β-adrenergic receptor-regulated gene involved in adipose tissue lipolysis.

Results

Hildpa is expressed in adipocytes

We first determined the distribution of *HILPDA* mRNA across various human and mouse tissues. Highest expression of *HILPDA* expression was found in white adipose tissue (WAT), with lower levels in muscle, intestine, liver, and kidney (Figures 1A and 1B). Considering the abundance of *HILPDA* mRNA in adipose tissue and its reported localization to lipid droplets we decided to focus on the potential role and regulation of HILPDA in adipose tissue. Separation of adipose tissue into adipocytes and stromal vascular fraction (SVF), which contains adipocyte progenitor cells and various immune cells, indicated that *Hilpda* expression was highly enriched in the adipocyte fraction (Figure 1C). Successful separation of adipose tissue was confirmed by the adipocyte- and SVF-specific expression of *Adipoq* and *Cd68* (Figure 1C). Human subcutaneous- and visceral adipose tissue separated into adipocytes and SVF similarly revealed enrichment of *HILPDA* mRNA in adipocytes (Figure 1D). Thus, HILPDA is highly expressed in adipose tissue where it is mainly confined to adipocytes.

We next determined whether HILPDA expression is influenced by diet-induced obesity and associated adipocyte hypertrophy. Intriguingly, high fat feeding, which caused a marked increase in bodyweight and expansion of adipose tissue mass (Figures 2A and 2B), led to a significant reduction in *Hilpda* mRNA in the adipocyte fraction (Figure 2C). Increased macrophage abundance, as illustrated by increased *Cd68* mRNA levels, did not associate with altered *Hilpda* expression in the SVF (Figure 2C). Another stimulus that causes major remodeling of the adipose tissue is fasting. Interestingly, fasting markedly increased *Hilpda* mRNA as well as protein levels in epididymal WAT (Figures 2D and 2E).
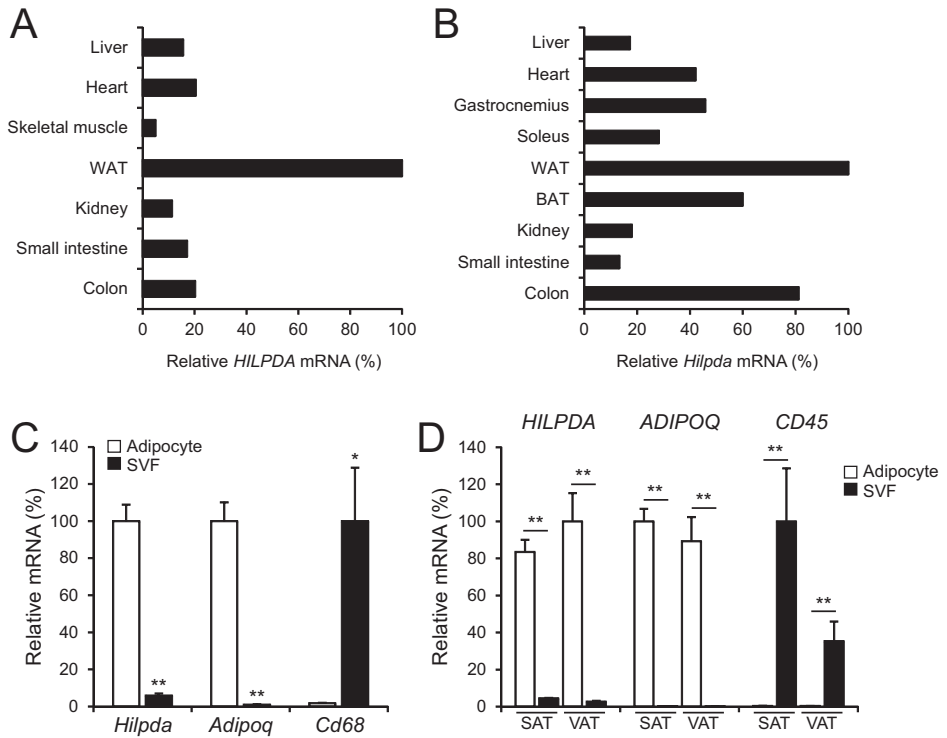
Figure 1. HILPDA is expressed in adipocytes
(A and B) *HILPDA* mRNA levels in various human (A, n =1) and mouse (B, n = 2) tissues.
(C) *Hilpda*, *Adipoq*, and *Cd68* expression in eWAT adipocytes and SVF of C57BL6 mice (n = 3).
(D) *HILPDA*, *ADIPOQ*, and *CD45* expression in adipocytes and SVF derived from human subcutaneous and visceral adipose tissue (n = 7).
Data are mean ± SEM. Asterisks indicate significant differences according to Student's *t*-test; *$P < 0.05$, **$P < 0.01$.

HILPDA does not affect adipogenesis

To gain insight into the expression of *Hilpda* during adipocyte differentiation, we employed the 3T3-L1 adipogenesis model. *Hilpda* mRNA levels increased 4-fold during 3T3-L1 adipogenesis (Figures 3A), which was copied at the protein level (Figure 3B). Similarly, *Hilpda* mRNA went up upon differentiation of mouse SVF cells into adipocytes, concurrent with established markers of adipogenesis (Figure 3C), as well as during SGBS (Simpson-Golabi-Behmel syndrome) pre-adipocyte differentiation (Figure 3D). Next, we explored the potential role of HILPDA in 3T3-L1 adipocyte differentiation by employing siRNA mediated knockdown of *Hilpda*. Although treatment of cells with siRNA against HILPDA
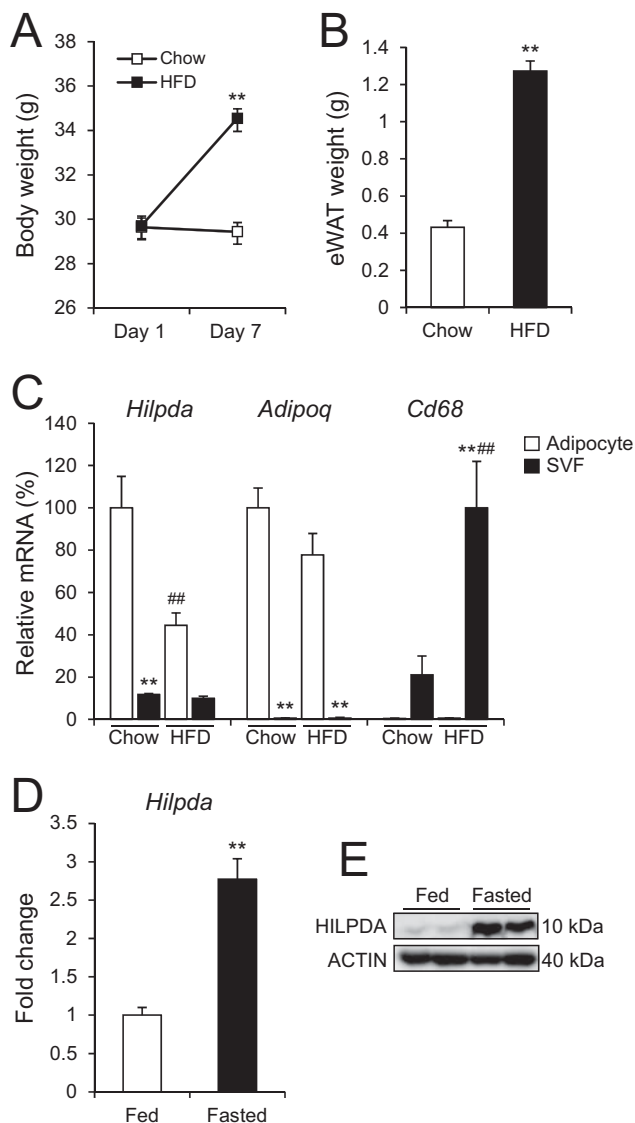
6

Figure 2. HILPDA expression during high-fat diet and fasting

(A and B) Increase in body weight (A) and eWAT weight of C57BL6 animals after 7 days of HFD (n = 3-4 animals per group).

(C) mRNA levels of *Hilpda*, *Adiponectin*, and *Cd68* in adipocytes and SVF of C57BL6 mice fed HFD for 7 days (n = 3-4 animals per group).

(D and E) Expression of *Hilpda* mRNA (D, n = 6 animals per group) and protein (E) in 18-hour fasted wild-type mice. ACTIN was used as loading control.

Data are mean ± SEM. Asterisks indicate significant differences according to Student's *t*-test or two-way ANOVA with Bonferroni post-hoc test (C); *$P < 0.05$, **$P < 0.01$, ##$P < 0.01$. In (C): *, difference between adipocyte and SVF; #, difference between chow and HFD.
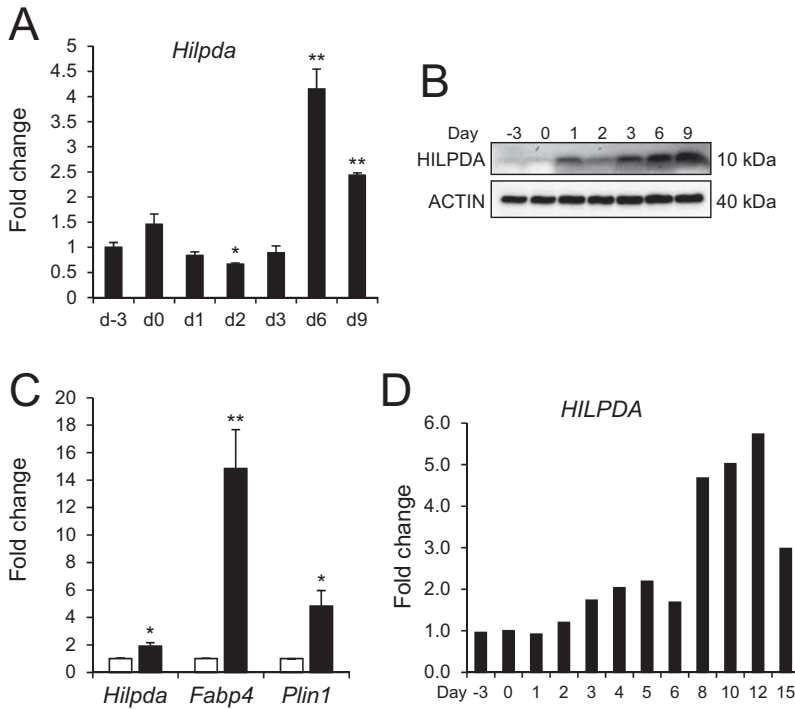
Figure 3. *Hilpda* expression during adipogenesis

(A and B) *Hilpda* mRNA (A, n = 3) and protein level (B) during 3T3-L1 adipogenesis.

(C) *Hilpda* mRNA during primary SVF differentiation into adipocytes. *Fabp1* and *Plin1* were measured to confirm successful differentiation. Adipose tissue from 3 C57BL6 animals was dissected, pooled, digested with collagenase and resulting SVF cells differentiated.

(D) SGBS cells were differentiated and *Hilpda* mRNA was measured at the indicated days (n =1).

Data are mean ± SEM. Asterisks indicate significant differences according to one-way ANOVA with Tukey's post-hoc test (A) or Student's *t*-test (C); *$P < 0.05$, **$P < 0.01$.

effectively reduced *Hilpda* mRNA and protein levels (Figures 4A and 4B), we observed no difference in adipogenic potential compared to cells treated with control siRNA, as illustrated by the lack of change in expression of adipogenic markers and the lack of change in Oil Red O staining (Figures 4C-4E). In congruence, adenovirus mediated overexpression of *Hilpda* also did not influence 3T3-L1 adipogenesis (Figures 5A and 5B).

Adipocyte HILPDA is regulated by PPARγ

HILPDA was recently identified as target of PPARs in liver, including PPARγ (Chapter 5). To explore the potential effect of PPARγ on *Hilpda* expression in adipocytes we treated
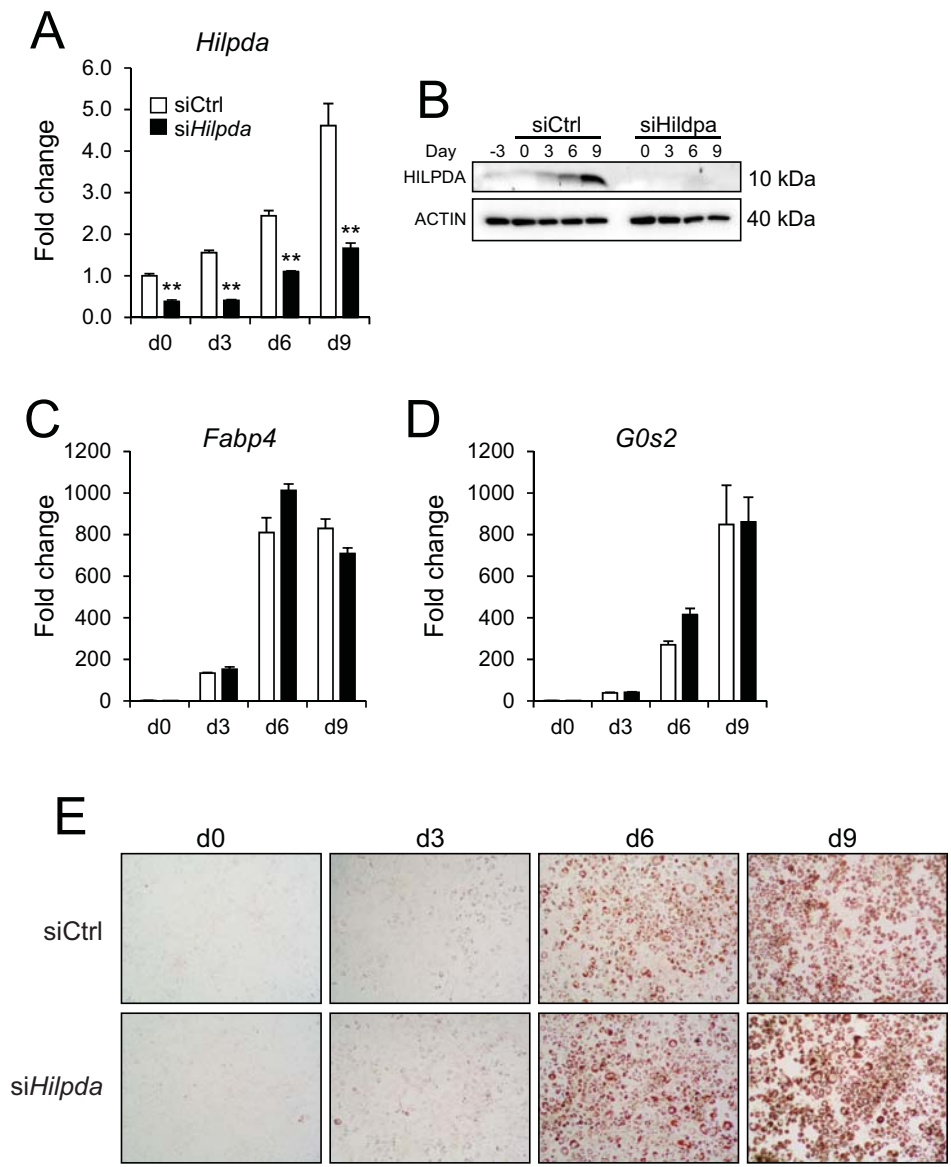
Figure 4. siRNA mediated HILPDA knockdown does not affect adipogenesis

(A and B) *Hilpda* mRNA (A) and protein (B) levels during 3T3-L1 adipogenesis. siRNAs were added two days before initiation of adipogenesis, at the start of differentiation and on day 3 and 6 of differentiation (n = 3). (C and D) *Fabp4* (C) and *G0s2* (D) expression in siCtrl and si*Hilpda* cells (n = 3).

(E) Oil Red O staining of siCtrl and si*Hilpda* cells at indicated days during the process of differentiation. Data are mean ± SEM. Asterisks indicate significant differences according to Student's *t*-test; **$P < 0.01$.
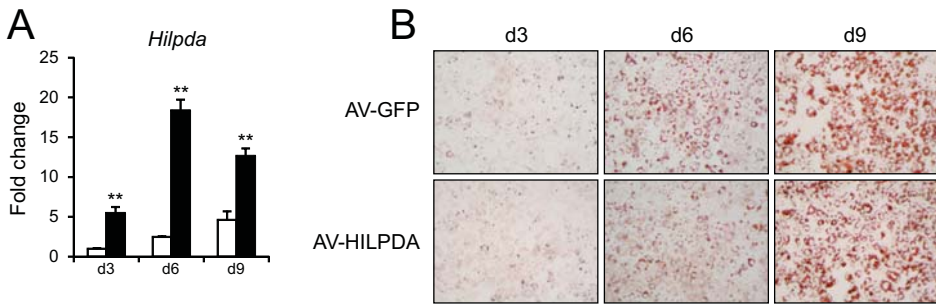
Figure 5. Adenovirus mediated overexpression of *Hilpda* does not affect adipogenesis
(A) Recombinant viruses expressing GFP of HILPDA were added at an MOI of 500 two days before initiation of differentiation and *Hilpda* mRNA was determined on the indicated days (n = 3).
(B) Oil Red O staining of parallel samples described in A.
Data are mean ± SEM. Asterisks indicate significant differences according to Student's *t*-test; **$P < 0.01$.

3T3-L1 adipocytes with the PPARγ agonist rosiglitazone. Rosiglitazone significantly induced *Hilpda* mRNA and protein in mature 3T3-L1 adipocytes but not undifferentiated 3T3-L1 fibroblasts (Figures 6A-6C). Consistent with PPARγ-dependent regulation, *Hilpda* expression in 3T3-L1 adipocytes was markedly decreased upon knockdown of *Pparg* (Figure 6D).

In chapter 5 we identified a functional PPAR response element (PPRE) around 1200 base pair upstream of the transcriptional start site (TSS) of the *HILPDA* gene. To examine whether PPARγ binds to this PPRE in adipocytes we performed ChIP-seq experiments in 3T3-L1 adipocytes. It was found that PPARγ binds to three loci upstream of the TSS (Figure 6E). The PPARγ binding site nearest to the TSS is identical to the binding site that binds PPARα (Chapter 5) and harbors a conserved and functional PPRE. Interestingly, PPARγ exclusively occupied the binding sites in 3T3-L1 adipocytes and not in fibroblasts (Figure 6E), which is consistent with exclusive induction of HILPDA by rosiglitazone in 3T3-L1 adipocytes and not fibroblasts (Figure 6B and 6C). Finally, despite the modest induction of *Hilpda* mRNA during 3T3-L1 adipocyte differentiation, binding of RNA polymerase II to the *Hilpda* promoter remained relatively stable during 3T3-L1 adipogenesis (Figure 6E).

Confirming regulation of HILPDA by PPARγ in human adipocytes, *HILPDA* was in the top 25 of most highly induced genes by rosiglitazone in differentiated human SGBS and MADs (multipotent adipose-derived stem cell) adipocytes, together with well-known PPARγ targets such as *PCK1* and *PDK4*, as assessed by microarray (Figure 7A and 7B). Again, consistent with PPARγ-dependent regulation, *HILPDA* expression in human SGBS

6

adipocytes was markedly decreased upon knockdown of *PPARG* (Figure 7C). Finally, ChIP-seq experiments indicated markedly enhanced binding of PPARγ to multiple binding sites in differentiated hMADs adipocytes, including the conserved binding site nearest to the TSS referred to above (Figure 7D). Binding of PPARγ upon differentiation of hMADs cells was accompanied by increased RNA polymerase II binding to the *HILPDA* promoter (Figure 7D). Together, these data suggest that HILPDA is regulated by PPARγ in human and mouse adipocytes via at least one functional PPRE.
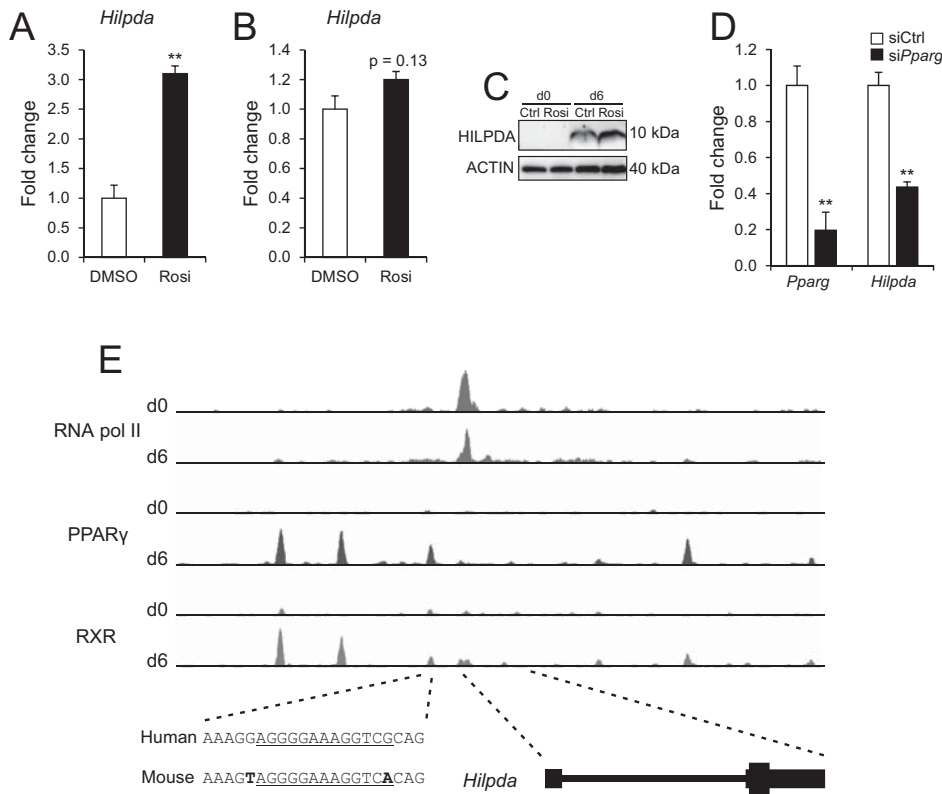

Figure 6. PPARγ binds to a conserved PPRE at the Hilpda loci in 3T3-L1 adipocytes

(A and B) Mature 3T3-L1 adipocytes (A) or 3T3-L1 fibroblasts (B) were exposed to 10 μM rosiglitazone for 24 hours and subsequently analyzed for *Hilpda* mRNA (n = 3).

(C) Western blot analysis on a subset of samples described in A and B.

(D) 3T3-L1 adipocytes were incubated with siRNA against PPARγ and three days later analyzed for expression of *Pparg* and *Hilpda* (n = 3).

(E) ChIP-seq profiles of RXR, PPARγ, and RNA polymerase II in 3T3-L1 fibroblasts and adipocytes at the *Hilpda* loci. Sequences indicate a conserved PPRE located 1200 base pair upstream of the TSS.

Data are mean ± SEM. Asterisks indicate significant differences according to Student's *t*-test; **$P < 0.01$.
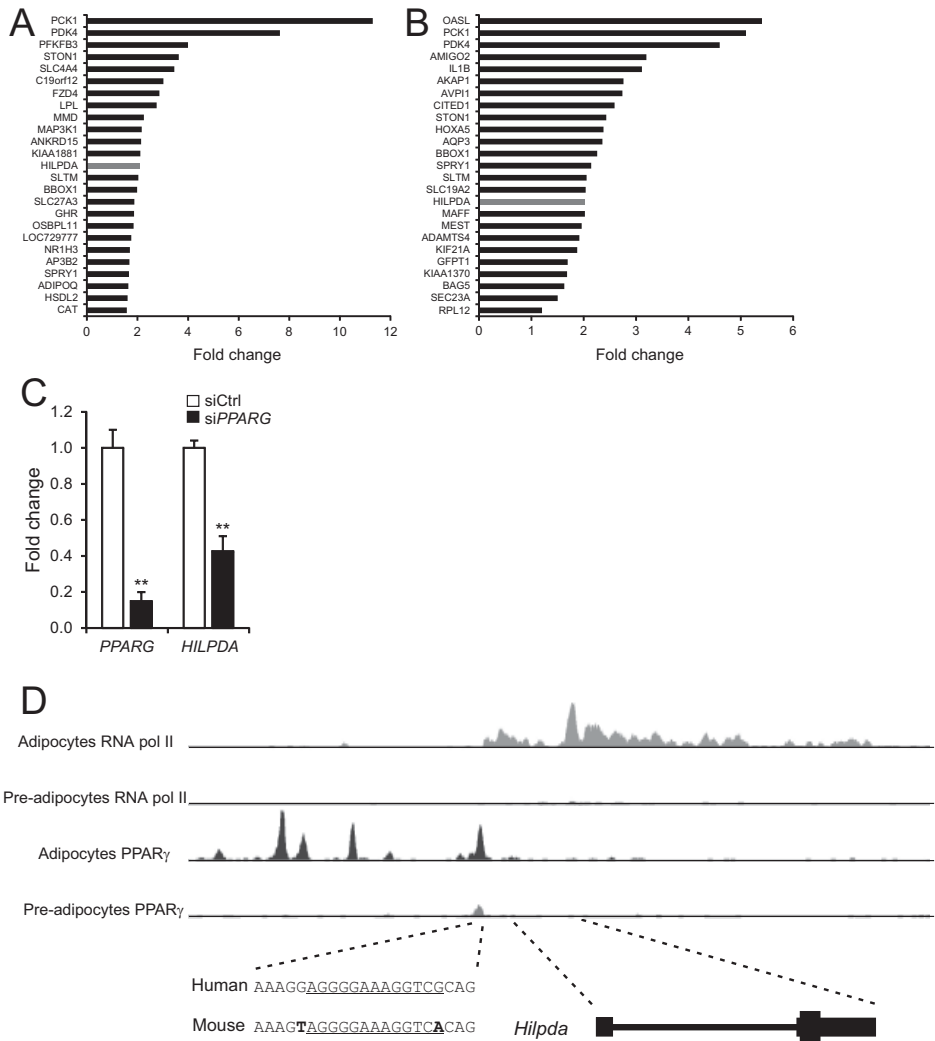
Figure 7. *HILPDA* is regulated by PPARγ in human adipocytes

(A and B) Gene expression profiling identified *HILPDA* to be in the top 25 of most highly induced genes upon rosiglitazone treatment of hMADs adipocytes (A) and SGBS (B) adipocytes.

(C) *PPARG* was knocked-down in SGSB cells and mRNA levels of *PPARG* and *HILPDA* were analyzed with qPCR (n = 3).

(D) ChIP-seq profiles of PPARγ and RNA polymerase II at the human *HILPDA* loci. hMADs fibroblasts and adipocytes were used for IP. Sequences show the location of the conserved PPRE.

Data are mean ± SEM. Asterisks indicate significant differences according to Student's *t*-test; **P < 0.01.

β-adrenergic receptor agonists induce Hilpda expression

To identify additional regulators of HILPDA expression we exposed 3T3-L1 adipocytes to a variety of compounds including insulin and dexamethasone. None of these metabolic cues affected HILPDA expression (data not shown). However, we noticed marked induction of *Hilpda* expression when 3T3-L1 adipocytes were exposed to β-adrenergic receptor agonists or forskolin, suggesting that HILPDA is responsive to cAMP levels (Figure 8A). *Hilpda* mRNA levels peaked after 3 hours of exposure to isoproterenol or forskolin (Figure 8B), which translated into increased protein levels (Figure 8C). Similarly, we found significant induction of *Hilpda* expression in primary mouse epididymal and inguinal adipocytes exposed to isoproterenol (Figure 8D). Moreover, the induction of *Hilpda* by isoproterenol was apparent at low concentrations and saturated at 1 μM (Figures 8E and 8F). Interestingly, the effect of isoproterenol was specific for mature adipocytes as we failed to observe induction of *Hilpda* expression in 3T3-L1 fibroblasts and non-differentiated SVF cells (Figures 8G and 8H). Adding to a β-AR mediated regulation of HILPDA we observed a robust increase in *Hilpda* expression in mice injected with the β3-adrenergic receptor agonist CL316,243, suggesting in vivo relevance (Figure 8I). Thus, adipocyte HILPDA is under strong positive control of β-adrenergic receptor signaling in vitro and in vivo.

To examine the induction of HILPDA by β-adrenergic receptor agonists in more detail we pretreated mature adipocytes with inhibitors for RNA polymerase II or translation, followed by exposure to isoproterenol or forskolin. Blocking RNA polymerase II partially reduced *Hilpda* mRNA levels whereas interfering with translation induced the expression of *Hilpda* (Figure 9A). Immunoblot analysis indicated partially reduced HILPDA protein levels upon RNA polymerase II inhibition while blocking protein synthesis completely abolished the isoproterenol- and forskolin-induced increase in HILPDA protein expression (Figure 9B). Many proteins involved in the regulation of lipolysis undergo phosphorylation. Nonetheless, we found no evidence for HILPDA being phosphorylated in 3T3-L1 adipocytes exposed to β-adrenergic receptor agonists (Figure 9C). These data suggest that isoproterenol and forskolin increase HILPDA protein via transcriptional and translational mechanisms but do not induce phosphorylation.

Adipose tissue-specific Hilpda⁻/⁻ animals show no major metabolic perturbations

To explore the functional role of HILPDA in adipose tissue we generated adipose tissue-specific null mice by crossing floxed *Hildpa* mice with Adiponectin-Cre mice, resulting in WAT- and BAT-specific deletion of *Hilpda* (AT*Hilpda*⁻/⁻) and concomitant transcription of human placental alkaline phosphatase (*ALPP*) reporter gene (Figures 10A and 10B).
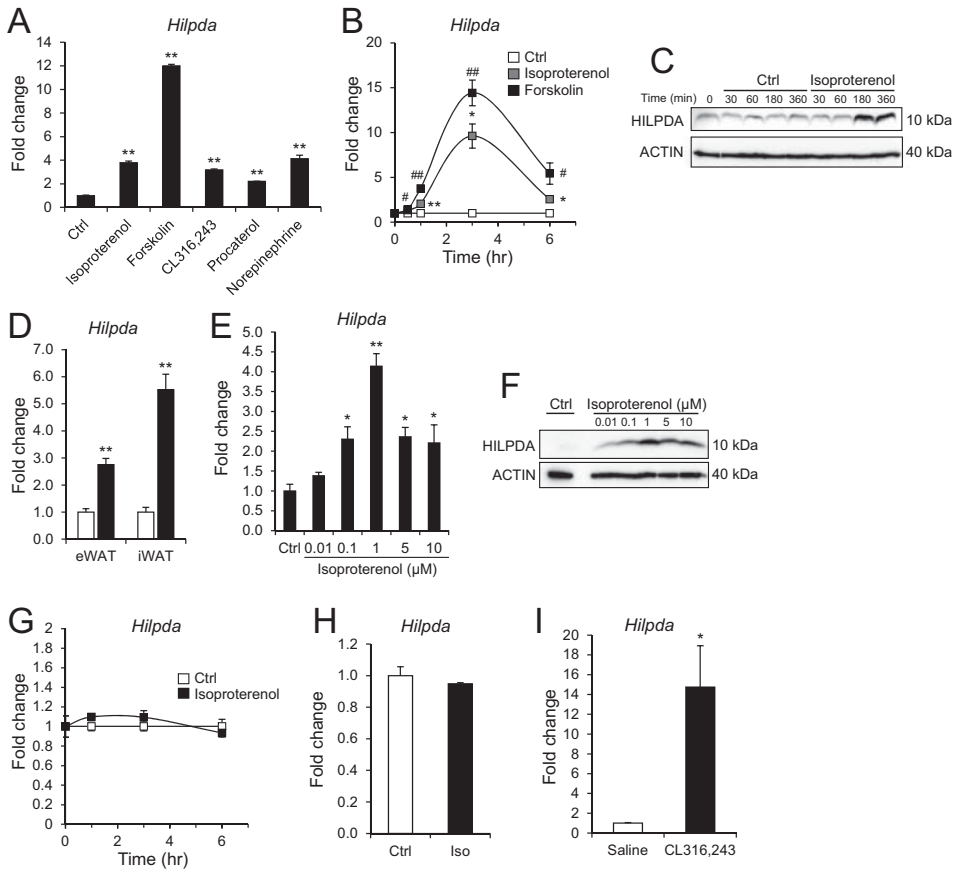
Figure 8. HILPDA is highly responsive to β-adrenergic receptor stimulation

(A) *Hilpda* mRNA levels in 3T3-L1 cells exposed to β-adrenergic receptor agonists and forskolin, an activator of adenylate cyclase, for 3 hours. Isoproterenol is a general β-adrenergic agonist. CL316,243 is specific for β3 receptors, procaterol for β2, and norepinephrine acts as a general adrenergic receptor agonist (n = 3).

(B) Time course of *Hilpda* expression upon exposure to 10 μM isoproterenol or 5 μM forskolin (n = 3).

(C) HILPDA protein expression in samples described in B.

(D) Primary adipocytes differentiated from epididymal and inguinal SVF were exposed to 10 μM isoproterenol for 3 hours and subsequently analyzed for *Hilpda* mRNA levels (n = 3).

(E and F) 3T3-L1 adipocytes were exposed to different concentrations isoproterenol for 6 hours after which the cells were analyzed for *Hilpda* mRNA (E, n = 3) and HILPDA protein.

(G) 3T3-L1 fibroblasts were treated as described for E and F (n = 3).

(H) SVF from eWAT was plated, exposed to 10 μM isoproterenol for 6 hours and subsequently analyzed for *Hilpda* expression (n = 3).

(I) Female NMRI mice were injected intraperitoneally with 1 mg/kg CL316,24 and eWAT was collected 4 hours later (n = 5 animals per group).

Data are mean ± SEM. Asterisks indicate significant differences according to Student's *t*-test or one-way ANOVA with Tukey's post-hoc test (A and E); *$P < 0.05$, **$P < 0.01$.

6

AT*Hilpda*⁻/⁻ mice developed normally over time. However, a small increase in body weight was detected in female AT*Hilpda*⁻/⁻ mice compared to wild-type mice (Figure 10C).

Since we observed a prominent increase in *Hilpda* expression in epididymal white adipose tissue (eWAT) upon fasting, we characterized wild-type and AT*Hilpda*⁻/⁻ mice after an overnight fast. Weight loss was similar between the two sets of mice (Figure 10D). Moreover,
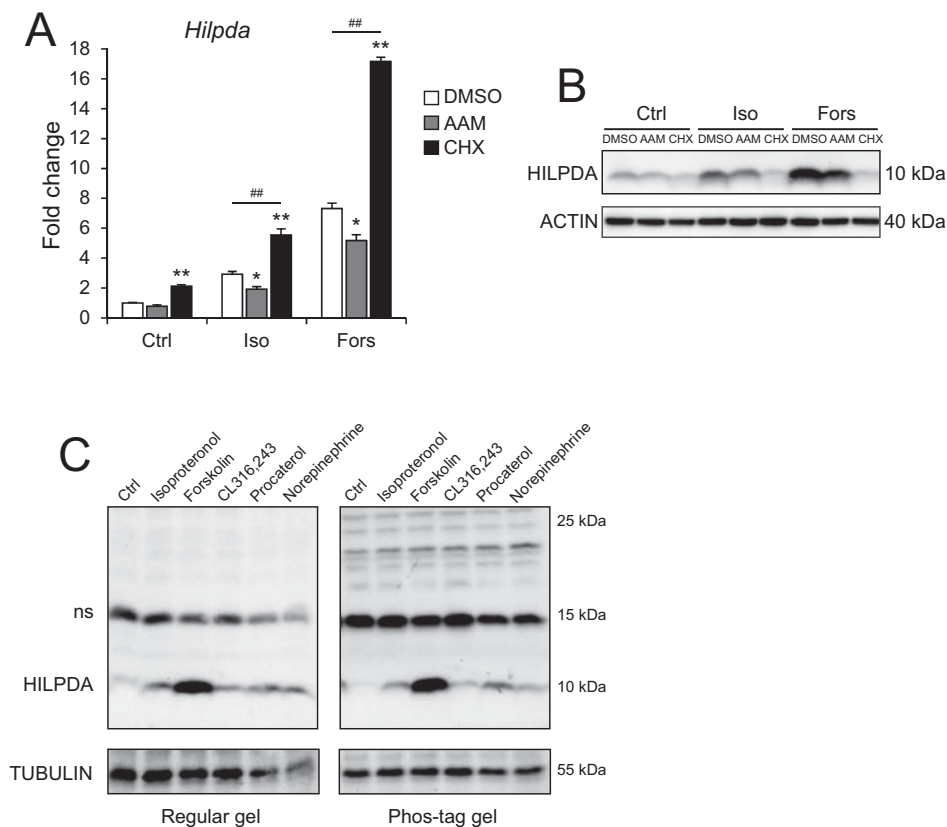

Figure 9. HILPDA is translated upon exposure to isoproterenol and forskolin

(A) Mature 3T3-L1 adipocytes were preincubated with 10 µg/ml alpha-amanitin or cycloheximide for 45 minutes followed by exposure to isoproterenol or forskolin for 3 hours. Following RNA isolation and cDNA synthesis, *Hilpda* mRNA levels were determined by qPCR (n = 3).

(B) Western blot analysis of samples used in described in A.

(C) 3T3-L1 adipocytes were exposed to isoproterenol (10 µM), forskolin (10 µM), CL316,243 (10 µM), procaterol (5 µM), and norepinephrine (1 µM) for 3 hours and analyzed for potential phosphorylation with Phos-tag gel. ns = non-specific immunodetection.

Data are mean ± SEM. Asterisks and number signs indicate significant differences according to two-way ANOVA with Bonferroni post-hoc test; *$P < 0.05$, **$P < 0.01$, ##$P < 0.01$. *, difference between DMSO, AAM or CHX; #, difference between control, isoproterenol or forskolin.

no differences were observed between the weights of several tissues from wild-type and AT*Hilpda*⁻/⁻ animals (Figures 10E-10H). Heamatoxylin and eiosin staining revealed no major differences in eWAT or BAT histology between the two sets of mice (Figures 10I and 10J).

To gain insight in the potential function of adipose tissue HILPDA, we assayed several serum parameters. No changes were observed in serum triglycerides, non-esterified fatty acids (NEFAs), glucose, ketone bodies, or glycerol, though a minor reduction in serum cholesterol was apparent in the male AT*Hilpda*⁻/⁻ animals (Figure 11A-11F). Likewise, serum adiponectin and insulin levels were similar between wild-type and AT*Hilpda*⁻/⁻ animals (Figures 11G and 11H). Thus, deletion of adipose *Hilpda* does not seem to alter the metabolic response to fasting.

Hilpda reduces isoproterenol induced NEFA release

We observed a striking induction of HILPDA expression with β-adrenergic receptor agonists (Figures 8A-8F). β-adrenergic activation leads to stimulation of intracellular lipolysis in adipose tissue. To explore a potential role for HILPDA in β-adrenergic receptor-mediated lipolysis, we exposed eWAT explants from wild-type and AT*Hilpda*⁻/⁻ mice to isoproterenol. No difference in NEFA and glycerol release was observed (Figures 12A and 12B). Similarly, siRNA mediated knockdown of HILPDA in mature 3T3-L1 adipocytes did not alter isoproterenol-induced NEFA and glycerol release (Figures 12C-12E). Thus, deletion of HILPDA does not affect the capacity of adipocytes to release fatty acids. However, we hypothesized that if HILPDA acts as an inhibitor of lipolysis, its function may be better revealed by overexpression. Therefore, we infected 3T3-L1 adipocytes with adenovirus to overexpress HILPDA followed by isoproterenol treatment. Consistent with our hypothesis, isoproterenol-induced release of NEFAs was significantly lower upon HILPDA overexpression (Figure 12F-12H). Taken together, these data suggest that Hilpda functions as an inhibitor of adipocyte lipolysis, potentially as part of a feedback mechanism induced by β-adrenergic receptor activation.

Discussion

The findings reported in this paper identify HILPDA as a novel regulator of adipocyte lipolysis. HILPDA expression was found to be regulated by fasting and high-fat diet feeding. Moreover, HILPDA expression was revealed to be under the control of both PPARγ and β-adrenergic receptor stimulation. Genetic manipulation of HILPDA expression did not affect the differentiation of fibroblasts into mature adipocyte. The metabolic response to
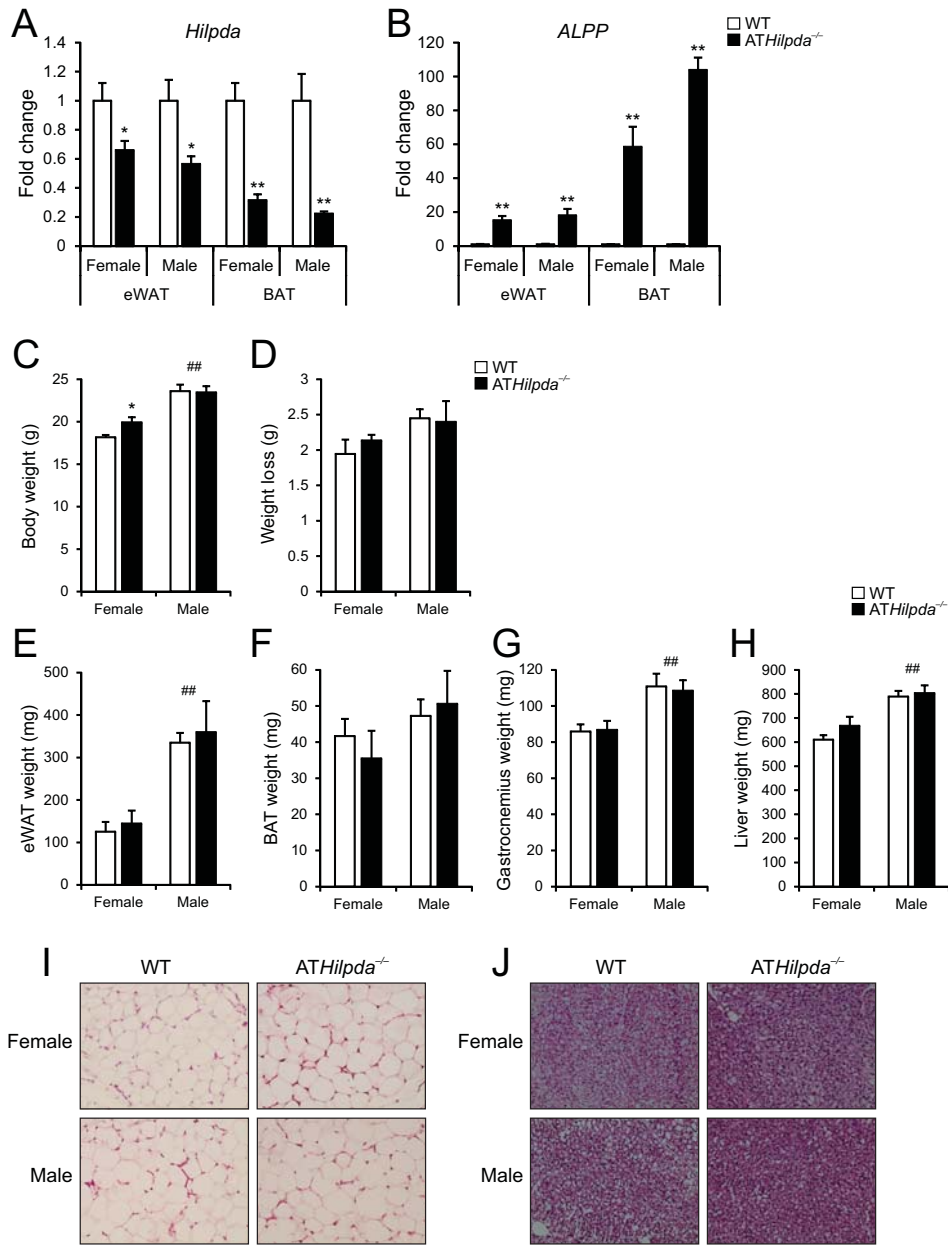
6

Figure 10. Adipose tissue-specific Hilpda knockout mice have normal adipose mass upon fasting

(A and B) *Hilpda* (A) and *ALPP* (B) expression in eWAT and BAT from wild-type and AT*Hilpda*$^{-/-}$ mice (n = 7-9 animals per group).

(C) Body weight of female and male wild-type or AT*Hilpda*$^{-/-}$ mice (n = 7-9 animals per group).

fasting in adipose tissue-specific *Hilpda* knockout mice was comparable to that of wild-type mice. However, adenoviral-mediated overexpression of HILPDA reduced NEFA release from adipocytes upon β-adrenergic stimulation.

Central to the induction of adipocyte lipolysis upon stimulation of β-adrenergic receptors is the cAMP/protein kinase A (PKA) mediated phosphorylation of hormone sensitive lipase (HSL) and perilipin 1 (PLIN1). Consequently, PLIN1 releases comparative gene identification-58 (CGI-58) which subsequently serves as a coactivator for ATGL/PNPLA2. Simultaneously, PLIN1 interacts with and translocates HSL to the surface of lipid droplets. Together, these actions lead to increased activity of ATGL and HSL that catalyze the hydrolysis of TAG and DAG, respectively. Following the final hydrolysis of MAG by MGL, resulting NEFAs are released in to the circulation (35). Despite the presence a number of potential phosphorylation sites, as determined by computational analysis (34), we found no evidence for phosphorylation of HILPDA upon β-adrenergic receptor stimulation using a Phos-tag method. Future experiments will have to address if HILPDA may be phosphorylated in response to other stimuli.

Besides causing the phosphorylation of several protein substrates including PLIN1 and HSL, PKA phosphorylates the transcription factor cAMP response element binding protein (CREB), leading to recruitment of several coactivators such as CREB binding protein (CBP/p300) and subsequent induction the transcription of numerous target genes such as phosphoenolpyruvate carboxykinase (PEPCK) and activating transcription factor 3 (ATF3) (36-39). siRNA mediated knockdown of CREB modestly decreased the cAMP-induced increase in *Hilpda* mRNA (data not shown). However, CREB expression was only 40% lower compared to control cells and adenoviral mediated knockdown of CREB will have to provide conclusive evidence. It should be noted that in silico analysis did not reveal the presence of conserved CREB responsive elements (CREs) in the proximity of the *Hilpda* gene. Thus, additional studies are required to delineate a potential induction of *Hilpda* expression by cAMP/PKA/CREB.

6

(D) Weight loss in 16-hour fasted female and male wild-type or AT*Hilpda*$^{-/-}$ mice (n = 7-9 animals per group).

(E-H) eWAT (E), BAT (F), gastrocnemius (G), and liver (H) weight of 16-hour fasted wild-type and AT*Hilpda*$^{-/-}$ mice (n = 7-9 animals per group).

(I and J) Representative H&E staining of eWAT (I) and BAT (J) of 16-hour fasted wild-type and AT*Hilpda*$^{-/-}$ mice.

Data are mean ± SEM. Asterisks and number signs indicate significant differences according to Student's *t*-test (A and B) or two-way ANOVA with Bonferroni post-hoc test; *P < 0.05, **P < 0.01, ##P < 0.01. *, difference between genotype; #, difference between female and male mice.
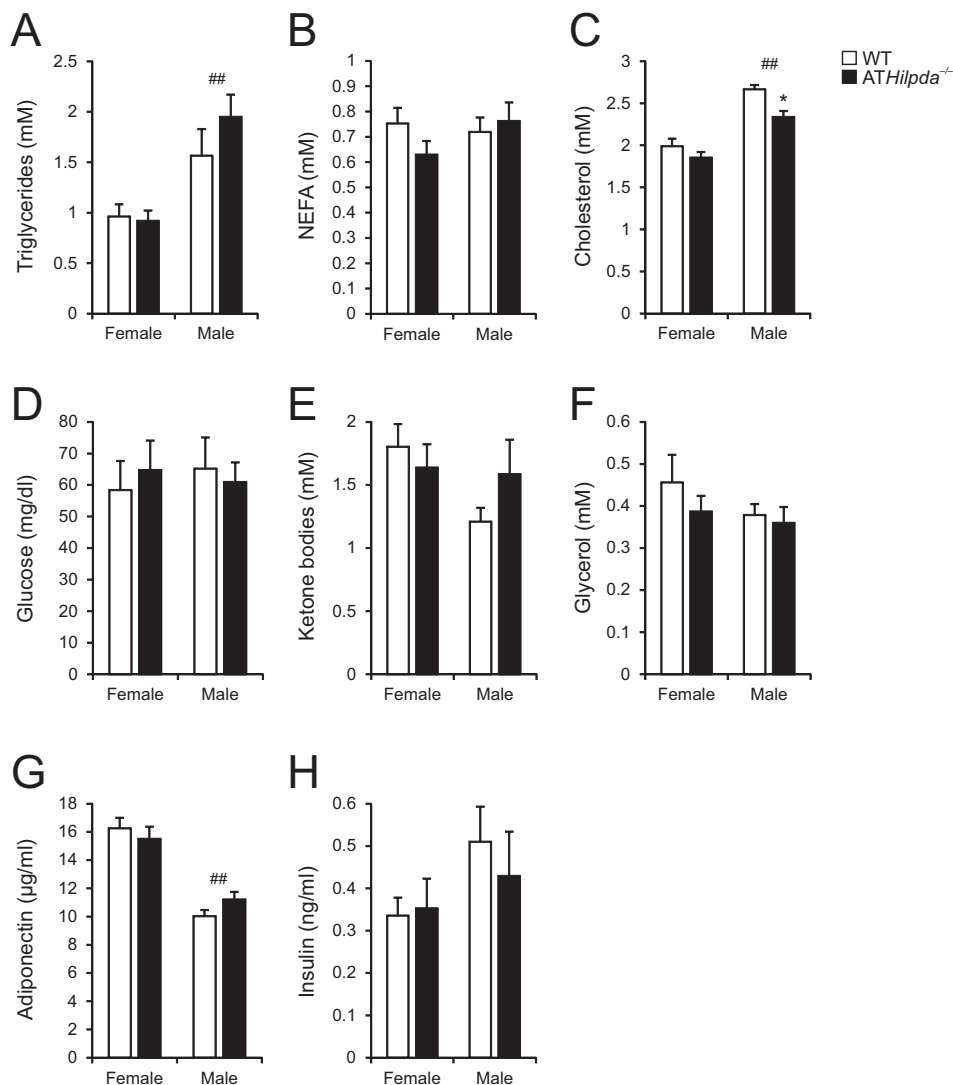
Figure 11. Fasting provokes no major alterations in serum parameters of AT*Hilpda*^{–/–} mice

(A-F) Serum from 16-hour fasted wild-type and AT*Hilpda*^{–/–} was analyzed for triglycerides (A), NEFAs (B), cholesterol (C), glucose (D), ketone bodies (E), and glycerol (F) (n = 6-9 animals per group).

(G and H) ELISA for adiponectin (G) and insulin (H) on serum samples of wild-type and AT*Hilpda*^{–/–} mice fasted for 16 hours (n = 6-9 animals per group).

Data are mean ± SEM. Asterisk and number signs indicate significant differences according to two-way ANOVA with Bonferroni post-hoc test; *$P < 0.05$, ##$P < 0.01$. *, difference between genotype; #, difference between female and male mice.

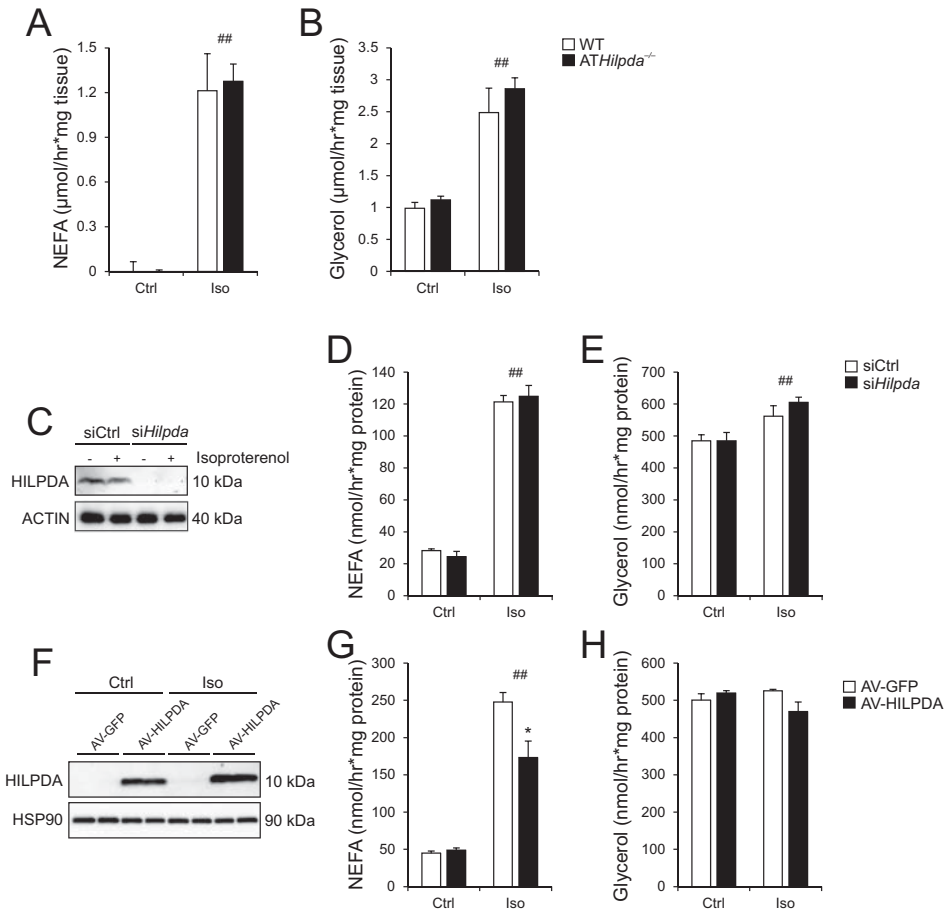**Figure 12. Effect of HILPDA on adipocyte lipolysis**

(A and B) NEFA (A) and glycerol (B) release in eWAT explants of wild-type and AT*Hilpda*$^{-/-}$ mice upon exposure to isoproterenol (n = 4 animals per group).

(C-E) siRNA against HILPDA was applied to mature 3T3-L1 adipocytes replated at 70% confluency leading to robust reductions in HILPDA levels (C). Cells were starved for 2 hours and subsequently exposed to 5 μM isoproterenol for 2 hours. Media were analyzed for NEFAs (D) and glycerol (E) (n = 3).

(F-H) Recombinant adenoviruses expressing GFP or HILPDA under the control of a CMV promoter were added to replated 3T3-L1 at an MOI of 750. Three days later the cells were serum starved (DMEM + 1% BSA) for 2 hours and subsequently incubated with DMEM supplemented with 5 μM isoproterenol for 3 hours. Cell lysates were analyzed for HILPDA protein levels (F) and media for NEFAs (G) and glycerol (H) content (n = 3).

Data are mean ± SEM. Asterisk and number signs indicate significant differences according to two-way ANOVA with Bonferroni post-hoc test; *$P < 0.05$, ##$P < 0.01$. *, difference between AV-GFP and AV-HILPDA; #, control versus isoproterenol.

6

Our experiments in AT*Hilpda*^{−/−} animals revealed no major perturbations in the metabolic response to fasting in the absence of adipose tissue HILPDA. Moreover, siRNA-mediated knockdown of HILPDA in adipocytes did not result in a change in NEFA release induced by catecholamines. By contrast, adenovirus-mediated HILPDA overexpression resulted in a significant reduction in NEFA release upon β-adrenergic receptor stimulation. Based on these results we postulate that HILPDA functions as a negative regulator of adipose tissue lipolysis, and that induction of HILPDA serves as a negative feedback mechanism to control the amount of NEFAs released. The mechanism behind impairment of adipocyte lipolysis by HILPDA remains elusive and will be studied in future experiments. It is tempting to speculate on the potential inhibition of one or more lipases such as ATGL or HSL by HILPDA, although evidence provided in chapter 5 argues against such a mechanism, at least in liver.

Gimm et al. (34) reported that HILPDA is localized to lipid droplets. Many lipid droplet associated proteins are under transcriptional control of PPARγ. Using a variety of techniques we firmly establish the direct regulation of HILPDA by PPARγ via at least one conserved functional PPRE. Considering the role of PPARγ as master regulator of adipogenesis, we expected a substantial increase in HILPDA expression upon adipogenesis. However, the inductions we observed were relatively modest compared to other lipid droplet proteins such as PLIN1, PLIN2, and G0S2. On the other hand, expression of the lipid droplet associated protein PLIN3/TIP47 remains unaltered during adipogenesis (22). It can be hypothesized that HILPDA has specific functions at the surface of lipid droplets during fasting and β-adrenergic receptor activation but not in the biogenesis of lipid droplets.

Compelling evidence suggest that the function of PPARγ goes beyond the anabolic lipogenic pathway (4). Indeed, PPARγ was found to regulate many genes involved in the lipolytic response upon catecholamine induced lipolysis, including *Adrb3* (β3 adrenergic receptor) *Atgl*, *Hsl*, and the lipid droplet associated proteins *Plin2* and *Cidec* (40-43). Mutations in PPARγ or *Pparg2* deletion were found to impair the catecholamine-induced lipolytic response (43, 44). Thus, coordinate induction of HILPDA by PPARγ and cAMP might be aimed at balancing the amount of NEFAs released from adipocytes during fasting. It should be noted that HILPDA appears to be the only gene known to be regulated by PPARγ and involved in lipolysis that is also regulated at the transcriptional level by β-adrenergic receptor stimulation.

Despite the absence of clear defects in the response to fasting in AT*Hilpda*^{−/−} animals, we did observe a reduction in the number of lipid droplets in brown adipose tissue of some but not all AT*Hilpda*^{−/−} animals. Accordingly, analysis of the adipose tissue of a larger number

of animals is warranted. Additionally, gene expression data showed increased expression of *G0s2* and *Pnpla3* in the brown adipose tissue of fasted AT*Hilpda*$^{-/-}$ animals (data not shown). Thus, in brown adipose tissue HILPDA might play a role in the response to fasting potentially via regulation of two known players involved in the lipolytic pathway. In white adipose tissue, however, knockdown of *Hilpda* did not lead to changes in the expression of genes involved in lipolysis.

Despite successful adipose tissue HILPDA deletion as determined by PCR and mRNA expression of the recombination marker *ALPP*, the reduction in *Hilpda* mRNA was relatively minor, especially in the white adipose tissue depot. A potential explanation for this observation might be increased expression of *Hilpda* in the macrophage fraction of the adipose tissue. Interestingly, experiments performed in our laboratory indicate that *Hilpda* is highly induced upon lipid loading of macrophages. Fractionation of adipose tissue from wild-type and AT*Hilpda*$^{-/-}$ animals will be carried out to examine the possibility that HILPDA expression is increased in adipose tissue macrophages.

Taken together, we demonstrate that HILPDA is under positive regulation by PPARγ and the β-adrenergic receptor. Induction of HILPDA may be aimed at regulating the amount of NEFAs released during β-adrenergic receptor stimulation. Given the induction of HILPDA during fasting, we anticipate a similar mechanism of action in vivo.

Methods

Animal studies

For generation of a tissue library, two male wild-type C57BL6 animals were anesthetized with isoflurane killed by cervical dislocation and several tissues were excised and snap-frozen.

Male wild-type C57BL6 animals (4 months old) were fed a chow diet or a high-fat diet containing 60en% fat (D12492, Research Diet Services, Wijk bij Duurstede, The Netherlands). One week later, the animals were anesthetized with isoflurane and killed by cervical dislocation. Epididymal adipose tissues were dissected and separated into the adipocyte fraction and stromal vascular fraction (SVF) as described below.

For in vivo β3-adrenergic receptor activation, 9-10-week-old female NMRI mice were injected intraperitoneally with 1 mg/kg CL316,243 (Tocris Bioscience, Bristol, United Kingdom) in 0.9% saline. Control animals were injected with an equal volume of saline. Four hours later, the mice were killed by cervical dislocation and the epididymal was WAT dissected and snap-frozen.

Male 4-6-months-old C57BL6 animals were fasted for 18 hours after which the epididymal WAT was dissected and snap-frozen in liquid nitrogen.

Heterozygous floxed *Hilpda* animals on a mixed C57BL/6 and Sv129 background were purchased from The Jackson Laboratory (Bar Harbor, ME, USA). LoxP sites were introduced to flank the second

6

exon of *Hilpda* followed by the open reading frame for membrane-tethered human placental alkaline phosphatase (*ALPP*) after the second loxP site. Following Cre-recombination, *ALPP* is expressed under the control of the HILPDA promoter. Floxed *Hilpda* mice were crossed with Adiponectin-Cre mice (The Jackson Laboratory) on a C57BL6 background. After initial crosses, *Hilpda*$^{fl/fl}$ mice were crossed with *Hilpda*$^{fl/fl}$ heterozygous for adiponectin-Cre, yielding 50% wild-type animals and 50% adipose tissue-specific *Hilpda* null animals (AT*Hilpda*$^{-/-}$), equally distributed among males and females. Nine to- 13-week-old littermates were used for experiments.

All animal experiments performed were approved by the local animal welfare committee of Wageningen University or Cornell University (Ithaca, NY, USA), respectively.

Recombinant adenoviruses
Adenoviruses (AV) were generated by cloning GFP or *Hilpda* cDNA in human adenovirus type5 (dE1/E3). Expression was under the control of the CMV promoter. Viruses were produced and titrated by Vector Biolabs (Philadelphia, PA, USA).

Chemicals
Isoproterenol, norepinephrine, cycloheximide, alpha-amanitin, 3-isobutyl-1-methylxanthine (IBMX), insulin, dexamethasone, and rosiglitazone were purchased from Sigma-Aldrich (Schnelldorf, Germany). Forskolin, procaterol and CL316,243 were from Tocris (Tocris Bioscience, Bristol, United Kingdom).

Collagenase digestion
Dissected adipose tissue samples from the different experiments were kept on ice in Dulbecco's modified Eagle's medium (DMEM) (Lonza, Verviers, Belgium) supplemented with 1% bovine serum albumin (BSA) (Lonza). Samples were subsequently cut into small 1-2 mm3 pieces and incubated with collagenase solution (DMEM, 3.2 mM $CaCl_2$, 15 mM HEPES, 0.5% BSA, 10% fetal calf serum, 1.5 mg/ml collagenase type II (Sigma-Aldrich #C6885)) at 37°C for 45 minutes. Mixtures were strained through a 100 μm cell strainer and centrifuged at 900 rpm for 10 minutes at room temperature. Floating adipocytes were collected and snap-frozen for RNA isolation. Stromal vascular cells (SVF) were resuspended in red blood cell lysis buffer (155 mM NH_4Cl, 12 mM $NaHCO_3$, 0.1 mM EDTA) and incubated for 2 minutes at room temperature. Following the addition of 8 ml DMEM, the SVF cells were pelleted at 900 rpm for 10 minutes at room temperature. Cell pellets were snap-frozen for RNA isolation or counted and plated for differentiation into adipocytes as described below.

Paired subcutaneous and visceral (omentum) adipose tissue samples were collected according to a standardized procedure from patients admitted to the Radboud University Nijmegen Medical Centre (Nijmegen, The Netherlands) for laparoscopic cholecystectomy or inguinal hernia surgery. Samples were obtained from 7 patients aged between 41-63 years with and a BMI ranging from 25-28 kg/m².

WAT explants

Male wild-type and AT*Hilpda*$^{-/-}$ mice were sacrificed by cervical dislocation. Epididymal fat pads were dissected, cut into 20-40 mg pieces, and divided over 6 wells of a 24-well plate per animal. Then, explants were incubated in DMEM supplemented with 1% BSA for 30 minutes at 37°C. After thorough washing with warm PBS, the explants were incubated in DMEM + 1% BSA with or without 10 μM isoproterenol for 3 hours at 37°C. Media were assayed for NEFAs and glycerol using commercially available kits from Wako (Wako Chemicals GmbH, Neuss, Germany) and DiaSys (DiaSys Diagnostic Systems, Holzheim, Germany), respectively.

Cell culture

3T3-L1 fibroblasts were maintained in DMEM (Lonza) supplemented with 10% fetal calf serum (FCS) (Lonza) and 1% penicillin/streptomycin (P/S) (Lonza). Differentiation was initiated 2 days post-confluency by the addition of DMEM + 10% FCS + 1% P/S supplemented with 0.5 mM IBMX, 5 μg/ml insulin, and 1 μM dexamethasone. Three days later, the medium was replaced by insulin medium (DMEM, 10% FCS, 1% P/S, 5 μg/ml insulin). Two days later, the cells were provided with fresh DMEM + 10% FCS + 1% P/S and cultured for an additional 2-3 days.

Dharmacon ON-TARGET*plus* SMARTpool siRNAs were purchased from Thermo Fisher Scientific (Landsmeer, The Netherlands). siRNAs were diluted in Dharmacon siRNA buffer (final concentration 20 mM KCl, 6 mM HEPES pH 7.5, 0.2 mM MgCl2). Transfections were performed with Lipofectamine RNAiMAX transfection reagent (Life Technologies, Bleiswijk, The Netherlands). All siRNA transfections were carried out at a concentration of 40 nM siRNA and 2 μl transfection reagent for a 12-well plate well.

To study the effect of *Hilpda* knockdown on 3T3-L1 differentiation, siRNAs were added two days before initiation of differentiation, at the start of differentiation, and subsequently every 3rd day. To knockdown *Hilpda* or *Pparg* in mature adipocytes, cells were washed with PBS, trypsinized, and collected in 0.5 mg/ml collagenase in PBS. After centrifugation at 400 *g* for 5 minutes at 4°C, cells were strained over a 70 μm cell strainer and plated to 70% confluency. siRNAs were added two hours later, and experiments were carried out after an additional 48-72 hours incubation. siCtrl and *siHilpda* cells were incubated in DMEM + 1% BSA for 2 hours followed by 5 μM isoproterenol in DMEM + 1% BSA for 2 hours. Medium samples were assayed for NEFAs and glycerol as described above.

For overexpression experiments in 3T3-L1 adipocytes, recombinant adenoviruses were diluted in DMEM (low glucose, 1 g/l) supplemented with 0.5 μg/ml poly-L-lysine and incubated at room temperature for 100 minutes. Mixtures were added to the cells and allowed to incubate for 90 minutes followed by the addition of normal culture medium. Differentiation was initiated two days later. Adenoviruses were used at an MOI of 500. To study isoproterenol induced NEFA and glycerol release, mature 3T3-L1 adipocytes were replated to 70% confluency as described above and subsequently starved for in DMEM (low glucose) + 1% FCS for 12 hours followed by DMEM (low glucose) + 0.1% FCS for an additional 12 hours. Adenoviruses diluted in 0.5 μg/ml poly-L-lysine were added to serum starved cells at an MOI of 750. Regular culture medium was added after 90 minutes. Three days later,

6

cells were incubated in DMEM + 1% BSA for 2 hours and subsequently exposed to 5 µM isoproterenol for 3 hours. Medium samples were assayed for NEFAs and glycerol as described above.

SVF cells derived from eWAT or iWAT of wild-type mice were plated at a density of $2x10^4$ cells per cm^2 in DMEM + 10% FCS + 1% P/S. Once cells reached confluency, differentiation was initiated using DMEM supplemented with 0.5 mM IBMX, 5 µg/ml insulin, 1 µM dexamethasone, and 0.5 µM rosiglitazone. Three days later the medium was replaced with DMEM supplemented with 5 µg/ml insulin and 0.5 µM rosiglitazone. Another three days later, the medium was replaced with normal growth medium.

SGBS cells and hMADs cells were cultured and differentiated according to published methods (45, 46). For microarray analysis, cells were exposed to 1 µM rosiglitazone for 6 hours as described previously (47).

Serum analysis

Triglycerides were determined using a Triglycerides liquicolor[mono] kit (HUMAN, Wiesbaden, Germany), NEFAs were measured with a NEFA-HR(2) kit (Wako). Ketone bodies were determined with a Ketone bodies Autototal kit (Wako). Glycerol, cholesterol, and glucose were measured with commercially available kits from DiaSys. Serum adiponectin was determined using the Mouse Ultrasensitive Insulin ELISA (ALPCO Diagnostics, Salem, NH, USA). Serum insulin levels were quantified using the Quantikine ELISA (R&D Systems, Abingdon, United Kingdom).

Oil red O staining

3T3-L1 adipoctyes and primary adipocytes were fixed with 4% formaldehyde in PBS for 20 minutes at room temperature. Cells were subsequently washed with PBS and incubated with filtered Oil Red O solution (30 mg/ml in 60% isopropanol) for 10 minutes. Cells were washed 2-3 times with ddH$_2$O twice before taking pictures.

ChIP-seq experiments

ChIP-seq in 3T3-L1 cells and hMADs cells was performed as described previously (48).

Histology

Adipose tissues were collected, fixated in 4% formaldehyde and embedded in paraffin. WAT was cut to 8 µm sections, BAT to 5 µm sections. Haematoxylin and eiosin staining was performed according to standard protocols.

Western blot

Proteins were extracted from adipose tissue samples using homogenization buffer (50 mM Tris, pH 8.0, 150 mM NaCl, 1% v/v NP-40, 0.5% v/v sodium deoxycholate, 0.1% SDS supplemented with Complete EDTA-free protease inhibitor cocktail) and the Qiagen TissueLyser II (Qiagen, Venlo, The Netherlands). Lysates were rotated for 15 minutes at 4ºC and subsequently centrifuged at 15,000 *g*

for 15 minutes at 4°C. For extraction of protein from 3T3-L1 cells similar homogenization buffer was added to PBS washed cells and the cells were subsequently scraped.

Equal amounts of protein were diluted with 2x Laemmli sample buffer, boiled, and separated on 8-16% gradient Criterion gels. Proteins were transferred to PVDF membrane using a Transblot turbo system (BioRad, Veenendaal, The Netherlands). Antibodies to detect HILPDA (1:1000, Santa Cruz Biotechnology, Inc, #sc-137518), ACTIN (1:2000, Sigma-Aldrich #A2066), HSP90 (1:4000, Cell Signaling Technology, Inc, #4874), TUBULIN (1:5000, Cell Signaling Technology, Inc, #2125), and anti-rabbit (1:5000, Jackson ImmunoResearch, #111-035-003) were diluted in PBS-T containing 5% w/v skimmed milk powder. Quantification of Western blots was done using the ChemiDoc MP system (BioRad, Veenendaal, The Netherlands) and Pierce ECL Plus (Thermo Fisher Scientific, Landsmeer, The Netherlands). Analysis of phosphorylation with Phos-tag gels was performed according to published methods (49). Phos-tag gels allow for the usage of the same antibody to detect native and phosphorylated protein.

RNA isolation and qPCR

RNA was isolated from tissues and cells using TRIzol® (Life Technologies Europe BV, Bleiswijk, The Netherlands). Homogenization of tissues was performed using a Qiagen TissueLyser II, whereas cells were lysed by pipetting up and down several times. Isolated RNA and RNA from the The FirstChoice Human Total RNA Survey Panel (Ambion) was reverse transcribed using the First Strand cDNA synthesis kit (Thermo Scientific, Landsmeer, The Netherlands). Gene expression analysis was performed on a CFX384 Real-Time PCR platform (BioRad, Veenendaal, The Netherlands). SensiMix PCR mix was purchased from Bioline (GC biotech, Alphen aan den Rijn, The Netherlands) Primer sequences were derived from the Harvard PrimerBank and synthesized by Eurogentec (Eurogentec S.A., Seraing, Belgium).

Microarray analysis

RNA from SGBS and hMADs cells (47) was purified with an RNAeasy Minikit (Qiagen). RNA quality was verified with the RNA 6000 Nano assay on an Agilent 2100 Bioanalyzer (Agilent Technologies, Amsterdam, the Netherlands). Hybridization, washing, and scanning of the Affymetrix Human Gene 1.1 ST array plate was performed according to standard protocols on an Affymetrix GeneTitan platform. Bioconductor packages were used to analyze the scans of the arrays (50). Robust multiarray (RMA) normalization was applied to obtain raw signal intensities (51). Probe sets were defined using remapped chip definition file (CDF, version 15) based on the Entrez gene database using published methods (52).

Statistical analysis

Student's *t*-tests, two-way ANOVAs with Bonferroni post-hoc test or one-way ANOVAs with Tukey's post-hoc test were performed in GraphPad Prism (GraphPad Software, La Jolla, CA, USA). The significance level was set at $P < 0.05$.

6

Acknowledgements

References

1. Tontonoz P, Hu E, Graves RA, Budavari AI, Spiegelman BM. mPPAR gamma 2: tissue-specific regulator of an adipocyte enhancer. *Genes Dev.* 1994;8(10):1224-1234.

2. Mandard S, Muller M, Kersten S. Peroxisome proliferator-activated receptor alpha target genes. *Cell Mol Life Sci.* 2004;61(4):393-416.

3. Bojic LA, Huff MW. Peroxisome proliferator-activated receptor delta: a multifaceted metabolic player. *Curr Opin Lipidol.* 2013;24(2):171-177.

4. Tontonoz P, Spiegelman BM. Fat and beyond: the diverse biology of PPARgamma. *Annu Rev Biochem.* 2008;77:289-312.

5. Poulsen L, Siersbaek M, Mandrup S. PPARs: fatty acid sensors controlling metabolism. *Semin Cell Dev Biol.* 2012;23(6):631-639.

6. Dowell P, Ishmael JE, Avram D, Peterson VJ, Nevrivy DJ, Leid M. p300 functions as a coactivator for the peroxisome proliferator-activated receptor alpha. *J Biol Chem.* 1997;272(52):33435-33443.

7. Gelman L, Zhou G, Fajas L, Raspe E, Fruchart JC, Auwerx J. p300 interacts with the N- and C-terminal part of PPARgamma2 in a ligand-independent and -dependent manner, respectively. *J Biol Chem.* 1999;274(12):7681-7688.

8. DiRenzo J, Soderstrom M, Kurokawa R, Ogliastro MH, Ricote M, Ingrey S, Horlein A, Rosenfeld MG, Glass CK. Peroxisome proliferator-activated receptors and retinoic acid receptors differentially control the interactions of retinoid X receptor heterodimers with ligands, coactivators, and corepressors. *Mol Cell Biol.* 1997;17(4):2166-2176.

9. Perissi V, Aggarwal A, Glass CK, Rose DW, Rosenfeld MG. A corepressor/coactivator exchange complex required for transcriptional activation by nuclear receptors and other regulated transcription factors. *Cell.* 2004;116(4):511-526.

10. Kulozik P, Jones A, Mattijssen F, Rose AJ, Reimann A, Strzoda D, Kleinsorg S, Raupp C, Kleinschmidt J, Muller-Decker K, et al. Hepatic deficiency in transcriptional cofactor TBL1 promotes liver steatosis and hypertriglyceridemia. *Cell Metab.* 2011;13(4):389-400.

11. Yu C, Markan K, Temple KA, Deplewski D, Brady MJ, Cohen RN. The nuclear receptor corepressors NCoR and SMRT decrease peroxisome proliferator-activated receptor gamma transcriptional activity and repress 3T3-L1 adipogenesis. *J Biol Chem.* 2005;280(14):13600-13605.

12. Horlein AJ, Naar AM, Heinzel T, Torchia J, Gloss B, Kurokawa R, Ryan A, Kamei Y, Soderstrom M, Glass CK, et al. Ligand-independent repression by the thyroid hormone receptor mediated by a nuclear receptor co-repressor. *Nature.* 1995;377(6548):397-404.

13. Perissi V, Jepsen K, Glass CK, Rosenfeld MG. Deconstructing repression: evolving models of co-repressor action. *Nat Rev Genet.* 2010;11(2):109-123.

14. Issemann I, Green S. Activation of a member of the steroid hormone receptor superfamily by peroxisome proliferators. *Nature.* 1990;347(6294):645-650.

15. Dreyer C, Krey G, Keller H, Givel F, Helftenbein G, Wahli W. Control of the peroxisomal beta-oxidation pathway by a novel family of nuclear hormone receptors. *Cell.* 1992;68(5):879-887.

16.   Barak Y, Nelson MC, Ong ES, Jones YZ, Ruiz-Lozano P, Chien KR, Koder A, Evans RM. PPAR gamma is required for placental, cardiac, and adipose tissue development. *Mol Cell.* 1999;4(4):585-595.

17.   Rosen ED, Sarraf P, Troy AE, Bradwin G, Moore K, Milstone DS, Spiegelman BM, Mortensen RM. PPAR gamma is required for the differentiation of adipose tissue in vivo and in vitro. *Mol Cell.* 1999;4(4):611-617.

18.   Ahmadian M, Suh JM, Hah N, Liddle C, Atkins AR, Downes M, Evans RM. PPARgamma signaling and metabolism: the good, the bad and the future. *Nat Med.* 2013;19(5):557-566.

19.   Schoonjans K, Peinado-Onsurbe J, Lefebvre AM, Heyman RA, Briggs M, Deeb S, Staels B, Auwerx J. PPARalpha and PPARgamma activators direct a distinct tissue-specific transcriptional response via a PPRE in the lipoprotein lipase gene. *EMBO J.* 1996;15(19):5336-5348.

20.   Motojima K, Passilly P, Peters JM, Gonzalez FJ, Latruffe N. Expression of putative fatty acid transporter genes are regulated by peroxisome proliferator-activated receptor alpha and gamma activators in a tissue- and inducer-specific manner. *J Biol Chem.* 1998;273(27):16710-16714.

21.   Cao W, Daniel KW, Robidoux J, Puigserver P, Medvedev AV, Bai X, Floering LM, Spiegelman BM, Collins S. p38 mitogen-activated protein kinase is the central regulator of cyclic AMP-dependent transcription of the brown fat uncoupling protein 1 gene. *Mol Cell Biol.* 2004;24(7):3057-3067.

22.   Dalen KT, Schoonjans K, Ulven SM, Weedon-Fekjaer MS, Bentzen TG, Koutnikova H, Auwerx J, Nebb HI. Adipose tissue expression of the lipid droplet-associating proteins S3-12 and perilipin is controlled by peroxisome proliferator-activated receptor-gamma. *Diabetes.* 2004;53(5):1243-1252.

23.   Targett-Adams P, McElwee MJ, Ehrenborg E, Gustafsson MC, Palmer CN, McLauchlan J. A PPAR response element regulates transcription of the gene for human adipose differentiation-related protein. *Biochim Biophys Acta.* 2005;1728(1-2):95-104.

24.   Puri V, Ranjit S, Konda S, Nicoloro SM, Straubhaar J, Chawla A, Chouinard M, Lin C, Burkart A, Corvera S, et al. Cidea is associated with lipid droplets and insulin sensitivity in humans. *Proc Natl Acad Sci U S A.* 2008;105(22):7833-7838.

25.   Kim YJ, Cho SY, Yun CH, Moon YS, Lee TR, Kim SH. Transcriptional activation of Cidec by PPARgamma2 in adipocyte. *Biochem Biophys Res Commun.* 2008;377(1):297-302.

26.   Tontonoz P, Hu E, Devine J, Beale EG, Spiegelman BM. PPAR gamma 2 regulates adipose expression of the phosphoenolpyruvate carboxykinase gene. *Mol Cell Biol.* 1995;15(1):351-357.

27.   Forman BM, Chen J, Evans RM. The peroxisome proliferator-activated receptors: ligands and activators. *Ann N Y Acad Sci.* 1996;804:266-275.

28.   Schupp M, Lazar MA. Endogenous ligands for nuclear receptors: digging deeper. *J Biol Chem.* 2010;285(52):40409-40415.

29.   Denko N, Schindler C, Koong A, Laderoute K, Green C, Giaccia A. Epigenetic regulation of gene expression in cervical cancer cells by the tumor microenvironment. *Clin Cancer Res.* 2000;6(2):480-487.

30.   Seo T, Konda R, Sugimura J, Iwasaki K, Nakamura Y, Fujioka T. Expression of hypoxia-inducible protein 2 in renal cell carcinoma: A promising candidate for molecular targeting therapy. *Oncol Lett.* 2010;1(4):697-701.

31.   Nishimura S, Tsuda H, Ito K, Takano M, Terai Y, Jobo T, Kigawa J, Sugiyama T, Yaegashi N, Aoki D. Differential expression of hypoxia-inducible protein 2 among different histological types of epithelial ovarian cancer and in clear cell adenocarcinomas. *Int J Gynecol Cancer.* 2010;20(2):220-226.

32.   Wang X, Bjorklund S, Wasik AM, Grandien A, Andersson P, Kimby E, Dahlman-Wright K, Zhao C, Christensson B, Sander B. Gene expression profiling and chromatin immunoprecipitation identify DBN1, SETMAR and HIG2 as direct targets of SOX11 in mantle cell lymphoma. *PLoS One.* 2010;5(11):e14085.

6

33. Kim SH, Wang D, Park YY, Katoh H, Margalit O, Sheffer M, Wu H, Holla VR, Lee JS, Dubois RN. HIG2 promotes colorectal cancer progression via hypoxia-dependent and independent pathways. *Cancer Lett.* 2013;341(2):159-165.

34. Gimm T, Wiese M, Teschemacher B, Deggerich A, Schodel J, Knaup KX, Hackenbeck T, Hellerbrand C, Amann K, Wiesener MS, et al. Hypoxia-inducible protein 2 is a novel lipid droplet protein and a specific target gene of hypoxia-inducible factor-1. *FASEB J.* 2010;24(11):4443-4458.

35. Zechner R, Zimmermann R, Eichmann TO, Kohlwein SD, Haemmerle G, Lass A, Madeo F. FAT SIGNALS--lipases and lipolysis in lipid metabolism and signaling. *Cell Metab.* 2012;15(3):279-291.

36. Mayr B, Montminy M. Transcriptional regulation by the phosphorylation-dependent factor CREB. *Nat Rev Mol Cell Biol.* 2001;2(8):599-609.

37. Altarejos JY, Montminy M. CREB and the CRTC co-activators: sensors for hormonal and metabolic signals. *Nat Rev Mol Cell Biol.* 2011;12(3):141-151.

38. Liu JS, Park EA, Gurney AL, Roesler WJ, Hanson RW. Cyclic AMP induction of phosphoenolpyruvate carboxykinase (GTP) gene transcription is mediated by multiple promoter elements. *J Biol Chem.* 1991;266(28):19095-19102.

39. Qi L, Saberi M, Zmuda E, Wang Y, Altarejos J, Zhang X, Dentin R, Hedrick S, Bandyopadhyay G, Hai T, et al. Adipocyte CREB promotes insulin resistance in obesity. *Cell Metab.* 2009;9(3):277-286.

40. Deng T, Shan S, Li PP, Shen ZF, Lu XP, Cheng J, Ning ZQ. Peroxisome proliferator-activated receptor-gamma transcriptionally up-regulates hormone-sensitive lipase via the involvement of specificity protein-1. *Endocrinology.* 2006;147(2):875-884.

41. Festuccia WT, Laplante M, Berthiaume M, Gelinas Y, Deshaies Y. PPARgamma agonism increases rat adipose tissue lipolysis, expression of glyceride lipases, and the response of lipolysis to hormonal control. *Diabetologia.* 2006;49(10):2427-2436.

42. Yajima H, Kobayashi Y, Kanaya T, Horino Y. Identification of peroxisome-proliferator responsive element in the mouse HSL gene. *Biochem Biophys Res Commun.* 2007;352(2):526-531.

43. Rodriguez-Cuenca S, Carobbio S, Vidal-Puig A. Ablation of Pparg2 impairs lipolysis and reveals murine strain differences in lipolytic responses. *FASEB J.* 2012;26(5):1835-1844.

44. Rodriguez-Cuenca S, Carobbio S, Velagapudi VR, Barbarroja N, Moreno-Navarrete JM, Tinahones FJ, Fernandez-Real JM, Oresic M, Vidal-Puig A. Peroxisome proliferator-activated receptor gamma-dependent regulation of lipolytic nodes and metabolic flexibility. *Mol Cell Biol.* 2012;32(8):1555-1565.

45. Wabitsch M, Brenner RE, Melzner I, Braun M, Moller P, Heinze E, Debatin KM, Hauner H. Characterization of a human preadipocyte cell strain with high capacity for adipose differentiation. *Int J Obes Relat Metab Disord.* 2001;25(1):8-15.

46. Rodriguez AM, Elabd C, Delteil F, Astier J, Vernochet C, Saint-Marc P, Guesnet J, Guezennec A, Amri EZ, Dani C, et al. Adipocyte differentiation of multipotent cells established from human adipose tissue. *Biochem Biophys Res Commun.* 2004;315(2):255-263.

47. Jeninga EH, Bugge A, Nielsen R, Kersten S, Hamers N, Dani C, Wabitsch M, Berger R, Stunnenberg HG, Mandrup S, et al. Peroxisome proliferator-activated receptor gamma regulates expression of the anti-lipolytic G-protein-coupled receptor 81 (GPR81/Gpr81). *J Biol Chem.* 2009;284(39):26385-26393.

48. Nielsen R, Pedersen TA, Hagenbeek D, Moulos P, Siersbaek R, Megens E, Denissov S, Borgesen M, Francoijs KJ, Mandrup S, et al. Genome-wide profiling of PPARgamma:RXR and RNA polymerase II occupancy reveals temporal activation of distinct metabolic pathways and changes in RXR dimer composition during adipogenesis. *Genes Dev.* 2008;22(21):2953-2967.

49. Yang L, Xue Z, He Y, Sun S, Chen H, Qi L. A Phos-tag-based approach reveals the extent of physiological endoplasmic reticulum stress. *PLoS One.* 2010;5(7):e11621.

50. Gentleman RC, Carey VJ, Bates DM, Bolstad B, Dettling M, Dudoit S, Ellis B, Gautier L, Ge Y, Gentry J, et al. Bioconductor: open software development for computational biology and bioinformatics. *Genome Biol.* 2004;5(10):R80.

51. Irizarry RA, Hobbs B, Collin F, Beazer-Barclay YD, Antonellis KJ, Scherf U, Speed TP. Exploration, normalization, and summaries of high density oligonucleotide array probe level data. *Biostatistics.* 2003;4(2):249-264.

52. Dai M, Wang P, Boyd AD, Kostov G, Athey B, Jones EG, Bunney WE, Myers RM, Speed TP, Akil H, et al. Evolving gene/transcript definitions significantly alter the interpretation of GeneChip data. *Nucleic Acids Res.* 2005;33(20):e175.

6

7

General discussion

The angiopoietin-like 4 gene (*Angptl4*) was identified as a peroxisome proliferator activated receptor (PPAR) target gene by three independent groups in 2000 (1-3). Since then, interest in ANGPTL4 has increased gradually, partly fueled by the finding that ANGPTL4 regulates lipoprotein lipase (LPL) and the observation that sequence variants of *ANGPTL4* are associated with changes in plasma triglyceride levels in large human studies(4, 5). In this thesis, we uncover ANGPTL4 as an important player in the protection of mesenteric lymph node (MLN)-resident macrophages from aberrant lipid accumulation and in the regulation of lipid digestion by pancreatic lipase (PL).

ANGTPL4 as a regulator of lipid digestion

In chapter 4 we provide evidence for regulation of dietary lipid digestion by ANGPTL4 via inhibition of pancreatic lipase (PL). Although the results clearly point to an effect of ANGPTL4 on intraluminal lipase activity, several aspects remain that warrant further attention and investigation. Of particular importance is the need to identify the specific cell(s) that secrete ANGPTL4 towards the intestinal lumen and to show the presence of ANGPTL4 in the lumen. The small intestine contains a multitude of cells such as enterocytes, enteroendocrine cells and Goblet cells (6, 7). Recent work from our group indicates that C-terminal ANGPTL4 is produced in enteroendocrine cells, suggesting secretion into the circulation (8). By contrast, we suspect that N-terminal ANGPTL4 is produced by enterocytes, possibly via cell-specific expression of proprotein convertases involved in ANGPTL4 processing. Unfortunately, the absence of functional antibodies for N-terminal ANGPTL4 has made it very difficult to verify this notion. Accordingly, concrete experimental evidence is still lacking that N-terminal ANGPTL4 is secreted towards the intestinal lumen. Antibody-based strategies to determine either n- or cANGPTL4 in the intestinal lumen did not succeed and it will require more sophisticated techniques such as mass spectrometry and peptide sequencing to be able to confirm the presence of ANGPTL4. Nevertheless, since we observed increased lipase activity in fecal waters of *Angptl4*$^{-/-}$ mice, inhibition of lipid digestion by ANGPTL4 most likely takes place intraluminally.

In addition to pancreatic lipase and colipase, the pancreas also secretes several proteases. The presence of high quantities of proteases in the intestinal lumen raises the question whether actual interactions between ANGPTL4 and PL are possible. Indeed, it would require significant amounts of ANGPTL4 to be secreted in order to reduce intraluminal lipase activity. Alternatively, experiments performed in the late 1980s show that heparin binds PL to the brush border which promotes the absorption of fatty acids (9, 10). It is

therefore tempting to speculate that ANGPTL4 mainly inhibits and/or releases active PL that is bound to heparin at the brush border. Consequently, such a mechanism could reduce the amount of ANGPTL4 required to inhibit lipid uptake. Experiments to delineate potential differences in PL binding capacity of intestinal explants of wild-type and *Angptl4*$^{-/-}$ using radioactively labeled pancreatic lipase would be extremely valuable to explore this option.

The constant rate of appearance of radio-labelled lipid in the circulation in our lipid absorption test supports the well-established notion that chylomicron synthesis is saturable and rate limiting for fat absorption (11). The lack of difference in tracer appearance between wild-type and *Angptl4*$^{-/-}$ animals suggests that ANGPTL4 does not influence chylomicron synthesis. Nevertheless, we did observe enhanced accumulation of lipid in the enterocytes of *Angptl4*$^{-/-}$ animals. Hence, we propose that *Angptl4*$^{-/-}$ mice produce chylomicrons at a similar rate but for a prolonged time, leading to a net increase in energy delivery. A potential confounding factor in the interpretation of the effect of PL inhibition by ANGPTL4 is the utilization of whole-body knockout. Indeed, ANGPTL4 is a known inhibitor of LPL and an increase in the capacity of the adipose tissue in *Angptl4*$^{-/-}$ mice to hydrolyze chylomicrons could lead to increased fat deposition (12). However, it should be mentioned that transgenic animals with adipose tissue-specific LPL absence or overexpression do not develop a phenotype regarding fat mass or body weight (13, 14). Also, a change in adipose tissue LPL activity is not expected to affect bodyweight gain and fat mass, as it does not influence energy balance. Therefore, we believe that the increase in adiposity is mainly attributable to increased harvesting of lipids from the ingested food.

Expression of *Angptl4* in the small intestine is known to be regulated by PPARα and it is therefore likely that increased lipid accumulation in enterocytes leads to PPARα mediated induction of *Angptl4* (15). Subsequent secretion of ANGPTL4 results in a reduction of lipid digestion and uptake via inhibition of PL. Thus, ANGPTL4 assures a controlled uptake of lipid in enterocytes and at the same time reduces the total amount of dietary lipid harvested. Interestingly, enterocytes are also capable to take up lipids basolaterally (16). Lipid taken up from the circulation is thought to represent a distinct pool of lipid from those apically absorbed. Indeed, apical acquired lipid is mainly incorporated into chylomicrons whereas basolateral derived lipids are used for β-oxidation or phospholipid synthesis (17, 18). Currently, there is no evidence that basolateral uptake of lipids requires LPL, which is expressed at very low levels in the small intestine, and uptake likely occurs in the form of free fatty acids. Accordingly, it is difficult to envision how ANGPTL4 may be involved in the regulation of basolateral lipid accumulation.

7

Macrophage LPL is required for a normal immune response

Chylomicrons mainly transport triglycerides. Upon high-fat diet feeding in rats, TG concentrations in the chyle that traverses the mesenteric lymphatics are much higher compared to plasma levels and can increase up to 55 mM. Consequently, cells residing in the MLNs are exposed to extremely high concentrations of TGs. In chapter 3 we provide evidence that MLN-resident macrophages require ANGPTL4-mediated inhibition of LPL to protect them from becoming engorged with lipid after a high-fat meal. The reason for these MLN-resident macrophages to take up lipids is not completely clear. Interestingly, chylomicrons have been described as transporters for dietary antigens such as ovalbumin (19). Similarly, LPS produced by the gut microbiota and lipid antigens are incorporated into lipoproteins (20, 21). Thus, it is conceivable that chylomicrons transport a variety of antigens that can be captured by macrophages in an LPL dependent manner for subsequent presentation to lymphocytes. Delivery of antigens to the immune cells that reside within the mesenteric lymph node represents an important process in the development of a normal immune response (22).

It has been suggested that under certain circumstances including high-fat feeding, bacteria translocate from the intestinal lumen to the circulation during which they are partially captured in the mesenteric lymph nodes (23, 24). Previous reports suggest that fatty acids are an important energy source to fuel phagocytosis (25, 26). More recently it was shown that macrophage β-oxidation and OXPHOS results in the production of mitochondria-derived reactive oxygen species (ROS) that contribute to eliminating phagocytized bacteria (27). It is therefore possible that the uptake of lipid by MLN-resident macrophages is required for efficient phagocytosis of bacteria that otherwise would traverse to the circulation. The high levels of chylomicrons that traverse these MLN-resident macrophages assures an ample supply of fatty acids to generate ROS but also poses a risk for excessive lipid uptake. Indeed, the capacity of macrophages to take up lipid is much larger than the amount used in oxidation, leading to storage of the surplus (28). Thus, LPL-mediated hydrolysis of chylomicrons by MLN-resident macrophages might be aimed at the uptake of antigens and lipid in order to develop a normal immune response. Without a tight regulation of this process, inappropriate amounts of antigen and lipid may accumulate, ultimately culminating in the development of an uncontrolled inflammatory response. Considering a potential deficit in fatty acid supply in macrophages of mice with ANGPTL4 overexpression it would be interesting to test if these animals have an impaired capacity to phagocytose bacteria in MLNs.

Saturated fatty acids affect chylomicron characteristics

Increased lipid accumulation in cells that are not professional lipid storing cells can lead to severe adverse effects such as mitochondrial dysfunction, endoplasmic reticulum stress, inflammation, and apoptosis. Hence, lipids can have so-called lipotoxic effects (29). Our experiments performed in chapter 3 revealed that the high-fat diet-induced lethal phenotype in *Angptl4*$^{-/-}$ mice was specific for high-fat diets containing mainly saturated fatty acids. Moreover, induction of ER stress and inflammation in macrophages was observed when they were exposed to saturated fatty acids but not unsaturated fatty acids. Indeed, compelling data indicate that saturated fatty acids are highly lipotoxic whereas unsaturated fatty acids may prevent lipotoxicity (30-32). The high lipotoxic potential of saturated fatty acids is thought to be linked to several mechanisms including a low efficiency of esterification into TGs and increased synthesis of ceramides and diacylglycerol (DAG). However, in addition to the lipotoxic potential of saturated fatty acids it is important to note that the consumption of dietary saturated fat changes the characteristics of chylomicrons that are produced in the intestine. Diets rich in saturated fatty acids lead to the production of smaller chylomicrons with higher apolipoprotein B to triglyceride ratios compared to chylomicrons containing unsaturated fatty acids (33, 34). Consequently, chylomicrons containing saturated fat are cleared from the circulation at a faster rate (33). Thus, saturated fatty acids not only have the inherent property of being lipotoxic, they also lead to faster hydrolysis of lipids from lipoproteins, further challenging the cellular response to lipid accumulation. Whether the chylomicrons produced upon consumption of saturated or unsaturated fat have divergent capacities for the transport of antigens is not known. Nevertheless, it is conceivable that in conjunction with increased delipidation of saturated fat based chylomicrons, higher levels of antigens accumulate in macrophages. Finally, it should be noted that the inflammatory response in macrophages elicited by chyle could be completely blocked by inhibiting LPL indicating that other components that are present in chyle such as fibrinogen do not contribute to the observed phenotype.

Growing family of ANGPTL proteins

ANGPTL4 is part of the family of ANGPTL proteins of which ANGPTL3 and ANGPTL4 are known to regulate LPL (35). Recently, a new member of the family was described with the identification of ANGPTL8 (36, 37). Interestingly, although the function of these ANGPTL proteins seems to be related to the inhibition of LPL, the regulation of these proteins as well as their mode of action toward LPL seems to be different. Indeed, ANGPTL3 is exclusively

7

expressed in the liver, mainly active during the fed state and inhibits LPL in a reversible manner. ANGPTL4 is expressed in multiple tissues and active in the fed and fasted state via non-reversible and reversible inhibition of LPL. ANGPTL8 was found to inhibit LPL activity primarily in oxidative tissues upon refeeding. Furthermore, ANGPTL8 would at the same time spare adipose tissue LPL in order to preserve uptake of lipid in the adipose tissue during the postprandial phase (37). LPL is known to be anchored to the cell surface of endothelial cells via several receptors including heparan sulfate proteoglycans (HSPGs) and glycosylphosphatidylinositol (GPI)-anchored high density lipoprotein-binding protein (GPIHBP1), of which the latter acts as an LPL transporter across endothelial cells (38, 39). In vitro experiments suggest that LPL bound to GPIHBP1 but not heparin is prevented from being inactivated by ANGPTL4 (40). In contrast, ANGPTL3 is unable to inhibit LPL in the presence of both GPIHBP1 and heparin (40). It can be hypothesized that the presence of specific anchor proteins that bind LPL prevent ANGPTL8 from inhibiting the catalytic function of LPL in adipose tissue. Together, these observations indicate that the family of ANGPTL proteins is highly important in the control of the amount of lipid that is allowed to enter a specific organ during the fed and fasted state.

Mechanism of HILPDA induced lipid accumulation

In chapter 5 we identified *Hilpda* as new PPAR target in mouse liver. Hepatic overexpression of HILPDA resulted in the induction of fatty liver, which we could attribute to a marked inhibition of VLDL-TG secretion. Inhibition of VLDL secretion did not result in a change in plasma TG levels. Consequently, it can be hypothesized that TGs secreted from mice with increased hepatic HILPDA expression are cleared from the circulation at a slower rate. This notion should be verified by plasma TG clearance studies using radiolabeled VLDL-like particles. A potential explanation for such an increase in TG clearance may be that hepatic HILPDA overexpression affects the apolipoprotein composition of VLDL. Indeed, multiple apolipoproteins including APOA5, APOC2, and APOE have been implicated in the clearance of lipoprotein-derived TG (41-44). Moreover, it has been reported that APOE3 overexpression in livers of APOE deficient mice leads to increased VLDL-TG secretion without inducing major changes in plasma TG levels, potentially via increased clearance of TG-rich lipoproteins in peripheral tissues (45). Thus, interference with the function and/or incorporation of APOE3 into VLDL by HILPDA could be a potential explanation for the observed discrepancy between hepatic VLDL production and plasma TG levels. In this context, it will be interesting to try to identify the specific apolipoproteins that are associated with the VLDL secreted from livers with increased

HILPDA expression using a proteomics approach. Many apolipoproteins including those of the APOC family are of low molecular weight (46). Given the small size of HILPDA it is tempting to speculate that HILPDA itself could represent an apolipoprotein that interacts with LPL to modulate the lipolytic activity. However, we did not find HILPDA to be secreted suggesting that any possible change in plasma TG clearance is likely to be related to perturbations in the liver.

At this point we have no information on the type of lipids accumulating upon HILPDA overexpression or where within the liver the surplus lipids are stored. Delineating this riddle would be very helpful in order to identify the function of HILPDA in liver lipid metabolism. Changes in the abundance of specific lipids might provide clues about the molecular targets of HILPDA involved in VLDL assembly and synthesis (47).

Important work by Gimm et al. suggests that HILPDA is a novel lipid droplet associated protein that colocalizes with PLIN2 and PLIN3 at the surface of some but not all lipid droplets (48). Both PLIN2 and HILPDA are regulated by PPARα in the liver and increased expression of PLIN2 leads to a reduction in VLDL synthesis (49, 50). Conversely, liver-specific knockdown of PLIN2 significantly reduces hepatic lipid accumulation, while causing no change in plasma TG levels (51, 52). Based on these observations it can be hypothesized that HILPDA may function similarly to PLIN2 and increase storage of TGs in lipid droplet, thereby preventing them from being incorporated into VLDL. It should be noted that incorporation of TG within lipid droplets into VLDL likely requires their hydrolysis into fatty acids, followed by re-esterification of the fatty acids to become VLDL-TG. Accordingly, it is conceivable that HILPDA may impair the accessibility of lipid droplets to cytosolic lipases such as adipose tissue triglyceride lipase (ATGL/PNPLA2), without directly impairing ATGL activity. Whether HILPDA and PLIN2 cooperate and/or physically interact requires further investigation. In future work, we intend to follow two different approaches to unravel the specific function of HILPDA in the VLDL secretory pathway: 1) the identification of specific lipids that accumulate, and 2) the pull-down assays to characterize proteins that potentially bind to HILPDA. Since we have access to floxed *Hilpda* mice it will be interesting to generate liver-specific knockout mice and examine if these animals are protected from hepatic steatosis due to increased VLDL-TG secretion. Also, generation of intestine-specific knockout mice would be very helpful to study if HILPDA is affecting chylomicron synthesis and secretion, as this process shares many similarities with VLDL synthesis.

Hepatic steatosis is a hallmark of many metabolic disturbances and associated with insulin resistance. Based on the plasma lipid and glucose parameters, we have no evidence for the development of insulin resistance upon hepatic steatosis following hepatic HILPDA

7

overexpression. Whether HILPDA is associated with accumulation of lipotoxic lipids such as ceramides and DAG is not clear (53). Nevertheless, it will be important to elucidate the potential effect of HILPDA-induced hepatic steatosis on the development of insulin resistance.

Interestingly, HFD-induced hepatic steatosis did not lead to the induction of HILPDA in mice. The unaltered expression of HILPDA upon the development of a fatty liver seems to correspond to our observations in the differentiation of fibroblast to adipocytes, in which we fail to observe major increases in HILPDA expression. Based on the results from these experiments we hypothesize that HILPDA is not directly required for lipid droplet biogenesis. Instead, HILPDA probably resides at the surface of lipid droplets to perform a specific task under certain conditions such as β-adrenergic stimulation (discussed below).

HILPDA regulates adipocyte lipolysis

In chapter 6 we revealed that HILPDA expression is highly induced upon stimulation of β-adrenergic receptors. Moreover, fasting resulted in a marked increase in HILPDA expression in white adipose tissue (WAT). Activation of β-adrenergic receptors leads to the phosphorylation and of numerous downstream targets such as protein kinase A and perilipin 1 (PLIN1). As a result, PLIN1 directs hormone sensitive lipase (HSL) to surface of lipid droplets. Moreover, comparative gene identification-58 (CGI-58), which is bound to PLIN1 under basal conditions, now binds to ATGL serving as a coactivator (54). These events increase the activity of ATGL and HSL leading the release of non-esterified fatty acids (NEFAs). Given the prominent induction of HILPDA by fasting and β-adrenergic receptor stimulation we initially reasoned that HILPDA would serve as an activator of lipolysis in adipose tissue, potentially as a cofactor for one of the aforementioned lipases. However, experiments with adipose tissue-specific *Hilpda* knockout mice clearly demonstrated that deletion of HILPDA has no major impact on the response to fasting. In contrast, overexpression of HILPDA in adipocytes consistently led to reduced NEFA release upon β-adrenergic receptor activation. Thus, it is likely that HILPDA is induced by β-adrenergic receptor and subsequently inhibits lipolysis to ensure controlled release of NEFAs in the circulation. Such feedback mechanisms are not uncommon as exemplified by the induction of both LPL and ANGPTL4 by PPAR.

An interesting question based on our data is why there is no increase in NEFA release with knockdown of HILPDA during fasting or in cell culture with siRNA? One possible answer is that increased lipolysis upon HILPDA knockout leads to increased production of

PPAR ligands. Indeed, intracellular lipolysis is known to stimulate the activation of PPARs in brown adipose tissue (BAT) (55). In congruence, we observed increased expression of the PPAR target *G0s2* in BAT of AT*Hilpda$^{-/-}$* animals (56). G0S2 is an inhibitor of ATGL and its increased expression could compensate for increased lipolysis upon HILPDA knockout (57). Thus, a potential effect of *Hilpda* deletion might be obscured via increased PPAR activity and subsequent induction of G0S2. Alternatively, a potential increased lipolytic rate upon HILPDA knockout may be counteracted by increased re-esterification of NEFAs into TGs. Future microarray experiments would provide a good opportunity to characterize additional differentially regulated genes upon knockout of adipose tissue HILPDA.

Experiments in chapter 5 revealed that HILPDA does not directly regulate ATGL or HSL activity in liver samples or in an in vitro system. However, this does not exclude a possibility for HILPDA to regulate lipolysis and lipase function in adipocytes. As mentioned above, PLIN1 plays an important role in the regulation of adipocyte lipolysis. Since PLIN1 is not expressed in liver it can be speculated that it contributes to a potential tissue-specific function of HILPDA in adipose tissue. Consequently, additional experiments will have to address a (indirect) inhibitory effect of HILPDA on several key lipases involved in the release of NEFAs in adipocytes.

Expression of HILPDA in macrophages

Unpublished work of our laboratory indicates that HILPDA expression is highly induced upon lipid loading of macrophages. In fact, *Hilpda* is consistently found in the top 15 of most highly induced genes upon exposure of macrophages to fatty acids or TG-rich lipoproteins. Hence, we initially anticipated HILPDA expression in adipose tissue to be mainly localized in the SVF, which contains numerous cells including adipocyte progenitor cells and macrophages. Moreover, we expected to find major increases in HILPDA expression upon high-fat diet intervention or fasting, two challenges that are known to increase lipid deposition in adipose tissue macrophages (58, 59). However, despite a marked increase in the expression of *Cd68* in the SVF fraction upon high-fat diet feeding we failed to observe changes in the abundance of *Hilpda* in the SVF. A potential explanation could be that HILPDA is expressed in lipid laden macrophages that separate together with adipocytes as has been described in literature (60, 61). Nevertheless, it can be expected that a major fraction of macrophages that have accumulated some lipid are in the SVF and future experiments will have to address this issue. Immunohistochemistry of crown-like structure in adipose tissue of wild-type animals revealed the presence of HILPDA positive cells providing evidence for the presence of HILPDA in lipid laden

7

macrophages in vivo. Similar experiments will be performed in adipose tissue of adipose tissue-specific *Hilpda* knockout mice to provide conclusive evidence on the presence of HILPDA in macrophages in vivo. Another intriguing observation is the absence of induction of *Hilpda* expression upon exposure of macrophages to potent PPAR ligands. In the same experiments the expression of *Plin2*, a known PPAR target, was increased upon exposure to ligands for PPARβ/δ and PPARγ. At this stage it is difficult to explain the absence of PPAR induced *Hilpda* expression in macrophages. Possibly, the PPRE is physically not accessible for PPARβ/δ or PPARγ due to occupancy of proximal response elements by other transcription factors that bind with higher affinity. Future experiments will take advantage of this interesting observation to get a better understanding tissue-specific induction of target genes by PPARs.

Conclusion

In this thesis we have extended our knowledge on the function of ANGPTL4 in lipid metabolism. We demonstrated that ANGPTL4 plays an important role in the protection of mesenteric lymph node resident macrophages from becoming engorged with lipid. Accumulation of saturated fat in macrophages upon loss of ANGPTL4-mediated inhibition of LPL activity elicited an inflammatory process in the lymph nodes ultimately culminating in fibrinopurulent peritonitis. *Angptl4*$^{-/-}$ mice initially gain more weight when fed a high-fat diet in the absence of inflammation. We provided evidence for this observation being dependent on inhibition of PL by ANGPTL4. As a result, mice lacking ANGPTL4 harvest more lipids from dietary sources leading to increased body weight and adiposity. We identified HILPDA as a novel PPAR target in mouse liver and adipose tissue. Overexpression of HILPDA in liver led to a significant decrease in hepatic VLDL-TG secretion and the development of a fatty liver. In addition to regulation of HILPDA by PPARγ we observed marked inductions in HILPDA expression upon fasting and β-adrenergic receptor activation in adipose tissue. Deletion of *Hilpda* in adipose tissue had no major impact on the metabolic response to fasting. In contrast, overexpression of HILPDA in adipocytes resulted in a reduction of NEFA release upon β-adrenergic receptor stimulation. Thus, HILPDA represents a novel PPAR target involved in hepatic and adipose tissue lipid metabolism via regulation of VLDL-TG secretion and adipocyte lipolysis, respectively.

References

1. Kersten S, Mandard S, Tan NS, Escher P, Metzger D, Chambon P, Gonzalez FJ, Desvergne B, Wahli W. Characterization of the fasting-induced adipose factor FIAF, a novel peroxisome proliferator-activated receptor target gene. *J Biol Chem.* 2000;275(37):28488-28493.

2. Yoon JC, Chickering TW, Rosen ED, Dussault B, Qin Y, Soukas A, Friedman JM, Holmes WE, Spiegelman BM. Peroxisome proliferator-activated receptor gamma target gene encoding a novel angiopoietin-related protein associated with adipose differentiation. *Mol Cell Biol.* 2000;20(14):5343-5349.

3. Kim I, Kim HG, Kim H, Kim HH, Park SK, Uhm CS, Lee ZH, Koh GY. Hepatic expression, synthesis and secretion of a novel fibrinogen/angiopoietin-related protein that prevents endothelial-cell apoptosis. *Biochem J.* 2000;346 Pt 3:603-610.

4. Yoshida K, Shimizugawa T, Ono M, Furukawa H. Angiopoietin-like protein 4 is a potent hyperlipidemia-inducing factor in mice and inhibitor of lipoprotein lipase. *J Lipid Res.* 2002;43(11):1770-1772.

5. Romeo S, Pennacchio LA, Fu Y, Boerwinkle E, Tybjaerg-Hansen A, Hobbs HH, Cohen JC. Population-based resequencing of ANGPTL4 uncovers variations that reduce triglycerides and increase HDL. *Nat Genet.* 2007;39(4):513-516.

6. Cheng H, Leblond CP. Origin, differentiation and renewal of the four main epithelial cell types in the mouse small intestine. V. Unitarian Theory of the origin of the four epithelial cell types. *Am J Anat.* 1974;141(4):537-561.

7. Gerbe F, Legraverend C, Jay P. The intestinal epithelium tuft cells: specification and function. *Cell Mol Life Sci.* 2012;69(17):2907-2917.

8. Alex S, Lichtenstein L, Dijk W, Mensink RP, Tan NS, Kersten S. ANGPTL4 is produced by entero-endocrine cells in the human intestinal tract. *Histochem Cell Biol.* 2013.

9. Bosner MS, Gulick T, Riley DJ, Spilburg CA, Lange LG, 3rd. Receptor-like function of heparin in the binding and uptake of neutral lipids. *Proc Natl Acad Sci U S A.* 1988;85(20):7438-7442.

10. Bosner MS, Gulick T, Riley DJ, Spilburg CA, Lange LG. Heparin-modulated binding of pancreatic lipase and uptake of hydrolyzed triglycerides in the intestine. *J Biol Chem.* 1989;264(34):20261-20264.

11. Xiao C, Hsieh J, Adeli K, Lewis GF. Gut-liver interaction in triglyceride-rich lipoprotein metabolism. *Am J Physiol Endocrinol Metab.* 2011;301(3):E429-446.

12. Kroupa O, Vorrsjo E, Stienstra R, Mattijssen F, Nilsson SK, Sukonina V, Kersten S, Olivecrona G, Olivecrona T. Linking nutritional regulation of Angptl4, Gpihbp1, and Lmf1 to lipoprotein lipase activity in rodent adipose tissue. *BMC Physiol.* 2012;12:13.

13. Hensley LL, Ranganathan G, Wagner EM, Wells BD, Daniel JC, Vu D, Semenkovich CF, Zechner R, Kern PA. Transgenic mice expressing lipoprotein lipase in adipose tissue. Absence of the proximal 3'-untranslated region causes translational upregulation. *J Biol Chem.* 2003;278(35):32702-32709.

14. Kratky D, Zimmermann R, Wagner EM, Strauss JG, Jin W, Kostner GM, Haemmerle G, Rader DJ, Zechner R. Endothelial lipase provides an alternative pathway for FFA uptake in lipoprotein lipase-deficient mouse adipose tissue. *J Clin Invest.* 2005;115(1):161-167.

15. Bunger M, van den Bosch HM, van der Meijde J, Kersten S, Hooiveld GJ, Muller M. Genome-wide analysis of PPARalpha activation in murine small intestine. *Physiol Genomics.* 2007;30(2):192-204.

16. Mansbach CM, Siddiqi SA. The biogenesis of chylomicrons. *Annu Rev Physiol.* 2010;72:315-333.

17. Gangl A, Ockner RK. Intestinal metabolism of plasma free fatty acids. Intracellular compartmentation and mechanisms of control. *J Clin Invest.* 1975;55(4):803-813.

18. Storch J, Zhou YX, Lagakos WS. Metabolism of apical versus basolateral sn-2-monoacylglycerol and fatty acids in rodent small intestine. *J Lipid Res.* 2008;49(8):1762-1769.

7

19. Wang Y, Ghoshal S, Ward M, de Villiers W, Woodward J, Eckhardt E. Chylomicrons promote intestinal absorption and systemic dissemination of dietary antigen (ovalbumin) in mice. *PLoS One.* 2009;4(12):e8442.

20. Ghoshal S, Witta J, Zhong J, de Villiers W, Eckhardt E. Chylomicrons promote intestinal absorption of lipopolysaccharides. *J Lipid Res.* 2009;50(1):90-97.

21. van den Elzen P, Garg S, Leon L, Brigl M, Leadbetter EA, Gumperz JE, Dascher CC, Cheng TY, Sacks FM, Illarionov PA, et al. Apolipoprotein-mediated pathways of lipid antigen presentation. *Nature.* 2005;437(7060):906-910.

22. Ohtani O, Ohtani Y. Structure and function of rat lymph nodes. *Arch Histol Cytol.* 2008;71(2):69-76.

23. Amar J, Chabo C, Waget A, Klopp P, Vachoux C, Bermudez-Humaran LG, Smirnova N, Berge M, Sulpice T, Lahtinen S, et al. Intestinal mucosal adherence and translocation of commensal bacteria at the early onset of type 2 diabetes: molecular mechanisms and probiotic treatment. *EMBO Mol Med.* 2011;3(9):559-572.

24. Yue C, Ma B, Zhao Y, Li Q, Li J. Lipopolysaccharide-induced bacterial translocation is intestine site-specific and associates with intestinal mucosal inflammation. *Inflammation.* 2012;35(6):1880-1888.

25. Yin B, Loike JD, Kako Y, Weinstock PH, Breslow JL, Silverstein SC, Goldberg IJ. Lipoprotein lipase regulates Fc receptor-mediated phagocytosis by macrophages maintained in glucose-deficient medium. *J Clin Invest.* 1997;100(3):649-657.

26. Chandak PG, Radovic B, Aflaki E, Kolb D, Buchebner M, Frohlich E, Magnes C, Sinner F, Haemmerle G, Zechner R, et al. Efficient phagocytosis requires triacylglycerol hydrolysis by adipose triglyceride lipase. *J Biol Chem.* 2010;285(26):20192-20201.

27. Hall CJ, Boyle RH, Astin JW, Flores MV, Oehlers SH, Sanderson LE, Ellett F, Lieschke GJ, Crosier KE, Crosier PS. Immunoresponsive gene 1 augments bactericidal activity of macrophage-lineage cells by regulating beta-oxidation-dependent mitochondrial ROS production. *Cell Metab.* 2013;18(2):265-278.

28. Newsholme P, Gordon S, Newsholme EA. Rates of utilization and fates of glucose, glutamine, pyruvate, fatty acids and ketone bodies by mouse macrophages. *Biochem J.* 1987;242(3):631-636.

29. Unger RH, Scherer PE. Gluttony, sloth and the metabolic syndrome: a roadmap to lipotoxicity. *Trends Endocrinol Metab.* 2010;21(6):345-352.

30. Lee JN, Kim H, Yao H, Chen Y, Weng K, Ye J. Identification of Ubxd8 protein as a sensor for unsaturated fatty acids and regulator of triglyceride synthesis. *Proc Natl Acad Sci U S A.* 2010;107(50):21424-21429.

31. Kato T, Shimano H, Yamamoto T, Ishikawa M, Kumadaki S, Matsuzaka T, Nakagawa Y, Yahagi N, Nakakuki M, Hasty AH, et al. Palmitate impairs and eicosapentaenoate restores insulin secretion through regulation of SREBP-1c in pancreatic islets. *Diabetes.* 2008;57(9):2382-2392.

32. Nolan CJ, Larter CZ. Lipotoxicity: why do saturated fatty acids cause and monounsaturates protect against it? *J Gastroenterol Hepatol.* 2009;24(5):703-706.

33. Renner F, Samuelson A, Rogers M, Glickman RM. Effect of saturated and unsaturated lipid on the composition of mesenteric triglyceride-rich lipoproteins in the rat. *J Lipid Res.* 1986;27(1):72-81.

34. Feldman EB, Russell BS, Hawkins CB, Forte T. Intestinal lymph lipoproteins in rats fed diets enriched in specific fatty acids. *J Nutr.* 1983;113(11):2323-2334.

35. Mattijssen F, Kersten S. Regulation of triglyceride metabolism by Angiopoietin-like proteins. *Biochim Biophys Acta.* 2012;1821(5):782-789.

36. Quagliarini F, Wang Y, Kozlitina J, Grishin NV, Hyde R, Boerwinkle E, Valenzuela DM, Murphy AJ, Cohen JC, Hobbs HH. Atypical angiopoietin-like protein that regulates ANGPTL3. *Proc Natl Acad Sci U S A.* 2012;109(48):19751-19756.

37. Wang Y, Quagliarini F, Gusarova V, Gromada J, Valenzuela DM, Cohen JC, Hobbs HH. Mice lacking ANGPTL8 (Betatrophin) manifest disrupted triglyceride metabolism without impaired glucose homeostasis. *Proc Natl Acad Sci U S A.* 2013;110(40):16109-16114.

38. Davies BS, Beigneux AP, Barnes RH, 2nd, Tu Y, Gin P, Weinstein MM, Nobumori C, Nyren R, Goldberg I, Olivecrona G, et al. GPIHBP1 is responsible for the entry of lipoprotein lipase into capillaries. *Cell Metab.* 2010;12(1):42-52.

39. Lutz EP, Merkel M, Kako Y, Melford K, Radner H, Breslow JL, Bensadoun A, Goldberg IJ. Heparin-binding defective lipoprotein lipase is unstable and causes abnormalities in lipid delivery to tissues. *J Clin Invest.* 2001;107(9):1183-1192.

40. Sonnenburg WK, Yu D, Lee EC, Xiong W, Gololobov G, Key B, Gay J, Wilganowski N, Hu Y, Zhao S, et al. GPIHBP1 stabilizes lipoprotein lipase and prevents its inhibition by angiopoietin-like 3 and angiopoietin-like 4. *J Lipid Res.* 2009;50(12):2421-2429.

41. Schaap FG, Rensen PC, Voshol PJ, Vrins C, van der Vliet HN, Chamuleau RA, Havekes LM, Groen AK, van Dijk KW. ApoAV reduces plasma triglycerides by inhibiting very low density lipoprotein-triglyceride (VLDL-TG) production and stimulating lipoprotein lipase-mediated VLDL-TG hydrolysis. *J Biol Chem.* 2004;279(27):27941-27947.

42. Garelnabi M, Lor K, Jin J, Chai F, Santanam N. The paradox of ApoA5 modulation of triglycerides: evidence from clinical and basic research. *Clin Biochem.* 2013;46(1-2):12-19.

43. Kinnunen PK, Jackson RL, Smith LC, Gotto AM, Jr., Sparrow JT. Activation of lipoprotein lipase by native and synthetic fragments of human plasma apolipoprotein C-II. *Proc Natl Acad Sci U S A.* 1977;74(11):4848-4851.

44. Hofmann SM, Perez-Tilve D, Greer TM, Coburn BA, Grant E, Basford JE, Tschop MH, Hui DY. Defective lipid delivery modulates glucose tolerance and metabolic response to diet in apolipoprotein E-deficient mice. *Diabetes.* 2008;57(1):5-12.

45. Tsukamoto K, Maugeais C, Glick JM, Rader DJ. Markedly increased secretion of VLDL triglycerides induced by gene transfer of apolipoprotein E isoforms in apoE-deficient mice. *J Lipid Res.* 2000;41(2):253-259.

46. Jong MC, Hofker MH, Havekes LM. Role of ApoCs in lipoprotein metabolism: functional differences between ApoC1, ApoC2, and ApoC3. *Arterioscler Thromb Vasc Biol.* 1999;19(3):472-484.

47. Yao ZM, Vance DE. The active synthesis of phosphatidylcholine is required for very low density lipoprotein secretion from rat hepatocytes. *J Biol Chem.* 1988;263(6):2998-3004.

48. Gimm T, Wiese M, Teschemacher B, Deggerich A, Schodel J, Knaup KX, Hackenbeck T, Hellerbrand C, Amann K, Wiesener MS, et al. Hypoxia-inducible protein 2 is a novel lipid droplet protein and a specific target gene of hypoxia-inducible factor-1. *FASEB J.* 2010;24(11):4443-4458.

49. Edvardsson U, Ljungberg A, Linden D, William-Olsson L, Peilot-Sjogren H, Ahnmark A, Oscarsson J. PPARalpha activation increases triglyceride mass and adipose differentiation-related protein in hepatocytes. *J Lipid Res.* 2006;47(2):329-340.

50. Chang BH, Li L, Saha P, Chan L. Absence of adipose differentiation related protein upregulates hepatic VLDL secretion, relieves hepatosteatosis, and improves whole body insulin resistance in leptin-deficient mice. *J Lipid Res.* 2010;51(8):2132-2142.

51. Li X, Ye J, Zhou L, Gu W, Fisher EA, Li P. Opposing roles of cell death-inducing DFF45-like effector B and perilipin 2 in controlling hepatic VLDL lipidation. *J Lipid Res.* 2012;53(9):1877-1889.

52. Chang BH, Li L, Paul A, Taniguchi S, Nannegari V, Heird WC, Chan L. Protection against fatty liver but normal adipogenesis in mice lacking adipose differentiation-related protein. *Mol Cell Biol.* 2006;26(3):1063-1076.

7

53. Cohen JC, Horton JD, Hobbs HH. Human fatty liver disease: old questions and new insights. *Science.* 2011;332(6037):1519-1523.

54. Zechner R, Zimmermann R, Eichmann TO, Kohlwein SD, Haemmerle G, Lass A, Madeo F. FAT SIGNALS--lipases and lipolysis in lipid metabolism and signaling. *Cell Metab.* 2012;15(3):279-291.

55. Mottillo EP, Bloch AE, Leff T, Granneman JG. Lipolytic products activate peroxisome proliferator-activated receptor (PPAR) alpha and delta in brown adipocytes to match fatty acid oxidation with supply. *J Biol Chem.* 2012;287(30):25038-25048.

56. Zandbergen F, Mandard S, Escher P, Tan NS, Patsouris D, Jatkoe T, Rojas-Caro S, Madore S, Wahli W, Tafuri S, et al. The G0/G1 switch gene 2 is a novel PPAR target gene. *Biochem J.* 2005;392(Pt 2):313-324.

57. Yang X, Lu X, Lombes M, Rha GB, Chi YI, Guerin TM, Smart EJ, Liu J. The G(0)/G(1) switch gene 2 regulates adipose lipolysis through association with adipose triglyceride lipase. *Cell Metab.* 2010;11(3):194-205.

58. Lumeng CN, Deyoung SM, Bodzin JL, Saltiel AR. Increased inflammatory properties of adipose tissue macrophages recruited during diet-induced obesity. *Diabetes.* 2007;56(1):16-23.

59. Kosteli A, Sugaru E, Haemmerle G, Martin JF, Lei J, Zechner R, Ferrante AW, Jr. Weight loss and lipolysis promote a dynamic immune response in murine adipose tissue. *J Clin Invest.* 2010;120(10):3466-3479.

60. Weisberg SP, McCann D, Desai M, Rosenbaum M, Leibel RL, Ferrante AW, Jr. Obesity is associated with macrophage accumulation in adipose tissue. *J Clin Invest.* 2003;112(12):1796-1808.

61. Xu X, Grijalva A, Skowronski A, van Eijk M, Serlie MJ, Ferrante AW, Jr. Obesity activates a program of lysosomal-dependent lipid metabolism in adipose tissue macrophages independently of classic activation. *Cell Metab.* 2013;18(6):816-830.

7

Nederlandse samenvatting

De peroxisoomproliferatorgeactiveerde receptoren (PPARs) omvatten een groep van nucleaire receptoren die een belangrijke rol spelen in de regulatie van het vetmetabolisme. Verschillende componenten uit onze voeding waaronder onverzadigde vetzuren kunnen dergelijke PPARs activeren. Actief PPAR bindt aan specifieke plaatsen op het DNA en stimuleert de productie van mRNA, wat leidt tot de productie van een eiwit. Drie verschillende PPARs zijn er geïdentificeerd: PPARα, PPARβ/δ en PPARγ. De specifieke functies die deze PPARs uitoefenen worden bepaald door zowel de relatieve expressie van een PPAR in een cel alsook de set van genen die door de PPAR wordt gereguleerd.

Angiopoietin-like 4 (ANGPTL4) is één van de vele genen die door deze PPARs wordt gereguleerd. ANGPTL4 wordt in verschillende organen geproduceerd waaronder de lever en vetweefsel en ondergaat vervolgens verschillende modificaties. Zo wordt ANGPTL4 in twee delen geknipt: nANGPTL4 en cANGPTL4, die beide verschillende functies uitvoeren. nAGPTL4 remt de werking van lipoproteïnelipase (LPL), een belangrijk eiwit dat betrokken is bij de afbraak en opname van triglyceriden uit het plasma. cANGPTL4 is niet betrokken in het vetmetabolisme maar speelt een rol in tumorgroei en wondheling. In dit proefschrift hebben we getracht de huidige kennis over de moleculaire functies van ANGPTL4 in het vetmetabolisme verder uit te diepen. Daartoe hebben we verschillende technieken gebruikt waaronder dierproeven, celkweek experimenten, biochemische experimenten en andere functionele metingen.

Gedurende één van die experimenten hebben we muizen zonder ANGPTL4, zogeheten *Angptl4* knockout muizen (*Angptl4*−/−), een hoog-vet dieet gegeven dat voornamelijk uit lange-keten verzadigde vetzuren bestond. Hierbij werden de muizen zonder ANGPTL4 al snel erg ziek en stierven ze aan fibrinopurulente peritonitis, terwijl wild-type dieren deze problemen niet ontwikkelden. Wanneer het vet in het dieet werd vervangen door lange-keten onverzadigde vetzuren of middellange-keten vetzuren ontstond er ook in de *Angptl4*−/− muizen geen ontstekingsreactie. Dit was een belangrijke aanwijzing in het vinden van de oorzaak van het ziek worden van *Angptl4*−/− dieren bij een dieet bestaande uit lange-keten verzadigde vetzuren. Daar waar lange-keten vetzuren via het mesenteriaal lymfatisch stelsel naar de vena subclavia worden getransporteerd in zogeheten chylomicronen, worden korte-keten vetzuren via de poortader naar de lever getransporteerd. Bij nauwkeurige inspectie van het mesenteriaal lymfatisch stelsel viel het op dat *Angptl4*−/− dieren vergrote lymfeklieren in het mesenterium ontwikkelden wanneer ze een dieet uit lange-keten verzadigde vetzuren kregen aangeboden. Microscopisch onderzoek toonde aan dat deze mesenteriale lymfeklieren veel met vet gevulde macrofagen bevatten. Daaropvolgende in vitro experimenten toonden aan dat PPARβ/δ de productie van ANGPTL4 in deze macrofagen stimuleert wanneer er vet de cel binnenkomt. Vervolgens remt ANGPTL4

de werking van LPL om op die manier de vetopname in deze macrofagen te voorkómen. Wanneer er geen ANGPTL4 aanwezig is zoals in het geval van de *Angptl4^{-/-}* muizen, nemen macrofagen ongelimiteerd vet op. Uiteindelijk leidt dit tot een verstoring van de werking van het endoplasmatisch reticulum en een ongecontroleerde ontstekingsreactie die vervolgens uitmondt in fibrinopurulente peritonitis.

Naast de waargenomen ontstekingsreactie die wordt veroorzaakt door lange-keten verzadigde vetzuren, komen dieren zonder ANGPTL4 sterker aan in gewicht wanneer ze een dieet krijgen aangeboden dat is gebaseerd op lange-keten onverzadigde vetzuren. Deze toename in lichaamsgewicht was niet gerelateerd aan een toename in voedselinname, lichaamsactiviteit, of een afname in energieverbruik. Echter, *Angplt4^{-/-}* dieren scheidden minder vet uit via de ontlasting in vergelijking met wild-type dieren. Vervolgexperimenten lieten zien dat muizen zonder ANGPTL4 zich kenmerken door een verhoogde lipase-activiteit in hun darminhoud. Pancreatisch lipase is de belangrijkste lipase die door de alvleesklier wordt geproduceerd en het grootste gedeelte van het aanwezige vet in voedsel verteert. In vitro experimenten toonden vervolgens aan dat ANGPTL4 de werking van pancreatisch lipase remt.

In het tweede deel van dit proefschrift beschrijven we de identificatie en karakterisatie van hypoxia inducible lipid droplet associated (HILPDA) als een PPAR gereguleerd gen. In initiële experimenten waarbij we dunne plakjes lever van muizen blootstelden aan een ligand voor PPARα kwam HILPDA uit de analyse als een mogelijk door PPAR gereguleerd gen. Vervolgens observeerden we een substantiële toename in de expressie van HILPDA wanneer we normale muizen voerden met een ligand voor PPARα, terwijl deze toename niet zichtbaar was wanneer dezelfde ligand aan muizen zonder PPARα werd gegeven. Vervolgexperimenten lieten zien dat de regulatie van HILPDA door PPARα is gebaseerd op een bindingsplaats voor PPAR op het DNA op ongeveer 1200 basenparen van de plaats waar de productie van *Hilpda* mRNA start. Deze bindingsplaats is zowel in muizen als in mensen aanwezig.

Om een eventuele functie van HILPDA in de lever te onderzoeken hebben we wild-type muizen met een adeno-geassocieerd virus geïnjecteerd dat specifiek de expressie van HILPDA in de lever verhoogt. Muizen met een lever-specifieke overexpressie van HILPDA ontwikkelden een vette lever. Daaropvolgende experimenten lieten zien dat muizen met een verhoogde HILPDA-expressie in hun lever minder very-low-density-lipoproteïnen (VLDL)-triglyceriden produceren, met als gevolg het ontstaan van een vette lever.

Naast de hierboven bescheven functie van HILPDA in de regulatie van VLDL-triglyceriden secretie in de lever, observeerden we een susbtantieel expressieniveau van HILDPA in vetweefsel van zowel muizen als mensen. In het vetweefsel vonden we dat de

expressie van HILPDA wordt gereguleerd door zowel PPARγ en β-adrenerge receptoren. Daarnaast was er een toename in de expressie van HILPDA in vetweefsel te zien wanneer muizen werden gevast, terwijl er een afname te zien was bij een hoog-vet interventie. Meerdere experimenten waarbij gebruik is gemaakt van zowel knockdown als overexpressie van HILPDA, hebben laten zien dat HILPDA geen effect heeft op vetceldifferentiatie. Muizen die het *Hilpda*-gen specifiek in het wit en bruin vetweefsel missen vertoonden geen metabole afwijking nadat ze werden gevast. Echter, overexpressie van HILPDA in vetcellen verlaagde de hoeveelheid vrije vetzuren die werd afgegeven bij activatie van de β-adrenerge receptoren. De toename in HILPDA-expressie na stimulatie van β-adrenerge receptoren is mogelijk een feedbackmechanisme gericht op het reguleren van de hoeveelheid vetzuren die wordt afgegeven.

Samengevat, in dit proefschrift hebben we belangrijke nieuwe kennis vergaard over de functie van ANGPTL4. We laten zien dat ANGPTL4 een belangrijke rol speelt in de regulatie van het proces van vetvertering en ook in het voorkómen van ongecontroleerde vetopname in macrofagen die zich in mesenteriale lymfeklieren bevinden. Vervolgens hebben we aangetoond dat HILDPA een nieuw doelgen van PPARα is en betrokken bij de regulatie van VLDL-triglyceriden secretie en vetzuurafgifte in het vetweefsel. Toekomstig onderzoek richt zich op de mechanistische aspecten die ten grondslag liggen aan de regulatie en functies van HILPDA in de lever en vetweefsel

Dankwoord

Daar komen ze dan. De meest gelezen pagina's van een proefschrift. Vaak ook de enige. En dat terwijl hoofdstuk 6 toch echt een aanrader is.

Hoewel het fijn is om dingen af te kunnen ronden, komt met elke letter in dit dankwoord mijn vertrek uit Wageningen dichterbij. Waarschijnlijk is dat ook de reden dat ik het schrijven ervan zo lang mogelijk heb uitgesteld. Ik heb altijd met veel plezier in Wageningen gewerkt en zal met veel goede herinneringen aan deze periode terugdenken. Dit is met name te danken aan de prettige werksfeer op het lab.

Allereerst wil ik een paar woorden richten aan mijn promotor, Sander Kersten. Sander, zonder jouw kennis, hulp, geduld, maar ook de vrijheid en kansen die je me hebt gegeven, had ik de eindstreep nooit gehaald. Je hebt me veel geleerd over het doen van goed en solide onderzoek. Het was altijd erg prettig om 's avonds laat via de mail nog wat ideeën uit te wisselen of wat advies te kunnen vragen. Dankzij jouw kritische blik en een discussietje zo af en toe heb ik ook veel over mezelf geleerd. Waarschijnlijk zul je niet veel eigenwijzere AIO's meer tegenkomen, dus het ergste heb je maar meteen gehad. Heel erg bedankt voor alles. Ik had me geen betere promotor kunnen wensen.

Michael, erg fijn dat ik binnen jouw NMG-groep onderzoek heb mogen doen. Je kritische blik en visie hebben me geleerd dat je je niet altijd maar op je eilandje moet blijven focussen. Heel erg bedankt.

Soms kom je iemand tegen waar het meteen mee klikt, zonder al te veel woorden te hebben gewisseld. Zo iemand trof ik een tijdje na de start van mijn PhD. Rinke, ik wil je bedanken voor al die gezellige koffiepauzes waarin we het laatste wielernieuws bespraken, een uitzending van Voetbal International nog eens analyseerden, ideeën uitwisselden met betrekking tot het onderzoek en hele ladingen aan slechte grappen aan het adres van Sander maakten. Een paar honderd liter koffie later durf ik wel te zeggen dat het zonder jouw aanwezigheid in het lab niet hetzelfde zou zijn geweest. Ik wens je veel succes met je toekomstige onderzoek. Bedankt dat je naast me gaat staan tijdens de verdediging.

Uiteraard wil ik ook graag mijn kamergenoten bedanken voor de gezellige tijd in 0049b. Karin, heel erg bedankt voor al die ELISAs, het zijn van een gezellige buurvrouw, alle last-minute bestellingen en voor het onderhouden van de plant. Shohreh, I have to make an exemption for you, as I am not sure whether I should thank you or not. I mean, you are the one who provided all the candy resulting in my occasional weight gain… Just kidding, I want to thank you for all your help and for being such a nice roommate. Ya, I wish you all the best with the remainder of your time as a PhD student, finding 'your compound', and of course lots of joy with your son. It was always nice to talk about the kids. Thanks Fenni for being such a nice roommate and good luck with your thesis. I'm sure you will manage. I would also like to thank Sheril for the help with the initial

pancreatic lipase assays and for being such a kind roommate. Good luck with your carreer. (s)Jenny (s)Jansen, bedankt voor het zijn van een lieve kamergenoot en je humor. Je rust en relaxte manier van werken heb ik altijd erg fijn gevonden. Waarschijnlijk ben je ook de enige hier op het lab die me ooit heeft verstaan met mijn rare dialect. Super dat je me wil bijstaan tijdens m'n promotie.

Guido (Bontempi) Hooiveld, man naar mijn hart. Altijd behulpzaam en lekker direct. Niets meer aan veranderen. Bedankt voor je gezelligheid, enthousiasme en natuurlijk het niet te vergeten practicum tijdens het WK voetbal. Eigenlijk zou elk lab een 'Guido' moeten hebben.

Dan de collega-AIO's binnen het groepje van Sander. Wieneke, heel veel succes met de rest van je PhD. Ik weet zeker dat je er iets moois van gaat maken. Het was erg prettig om met je samen te werken. Milène, nog even en je bent de volgende die mag promoveren. Je bent al erg goed op weg, dus dat gaat, kinda… wel lukken. Aafke en Lily. Jullie zijn nog maar relatief kort geleden toegetreden tot het groepje van Sander maar ik ben er van overtuigd dat het allemaal goed komt. Jullie zijn allebei een echte aanwinst die ook veel gezelligheid hebben toegevoegd. Veel succes voor de toekomst.

Vervolgens Diederik, Juri, Sophie, en alle eerdere bewoners van kamer 0051. Het was erg prettig om zo af en toe bij jullie binnen te vallen om wat slechte grappen en andere zaken te kunnen ventileren. Dank hiervoor. Ik wens jullie allemaal veel succes met jullie toekomstige onderzoek. Diederik, nog erg bedankt voor al je advies tijdens het afronden van mijn proefschrift.

Uiteraard wil ik nog meer collega's bedanken.

Mieke: zonder jou zou de celkweek een puinhoop zijn. Ik wil je bedanken voor al je hulp, kunde, en gezelligheid. Carolien, erg bedankt voor de gezellige babbeltjes en veel succes nog. Katja, Inge, Jvalini, Neeraj en Nikkie: heel erg bedankt voor de leuke tijd en veel succes allemaal nog met het afronden van jullie PhD. Echt super dat onze vis een plaatsje krijgt op jullie kantoor. O, Katja, sorry for all my pranks in the hallway. Bedankt Mark voor je hulp met de arrays zo af en toe maar vooral voor je humor en alle nutteloze feitjes via Wikipedia en al die andere apps. Lydia, Wilma en Mechteld, erg bedankt voor jullie gezelligheid. Respect Wilma dat je altijd maar weer zo vroeg op het lab bent. Ik heb het een tijdje geprobeerd, maar elke dag om 7 uur beginnen is me toch iets te gortig. Verder Philip, Michiel, Parastoo, Marco, Renger, Jocelijn en Klaske allemaal heel veel succes met jullie werkzaamheden en bedankt voor de fijne tijd op het lab.

Vervolgens wil ik ook graag de mensen van het CKP bedanken voor al hun hulp en kunde. René, Wilma, Judith, Bert, Lisette, Romy, en Rob. Zonder jullie bijdrage was dit boekje er zeker niet gekomen en daarom: hartelijk bedankt!

Mijn zus Bouke met aanhanger Joris en schoonzus Carola met aanhanger Jeroen: ik wil jullie bedanken voor jullie interesse, hulp en geduld.

Marleen, we hebben als familie geen gemakkelijke periode achter de rug met het overlijden van Hub. Ik vind het bewonderenswaardig hoe jij je hier doorheen weet te slaan en altijd interesse in mijn werk hebt getoond. Heel erg bedankt.

Pa en Ma, meestal hadden jullie geen flauw idee waar ik me precies mee bezig hield anders dan 'iets in het lab' of 'wat muizen opensnijden'. Toch hebben jullie me altijd vrij gelaten in mijn keuzes en me hier ook in gesteund. Ik heb dat altijd erg fijn gevonden. Ik wil jullie bedanken voor de onvoorwaardelijke hulp. Zonder jullie aanwezigheid was het niet gelukt, zeker niet in de afgelopen 1.5 jaar na de geboorte van Fabian.

Als laatste wil ik mijn lieve Christel bedanken. Om jou te bedanken Christel zou ik eigenlijk een boek moeten schrijven. Al je opofferingen omdat ik zonodig de wetenschapper uit wil hangen zijn te gek voor woorden: verhuizen, parttime gaan werken, en veel reizen. Ik vind het stoer dat je het ook nu weer aandurft om 'eens iets anders te doen'. Je bent een geweldige moeder en een fantastische vrouw. We hebben samen altijd veel lol en zonder jouw 'schop onder mijn kont' en liefde ben ik nergens. Ik weet zeker dat we samen met Fabian een hele leuke tijd tegemoet gaan in Heidelberg.

Frits

About the author

Curriculum vitae

Frits Mattijssen was born on May 17, 1984 in Doornenburg, The Netherlands. He completed secondary school at the Over Betuwe College in Bemmel. Frits became interested in the topic of nutrition during his time as a competitive cyclist. This led to enrollment in the Nutrition and Dietetics study program at the Hogeschool van Arnhem en Nijmegen in 2003. After receiving a bachelor degree in Nutrition and Dietetics, he continued with the Master program in Nutrition and Health at Wageningen University in 2007. Frits specialized in Molecular Nutrition with a Master thesis on the topic of fatty acid transporters in hepatocytes. He then performed an internship at the German Cancer Research Center (DKFZ) in Heidelberg, Germany, working on the transcriptional cofactor TBLR1. Upon completion of his MSc training he started a PhD project within the Nutrition, Metabolism and Genomics group at Wageningen University in September 2009. Guided by his promotor Prof. Dr. Ir. Sander Kersten, he finished his PhD of which the results are described in this thesis. Frits recently started as a postdoc with Prof. Dr. Stephan Herzig at the DKFZ in Heidelberg, Germany.

List of publications

Mattijssen F, Xue Z, Dijk W, Tasdelen I, Vegiopoulos A, Kalkhoven E, Stienstra R, Mandrup S, Qi L, Kersten S. Hypoxia inducible lipid droplet associated (HILPDA) is a PPARγ and β-adrenergic receptor target gene involved in adipose tissue lipolysis. *(manuscript in preparation)*

Mattijssen F, Georgiadi A, Andasarie T, Szalowska E, Zota A, Krones-Herzig A, Heier C, Ratman D, De Bosscher K, Qi L, Zechner R, Herzig S, Kersten S. Hypoxia inducible lipid droplet associated (HILPDA) is a novel PPAR target involved in hepatic triglyceride secretion. *(submitted for publication)*

Catoire M, Alex S, Paraskevopulos N, **Mattijssen F**, Evers-van Gogh I, Schaart G, Jeppesen J, Kneppers A, Mensink M, Voshol PJ, Olivecrona G, Soon Tan N, Hesselink MK, Berbee JF, Rensen PC, Kalkhoven E, Schrauwen P, Kersten S. Fatty acid-inducible ANGPTL4 governs lipid metabolic response to exercise. *Proc Natl Acad Sci U S A.* 2014. *(in press)*

Mattijssen F, Alex S, Swarts HJ, Groen AK, van Schothorst EM, Kersten S. Angptl4 serves as an endogenous inhibitor of intestinal lipid digestion. *Mol Metab.* 2014;3(2):135-144.

Jonker JT, Smit JW, Hammer S, Snel M, van der Meer RW, Lamb HJ, **Mattijssen F**, Mudde K, Jazet IM, Dekkers OM, de Roos A, Romijn JA, Kersten S, Rensen PC. Dietary modulation of plasma angiopoietin-like protein 4 concentrations in healthy volunteers and in patients with type 2 diabetes. *Am J Clin Nutr.* 2013;97(2):255-260.

Mattijssen F, Kersten S. Regulation of triglyceride metabolism by Angiopoietin-like proteins. *Biochim Biophys Acta.* 2012;1821(5):782-789.

Kroupa O, Vorrsjo E, Stienstra R, **Mattijssen F**, Nilsson SK, Sukonina V, Kersten S, Olivecrona G, Olivecrona T. Linking nutritional regulation of Angptl4, Gpihbp1, and Lmf1 to lipoprotein lipase activity in rodent adipose tissue. *BMC Physiol.* 2012;12:13.

Bosma M, Hesselink MK, Sparks LM, Timmers S, Ferraz MJ, **Mattijssen F**, van Beurden D, Schaart G, de Baets MH, Verheyen FK, Kersten S, Schrauwen P. Perilipin 2 improves insulin sensitivity in skeletal muscle despite elevated intramuscular lipid levels. *Diabetes.* 2012;61(11):2679-2690.

Mattijssen F, Kersten S. Saturated fatty acids and snoRNAs: partners in crime. *Cell Metab.* 2011;14(1):1-2.

Kulozik P, Jones A*, **Mattijssen F***, Rose AJ, Reimann A, Strzoda D, Kleinsorg S, Raupp C, Kleinschmidt J, Muller-Decker K, Wahli W, Sticht C, Gretz N, von Loeffelholz C, Stockmann M, Pfeiffer A, Stohr S, Dallinga-Thie GM, Nawroth PP, Berriel Diaz M, Herzig S. Hepatic deficiency in transcriptional cofactor TBL1 promotes liver steatosis and hypertriglyceridemia. *Cell Metab.* 2011;13(4):389-400.

Lichtenstein L*, **Mattijssen F***, de Wit NJ*, Georgiadi A, Hooiveld GJ, van der Meer R, He Y, Qi L, Koster A, Tamsma JT, Tan NS, Muller M, Kersten S. Angptl4 protects against severe proinflammatory effects of saturated fat by inhibiting fatty acid uptake into mesenteric lymph node macrophages. *Cell Metab.* 2010;12(6):580-592.

*Equal contribution

Overview of completed educational activities

Discipline specific activities

NWO Voedingsdagen (Deurne, The Netherlands, 2009-2011)

2nd Benelux Nuclear Receptor meeting (Leiden, The Netherlands, 2009)

Gordon Research Conference on Lipoprotein Metabolism (Waterville Valley, NH, USA, 2010)

3rd Benelux Nuclear Receptor meeting (Ghent, Belgium, 2010)

Deuel Conference on Lipids (Napa, CA, USA, 2011)

27th Ernst Klenk Symposium in Molecular Medicine (Cologne, Germany, 2011)

4th Benelux Nuclear Receptor meeting (Amsterdam, The Netherlands, 2011)

Training at laboratory of Dr. Ling Qi, Cornell University (Ithaca, NY, USA, 2013)

Nederlandse Vereniging voor Diabetes Onderzoek (NVDO) meeting (Oosterbeek, The Netherlands, 2013)

General courses

Academic Writing II (2009)

VLAG PhD week (Baarlo, The Netherlands, 2009)

Course on Laboratory Animal Science (Utrecht, The Netherlands, 2010)

Workshop: how to write a world-class paper (2011)

Optionals

Preparation research proposal (2009)

Scientific meetings NMG group (2009-2014)

Journal club (2010-2014)

Scientific meetings TSK (2012-2014)